UiT The Arctic University of Norway

Faculty of Science and Technology

Department of Geosciences

Late Quaternary tephra stratigraphy and paleoenvironmental reconstruction based on lake sediments from North and Northeast Iceland

Emma Marie Bender

Master's Thesis in Geology GEO-3900

July 2020

Abstract

Due to Iceland's position in the middle of the North Atlantic, the island is highly sensitive to oceanic and atmospheric fluctuations, which lead to changes in the environment. These fluctuating environmental conditions in addition to Iceland's high volcanic activity make it a strategic study area for paleoenvironmental and tephra studies. Lake sediments contain information about such past climate and environmental changes, and also have the ability to preserve tephra deposits. For this thesis, sediments cores were collected from four lakes: Torfdalsvatn, located on Skagi peninsula in North Iceland, and Þuríðarvatn, Nykurvatn and Ásbrandsstaðavatn, located near Vopnafjörður in Northeast Iceland. Multi-proxy analyses of the sediment records have been performed with the aim to construct a reliable alignment of individual core sections, to establish age models and tephra stratigraphy by identifying tephra marker layers, and to reconstruct the paleoenvironment during the Late Quaternary.

Alignments for the core sections of the four lakes were established based on ^{14}C ages, identified tephra layers and geochemical composition of the sediments. The alignments allowed the construction of continuous core records for each lake.
Analysis of major element compositions from tephra layers contained in the Torfdalsvatn sediment core revealed four tephra marker layers, including Hekla 1104, Hekla 3, Hekla 4, and the Saksunarvatn Ash. In sediment records from Northeast Iceland the major element analysis of tephra layers showed that five tephra marker layers, including V1477, Hekla 3, Hekla 4, the Saksunarvatn Ash and Askja S, were deposited in the study area.
Sedimentological and geochemical analysis of Torfdalsvatn revealed a clayey facies, which is believed to indicate that a glacial advance occurred on Skagi between ca. 12.0 to 10.3 cal. kyr BP. A gyttja facies found above the clay has been interpreted as a deposit formed during lacustrine conditions without the inflow of glacial meltwater, which would have coincided with warmer temperatures from 10.3 cal. kyr BP until presently. Skagi is therefore believed to have been fully deglaciated by 10.3 cal. kyr BP.
A clayey facies in the bottom of the Ásbrandsstaðavatn core is believed to have formed in a glaciated environment in the Vopnafjörður area between 10.8-10.3 cal. kyr BP. After 10.3 cal. kyr BP the presence of gyttja suggests that lacustrine sedimentation persisted in Þuríðarvatn, Nykurvatn and Ásbrandsstaðavatn (Vopnafjörður area). Based on the findings it is believed that the Vopnafjörður area has been fully deglaciated by 10.3 cal. kyr BP.

Acknowledgements

First, I would like to thank my main supervisor Anders Schomacker for your support throughout this project, feedback on the text and many encouraging words. Sofia Kjellman and Alexandra Rouillard, thank you for devoting your time for reading my thesis and for the guidance and time spend in the lab. I truly am grateful for all your support and I'm sincerely glad to have chosen this project.

I would also like to thank Esther Ruth Guðmundsdóttir for introducing me to the 'world' of tephra and for giving me great guidance and insight for this project. I would further like to thank Ingvild Hald, Karina Monsen and Trine Dahl for your great assistance in the Geology Laboratory at UiT. It was always great working in the lab and I'm grateful for the time you devoted to help me. Another thanks go to Marie Merkel for your help and assistance in the UiT University Museum lab. Furthermore, I would like to thank Egill Erlendsson, University of Iceland and his collaborators for retrieving the sediments cores of Lake Torfdalsvatn.

Finally, I would like to my friends and family for making my time in Tromsø so special. Kevin, your support has been so important to me especially through time's I hadn't been so sure. To my sister, thank you for always giving me the feeling to be home, even if we're so far away. And to my parents, thank you for supporting yet another little Arctic adventure.

Von guten Mächten wunderbar geborgen,
erwarten wir getrost, was kommen mag.
Du bist mit uns am Abend und am Morgen
und ganz gewiss an jedem neuen Tag.
Dietrich Bonhoeffer

Table of Content

1 Introduction

Lake sediments are valuable records that contain information about fluctuations in past climates making them particularly useful for investigations of paleoenvironmental conditions (Fritz, 2008). These reconstructions of the paleoenvironment and paleoclimate are often based on a broad range of physical, geochemical and biological proxies, used to infer past changes in the depositional environment of natural lake systems (e.g., Ólafsdóttir & Guðmundsson, 2002; Axford et al., 2009; Kaufman, 2009). Lake records allow for detailed reconstructions of the climatic and environmental history as they provide high-resolution multi-proxy data covering long time spans (e.g., Cherapanova et al., 2007). The high abundancy of lakes at high latitudes also makes them especially useful for studies in the Northern Hemisphere (Kaufman, 2009).

For a reliable paleoreconstruction, it is crucial to have a precise and accurate age control of the sedimentary record. Tephra marker layers within a sediment sequence are especially favorable for dating sediments because of the instantaneous deposition of tephra, and their wide geographical distribution (Lowe, 2011; Óladóttir et al., 2011). Additionally, tephra layers are well preserved in lacustrine sediments, making them a useful tool for establishing a chronology for a lake sediment sequence (Larsen & Eiríksson, 2008; Davies, 2015). However, one challenge using lake sediments for paleoenvironmental reconstructions is the construction of continuous core records. Lake cores often require alignment of individual overlapping core sections collected from a single lake, to establish a continuous sediment sequence. Correlations can be difficult to determine due to lack of visual similarities, clear stratigraphic tie-points or hiati between core sections. Nonetheless, it is important to construct a reliable continuous record to avoid possible misalignments that might lead to an incorrect interpretation of proxy data (e.g., Lisiecki & Herbert, 2007; Turner et al., 2008).

Because of their high potential to help reconstruct past climate changes, the use of lake sediments as paleoclimate archives has also been widely established for studies in Iceland (e.g., Caseldine et al., 2003; Axford et al., 2009; Striberger et al., 2012; Schomacker et al., 2016). The location of Iceland in the middle of the North Atlantic (Fig. 1A) makes it highly sensitive to changes in water masses and the atmosphere. Even small-scale changes in the oceanic or atmospheric circulation can affect the climate on Iceland and cause many of the glaciers on the island to fluctuated in size (Ingólfsson, 1991; Gudmundsson, 1997; Bianchi &

McCave, 1999; Geirsdóttir et al., 2009). The islands is therefore an especially interesting study area regarding variations in the environmental and climatic conditions through time (Axford et al., 2007; Geirsdóttir et al., 2009). Another reason for Iceland being especially interesting for paleoenvironmental studies is the high volcanic activity. Due to the high quantity of tephra-producing, phreatomagmatic eruptions, terrestrial, marine and ice-core records from Iceland have the potential to preserve high-resolution geochronological records (e.g., Larsen et al., 2012; Blair et al., 2015; Harning et al., 2016; Schomacker et al., 2016; Eddudóttir et al., 2017; Geirsdóttir et al., 2009, 2019). While some parts of Iceland, especially South and Central Iceland, are relatively well studied (e.g., Dugmore & Buckland, 1991; Syvitski et al., 1999; Schomacker et al., 2003; Flowers et al., 2008; Larsen et al., 2011), there are fewer studies of the northern and especially northeastern section of the island. Analyses of lake sediments collected from these areas could therefore provide new insight into the climatic and environmental history of the region and reveal details about the paleoclimate.

1.1 Objectives

In this project, sediment cores from four lakes: Lake Torfdalsvatn on Skagi peninsula, North Iceland and lakes Þuríðarvatn, Nykurvatn and Ásbrandsstaðavatn in Northeast Iceland close to Vopnafjörður (Fig. 1B), were analyzed in order to address multiple objectives. The main objectives of this thesis are to:

- Construct a continuous core record for each lake, by aligning sediment core sections based on lithostratigraphy and geochemical composition.
- Establish or improve the tephra stratigraphy for North and Northeast Iceland during the Late Glacial and Holocene by identifying and correlating tephra layers to silicic (and basaltic) tephra marker horizons.
- Reconstruct environmental conditions in North and Northeast Iceland during the Late Glacial and Holocene by describing and interpreting the assemblage of sedimentary processes and products and constructing age-depth models for the obtained sequences.

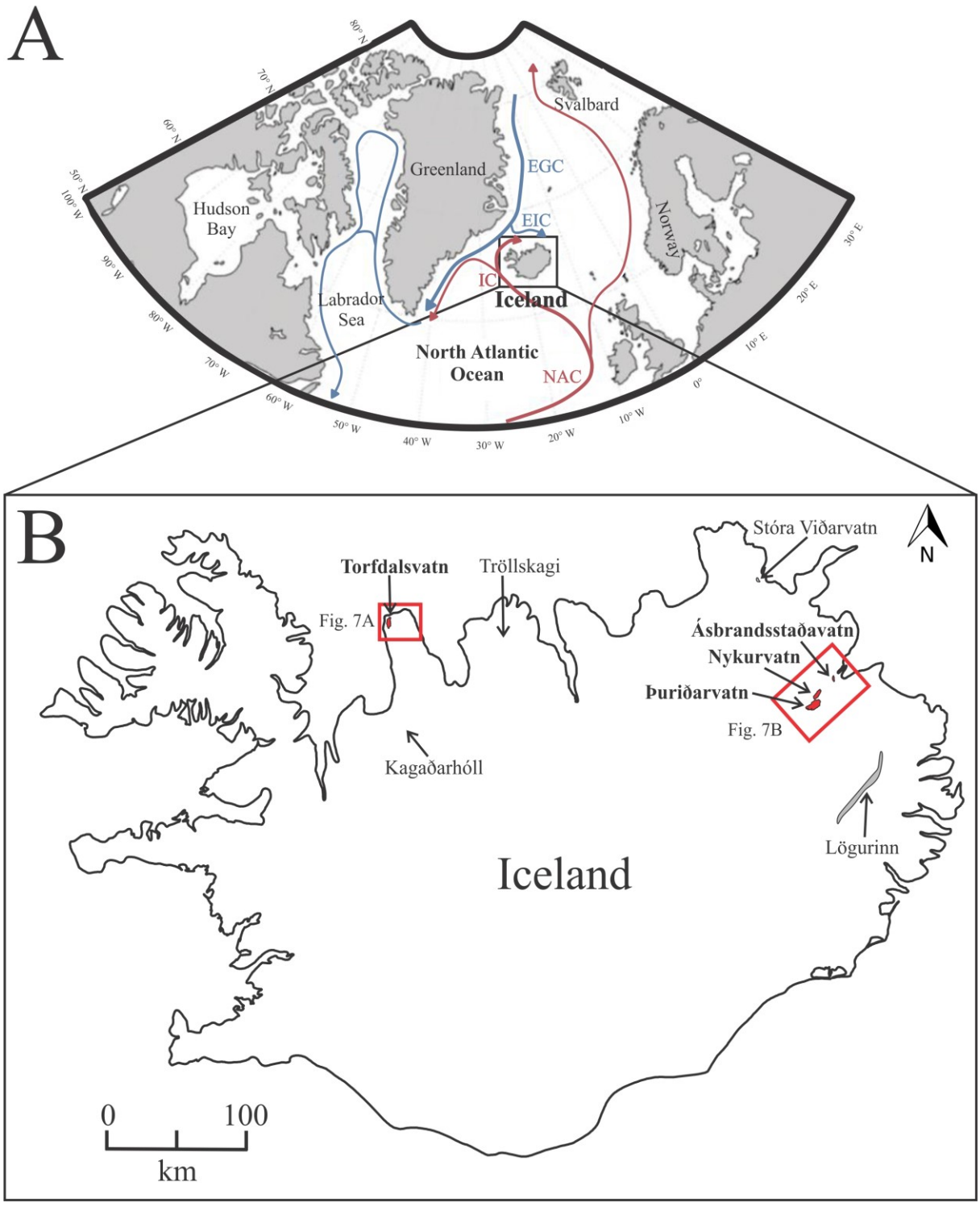

Figure 1. *A: Overview map of the North Atlantic showing the position of Iceland in its center. EGC = East Greenland Current, EIC = East Iceland Current, IC = Irminger Current, NAC = North Atlantic Current (modified from Geirsdóttir et al., 2019). B: Map of Iceland showing different localities that are important to this study. The red boxes show the study areas with the locations of the four studied lakes. The detailed study areas can be seen in Fig. 7.*

2 Glacial and environmental history of Iceland

2.1 Last Glacial Maximum and deglaciation

The glacial and environmental history of Iceland has been addressed by multiple authors, including Ingólfsson et al. (2010), who summarized Iceland's history since the Last Glacial Maximum (LGM). While the glacial history of northwestern Iceland is relatively well documented (e.g., Principato, 2008; Schomacker et al., 2016), northeastern Iceland's glacial history remains relatively poorly constrained. Variations of ice sheet extents and fluctuations in the climatic conditions reflect changes in the regional climate in the North Atlantic region, largely controlled by changes in the Atlantic ocean circulation (i.e., maritime processes) (Ingólfsson & Norðdahl, 1994; Ingólfsson et al., 1997).

During the LGM (ca. 28.1-22.8 cal. kyr BP) Iceland was completely covered by the Icelandic Ice Sheet (IIS) with a maximum ice extent and volume being reached at ca. 22.9 cal. kyr BP (Fig. 2A) (Ingólfsson, 1991; Norðdahl, 1991; Geirsdóttir et al., 2009; Spagnolo & Clark, 2009; Ingólfsson et al., 2010; Patton et al., 2017). Glacial striations and glacially formed landforms (e.g., terminal moraines) that have been identified on the continental shelves surrounding Iceland suggest that the IIS extended across the Icelandic shelf and in some regions even reached the shelf break (Fig. 2A; Syvitski et al., 1999; Principato et al., 2006; Spagnolo & Clark, 2009; Patton et al., 2017).

Following the LGM, the IIS began to retreat from the shelf break at approximately 22.8 cal. kyr BP and had reached the mid shelf before 18.5 cal. kyr BP (Andrews et al., 2000; Patton et al., 2017). Between 18.7-16.1 cal. kyr BP warm Atlantic water, with sea surface temperatures (SST) similar to present temperatures, reached North Iceland's shelf areas and the sea level started to rise around Iceland (Andrews et al., 2000; Ingólfsson & Norðdahl, 2001; Andrés et al., 2019). The warm SST initiated the Bølling-Allerød interstadial (Bølling:15.4-13.9 cal. kyr BP; Allerød: 13.9-13.0 cal. kyr BP) and the start of a gradual deglaciation on Iceland (Ingólfsson, 1988, 1991; Ingólfsson et al., 1997, 2010; Syvitski et al., 1999; Geirsdóttir et al., 2009; Patton et al., 2017). During the Bølling interstadial, at ca. 15.4 cal. kyr BP, the IIS retreated rapidily and collapsed, most likely caused by a northwards migration of the Polar Front and rising sea levels (Rundgren et al., 1997; Syvitski et al., 1999; Norðdahl et al., 2008; Geirsdóttir et al., 2009; Patton et al., 2017; Andrés et al., 2019). Pollen records and sea level

reconstructions from marine sediments indicate that at the end of the Bølling interstadial (ca. 14.0 cal. kyr BP) a cold period and glacial advances occured on Iceland (Ingólfsson et al., 1997; Pétursson et al., 2015; Andrés et al., 2019). It was reported that during the Allerød interstadial glaciers had retreated from Skagafjörður (Fig. 2B). Coastal lowlands including Skagi and the Vopnafjörður area, are believed to have been ice-free but submerged during this interstadial (Ingólfsson et al., 1997). The glacial retreat during the Bølling-Allerød interstadial was interrupted by short-lived glacial advance during the Older Dryas (Ingólfsson et al., 1997).

A rapid cooling of the coastal waters off southwestern Iceland marked the transition from Allerød to Younger Dryas (YD; Ingólfsson et al., 2010)). The YD occurred between ca. 13.0 to 11.7 cal. kyr BP (Pétursson et al., 2015; Patton et al., 2017). The ocean cooling led to a rapid decrease in atmospheric temperatures at the onset of the YD (Ingólfsson et al., 2010). This decrease in temperature is also indicated by pollen records showing a shift in the vegetation from dwarf-shrub tundra coverage to grass tundra (Rundgren, 1995, 1999). During the YD, coastal areas that have been ice-free since the beginning of the Bølling interstadial, were covered by the regrowing IIS (Norðdahl et al., 2008). On Iceland several regional indicators for readvances or standstill of glaciers have been observed. The regrowing ice sheet is not believed to have extended onto Skagi peninsula (Patton et al., 2017). However, cirque glaciers may have been abundant on the peninsula during the YD (and early Holocene) while the lowlands in North Iceland remained ice-free (Ingólfsson et al., 1997). Glacial striations dated to a YD age indicate that the IIS extended into the Vopnafjörður area during that time. It is believed that the Vopnafjörður area was completely covered by glaciers during the Younger Dryas (Sæmundsson, 1995; Patton et al., 2017). At the end of the YD the IIS started to retreat again (Pétursson et al., 2015; Andrés et al., 2019).

Following the YD is the Holocene epoch starting ca. 11.7 cal. kyr BP. The early Holocene glacial history is generally characterized by extensive retreat of glaciers to the highlands (Hallsdóttir & Caseldine, 2005). The early Holocene ice sheet was situated behind the coastline all over Iceland (Fig. 2C) (Norðdahl & Pétursson, 2005). However, around 11.5 cal. kyr BP the IIS readvanced again, reaching coastal areas in south, north and northeast Iceland (Fig. 2B; Pétursson et al., 2015; Patton et al., 2017; Andrés et al., 2019). According to Sæmundsson (1995), glaciers terminated in the inner parts of Vopnafjörður around 11.1 cal.

kyr BP. In the outer parts of Vopnafjörður, raised marine terraces at about 60 m a.s.l. indicate that glacier terminated at Hofsádalur and Selárdalur. This suggests that glaciers in the Vopnafjörður area were fairly extensive in early Holocene times (Fig. 2C) (Norðdahl, 1991). Ingólfsson (1991) also described that in northeast Iceland (Vopnafjörður area) glaciers reached the present coast during the early Holocene. However, the second readvance during the early Holocene seems to be less extensive compared to the Younger Dryas advance. While Skagi was mostly ice-free during the early Holocene, a large outlet glacier extended to the head of Skagafjörður (Fig. 2C) (Ingólfsson et al., 1997; Patton et al., 2017). The early Holocene displays most likely the last time when glaciers were situated in or close to both study areas. The ice sheet experienced a rapid retreat after 11.2 cal. kyr BP, and by the time the Saksunarvatn tephra was deposited (10.3 cal. kyr BP) the highlands of Iceland were almost ice-free (Kaldal & Víkingsson, 1990; Geirsdóttir et al., 2009; Andrés et al., 2019).

2.2 Holocene

The Holocene epoch describes a period of complex variations in climate (Fig. 3) and fluctuating glaciers (Geirsdóttir et al., 2009). During the early Holocene, summer insolation peaked at ca. 11 cal. kyr BP in the Northern Hemisphere. However, due to negative feedback mechanisms increasing temperatures were delayed (Kaufman et al., 2004). During the first stage of the early Holocene (11.7 – 10.1 cal. kyr BP), the climate was cold, later transitioning into an interglacial subpolar maritime climate with cool summer temperatures (Ingólfsson, 1991; Björck et al., 1992; Eiríksson et al., 2000; Axford et al., 2007). A gradual warming trend started after 11 cal. kyr BP but was interrupted by a substantial temperature depression around 8.2 cal. kyr BP. Marine, lacustrine and ice core studies revealed drastic decreases in temperatures during the 8.2 event and indicated that ice caps started to grow (e.g., Langjökull) (e.g., Eiríksson et al., 2000; Geirsdóttir et al., 2002; Alley & Ágústsdóttir, 2005; Flowers et al., 2008).

The highest temperatures that were reached during the early and mid Holocene occurred after 8 cal. kyr BP during the Holocene Thermal Maximum (HTM, Fig. 3) (Andersen & Koç, 2004; Geirsdóttir et al., 2009). In Iceland the HTM occurred between 8 and 6 cal. kyr BP, however the exact timing is indicated by a maximum expansion of birch forests in southern Iceland (Andersen & Koç, 2004; Hallsdóttir & Caseldine, 2005). The summer temperatures

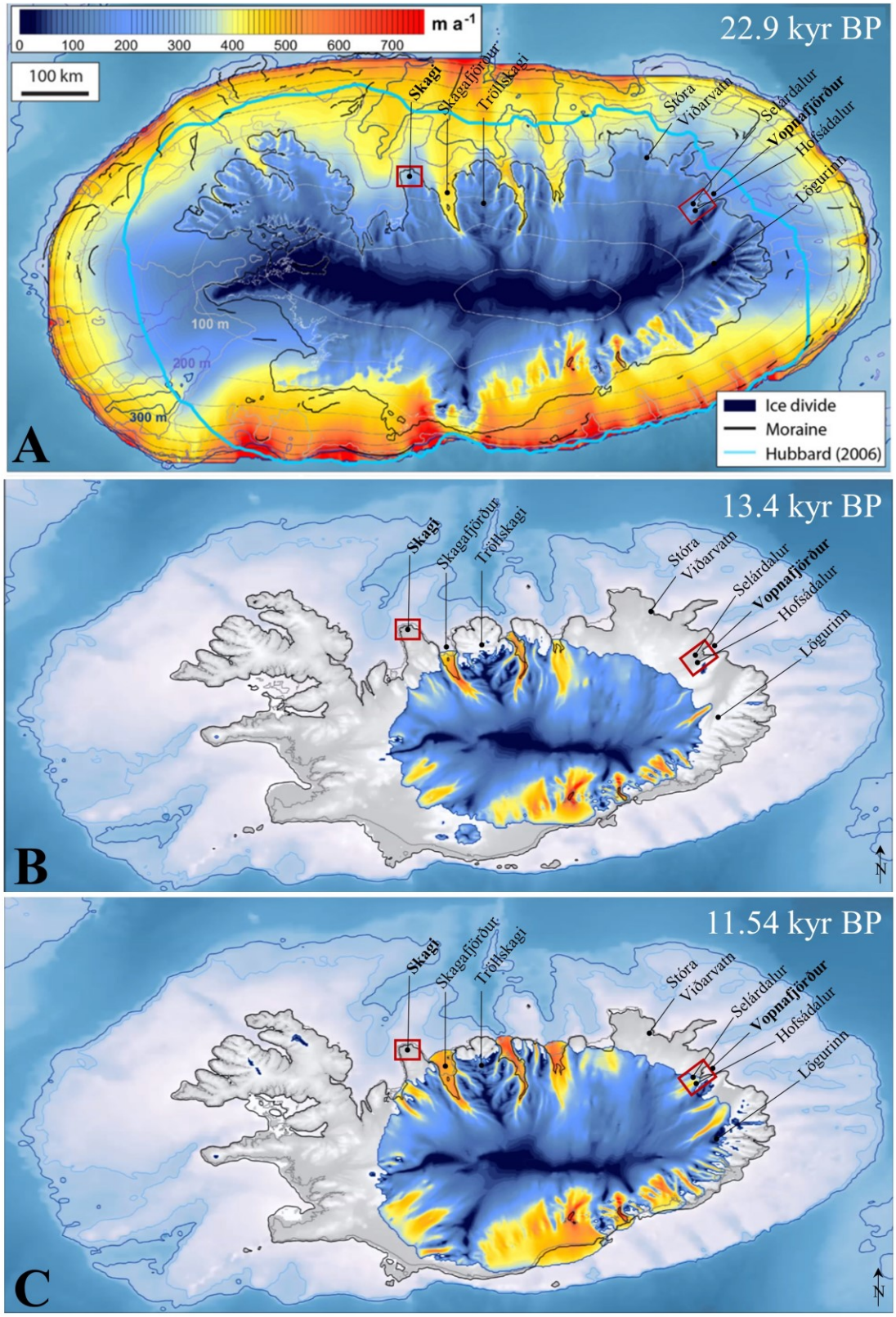

Figure 2. *A. Maximum size of the Icelandic ice sheet (IIS) during the Last Glacial Maximum at about 22.9 cal. kyr BP. B: Extent of the retreating IIS during the Bølling-Allerød interstadial at ca. 13.4 cal. kyr BP. C: Extent of the IIS during the Early Holocene at ca. 11.54 cal. kyr BP (modified from (Patton et al., 2017). The red boxes indicate the location of the study areas.*

during the HTM were 1.5 – 3 °C higher than the mean annual air temperature today in Iceland (Caseldine et al., 2003; 2006). The HTM was the warmest period of the Holocene in Iceland and was caused by an intensification of the Irminger Current combined with higher summer insolation occurring between 8.5 and 6.5 cal. kyr BP (Andersen & Koç, 2004; Geirsdóttir et al., 2009; Eddudóttir et al., 2017). North and Northeast Iceland were less affected by the HTM and maintained relatively cool temperatures even during summer (Axford et al., 2007). After 5.5 cal. kyr BP temperatures started to decrease, marking the beginning of a cooling phase, the Neoglacial period (Gudmundsson, 1997; Geirsdóttir et al., 2009; Larsen et al., 2012).

The environmental and climatic conditions of the late Holocene (4.2-0 cal. ykr BP) was characterized by the cold temperatures of the Neoglacial period with increased glacial activity (Gudmundsson, 1997; Geirsdóttir et al., 2009; Larsen et al., 2012; Eddudóttir et al., 2020). During the Neoglaciation, cold temperatures dominated and led to the re-formation and/or expansion of ice caps in the highlands (Gudmundsson, 1997; Geirsdóttir et al., 2019).The Neoglaciation is believed to have ended around 3.0 cal. kyr BP (Gudmundsson, 1997). Around 1.1 cal. kyr BP, during the Norse settlement, climate conditions on Icelandic were relatively warm (Axford et al., 2009; Geirsdóttir et al., 2009). The time of the Norse settlement might have taken place during the beginning of the Medieval Warm Period (MWP, Fig. 3). The MWP occurred between ca. AD 950 to 1200, however no distinct warming events could be detected from Icelandic lake records (Axford et al., 2009; Geirsdóttir et al., 2009). Between AD 1200 and 1300 cooler conditions have been noted in historical records from Iceland (Ogilvie, 1984; Doner, 2003). These cooling conditions have been identified to correspond to the end of the MWP (Doner, 2003). Following the MWP was the Little Ice Age (LIA), which occurred between ca. AD 1450-1900 (Ogilvie and Jónsson, 2001; Doner, 2003). The climate during the LIA was highly variable with cooling phases being interfered by milder intervals. These changes from cold to slightly milder temperatures occurred on both decadal and annual timescales. Mean annual air temperatures during the LIA decreased by 1-2 °C, displaying the coldest temperatures since the HTM (Jiang et al., 2002; Axford et al., 2009). The cold phase continued and warmer temperatures were first recorded at the end of the 19th century (Jiang et al., 2002; Axford et al., 2009; Geirsdóttir et al., 2009). The cold periods of the last 2000 years were defined by decreasing lake productivity and increasing soil erosion (Axford et al., 2009).

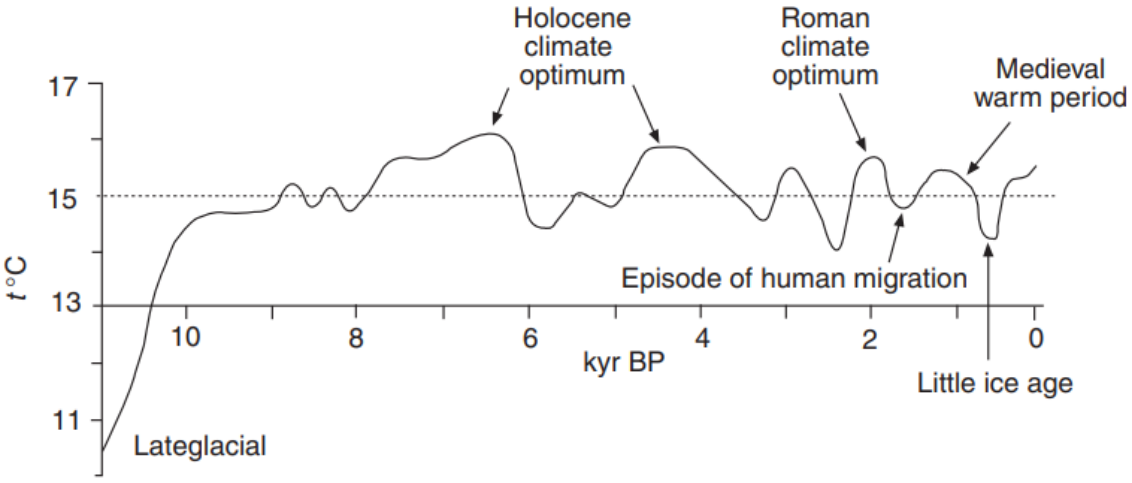

Figure 3. *Schematic reconstruction of the average temperatures during the Late Glacial and Holocene in the Northern Hemisphere (from Borgatti & Soldati, 2013).*

3 Background

3.1 Ocean currents and climate

Iceland is located in the middle of the North Atlantic between 13°29.6'W and 24°32.1'W and 63°23.4'N and 66°32.3'N (Fig. 1A) (Perry, 1986; Molina-Cruz, 1991). Several ocean currents influence the islands climatic and environmental conditions by carrying cold and warm water masses towards Iceland's coast (Einarsson, 1984). One of the currents flowing towards Iceland is the North Atlantic Current, that passes Iceland's southern coast on its northeastward course (Fig. 1A). The Irminger Current (IC), a branch the North Atlantic Current carrying warm water masses, flows along and encircles the southern, western and northern coast of Iceland (Fig. 1A; Einarsson, 1984; Geirsdóttir et al., 2019). Without the relatively warm (temperature 3 to 8 °C), and saline waters transported by the IC, temperatures on Iceland would be much colder (Einarsson, 1984; Eiríksson et al., 2000; Hansen & Østerhus, 2000; Ólafsson et al., 2007; Ólafsdóttir et al., 2010). North of Iceland, the cold waters of the East Greenland current (EGC) (temperature < 1°C) flow along Greenland's eastern coast towards Iceland (Fig. 1A), which also have an impact on the climate of Iceland. A branch of this cold ocean current, the East Iceland Current (EIC) (temperature -1 °C to 6 °C), passes the northeastern and eastern coast of Iceland and flows in a south-southeastern direction (Fig. 1A) (Einarsson, 1984; Ólafsson et al., 2007; Ólafsdóttir et al., 2010). When cold-temperate and low-saline waters of the EGC and the EIC meet with warm, southwards flowing saline waters of the IC, it results in the formation of the sub-polar temperature front, which can be observed off the southeastern and northwestern coasts of Iceland. The position of the Polar Front has varied over (geological) time and largely controls the climate of Iceland (Einarsson, 1984; Molina-Cruz, 1991; Eiríksson et al., 2000; Hansen & Østerhus, 2000; Østerhus et al., 2005; Ólafsson et al., 2007; Sicre et al., 2008; Ólafsdóttir et al., 2010). The mixing of IC and EIC water masses, combined with lower temperatures during the winter, cause the formation of an intermediate water mass in the Icelandic Sea. During spring or summer the intermediate water mass is non-existent (Eiríksson et al., 2000). Iceland's climate is strongly influenced by these ocean currents both directly at coastal areas and inland through the arrival of air masses that have traveled over the ocean (Einarsson, 1984).

Besides being directly influenced by ocean currents, Iceland's climate is controlled by air masses of polar or tropical origin (Einarsson, 1984). The cold air masses from the Arctic

interact with milder Atlantic air masses and cause fluctuations in the regional climate in regard to weather and storm events. The temperature differences between the polar and tropical air masses is the largest during winter (Einarsson, 1984; Marty et al., 2010; Denk et al., 2011). Another factor influencing Iceland's climate is the proximity to the Greenland Ice Sheet and sea ice extending from the Greenland Sea to the northern coast of Iceland, leading to a decrease in regional temperatures by causing an area of high air pressure (Bergthórsson, 1969; Ogilvie et al., 2000).

Iceland's climate is considerably milder than might be expected from its high latitude position (Marty et al., 2010; Denk et al., 2011). Einarsson (1984) described the climate of Iceland as cold-temperate humid maritime with cool summers and mild winters. The inner fjords generally experience a temperate and humid climate with cool and short summer (Ólafsdóttir et al., 2001; Kottek et al., 2006; Denk et al., 2011). The climate of the peninsulas in the northwest, north and east and on the highland can be described as Arctic (Einarsson, 1984). Figure 4A shows that the warmest mean annual temperatures occur along the southern and southwestern coast, while the coldest temperatures can be observed in the southeast (Marty et al., 2010). Generally, July is the warmest month (average 12 °C) except for the coastline in northern and eastern Iceland, where maximum temperatures are reached in August. The coldest temperatures generally occur in February (average 1°C) (Einarsson, 1984).

A passage of atmospheric low-pressure cyclones occurring across the North Atlantic Ocean is reflected by Iceland's precipitation pattern. The precipitation is also further influenced by the island's mountainous topography (Einarsson, 1984; Hanna et al., 2004; Marty et al., 2010). The cyclones, formed as disturbances on the Polar Front, often travel close to Iceland and cause large pressure variations and a mean low-pressure center (Icelandic Low), near the southwestern coast (Serreze et al., 1997). Precipitation and strong winds are brought along with these cyclones. Due to the large temperature differences between the air masses during winter, cyclones occur more frequently during this season (Einarsson, 1984; Hanna et al., 2004; Ólafsson et al., 2007). Precipitation rates over Iceland differ with highest precipitation rates in the southeast (Fig. 4B, max. > 4000 mm/year) on the ice caps Vatnajökull and Mýrdalsjökull (Einarsson, 1979). The mean annual precipitation rates in northern and northeastern Iceland range between 400 – 600 mm/year. The highest amount of precipitation generally occurs during autumn and early winter and peak in October. This is in contrast to

northeastern Iceland where the wettest months are July and August. The lowest amount of precipitation occurs in May and June (Einarsson, 1984). The annual number of days with precipitation in northern and northeastern Iceland is ca. 130 - 140 days (Einarsson, 1984). During winter, half of the precipitation falls as snow in northern Iceland. In this area complete snow cover occurs for weeks or even months (Einarsson, 1984; Ólafsson et al., 2007).

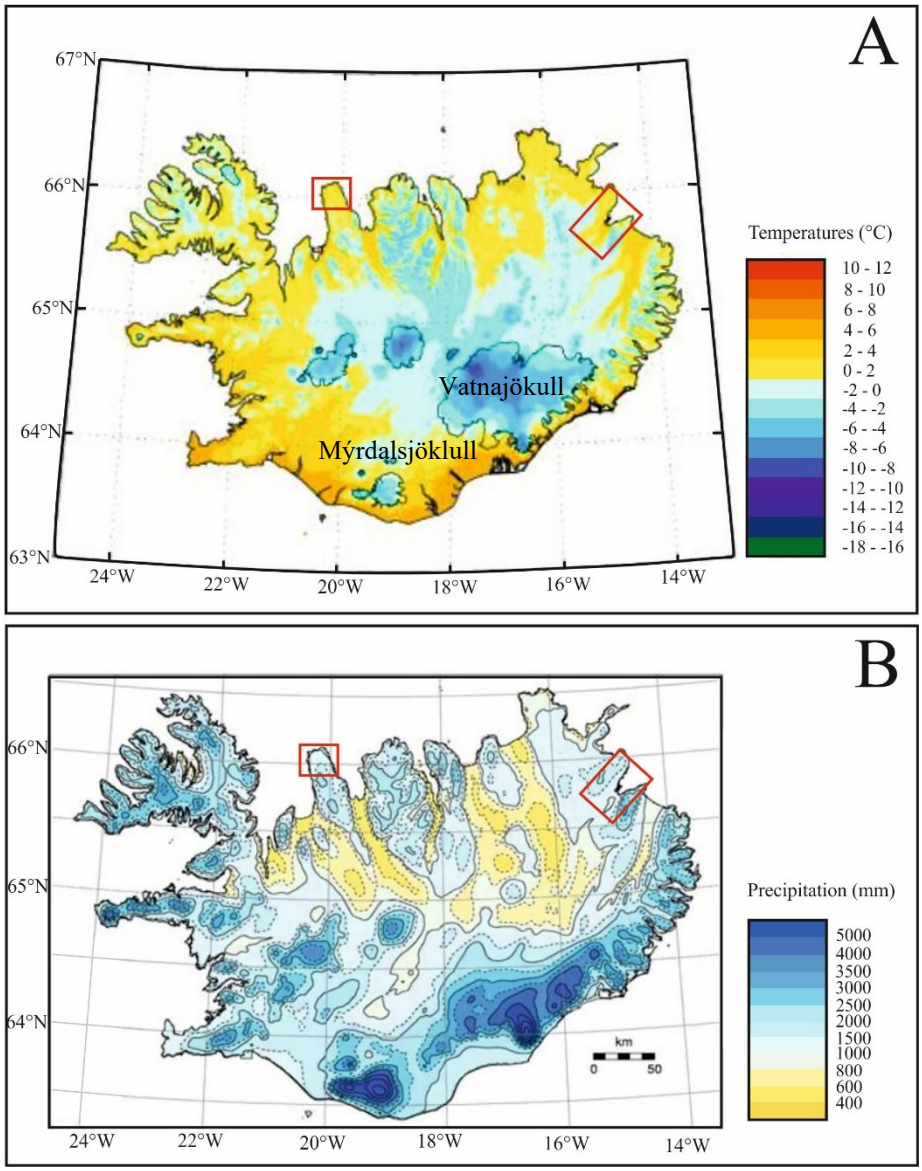

Figure 4. *A. Overview map showing the mean annual temperatures in Iceland (modified from Marty et al., 2010). B. Overview map showing the mean annual precipitation in Iceland (modified from Björnsson & Pálsson (2008) after Crochet et al. (2007)). The study areas are indicated by the red boxes.*

For the last 200 years, an increase in temperatures across Iceland has been be observed. Temperatures have gradually increase by ca. 0.7°C per century (Hanna et al., 2004). A similar trend can be seen all over the Northern Hemisphere (Rutgersson et al., 2014; Delworth et al.,

2016). Resulting from this general warming trend, sea ice along the northern coast of Iceland has become less common for the last 120 years (Hanna et al., 2004; Marty et al., 2010). However, this general warming trend was non-gradual and interrupted by periods of cooling. Three distinct warming phases have been observed between 1880-1990, 1925-1940 and 1983-2003. Especially during the period from 1925 to 1940 a rapid warming event occurred. Between 1940s and 1980s temperatures seemed to cool down (Hanna, Jónsson, & Box, 2001; Hanna et al., 2004). Besides this increase in temperatures, a shift in the mean annual precipitation rate occurred. Since the end of the 19th century, an increase in precipitation occurred on Iceland (Hanna et al., 2004; Marty et al., 2010).

3.2 Volcanic systems and geochemical composition of Icelandic volcanic rocks

Iceland's characteristic high volcanic activity results from the superimposition of the spreading Mid-Atlantic ridge and the Icelandic mantle plume (Vink, 1984; Wolfe et al., 1997; Óladóttir et al., 2008; Meara et al., 2019). This interaction of the Mid-Atlantic ridge with the mantle plume is represented on Iceland as neovolcanic zones (Fig. 5) (White et al., 1995; Wolfe et al., 1997; Óladóttir et al., 2011). Four distinct volcanic zones can be observed on Iceland, the Northern (NVZ), Western (WVZ), Snæfellsnes (SVZ) and Eastern Volcanic zones (EVZ) and the Öræfajökull-Snæfell zone (ÖVZ) (Fig. 5). The volcanic zones consist of individual volcanic systems that form both rift and flank zones (Sæmundsson, 1978; Jakobsson, 1979; Óladóttir et al., 2011, 2008).

The volcanic systems are composed of a central volcano with high magmatic activity, which are surrounded by fissure swarms (Sæmundsson, 1978; Jakobsson, 1979; Larsen & Eiríksson, 2008; Óladóttir et al., 2008; 2011). Each volcanic system is characterized by distinct magma generation processes leading to specific geochemical signatures for each individual system. The unique signature can be used to trace back volcanic products to their provenance (Meara et al., 2019). Volcanoes that are situated close to or directly above the rift zone are characterized by the production of tholeiitic magma series. The volcanic systems found in the flank zones produce alkali and transitional series (Jakobsson et al., 2008; Óladóttir et al., 2011). Tholeiitic magma series have relatively high Fe and Ti and low Al and Ca contents for tholeiitic series, transitional alkalic series are characterized by high Fe, Ti and alkali metals for a given SiO_2 concentration with low Al contents, and alkalic series can be identified by

their significantly higher Na and K contents (Jakobsson, 1979; Óladóttir et al., 2011). Most of the volcanic products found on Iceland are of tholeiitic composition (80%), 12% are transitional alkalic and 8% are alkalic (Jakobsson et al., 2008; Óladóttir et al., 2011). Iceland's volcanic activity is therefore defined by basaltic (tholeiitic) magmatism (Óladóttir et al., 2008).

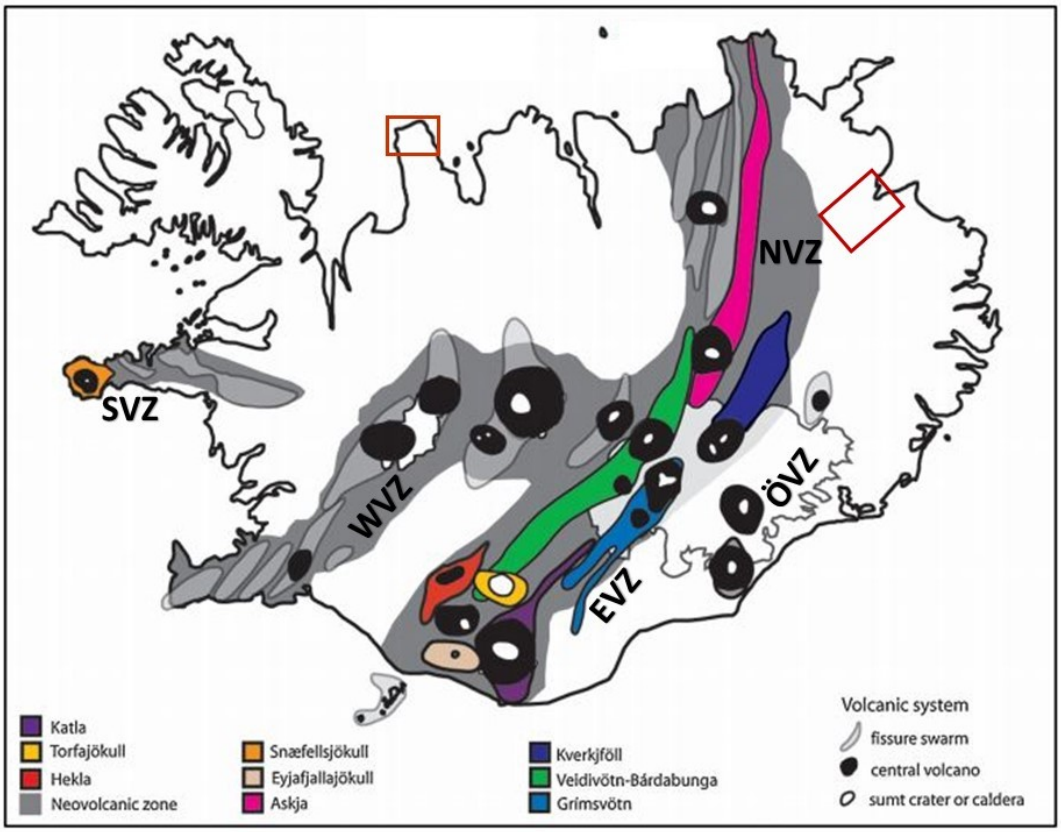

Figure 5. *Map showing the volcanic systems of Iceland. Different colors demonstrate different geochemical characteristic of the individual volcanic systems. EVZ = Eastern Volcanic zones, SVZ = Snæfellsnes Volcanic zones, WVZ = Western Volcanic Zones, ÖVZ = Öræfajökull-Snæfell Volcanic Zones, NVZ = Northern Volcanic Zone (taken from Gudmundsdóttir et al. (2011) and modified after Óladóttir et al. (2008)). The red boxes indicate the location of the study areas.*

Iceland has a typical phreatomagmatic volcanic activity with explosive, mainly basaltic eruptions, that is caused by eruptions occurring below thick ice caps (Larsen & Eiríksson, 2008; Óladóttir et al., 2008; Larsen, 2010; Óladóttir et al., 2011). During those explosive eruptions volcanic plumes, comprising of hot gas-rich pumice and tephra (ash), get released. If winds influence the plume ash will be deposited in a downwind direction and tephra deposits can be observed not only in proximal but also distal locations (Meara, 2011). The term tephra (gr. τέφρα = 'ashes') describes all explosively-erupted, unconsolidated pyroclastic volcanic products, comprising deposits arising from both pyroclastic density currents and fall

deposits (Jakobsson, 1979; Larsen & Eiríksson, 2008; Lowe, 2011; Óladóttir et al., 2011). Tephra consists of all volcanological grain sizes, including ash (particle <2 mm), lapilli (2-64 mm), angular blocks and subrounded bombs (both >64 mm) (Haldar & Tišljar, 2014).

Most of the tephra layers, that have been produced during explosive eruptions originate from the volcanic systems in the EVZ, making it the most active zone on Iceland (Sæmundsson, 1979; Thordarson et al., 2003; Thordarson & Larsen, 2007; Óladóttir et al., 2008). Nine active volcanic systems can be found in the EVZ. Four of these systems have produced the majority of tephra deposits that can be observed in soil profiles in southern Iceland, including Katla, Hekla, Grímsvötn and Veiðivötn-Bárðabunga (Fig. 5; Óladóttir et al., 2008; Gudmundsdóttir et al., 2012). The Katla volcano activity is characterized by its explosive basaltic and subglacial eruptions, while Hekla produces intermediate to silicic magma (Jakobsson, 1979; Larsen, 2000; Larsen et al., 2001; Óladóttir et al., 2008). The Veiðivötn-Bárðabunga and Grímsvötn volcanic systems are characterized by subglacial and subaerial phreatomagmatic volcanism producing basaltic tephra (Jakobsson, 1979; Óladóttir et al., 2008). Silicic tephras are characterized by their SiO_2 content being higher than 63% (rhyolitic ~68-77%; dacitic 63-68%), while basaltic tephra has a SiO_2 content of < 52%. Tephras that have an SiO_2 content of 52-63% are described as dacitic (Larsen & Eiríksson, 2008; Meara et al., 2019).

During the Holocene, approximately 30 active volcanic centres existed and still exist on Iceland (Larsen & Eiríksson, 2008; Meara et al., 2019). Tephra deposited on Iceland is generally divided into a historical record, including the volcanic activity since the Settlement of the Vikings (AD 871) and a prehistoric record, comprising the time from the end of the last deglaciation to the Settlement (approximate duration: ~9000 years) (Óladóttir et al., 2008). Icelandic's volcanic activity throughout the Holocene was characterized by often explosive eruptions with approximately 75-80% of the explosive eruptions producing tephra mainly of basaltic composition (Larsen & Eiríksson, 2008; Óladóttir et al., 2011).

Identified tephra layers that have been produced during the Holocene on Iceland include around 60 silicic marker layers, deposited and preserved in terrestrial soils and lake sediments. At least 51 of the acidic tephra layers could be correlated to a source and 19 of the layers got widely dispersed across the North Atlantic area (Larsen & Eiríksson, 2008; Meara et al., 2019). The volcanic sources of these silicic tephra layers were Hekla, Torfajökull,

Öræfajökull, Askja, Snæfellsjökull, Eyjafjallajökull and Katla central volcanoes (Fig. 6; Larsen & Eiríksson, 2008; Meara et al., 2019). The Hekla volcano can be described as the most active of those volcanic systems that produces silicic tephra. The largest Holocene eruption of the Hekla volcanic system produced the Hekla 3 (3144–2884 cal. yr BP) tephra layer (Larsen et al., 2002; Larsen & Eiríksson, 2008; Gudmundsdóttir et al., 2011; 2018). The number of identified basaltic tephra layers in Icelandic terrestrial soils is over 400 of which at least 170 are originating from the Katla volcanic system (Larsen, 2010; Larsen & Eiríksson, 2008; Óladóttir et al., 2005). Basaltic tephra layers were mainly erupted by Grímsvötn, Katla and Veidivötn-Bárdabunga (Larsen & Eiríksson, 2008).

In recent times the most active volcanic system has been the Grímsvötn system, producing over 70 tephra layers during the last 1100 years. One of the most prominent and most voluminous basaltic Grímsvötn tephra layers is the Saksunarvatn tephra, being ~ 10300 years old (Rasmussen et al., 2006). However, it is believed that this specific tephra layer might represents more than one eruption (Larsen & Eiríksson, 2008). The Saksunarvatn tephra is the only basaltic tephra layer that together with large silicic tephras is a potential widespread marker horizon overseas (Dugmore et al., 1995; Wastegård et al., 1998; Hall & Pilcher, 2002; Larsen & Eiríksson, 2008). It has been observed that such thick or voluminous tephra deposits, erupted during the Holocene have influenced Iceland's environmental by stripping the landscape of vegetation and triggering intensified soil erosion (Blair et al., 2015; Eddudóttir et al., 2017; Geirsdóttir et al., 2009, 2019).

3.3 Bedrock geology

Iceland was created during the past 25 Myr (Neogene and Quaternary period) and is therefore a relatively young island from a geological perspective. The bedrock of Iceland consists of ca. 90% basaltic rocks, and can be divided into four main stratigraphic groups (1) Neogene bedrock (Miocene-Pliocene; 16-3.1 Myr), (2) Plio-Pleistocene bedrock (ca. 2.6-0.8 Myr), (3) Late Pleistocene lavas and hyaloclastites (0.8-0.01 Myr) and (4) the Holocene succession (Fig. 6A) (Thorarinsson et al., 1959; Ward, 1971; Einarsson, 1973; Sæmundsson, 1979; Steinthórsson & Thorarinsson, 1997; Denk et al., 2011; Snæbjörnsdóttir et al., 2014). The rocks are subdivided based on their rock type (e.g., sedimentary, volcanic) and by their paleomagnetism (Sæmundsson, 1979; Steinthórsson & Thorarinsson, 1997). The bedrock can have an influence on the depositional environment of lakes, because the easily erodible

basaltic bedrock can lead to high sedimentation rates within lake catchments erosion (Blair et al., 2015; Eddudóttir et al., 2017; Geirsdóttir et al., 2009, 2019).

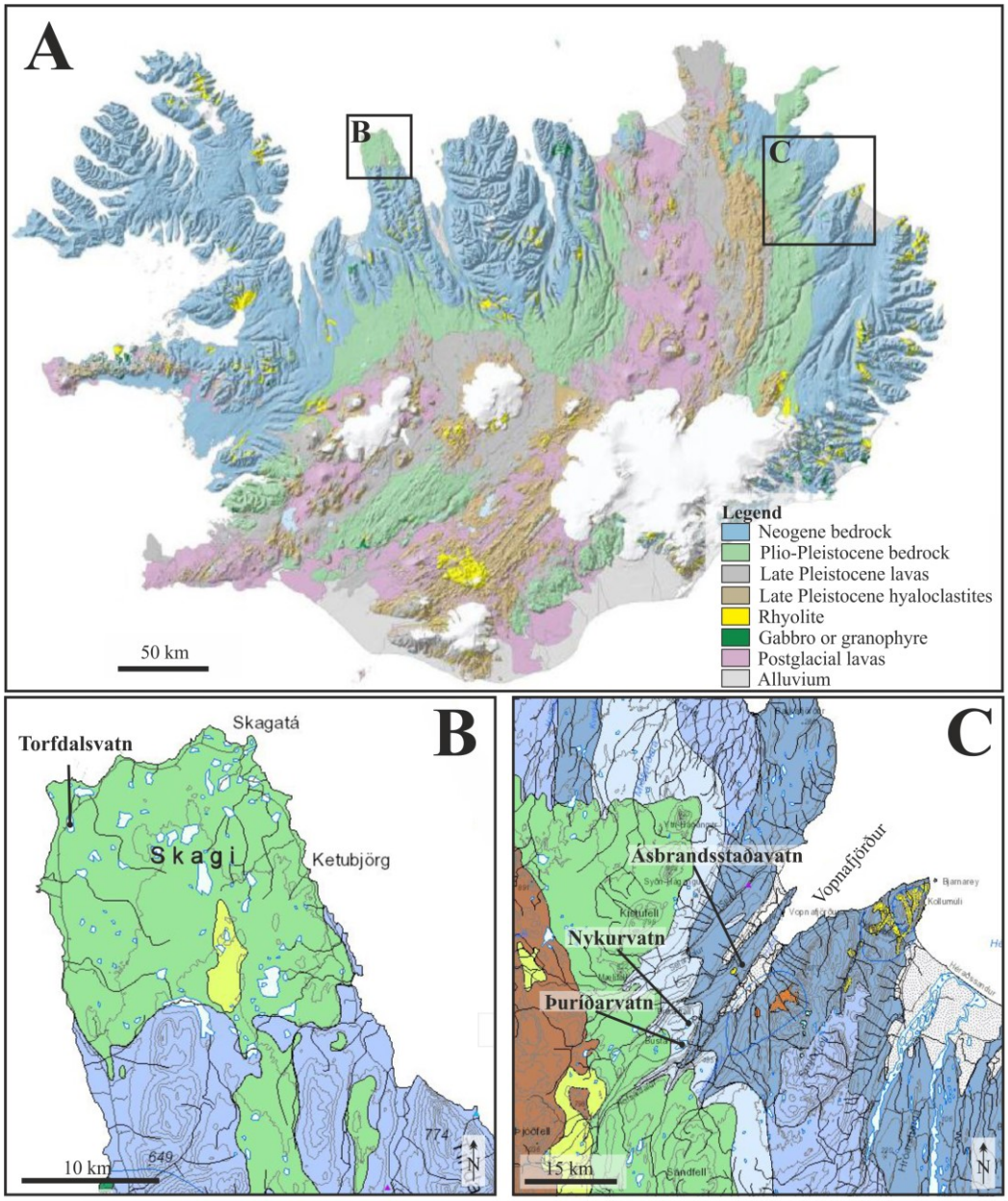

***Figure 6**. A. Geological overview map of Iceland showing different types of bedrock. Locations of the two study areas are indicated (modified from Snæbjörnsdóttir et al., 2014). B. Geological map of study area Skagi, located in North Iceland. C. Geological map of the study area Vopnafjörður, located in Northeast Iceland. Maps displaying bedrock geology of the two study areas from ISOR (http://jardfraedikort.is)*

3.4 Vegetation cover

Only about 28% of the total land area of Iceland is covered by vegetation. The vegetation density decreases with increasing elevation, indicated by the noticeably less dense plant coverage at 200-400 m a.s.l. Almost no vegetation can be found above 700 m a.s.l. Areas with relatively continuous vegetation cover are usually found in lowlands (Ólafsdóttir et al., 2001; Hallsdóttir & Caseldine, 2005). The most common vegetation types are grasslands and heath shrubs. However, in the lowlands, different types of lichens and mosses usually are the dominating types of plants. The dominant vegetation in the outermost coastal districts in north, northeast and northwest Iceland is Arctic-alpine species (Hallsdóttir & Caseldine, 2005). Only ca. 1% of Iceland's vegetation consists of trees dominated by birches and willows (Ólafsdóttir et al., 2001; Hallsdóttir & Caseldine, 2005). The sparse vegetation, and especially low number of trees, have been attributed to the Norse settlement on Iceland, where Vikings cut down and burned the forests (Hallsdóttir & Caseldine, 2005).

3.5 Study areas

This thesis focuses on the four lakes four lakes from two study areas situated in North and Northeast Iceland. Lake Torfdalsvatn is located on the Skagi peninsula and lakes Þuríðarvatn, Nykurvatn and Ásbrandsstaðavatn are situated close to the Vopnafjörður fjord.

3.5.1 Skagi peninsula, North Iceland

The northern study area, Skagi, is located at the northern coast of Iceland, characterized by a valley and fjord landscape. Skagi is situated between Skagafjörður on the eastern side and the Húnaflói bay on the western side (Fig. 7A). The southern parts of the peninsula are defined by mountainous terrain with peaks up to 1000 m a.s.l. The climate in Skagi is largely influenced by its coastal position. The mean annual air temperature in the northeastern part of the peninsula is ~2.5°C. The lowest temperatures of -1.8 °C occur in January, and the warmest temperatures are recorded during June with 8.2 °C (last normal period 1961-1990; vedur.is). The annual mean precipitation rate on Skagi is ca. 475 mm (Einarsson, 1984; Rundgren, 1997). On Skagi, two dominating bedrock formations can be found (Fig. 6B). In the southern

part of the peninsula upper Miocene basaltic and intermediate extrusive rocks are present (>11-5.3 Myr) consisting of 80% basaltic flows (Einarsson, 1973; Rundgren, 1997). The bedrock of the northern part of Skagi consists of basaltic and intermediate extrusive rocks and sedimentary rocks that are of lower Pleisotcene age (2.6-0.8 Myr; Fig. B) (Rundgren, 1997).

Lake Torfdalsvatn is situated in the northern part of Skagi, and the catchment of the lake can be described as a gently undulating lowland area, that reaches ca. 250 m a.s.l. Torfdalsvatn (66°061'N, 20°382'W, 47 m a.s.l.) is located in a depression surrounded by bedrock plateau (Fig. 7C; Rundgren, 1997). The vegetation on site is dominated by dwarf-shrub heaths, with *Betula nana*, *Salix herbacea* and *Empetrum nigrum* being the most common species (Rundgren, 1997; Rundgren & Ingólfsson, 1999). The lake has a maximum depth of 5.8 m (Florian, 2016), a surface area of ca. 0.4 km^2 and a north-south orientation (Fig. 7C). In the southern end, two small streams, one of them draining a small lake nearby, flow into the lake. A northward running outflow, that flows over a till threshold, can be found at the northern end of the lake. The lake has gravelly, steep shores (Rundgren, 1997). Torfdalsvatn is a non-glacial lake, i.e, it has not received glacial meltwater since the last deglaciation of the area (Rundgren, 1997).

3.5.2 Vopnafjörður area, Northeast Iceland

The study area in northeastern Iceland with lakes Þuríðarvatn, Nykurvatn and Ásbrandsstaðavatn is located close to the Vopnafjörður fjord (Fig. 7B). Vopnafjörður is situated south of Bakkafjörður and northwest of the Héraðsflói bay and has three parallel southwest to northeast trending valleys, Hofsárdalur, Vesturárdalur and Selárdalur, as main topographical features (Fig. 7B). The study area is confined by mountain Smjörfjöll to the south, and by extensive highlands to the west and north (Fig. 7B). In the east the study area is limited by Vopnafjörður (Sæmundsson, 1995). The meandering river Hofsá, located southwest of the lakes flows in northeast direction and enters the fjord (Fig. 7B). The climate of the Vopnafjörður area is (similar to Skagi) also influenced by its close proximity to the coast. Mean annual air temperatures lie between -4 and -2 °C during January and reach ca. 10°C in July (last normal period 1961-1990, vedur.is). Around Vopnafjörður the bedrock is of both Neogene and Quaternary ages (Fig. 6C) with the oldest rocks in the east and youngest rocks in the western part of the study area (Einarsson, 1973; Sæmundsson, 1977; Jóhannesson & Sæmundsson, 1989; Sæmundsson, 1995). On the Hraunlína ridge, intermediate and basaltic

rocks that are of middle Miocene age (>11 Myr) are abundant (Fig. 6C; Sæmundsson, 1977; Jóhannesson & Sæmundsson, 1989). Hraunlína is a low ridge, situated between the Hofsárdalur and the Vesturárdalur valley, that gradually rises from the valley mouth (ca. 180 m a.s.l.) to close to the Burstarfell mountain (300 m a.s.l). Southwest of this succession on Burstarfell, basaltic and intermediate extrusive rocks from the Pliocene (5.3-2.6 Myr) can be found (Fig. 6C; Sæmundsson, 1977; Jóhannesson & Sæmundsson, 1989).

Þuríðarvatn (Fig. 7F) and Nykurvatn (Fig. 7E) are located on Burstarfell (highest point 538 m a.s.l.) and are sourrounded by rocky, streamlined landforms (i.e., Burstarfell drumlin field) (Ingólfsson, 2019). The Burstarfell mountain is located between the valleys Hofsárdalur and Vesturárdalur (Fig. 7B; Sæmundsson, 1995). The two lakes are located in close proximity (ca. 1.5 km) to each other with Þuríðarvatn being situated southwest of Nykurvatn. Þuríðarvatn (65°603'N; 15°1677'W, ca. 416 m a.s.l.) covers a total surface area of ca. 1.6 km^2 and a northeast-southwest orientation (Fig. 7F). A stream enters Þuríðarvatn on its southwestern end and another stream (Þuríðará), located on the northeastern side, drains the lake. Þuríðará later flows into the larger river Hofsá. Nykurvatn (65°62905'N, 15°14157'W, ca. 490 m a.s.l.) has a surface area of ca. 0.62 km^2 (Fig. 7E). The lake is oriented in a northeast-sourthwest direction. On its southwestern end the lake is entered by two small streams. A second stream (Teigará) drains the lake on its northeastern end. The third lake in the northeastern study area, Lake Ásbrandsstaðavatn, is located closer to the Vopnafjörður mouth and ca. 12.7 km northwest of Þuríðarvatn and Nykurvatn. Ásbrandsstaðavatn (65°7085'N, 14°932'W, ca. 170 m a.s.l.) is the smallest of the four investigated lakes with a surface area of 0.04 km^2 (Fig. 7D**).** The official name of the lake is 'Lake Nykurvatn', but it is here refered to as 'Lake Ásbrandsstaðavatn' (i.e., Ásbrandsstaðir is a close-by farm) to avoid confusions with the other, larger Nykurvatn. Ásbrandsstaðavatn is located on the southeastern side of Hraunlína. The lake has a north-south orientation and lies within rocky landforms most likely formed through glacial erosion, with no permanent inflow nor outflow. No publications describing the vegetation occurring at the northeastern study site are available. Based on publications describing the surrounding vegetation of lakes situated relatively close to the study area (e.g., Simpson et al., 2004; Axford et al., 2009) it can be concluded that the vegetation at Vopnafjörður is very similar to the Skagi plant coverage with open dwarf-shrub heaths (i.e., *Betula nana, Empetrum nigrum*). All three lakes located in the northeastern study area are non-glacial lakes and have therefore not received glacial meltwater since deglaciation.

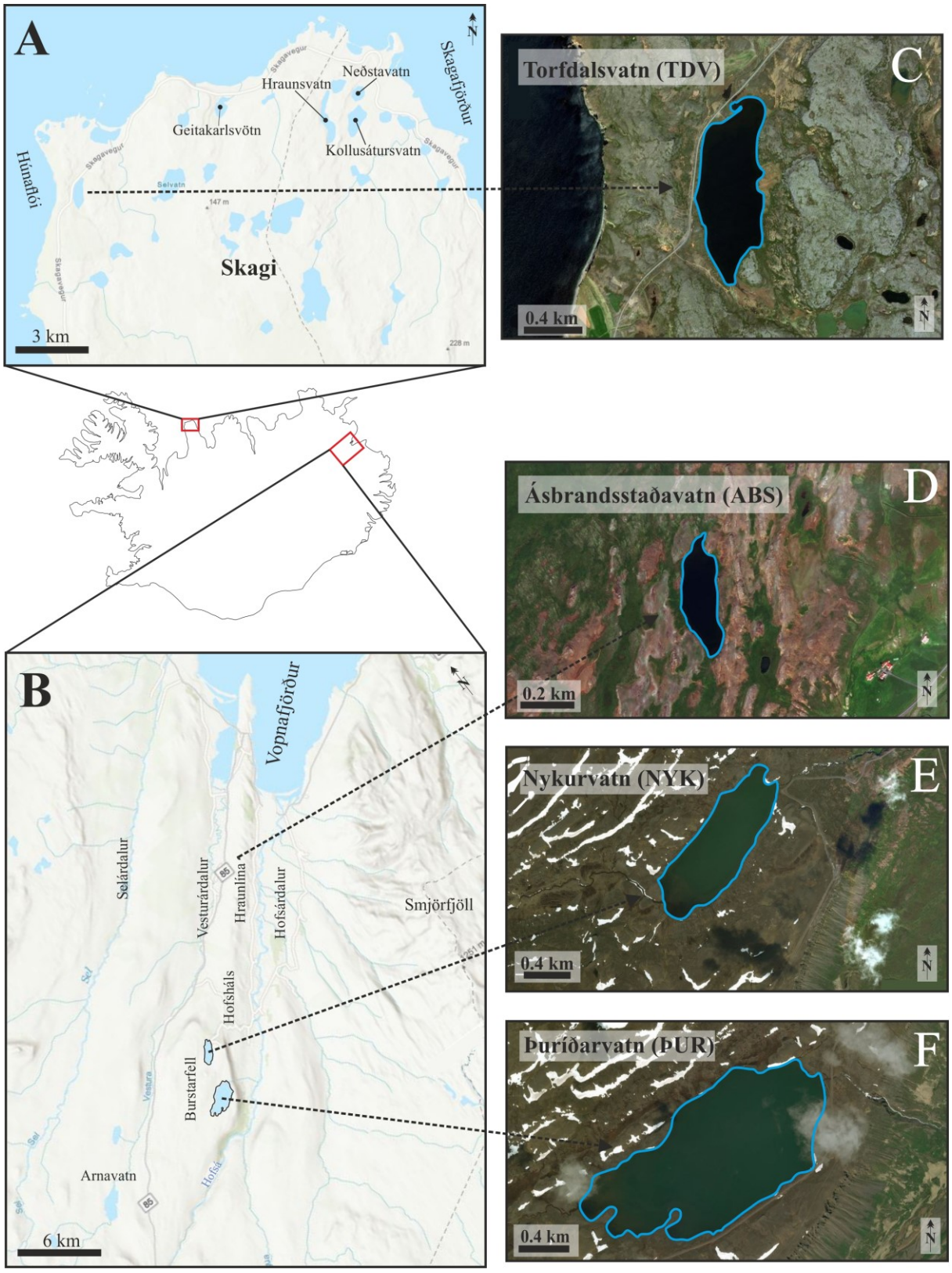

Figure 7. *Topographical maps showing the two study areas: A. Skagi in northern Iceland, B. Vopnafjörður area in northeast Iceland. Aerial photographs of the four lakes: C. Torfdalsvatn (TDV), D. Ásbrandsstaðavatn (ABS), E. Nykurvatn (NYK), F. Þuríðarvatn (ÞUR) Topographical maps and air photographs from NOAA (https://www.arcgis.com/).*

4 Material and Methods

This thesis is based on multi-proxy analyses of lake sediment cores collected from four lakes in North and Northeast Iceland. Paleo-environmental reconstructions for the study areas are made based on lithostratigraphic descriptions, loss-on-ignition (LOI) and X-ray fluorescence (XRF). Geochronological models were constructed using radiocarbon (^{14}C) dates and ages of identified tephra markers. Details of the methods are described in the following sections.

4.1 Sediment cores

Eighteen sediment cores (between 91-154 cm long) were retrieved using a hand-held lightweight piston corer (200 cm long and 60 mm diameter coring tubes). In Torfdalsvatn (TDV), seven sediment cores were collected. The TDV core sections were collected in 2012. The sediment record from Nykurvatn (NYK) consists of five core sections. Core sections NYK1-4 were collected in the center of the lake and NYK5 was collected at the NE end of the lake. The cores were collected on 7th of April 2018. At Ásbrandsstaðavatn (ABS), four core sections were taken. Two sediment cores were collected from Þuríðarvatn (ÞUR). The ABS and ÞUR cores from were collected on the 6th of April (ABS 1,2) and the 8th of April 2018 (ABS 3,4; ÞUR 1,2). Coring locations, water depths and exact lengths of the core sections are given in Table 1.

Parts of the laboratory work was carried out at the University of Copenhagen (Centre for GeoGenetics) in September 2019. The remaining work was completed at UiT The Arctic University of Norway (Department of Geoscience) from October 2019 to January 2020.

Table 1. *Core locations, water depths and recovery lengths of the sediment cores collected in North and Northeast Iceland.*

Lake	Location	Longitude (dec °N)	Langitude (dec °W)	Water depth (m)	Core section	Length sediments (cm)
Torfdalsvatn	N- Iceland, Skagi peninsula	66.061	20.382	5.1	TDV 2-1	125
					TDV 2-2	139.5
					TDV 2-3	141
					TDV 2-4	146
					TDV 2-5	139.5
					TDV 2-6	131
					TDV 2-7	91
Þuríðarvatn	NE-Iceland, Near Vopnafjörður	65.603	15.1677	5.2	ÞUR 1	151
					ÞUR 2	154
Nykurvatn	NE-Iceland, Near Vopnafjörður	65.62905	15.14157	10.0	NYK 1	126
					NYK 2	152
					NYK 3	151
					NYK 4	132
					NYK 5	152
Àsbrandsstaðir	NE-Iceland, Near Vopnafjörður	65.7085	14.932		ABS 1	147
					ABS 2	147
					ABS 3	152
					ABS 4	105

4.2 Lithostratigraphy and LOI

4.2.1 Lithostratigraphy

The cores were opened by cutting the plastic liner in half lengthwise with a core-liner saw (TDV, ABS) or a hand saw (NYK, ÞUR). A metal wire was used to split the sediments. Each core was divided into work and archive halves. The archive halves were used for XRF and X-ray scans before being covered with plastic wrap, put into a plastic sleeve and stored in a cooling room (4° C). The work halves, being used for further analyses, were packed similar and stored in a refrigerated storage area, when not in use.

The sediment surface of each core section was systematically described in terms of sediment type (e.g., minerogenic, organic), color, grain size and organic material content. Additionally, color and depth of visible tephra layers were noted. Based on the descriptions, lithological logs were made, and the cores were divided into stratigraphical units.

4.2.2 Loss-on-ignition

Loss-on-ignition (LOI) is a fast and inexpensive method for determining the organic content in sediments without pretreatment (Dean, 1974; Ben-Dor & Banin, 1989; Heiri et al., 2001). For obtaining reliable and comparable LOI results, it is essential to maintain a consistent ignition temperature, exposure time and sample size (Dean, 1974; Heiri et al., 2001). When burned at 500-550 °C, the organic material is completely ignited and oxidized to carbon dioxide and ash (Dean, 1974; Heiri et al., 2001). The weight loss is therefore closely correlated to the organic matter content of the sediments (Dean, 1974).

Methods for LOI followed Heiri et al. (2001). Samples were collected every 5 cm with additional samples at visible transitions. Each sample of approximately 2 cm^3 was placed into a ceramic crucible. To estimate the organic matter content, the samples were first dried in an oven at 110 °C for 24 h. The oven-dried samples were then burned in a furnace at 550 °C for 4 h, where the organic matter was combusted to ash and carbon dioxide. Before and after each step the ceramic crucibles with the samples were weighted. Between each sample run, the containers were rinsed with water and heated for 2 h at 1000 °C.

The water content of the samples was calculated by using following equation:

$$\text{Water content} = ((WW - DW_{110}) / WW) * 100 \quad (1)$$

where WW represents the weight of the wet sample and DW_{110} the dry weight after 110 °C (Heiri et al., 2001).

For calculating the LOI at 550 °C (LOI_{550}), the following equation (modified after Heiri et al., 2001) was used:

$$LOI_{550} = ((DW_{110} - DW_{550}) / DW_{110}) * 100 \quad (2)$$

where DW_{550} represents the weight of the sample after combustion at 550 °C (Heiri et al., 2001).

4.2.3 Interpretation and correlation between lithostratigraphy and LOI

Results of LOI and lithostratigraphy strongly agree with each other, because high LOI percentages typically are observed in organic-rich sediments and low LOI values indicate higher minerogenic content (Dean, 1974; Santisteban et al., 2004). Both lithostratigraphic

descriptions and LOI results give insight into depositional environments and can indicate climatic fluctuations. They are therefore important for (Holocene) paleoenvironmental reconstructions (Smith, 2003).

Sedimentation in Arctic lakes is mainly controlled or influenced by geological and climatic factors (Coakley & Rust, 1968). Sources of minerogenic sediments largely depend on the climatic conditions and properties of the catchment area (Carroll et al., 1999; Zolitschka et al., 2015). In non-glacial regimes, the main sediment contributors are rivers draining areas underlain by erodible bedrock and transporting fine sediments as suspended load into lakes (i.e., fluvial source) (Coakley & Rust, 1968; Hatfield & Maher, 2009). Surface runoff triggered by high precipitation rates or spring melt could also lead to sediments getting transported into a lake (Coakley & Rust, 1968). Fine minerogenic sediments can also be wind-derived (Leeder, 2011). Another source for minerogenic sediments are glaciers. During increased glacier activity, the ice may erode underlying bedrock, resulting in a higher input of clastic sediments into a lake (Karlén, 1976). Therefore, clastic or minerogenic material, including clay, silt or sand, that are deposited into a lake may have been derived from aeolian, fluvial, glacial or glaciofluvial sources (Schnurrenberger et al., 2003).

The deposition of fine-grained organic sediments (i.e., gyttja; Schnurrenberger et al., 2003), is typically found in non-glacial lake and therefore indicates warmer climatic conditions (Karlén, 1976; Kaplan et al., 2002; Cohen, 2003; Smith, 2003). The formation of gyttja occurs under oxygenated conditions in lakes (Cohen, 2003; Stolt & Lindbo, 2010). The sources of organic matter in lakes can be autochthonous and allochthonous (Meyers & Ishiwatari, 1993). Plants that are growing around a lake may get transported into the lake system through high precipitation or strong winds or be carried by rivers (Karlén, 1976). A low percentage of organic matter can also be caused by low production of organic content within the lake and/or the area surrounding the lake (Karlén, 1976).

4.3 Geophysical and geochemical properties

Two types of XRF core scanners were used for obtaining geophysical and geochemical properties of the analyzed lake sediment cores. The split TDV core sections were scanned using an Itrax Core scanner. The Itrax Core scanner was constructed to collect high-resolution data from split core sections, including X-ray fluorescence (XRF) and magnetic susceptibility,

and optical and radiographic images (Croudace et al., 2006). The core sections from ABS, NYK and ÞUR were analyzed with an Avaatech core scanner. The Avaatech core scanner carries out X-ray and XRF scans and collects optical images (Forwick, 2013), but does not measure the magnetic susceptibility. In both devices, the intensity of X-radiation, that is needed for X-ray and XRF scans, is transmitted through the sediments and gets recorded by the X-ray line camera located in the center of the device (Croudace et al., 2006; Forwick, 2013). Both core scanners have an X-ray source with a Rh (rhodium) anode (Forwick, 2013; Croudace et al., 2006).

Prior the being analyzed by the core scanners, the core sections were adjusted to room temperature, so potential water films on sediment surfaces dry out. The surfaces of all split sediment cores need to be flattened and smoothened before producing a visual color image or scanning for XRF (Kido et al., 2006; Richter et al., 2006). A 4 µm ultralene film was applied onto the sediment surfaces prior to the XRF scan to avoid contamination.

4.3.1 Optical images

High-quality optical images of the TDV core sections were taken with an optical-line camera installed in the Itrax Core scanner, using a light sensitive 2048 pixel device. Line-scan high quality color images of the NYK, ABS and ÞUR core sections were produced by the Avaatech core scanner. The core scanner incorporates a camera with three sensors that each have 4096 pixels. Optical images of lake sediment cores can be used for correlating XRF data and radiographic images to visual color features (Croudace et al., 2006).

4.3.2 X-radiographic images

X-ray photography is a non-destructive method allowing the imaging of a material, e.g. sediments, using electromagnetic radiation. It can be used to identify fine-scale sedimentary structures that cannot be observed from the sediment surface without destructing the sample (Lofi & Weber, 2001). The quality of images generated by X-ray photography is determined by the exposure time, contrast and image density (Croudace et al., 2006; Fujifilm Corperation, 2009).

X-radiographic photographs of the TDV half-core sections were taken using an Itrax core scanner. Values for voltage and current of 30 kV and 30 µA were used for acquiring the image, and a measurement was taken every 0.2 mm. The radiographic images of all NYK,

ABS and ÞUR unopened core sections were taken using a Geotek MSCL-XCT X-ray machine. For imaging whole cores (NYK, ÞUR, ABS), values of 130 kV and 300 µA were used.
The images produced by both Geotek MSCL-XCT and Itrax core scanner are 'radiographic positive', meaning that areas of high density appear darker and low-density areas are imaged lighter of color (Croudace et al., 2006).

4.3.3 X-ray fluorescence scans

X-ray fluorescence (XRF) core scanning is a standard analytical technique for rapid acquisition of the elemental composition of a sediment surface (Croudace et al., 2006; Löwemark et al., 2019). The scan provides high-quality data from terrestrial and marine sediments without destructing the sediments (Croudace et al., 2006). XRF core scanners consist of a cathode and an anode in a vacuum chamber. Electrons are emitted from the cathode when an electric current passes through the cathode. The energy (intensity) of the electric current can be changed in order to get varying numbers and accelerations of electrons. Such modifications can be made to measure different elements, e.g., a higher energy is needed to detect heavy elements (Forwick, 2013).

Each element is characterized by a specific wavelength of emitted radiation. It is therefore possible to use the detected energy of fluorescence to identify elements. The concentration of a corresponding element is proportional to the amplitudes of peaks in the XRF spectrum (Jenkins & Vries, 1970; Richter et al., 2006; Weltje & Tjallingii, 2008).
Measurements were conducted every 1 mm at 30 kV and 30 µA, with a 30 s exposure time. The split NYK, ABS and ÞUR core sequences were scanned with the Avaatech core scanner, set to 10 kV and 30 µA with a 2 mm resolution and 20 s counting time. Both instruments perform continuous down-core measurements.

XRF measurements can be altered by several factors. Variable grain size and water content downcore can lead to inhomogeneity of a sample which could cause alterations in elemental composition (Richter et al., 2006; Weltje & Tjallingii, 2008). The water content of a sample influences the degree of XRF absorption and can therefore lead to variable results as water films can absorb XRF of elements that are emitted from a wet sediment surface. Especially quantitative analyses of light elements (e.g., Al, Si, K) get affected by water content and grain

size variability (Kido et al., 2006). Another factor that can influence the XRF elemental composition measurements is the organic component of the sediment, therefore being especially important for lake sediments because of the often high organic content (Löwemark et al., 2011).

The geochemical results are usually presented as ratios of counts or elements (e.g., Fe/Ca) (Zuo, 2013). To minimize the artefacts caused by varying water and grain size content, the data were normalized with the incoherent (inc) and coherent (coh) scatter peaks from the X-ray tube (e.g., Ti/(inc+coh); Kylander et al., 2011). Another method to minimize these artefacts is to plot single elements against the sum of several elements (e.g., Fe/Sum, where Sum includes all element counts over 10 000; Weltje & Tjallingii, 2008).

The data obtained from XRF scans can be used for a broad range of fields, including paleoclimatology, paleoceanography and geology (Löwemark et al., 2019). The resulting high-resolution elemental profiles can help identify changes in the depositional environmental and sedimentological processes at the time of deposition. By correlating the results with other measurements (e.g., magnetic susceptibility), paleoenvironmental reconstructions can be conducted (Croudace et al., 2006).

4.3.4 Magnetic susceptibility

Magnetic susceptibility (MS) is a non-destructive method to determine the degree of magnetism a material shows in response to an applied magnetic field (Geotek, 2016). If paramagnetic, ferromagnetic or antiferromagnetic materials are present in the sediments, MS measurements will show positive values. Ferrimagnetic minerals (e.g., magnetite and maghemite) show MS values that are 3 to 4 orders of magnitude higher than the values of antiferromagnetic minerals (e.g., hematite). If no ferrimagnetic minerals are present, the concentration of diamagnetic (e.g., silica, biogenic carbonate) and paramagnetic (e.g., clay minerals) components can be measured. Negative values are recorded if diamagnetic material is measured (Stoner et al., 1996).

The MS measurement is a proxy that mainly gives indications about changes in sediment composition, and therefore changes in the sediment source or diagenetic environment (Geotek, 2016). The magnetic susceptibility was measured for the TDV core sections using the Itrax Core Scanner, with a 2 mm resolution.

4.4 Dating methods

Two dating methods were used in order to obtain ages that were used for the age-depth models and to be able to correlate the cores. Ten samples were sent for radiocarbon dating and 82 samples were collected for tephra analyses.

4.4.1 Radiocarbon dating

4.4.1.1 Basic principles

Radiocarbon dating is a method being widely used for constructing geochronological models (Hajdas, 2008; Wolfe et al., 2004). The method can be used to date organic material younger than ca. 50 000 years (Lowe & Walker, 2014). Carbon has three naturally occurring isotopes (^{12}C, ^{13}C and ^{14}C). Unlike ^{12}C and ^{13}C, ^{14}C is radioactive (Hajdas, 2008). ^{12}C represents ~98,89% of all natural carbon and is therefore the most abundant of the three isotopes, while ^{14}C (radiocarbon) contributes only ~1 ppm of all carbon (Meija et al., 2016). Radiocarbon is being produced in the upper atmosphere, where cosmic ray neutrons collide with ^{14}N atoms (Hajdas, 2008; Wolfe et al., 2004). The newly produced ^{14}C gets oxidized to ^{14}CO and $^{14}CO_2$. This process, taking weeks to a month, is followed by rapid mixing of $^{14}CO_2$ with the atmosphere. The production of radiocarbon over time is not constant. Changes in the solar activity result in fluctuating atmospheric radiocarbon content (Hajdas, 2008). Higher production rates result in radiocarbon plateaux during periods of low solar activity (Birks, 2001; Hajdas, 2008).

The principle of radiocarbon dating is based on both the amount of radiocarbon being present at the time of death in any kind of living organism and the half-life of ^{14}C ($T_{1/2}$ = 5730±40 yr) (Godwin, 1962; Hajdas, 2008; Wolfe et al., 2004). In a living plant, the metabolic uptake of ^{14}C through photosynthesis and the decay of radiocarbon are in steady state. The uptake of ^{14}C by the plant is assumed to be in equilibrium with atmospheric ^{14}C. After the plant dies, the only remaining process is the decay of the previously incorporated radiocarbon (Wolfe et al., 2004; Hajdas, 2008). By knowing the half-life of ^{14}C and counting the remaining ^{14}C atoms in an organic material, an age can be calculated. The radiocarbon activity when counting beta-particles can be measured by either counting the beta particles emitted by decaying ^{14}C, or by measuring the $^{14}C/^{12}C$ ratio using accelerator mass spectrometry (AMS), which is the prevailing procedure today (Hajdas, 2008).

The AMS ^{14}C technique allows high accuracy dating of small samples of Late Quaternary age (Wohlfarth et al., 1998). The principle of the AMS method is to accelerate C ions from the samples and to then subject the ions to a magnetic field (Wiedenbeck, 2015). Depending on their mass, particles that have the same velocity are deflecting in a different way from the applied magnetic field. The ^{14}C amount of heavy particles can be measured, since those particles get deflected the least (Bowman, 1990).

4.4.1.2 Sampling and analysis

Terrestrial plant macrofossils collected from the sediment cores of Nykurvatn, Ásbrandsstaðavatn and Þuríðarvatn were submitted for radiocarbon dating. Both macrofossils observed at the sediment surface of the split cores and found through specific searches were selected. Macrofossils were searched for by taking 1 cm thick sediment slices from the bottom, middle and top of each core. The sediments were then wet sieved, using a 63 µm meshed-sized sieve. After all sediments were removed, plant macrofossils were collected. The macrofossils were subsequently cleaned to remove any remaining organic sediments from them. This procedure was repeated until suitable macrofossils were found, by taking sediment slices from different depths within a core. The macrofossils were identified under a stereo microscope. After identification, the macrofossils were dried and weighed. Macrofossils were selected based on their location within the sediment core, their weight and terrestrial origin. The radiocarbon samples were submitted to the Ångström Laboratory, Uppsala University, Sweden. A Mini-Radiocarbon-Dating-System (MICADAS) was used to analyze the samples (Synal et al., 2007).

4.4.1.3 Calibration

For radiocarbon dating, macrofossils of terrestrial origin should be favored over aquatic plant remains. Terrestrial plants directly take up carbon from the atmosphere and should therefore be representative to the actual radiocarbon content at their time of death. Terrestrial plant macrofossils are, e.g., leaves, flowers, bark, wood and diaspores, such as fruits spores and seeds (Birks, 2001). Aquatic plants may be affected by the so-called reservoir or hard-water effect. This effect is caused by the uptake of HCO_3^-, derived from ground-water and ancient carbonate rocks, by an aquatic plant through photosynthesis. Plants affected by the hard-water effect give a too old age (Birks, 2001). Birks (2001) therefore advises to use terrestrial plant

macrofossils for AMS radiocarbon dating to prevent errors caused by reservoir or hard-water effects.

Fluctuations in the atmospheric ^{14}C content make the calibration of radiocarbon ages necessary (Hajdas, 2008). For terrestrial samples, two calibration curves are available; one for the Northern Hemisphere (IntCal) and one for the Southern Hemisphere (SHCal). The IntCal calibration curve was established through dendrochronology, varved lake sediments, speleothems and corals. It is well-defined for a time scale from 13.9 to 0 cal. kyr BP (Reimer et al., 2013). For this project, OxCal (v. 4.3, Ramsey et al., 2001) with the IntCal13 calibration curve was used for calibrating the radiocarbon ages.

4.4.2 Tephrochronology

4.4.2.1 Basic principles

Tephrochronology is a geochronological and stratigraphical technique that allows dating, correlation and synchronization of geological and paleoenvironmental events and sequences. Tephrochronology describes the use of tephra layers as isochrons to correlate paleoclimatic records (e.g., between different terrestrial records or between marine and ice-core records). Compared to other dating methods, tephrochronology allows the construction of an exceptionally precise volcanic-event stratigraphy. Tephra layers are often well preserved in lacustrine and marine sediments (Larsen & Eiríksson, 2008). Because of their high preservation potential combined with their high abundance on Iceland, tephra layers have the potential to improve the precision of tephrochronology in the North Atlantic area (Óladóttir et al., 2011).

For the application of tephrochronology, a characterization (also called geochemical 'fingerprint') of the tephra deposit is needed. The deposits can be characterized by physical properties visible in the field or through laboratory analyses. Every volcanic source has a certain geochemical signature that can link tephra back to its origin. Some volcanoes have a unique, easily distinguishable geochemical fingerprint, while others have similar geochemistry and are therefore are more difficult to identify (Lowe, 2011). The geochemical characterization of single grains can be conducted by analyzing the major elements as well as the trace elements (Davies, 2015).

4.4.2.2 Sampling and analysis

Electron Probe Microanalysis (EPMA) is a method that can be used for both analyzing minor and major elements (Larsen, 1981). EPMA allows the determination and quantification of major element geochemistry of individual glass shards (Coulter et al., 2010). The EPMA technique has a high spatial resolution, good analytical sensitivity, high accuracy and precision, and ability to differentiate between source volcanoes and between tephras produced by the same volcano (Hayward, 2012). The major elements that are measured as oxides with wavelength dispersive spectrometry are SiO_2, Al_2O_3, FeO, TiO_2, MnO, MgO, CaO, Na_2O, K_2O and P_2O_5 (Hunt & Hill, 2001; Hayward, 2012).

For the analysis, a focused beam of electrons gets directed onto a sample, leading to emission of X-rays. The emitted X-rays are characterized by particular energies and wavelengths that relate them to individual elements. The measured intensities of the X-rays are proportional to specific element abundance (Hunt & Hill, 1993). The produced X-ray signals can be detected or recorded by either energy-dispersive spectrometry (EDS) or wavelength-dispersive spectrometry (WDS) (Coulter et al., 2010). EDS analysis is faster, whereas WDS has a higher precision (Froggatt, 1992; Coulter et al., 2010). WDS has lower detection limits and better element discrimination, meaning that peaks of individual elements do not interfere (Froggatt, 1992). The downside is that the WDS is much slower than EDS because it requires higher beam current and longer counting times (Froggatt, 1992).

Samples from every visual layer of volcanic and suspected volcanic origin in the sediment cores were collected from all core sections of the four lakes, using a spatula. The layers were described in terms of color, grain size and thickness. The samples were sieved through two different mesh sizes, 63 µm and 125 µm and subsequently dried at 50 °C for 4 hours. The samples were sent to University of Iceland where they were geochemically identified using EPMA.

All tephra samples have been analyzed for major element chemical composition by WDS performed on a JEOL JXA-8230 electronic microprobe at the Institute of Earth Science, University of Iceland. For rhyolitic glass shards an accelerating voltage of 15 kV, a 5 nA beam current a beam diameter of 10 µm were used. For basaltic glass an accelerating voltage of 15 kV, a 10 nA beam current and a beam diameter of 10 µm were used. In the beginning and end of each session, a secondary glass standard was analyzed. For rhyolitic analyzing

sessions an ATHO rhyolitic glass was used as standard and for the basaltic sessions an A99 basaltic glass was used as standard.

4.4.2.3 Identification and correlation

Potential volcanic sources and events can be identified by comparing and matching the geochemistry of a sample with the geochemical fingerprint of previously identified tephra. A correct identification will result in a precise age determination of the analyzed tephra horizon (Davies, 2015). In study areas located in or around the North Atlantic, most tephras presumably originate from Icelandic volcanic systems (Haflidason et al., 2000). The identification of silicic tephra found on Iceland is based on their generally unique geochemical composition and stratigraphy (Larsen et al., 1999; 2001). Silicic tephra layers were correlated to specific volcanic events based on a series of element-element diagrams of TiO_2:SiO_2, K_2O:SiO_2, TiO_2:FeO, TiO_2:K2O, MgO:FeO, CaO:FeO (Larsen et al., 1999; Larsen & Eiríksson, 2008; Gudmundsdóttir et al., 2016; Meara et al., 2019). Because of the similar geochemistry, basaltic tephra derived from the same volcanic system is more difficult to identify (Óladóttir et al., 2011). Basaltic tephra produced by the most active volcanic systems; Veiðivötn-Bárðabunga, Grímsvötn, Kverkfjöll, and Katla, can be identified by element-element oxide bi-plots of TiO_2:FeO, TiO_2:K_2O, TiO_2:MgO, CaO:Al_2O_3, FeO:MgO and CaO:MgO (Óladóttir et al., 2008; Gudmundsdóttir et al., 2016). In this thesis, the focus is on silicic tephra layers, with both volcanic source and eruption being identified. For most basaltic tephra layers only the volcanic source is identified.

4.4.3 Age-depth models

Age-depth models for all four lakes were constrained based on the results of both radiocarbon ages and tephra analysis. The top cm of each core was determined to be the age in which the cores were collected. For the construction of the models, the Bayesian based code ‘Bacon’ v. 2.3.5 (Blaauw & Christen, 2011) was used in ‘R’ v. 3.5.2 (R Core Team, 2017). Constant accumulation rates were assumed between dated intervals. The IntCal13 calibration curve was used for calibrating the radiocarbon dates. Generally, a higher number of dates lead to lower uncertainties in the resulting model (Telford et al., 2004).

4.5 Alignment of cores

The individual core sections of all four lakes are overlapping and needed to be aligned for the construction of a continuous record. The core alignments started with the uppermost core section and continued downcore. The alignment of the core sections is based on visual correlation by studying element signals, MS and LOI results, identified tephra layers and stratigraphy (e.g., Fig. 8). Tephra layers that were correlated to a volcanic source or specific volcanic event and that were found in multiple cores were also used for the alignment. Identified tephra layers present in two cores are the most reliable tie-points. Tie-points identified from element signals are less reliable unless they are located near an identified tephra deposit. Generally, all elements showing clear trends or signals can be used for correlating core sections. Elements that were used for the alignment include Ti, Fe, Ca, Si. Ti/Sum was the element with the clearest signal for all core sections and correlation based on XRF data were therefore primary made by it. Additionally, differences in the lithology with changing grains sizes, colors or organic matter content were used for determining overlaps between cores.

Tie-points that were previously identified to connect two core sections with each other, were inserted into the program AnalySeries 2.0.4.2 (Fig. 8; Paillard et al., 1996). The program was (mainly) used for constructing the composite depth scales of the individual core sections. For correlating two sedimentary records, geochemical data vs depth of two overlapping core sequences were uploaded into AnalySeries (Paillard et al., 1996). AnalySeries does not correlate element signals automatically, but tie-points need to be added manually. Based on the tie-points, the position of the lower core shifts and thereby a new, composite depth of the lower core sequence is established. AnalySeries constructs a new depth for the analyzed data, based on the last two tie-points inserted into the program. The original length of a core section may get altered and data might get tuned (i.e., stretched or compressed), depending on the alignment with another core section (Fig. 8B).

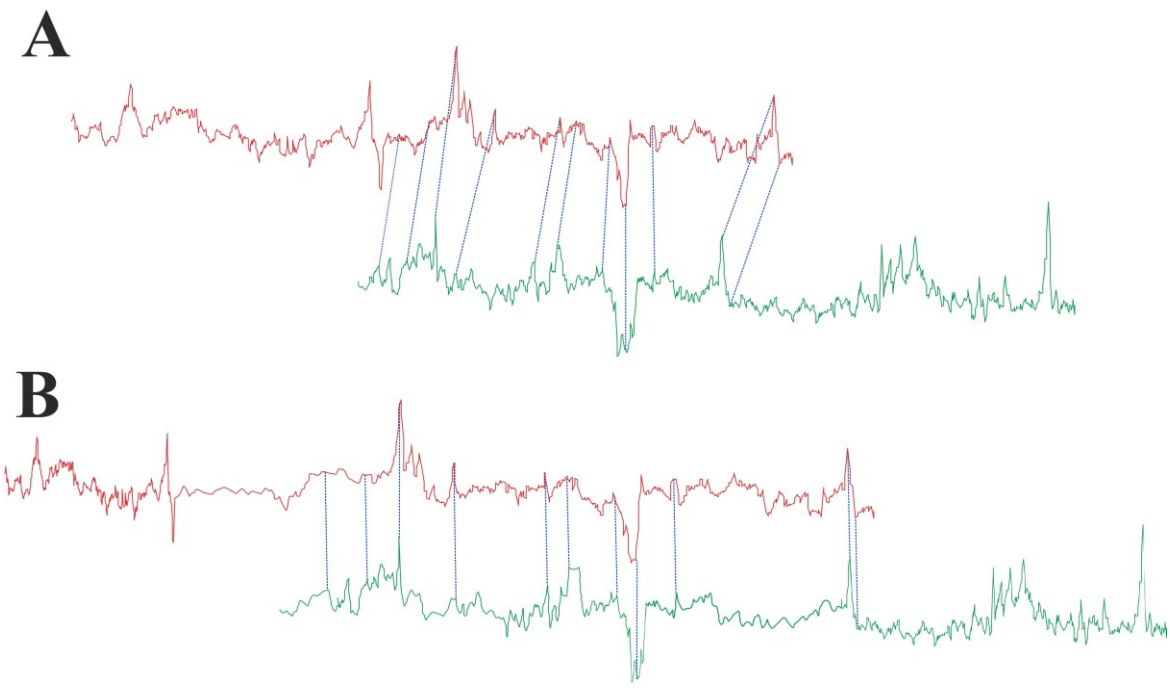

Figure 8. *Example of two overlapping core sections: NYK2 in red and NYK3 in green. Tie points are indicated by blue line. A. Ti/Sum curves showing the overlap and tie-points connecting the two sections. The tie-points were identified based on correlating identified tephra layer, element signals (or LOI/MS) and other lithostratigraphic characteristics. B. Data curves got stretched and/or compressed based on selected tie-points, so both curves directly align.*

5 Results

5.1 Radiocarbon dating

Dated plant macrofossils are presented in Fig. 9 and the results of the AMS radiocarbon dating and the calibrated ages are shown in Table 2**.** Calibrated ages are presented as the mean of the 2σ range. Five of the samples collected for radiocarbon dating could not be dated, including NYK2 75-76 cm, NYK3 143-144 cm, NYK4 11-12 cm, ABS4 63-64 cm and ÞUR2 125-126 cm (Fig. 9B, C, D, H, J**).** As a result, only one radiocarbon age could be obtained for both Ásbrandsstaðavatn and Þuríðarvatn. The age of sample NYK1 48-49 cm and the position of the dated material below a tephra layer identified as Hekla 3 marker layer (see Chapter 5.2) suggest that the twig was not deposited directly into the lake or may have been redeposited. The depths of the other radiocarbon ages have also been compared to the depth of ages of identified marker layers and therefore are considered to be reliable.

Table 2. *Results of the ^{14}C measurements.*

Core section	Depth in core section (cm)	Composite depth (cm)	^{14}C age (yr BP ± σ)	Dated material	calibrated age (cal. yr BP ± 2σ)	Lab no.	$\delta^{13}C$‰ V-PDB
NYK1	48-49	48-49	3 597 ± 31	Twig (*Betula* sp.) (Fig. 9A)	3 903 ± 45	Ua-65341	−23.9
NYK5	62-63	320-321	6 125 ± 45	Leaf (*Betula nana* /sp.) (Fig. 9E)	7 016 ± 79	Ua-65343	
NYK5	133-134	391-391	7 511 ± 38	Leaf (*Salix herbacea*) (Fig. 9F)	8 344 ± 51	Ua-65344	−28.0
ABS2	49-50	152-153	3 476 ± 66	Terrestrial leaf fragment (Fig. 9G)	3 750 ± 85	Ua-65342	
ÞUR1	135-136	135-136	308 ± 33	Leaf (*Betula nana* /sp.) (Fig. 9I)	387 ± 49	Ua-65345	−27.7

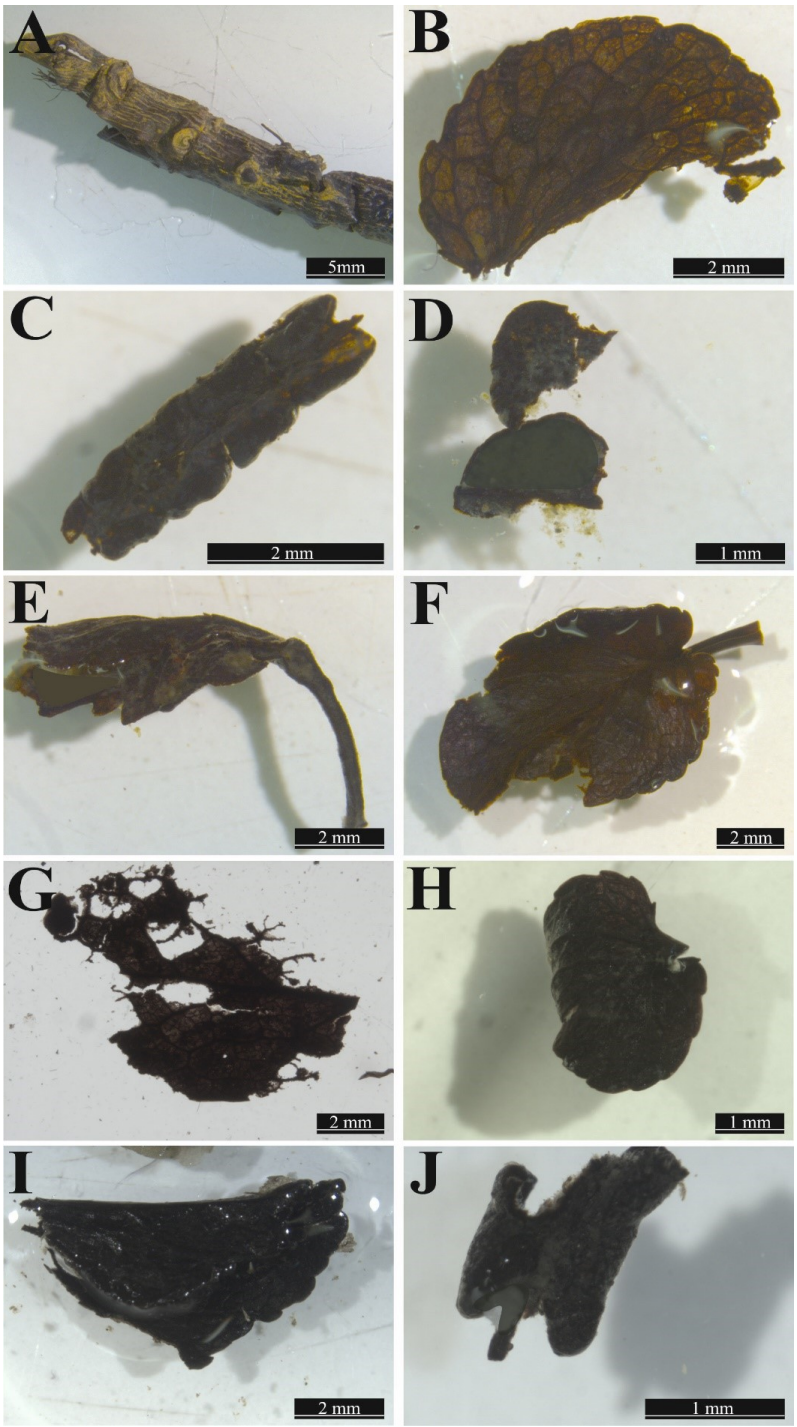

Figure 9. *Macrofossils from Nykurvatn, Ásbrandsstaðarvatn and Þuríðarvatn (NE Iceland) used for radiocarbon dating. In total, ten macrofossils were collected from nine core sections. A. Twig from a shrub (Betula sp.) collected in NYK1 at 48-49 cm. B. Terrestrial leaf (Salix herbacea) collected in NYK2 at 75-76 cm. C. Terrestrial leaf (Dryas sp.) collected in NYK3 at 143-144 cm. D. Terrestrial leaf fragments collected in NYK4 at 11-12 cm. E. Terrestrial leaf (Betula nana/sp.) collected in NYK5 at 62-63 cm. F. Terrestrial leaf (Salix herbacea) collected in NYK5 at 133-134 cm. G. Terrestrial leaf fragment collected in ABS2 at 49-50 cm. H. Terrestrial leaf (Salix herbacea) collected in ABS4 at 63-64 cm. I. Terrestrial leaf (Betula nana/sp.) collected in ÞUR1 at 135-136 cm. J. Terrestrial leaf fragment collected in ÞUR2 at 125-126 cm.*

5.2 Tephra marker identification

The volcanic sources of 53 primary tephra layers, collected from the TDV, THUR, NYK and ABS sediment sequences, have been identified based on their major element composition (e.g., Larsen et al., 1999; Óladóttir et al., 2008; Gudmundsdóttir et al., 2011). The source volcanoes include the Grímsvötn (n=19), Veiðivötn-Bárðarbunga (n=15), Katla (n=8), Askja (n=1) and Hekla (n=10) volcanic systems. However, some samples were collected from the same layer located in overlapping core sections and therefore identical layers may have been counted several times. Geochemical analysis showed that eleven layers consists of tephra from two or more volcanic systems or samples have been collected from disturbed layers and were therefore not viewed as primary layers. Eighteen primary tephra layers or samples have been further analyzed and correlated to specific volcanic events (i.e., known tephra marker layers) based on major element-composition, visual characteristic, stratigraphic position and potentially available ^{14}C ages. Six different regional and local marker tephra layers have been identified in the sediment sequences of the four studied lakes (Table 3). Identified tephra marker layers include V1477, originating from the Veiðivötn-Bárðarbunga system (ÞUR, NYK), Hekla 1104 (TDV), Hekla 3 (TDV, NYK, ABS), Hekla 4 (TDV, NYK, ABS), Saksunarvatn Ash from the Grímsvötn system (TDV, ABS) and Askja S (ABS) (Table 3). All identified tephra marker layers had sharp upper and lower boundaries to gyttja. The composite depths of all sampled tephra layers are shown in Figs 25 (TDV), 27 (ÞUR), 29 (NYK) and 31 (ABS) and can also be found in Table A.

Table 3. *Identified tephra layers in the studied lakes. Depth of each layer, source volcanic system, geochemical composition, identified tephra markers and age are listed. H: Historical, R: Radiocarbon, M: Age-model. Radiocarbon ages taken from previous publications have been calibrated using OxCal.*

Tephra layer name (core section, depth)	Lake	Volcanic system	Silicic (S) Basaltic (B)	Tephra markers	Age (cal. yr BP)	Type of date	References for ages
ÞUR2 1, NYK1 61, NYK3 1	ÞUR, NYK	Vei-Bar	B	V1477	470	H	Larsen et al., 2002
TDV2-1 115	TDV	Hekla	S	Hekla 1104	850	H	Larsen et al., 2002
TDV2-4 2, NYK4 29, ABS1 130, ABS2 22	TDV, NYK, ABS	Hekla	S	Hekla 3	3005 ± 57	R	Dugmore et al., 1995
TDV2-4 100, NYK3 98, ABS2 63	TDV, NYK, ABS	Hekla	S	Hekla 4	4196 ± 33	R	Dugmore et al., 1995
TDV2-6 129, TDV2-7 16, ABS3 117, ABS3 147, ABS4 18, ABS4 48	TDV, ABS	Grímsvötn	B	Saksunarvatn Ash	10267 ± 89	I	Rasmussen et al., 2006
ABS4 97	ABS	Askja	S	Askja S	10824 ± 97	M	Kearney et al., 2018

5.2.1.1 Torfdalsvatn sediment core – tephra marker layers

Five tephra layers, contained within the sediment sequence of Torfdalsvatn, have been correlated to four different tephra marker layers, displaying particular volcanic events. Three silicic tephra layers were identified to originate from Hekla and have been correlated to the tephra marker layers Hekla 1104 (H1104), Hekla 3 (H3) and Hekla 4 (H4) (Fig. 11). One basaltic tephra layer has been identified as the Saksunarvatn Ash (Fig. 12), originating from the Grímsvötn volcanic system. The Saksunarvatn Ash (ca. 10.3 cal. kyr BP; Rasmussen et al. 2006) is the oldest identified tephra marker layer in the TDV sediment sequence, and H1104 AD is the youngest identified layer. The position of the tephra layers in the TDV sediment sequences is show in Fig. 21.

Description of silicic tephra layers

Three silicic tephra layers (TDV2-1 115, TDV2-4 1 and TDV2-4 100) were correlated to a marker layer (Fig. 11). In core section TDV2-1, a continuous rhyolitic tephra layer with a thickness of ~1 cm is located at 115-116 cm. The tephra layer has a light grey color and consists of fine ash (Fig. 10). The silicic component of the TDV2-1 115 tephra shows a narrow range in the SiO_2 concentrations (69.12-72.38 wt%). The compositions of TiO_2 (0.14-

0.24 wt%), FeO (2.93-3.31 wt%), K_2O (2.41-2.79 wt%), MgO (0.08-0.14 wt%) and CaO (1.78-2.03 wt%) show similar small ranges as the SiO_2 concentration (Fig. 11). One outlier with higher concentrations in TiO_2 (0.62 wt%), FeO (4.65 wt%), MgO (0.85 wt%) and CaO (1.78 wt%) has been observed in the geochemical data (Fig. 11).

In core section TDV2-4 a thin (<5 mm) grey tephra layer, located between 1-2 cm (TDV2-4 2) consists of fine ash (Fig. 10). The tephra is characterized by a relatively broad range in SiO_2 (60.46-66.93 wt%) and FeO (4.96-8.57 wt%) concentrations. The concentrations of TiO_2 (0.35-0.78 wt%), K_2O (1.23-2.17 wt%), MgO (0.34-0.97 wt%) and CaO (3.01-4.66 wt%) show a narrow range.

A second continuous tephra layer has been observed in TDV2-4 at 98-100 cm (TDV2-4 100). The tephra layer consists of dark grey, fine to medium ash and is fining upwards (Fig. 10). The tephra is characterized by high SiO_2 concentrations (71.75-74.03 wt%). The concentrations of TiO_2 (0.03-0.16 wt%), FeO (1.85-2.09 wt%), K_2O (2.71-2.91 wt%), MgO (0.01-0.08 wt%) and CaO (1.19-1.37 wt%) all show narrow ranges.

Identification of silicic tephra layers

The three silicic tephra layers have been correlated to specific tephra marker layers. TDV2-1 115 was identified as H1104, TDV2-4 2 as H3 and TDV2-4 100 as H4 (Table 3). In all three layers high SiO_2 (> 60 wt%) and low TiO_2 (> 0.2 wt%) concentrations that are typical for the Hekla volcano, were measured (Larsen & Eiríksson, 2008).

The major element composition measured in TDV 2-1 115 is nearly identical to the composition of several tephra layers, that were previously identified as H1104 (Fig. 11; Larsen et al., 1999; Larsen, 2000; Meara et al., 2019). The Hekla 1104 tephra is characterized by high SiO_2 concentrations (rhyolitic) and low FeO concentrations with narrow ranges (Meara et al., 2019). As shown in Fig. 11, TDV2-1 115 appears to have a very similar narrow ranges in its major element composition as the previously published geochemical data of the H1104 tephra. During the H1104 eruption, volcanic material was primarily transported towards northern Iceland, including Skagi (Fig. 35; Larsen & Thorarinsson, 1977; Larsen et al., 2002; Gudmundsdóttir et al., 2011; Meara et al., 2019). Meara et al. (2019) suggested a thickness of ca. 1 cm for H1104 tephra layers deposited in northern Iceland. The thickness of TDV2-1 115 of 1 cm is therefore consistent with the suggested thickness of H1104. Florian

(2016) reported the presences of H1104 in a sediment sequence of Torfdalsvatn, confirming that the tephra has been transported to the lake.

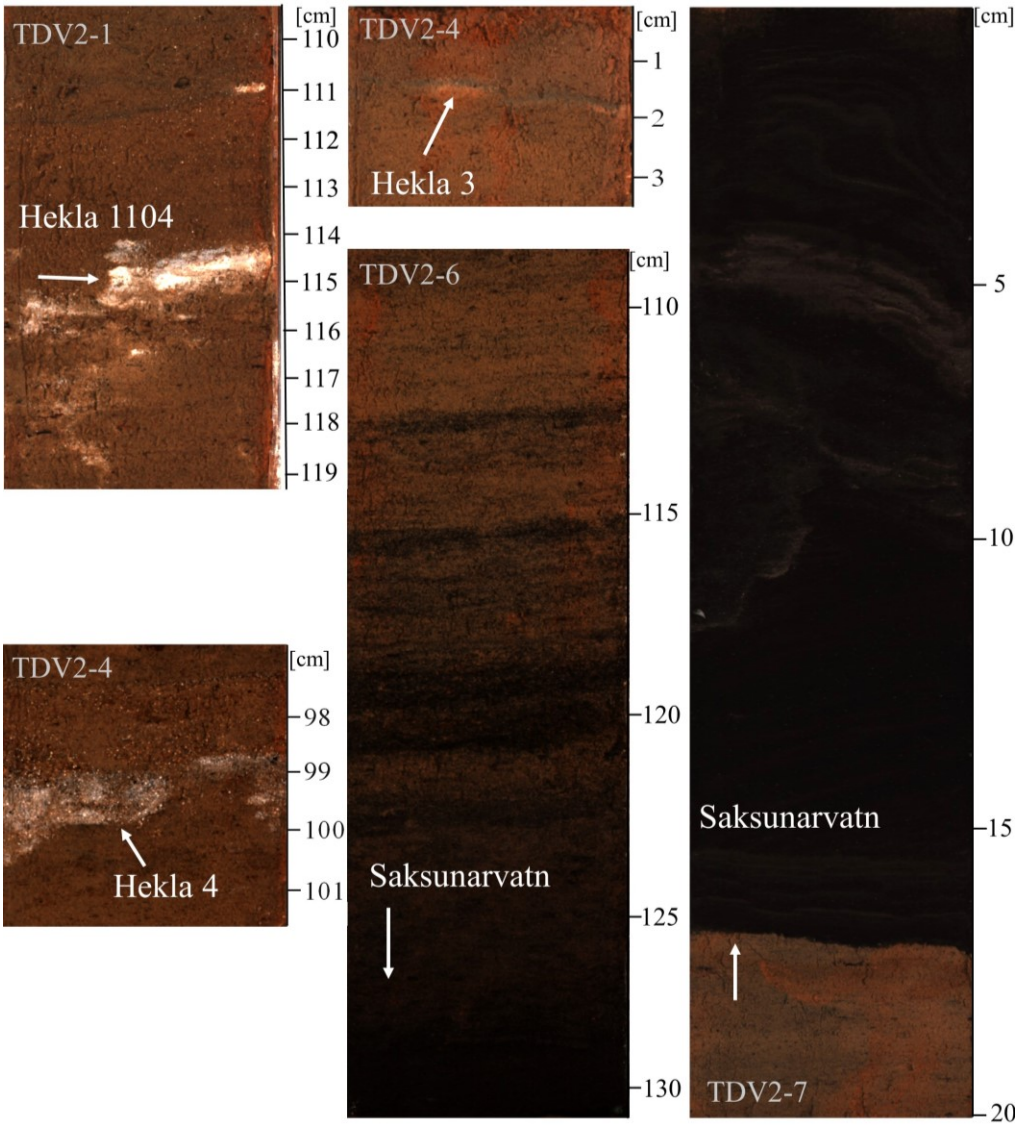

Figure 10. *Visual tephra layers contained in the sediment sequences of Torfdalsvatn. Four tephra markers are shown: three silicic layers (Hekla 1104, Hekla 3 and Hekla 4), and the basaltic Saksunarvatn Ash layer.*

TDV2-4 2 is compositionally identical to tephra layers that were identified as H3 (Fig. 11; Larsen et al., 2002; Sverrisdottir, 2007; Óladóttir, 2009; Meara, 2011; Óladóttir et al., 2011; Gudmundsdóttir et al., 2016; Meara et al., 2019). H3 and H1104 tephras show a near identical rhyolitic/dacitic composition with only minor differences. However, the concentration ranges of major elements (e.g., SiO_2, TiO_2, FeO) of the H3 tephra are typically broader than concentrations analyzed for Hekla 1104 (Meara et al., 2019). Similar trends with wider ranges have been observed in TDV2-4 2 (Fig. 11). The H3 eruption widely dispersed volcanic

material over an area of 80,000 km^2 on Iceland including Skagi (Fig. 35; Larsen & Thorarinsson, 1977; Larsen et al., 2002; Gudmundsdóttir et al., 2011; Meara et al., 2019). H3 tephra layers deposited in North Iceland typically have a thickness of ca. 1 cm or less (Larsen & Thorarinsson, 1977; Meara et al., 2019), matching the thickness of TDV2-4 2. Eddudóttir et al. (2017) reported the presence of a silicic tephra layer in a soil profile from a wetland close to Kagaðarhóll (~60 km southwest of Torfdalsvatn), and correlated it with the H3 marker layer. The grey color of the tephra layer described by Eddudóttir et al. (2017) is similar to TDV2-4 2, which further supports the idenfication as H3. The correlations of the compositionally similar tephra layers TDV2-1 115 with H1104 an TDV2-4 2 with H3 are further supported by their stratigraphic position within the TDV core sequence, where TDV2-1 115 is located stratigraphically above TDV2-4 2.

The major element composition of TDV2-4 100 is nearly identical to the composition of tephra layers that have been identified as H4 (Fig. 11; Dugmore et al., 1992; Sverrisdottir, 2007; Óladóttir, 2009; Gudmundsdóttir et al., 2016; Meara et al., 2019). Compared to the H1104 and H3 tephra, the H4 tephra typically is characterized by very high SiO_2 concentrations (71.25-77.19 wt%) and lower FeO concentrations (1.45-4.16 wt%) (Meara et al., 2019). As shown in Fig. 11, the major element composition of TDV2-4 100 correlates very well with the high SiO_2 and low FeO concentrations. The narrow ranges of other concentrations (e.g. MgO, K_2O, TiO_2, CaO) in TDV2-4 100 also overlap with the published geochemical composition of H4 (Fig. 11). The H4 tephra layer is a well-known tephra marker in Iceland`s tephra stratigraphy. H4 tephra deposit on Iceland cover an area of ca. 78,000 km^2 including Skagi (Fig., 35; Larsen & Thorarinsson, 1977; Larsen et al., 2002; Larsen & Eiríksson, 2008; Gudmundsdóttir et al., 2011; Meara et al., 2019). The ca. 2 cm thickness of TDV2-4 100 agrees with the thickness of H4 tephra layers deposited on Skagi of 2 cm, as suggested by an isopach map showing the dispersal of the H4 tephra (Larsen & Thorarinsson, 1977; Meara et al., 2019). A tephra layer with the same grey color as TDV2-4 100, that was found in a soil profile from a wetland close to Kagaðarhóll, was correlated to the H4 tephra marker (Eddudóttir et al., 2017). This visual correlation therefore supports the geochemical identification as H4. Florian (2016) previously correlated a tephra layer found in a sediment sequence of Torfdalsvatn with the H4 tephra marker, confirming that the tephra has been deposited in the lake.

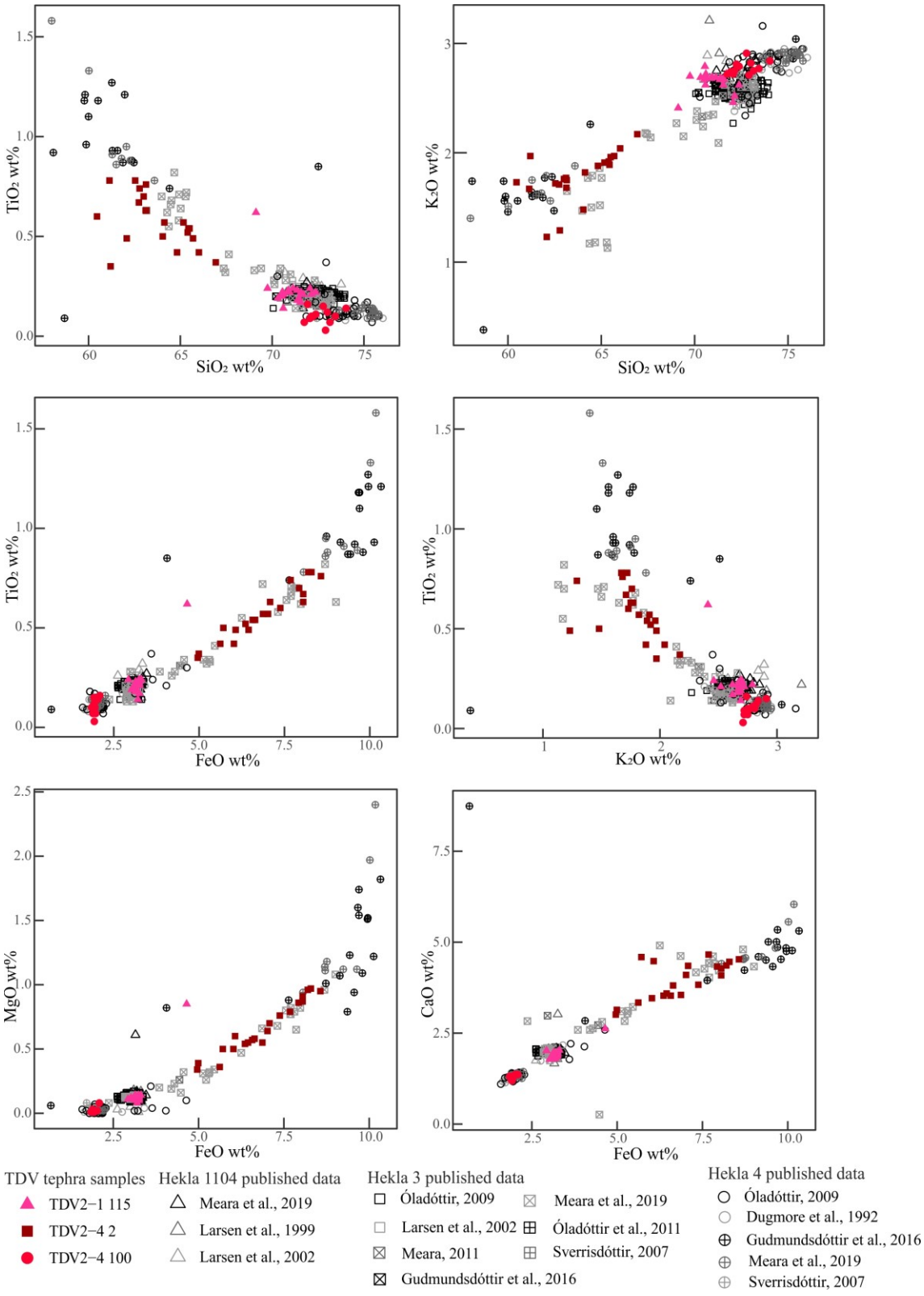

Figure 11. *Binary plots of major element oxide values analyzed for the silicic TDV tephra layers. Plots show the correlation of the TDV2-1 115, TDV2-4 2 and TDV2-4 100 tephra layers with the Hekla 1104, Hekla 3 and Hekla 4 marker layers.*

Description of basaltic tephra layers

Two tephra layers (TDV2-6 129 and TDV2-7 16) have been correlated to the same tephra marker layers. Both layers are of basaltic composition and show SiO_2 concentrations of <50 wt%.

In the bottom of core section TDV2-6 at 124-131 cm a black tephra layer consisting of fine ash is located (Fig. 10; TDV2-6 129). TDV2-6 129 is characterized by relatively narrow ranges in concentrations of TiO_2 (2.56-3.16 wt%), FeO (13.58-14.96 wt%), K_2O (0.37-0.48 wt%), MgO (4.77-6.04 wt%), CaO (9.47-10.57 wt%) and Al_2O_3 (12.91-13.62 wt%).
At the top of core section TDV2-7 between 0 and 17 cm a tephra layer consisting of fine ash is located (TDV2-7 16). The tephra layer is black with grey lineation between 4 and 5 cm (Fig. 10). TDV2-7 16 is geochemically characterized by narrow ranges in the TiO_2 (2.75-3.40 wt%), FeO (14.15-14.88 wt%), K_2O (0.43-0.48 wt%), MgO (4.69-5.58 wt%), CaO (9.52-10.24 wt %) and Al_2O_3 (12.84-13.64 wt%) concentrations (Fig. 12). The geochemical data shows one outlier with higher FeO (16.38 wt%) concentrations.

Identification of basaltic tephra layers

TDV2-6 129 and TDV2-7 16 have both been correlated to the Saksunarvatn Ash marker layer (Table 3). In both samples, low SiO_2 and TiO_2 concentrations of ~2.2-3.5 wt% were measured, which are typical for basaltic tephra originating at the Grímsvötn volcanic system (Larsen & Eiríksson, 2008).

The major element chemical compositions measured in TDV2-6 129 and TDV2-7 16 correlate with the composition of tephra layers, that were previously identified as Saksunarvatn Ash (Fig. 12; Mangerud et al., 1986; Björck et al., 1992; Ingólfsson, et al., 1995; Birks et al., 1996; Kristjánsdóttir et al., 2007; Gudmundsdóttir et al., 2011). The published composition of the Saksunarvatn Ash shows very similar concentrations in K_2O (0.24-0.57 wt%), MgO (4.58-9.57 wt%), TiO_2 (2.23-3.41 wt%) and FeO (12.08-16.20 wt%) to the concentrations analyzed in the basaltic TDV layers. The Saksunarvatn Ash is a marker layer characterized by its wide dispersal over the northern North Atlantic region and has been deposited almost all over Iceland (Fig. 35; Gudmundsdóttir et al., 2011; Óladóttir et al., 2020). Based on its wide dispersal, the Saksunarvatn tephra is expected to be found in Icelandic lacustrine sediment sequences covering the early Holocene.

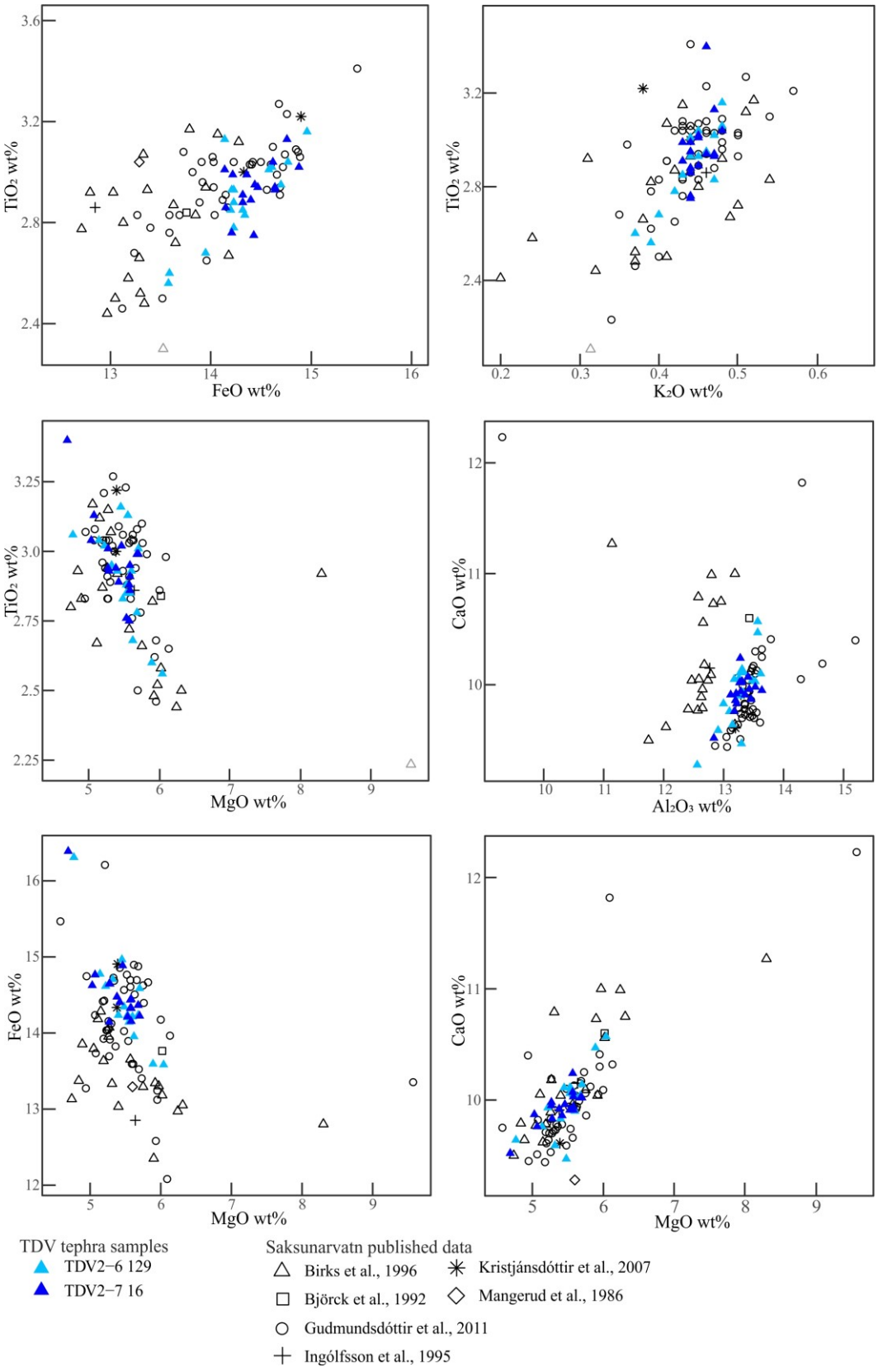

Figure 12. *Binary plots of major element oxide values analyzed for the basaltic TDV tephra layers. Plots show the correlation of TDV2-6 129 and TDV2-7 16 with the Saksunarvatn Ash.*

Björck et al. (1992), Rundgren (1995) and Florian (2016) described a ca. 20 cm thick dark tephra layer in sediment sequences of Torfdalsvatn and identified the layer as the Saksunarvatn ash. This previous discovery of the distinct and unique tephra layers further supports the geochemical identification of TDV2-6 129 and TDV2-7 16 as Saksunarvatn ash.

5.2.1.2 Þuridarvatn sediment core – tephra marker layers

In the sediment record of Þuridarvatn, one tephra layer has been correlated to a tephra marker. The basaltic tephra has been identified to originate from the Veiðivötn-Bárðarbunga system and was correlated with the V1477 marker layer (AD 1477). The stratigraphic position of the V1477 tephra layer is shown in Fig. 22.

Description of basaltic tephra layer

In core section ÞUR2, a continuous tephra layer is located between 0-4 cm. The tephra layer (ÞUR2 1) consists of dark grey, very fine ash (Fig. 13). The major element composition shows that the tephra has narrow ranges in the concentrations of SiO_2 (49.78-50.87 wt%), TiO_2 (1.75-1.94 wt%), Al_2O_3 (13.25-14.29 wt%), FeO (11.92-13.03 wt%), K_2O (0.21-0.25 wt%), MgO (6.29-6.77 wt%) and CaO (10.98-11.60 wt%) (Fig. 14).

Figure 13. *Visual tephra layers contained in the sediment sequences of Lake Þuridarvatn. One single tephra marker has been identified: V1477.*

Identification of basaltic tephra layer

The major element chemical composition measured in the ÞUR2 1 layer correlates with the composition of tephra layers identified as V1477 tephra marker layers (Fig. 14; Larsen et al.,

2002; Gudmundsdóttir et al., 2011, 2016; Vakhrameeva et al., 2020). The TiO_2 concentrations measured in ÞUR2 1 lie within the characteristic values for tephra layers originating from the Veiðivötn-Bárðarbunga system of ca. 1.3-2.1 wt% (Larsen et al., 2002). The published composition of the V1477 tephra shows very similar concentrations in K_2O (average: ~0.3 wt%), MgO (~6.7 wt%), Al_2O_3 (~15.2 wt%), CaO (11.5 wt%) and FeO (~13.4 wt%) to the concentrations analyzed in ÞUR2 1. However, the range in elemental concentrations are slightly narrower in ÞUR2 1 (Fig. 14). Dispersal maps show that during the V1477 eruption volcanic material was deposited in the eastern half of Iceland (Fig. 35), therefore the appearance of V1477 tephra deposits in lakes located in the Vopnafjörður area is likely (Larsen & Thorarinsson, 1977; Larsen et al., 2002; Gudmundsdóttir et al., 2011). The geochemical identification is supported by a visual correlation of ÞUR2 1 with a dark grey, 2 cm-thick and compositionally identical tephra layer situated in the sediment sequence of the lake Lögurinn, ~55 km southeast of Þuridarvatn (Gudmundsdóttir et al., 2016). A ^{14}C age of 387 ± 49 cal. yr BP obtained from the upper core section ÞUR1 at 135 cm further supports the identification of V1477 because the 470 cal. yr BP layer is located stratigraphically below the ^{14}C age (Larsen et al., 2002).

5.2.1.3 Nykurvatn sediment core – tephra marker layers

Four tephra layers situated in the sediment sequences of Nykurvatn have been correlated to four different tephra marker layers. Two silicic tephra layers were identified to originate from Hekla and have been correlated to the tephra marker layers H3 and H4 (Fig. 16). Two basaltic tephra layers have been identified as the V1477 tephra marker, (Fig. 17). The H4 layer (ca. 4200 cal. yr BP; Dugmore et al., 1995) is the oldest identified tephra marker layer contained in the NYK sediment sequence and the V1477 tephra (470 cal. yr BP; Larsen et al., 2002) is the youngest identified tephra marker. The positions of the tephra layers in the core sequences is shown in Fig. 23.

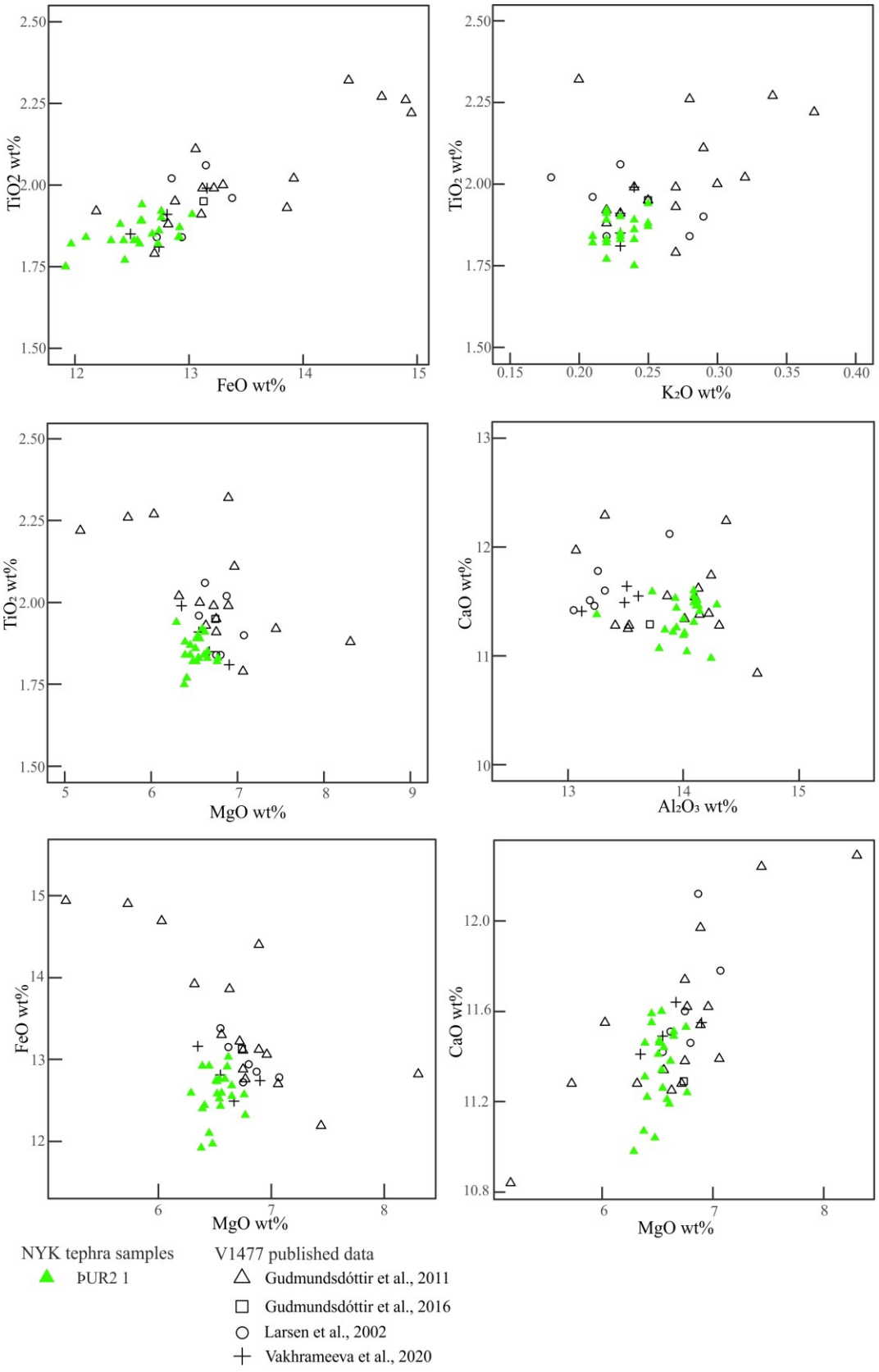

Figure 14. *Binary plots of major element oxide values analyzed for the ÞUR basaltic tephra layers. Plots show the correlation of ÞUR2 1 with the V1477 marker layer.*

Description of silicic tephra layers

Two silicic tephra layers (NYK3 98 and NYK4 29) were correlated to tephra marker layers (Fig. 16). In core section NYK3, a 3-cm thick tephra (NYK3 98) has been identified at 97-100 cm. The tephra layer consists of is dark grey, fine ash with coarser white ash grains (Fig. 15). SiO_2 concentrations in the NYK3 98 tephra show two trends with high concentrations, ranging between 69.97-72.42 wt% (rhyolitic), and lower concentrations, ranging between 60.86-61.65 wt% (andesitic; Fig. 16). Similar trends have been observed for TiO_2 (0.11-0.13 wt%; 0.83-0.97 wt%), FeO (1.94-2.02 wt%; 9.13-9.6 wt%), K_2O (2.52-2.8 wt%; 1.59-1.66 wt%), MgO (0.01-0.03 wt%; 0.80-1.25 wt%) and CaO (1.20-1.31 wt%; 4.50-5.04 wt%) with geochemical data clustering together at higher or lower concentrations (Fig. 16).

One tephra sample (NYK4 29) was collected from a discontinuous tephra patch located at the edge of core section NYK4 at 27-31 cm. The tephra patch consists of very fine ash with a light grey color (Fig. 15). It was assumed that the patch was dragged down during the coring processes and originates from a continuous tephra layer located in NYK2 116-117 cm and NYK3 at 55-58 cm. Both continuous tephra layers consist of light grey fine ash and are therefore very similar to the tephra sampled in NYK4. Based on their very similar visual characteristic and the absence of any comparable other tephra layer, it was assumed that both tephra layers and tephra patch consist of volcanic material from the same eruption. The correlation of the geochemical data obtained from NYK4 29 with a tephra marker was therefore used for identifying the tephra layers in NYK2 (116-117 cm) and NYK3 (55-58 cm). The NYK4 29 sample shows a wide range in the SiO_2 concentrations (60.05-72.32 wt%) (Fig. 16). A narrower range was observed in the concentrations of TiO_2 (0.14-0.46 wt%), K_2O (1.99-2.54 wt%), MgO (0.10-0.41 wt%) and CaO (1.65-3.31 wt%). The FeO concentration range (2.68-5.73 wt%) is comparably broader (Fig. 16).

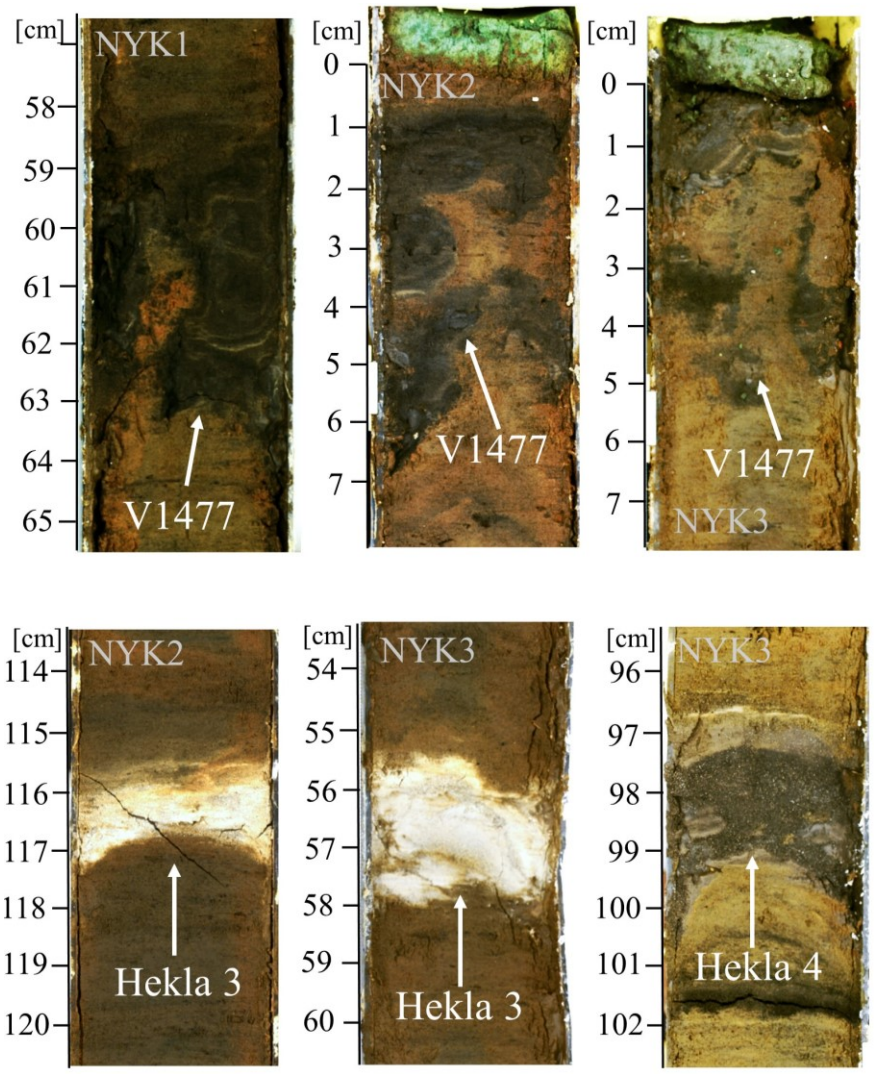

Figure 15. *Visual tephra layers contained in the sediment sequences of Nykurvatn. Three tephra marker layers have been identified: V1477, Hekla 3 and Hekla 4.*

Identification of silicic tephra layers

The silicic tephra layers are characterized by low TiO_2 concentrations, indicating that both layers originate from the Hekla volcano (Larsen et al., 2002). The major element chemical composition of NYK3 98 correlates with the geochemical composition of tephra layers identified as H4 (Fig. 16; Dugmore et al., 1992; Sverrisdottir, 2007; Óladóttir, 2009; Gudmundsdóttir et al., 2016; Meara et al., 2019). Published analyses of H4 show a similar trend as described in NYK3 98 with rhyolitic and andesitic chemical components. The rhyolitic component shows highly evolved SiO_2 (~73 wt%), and low TiO_2, K_2O, FeO, CaO and MgO concentrations. The andesitic component of the H4 tephra shows high concentrations in TiO_2, K_2O, FeO, CaO and MgO. The rhyolitic and andesitic components

measured in NYK3 98 show the same ranges in major element concentrations (Fig. 16). The geochemical correlation is further supported by a suggested thickness of 2 cm for H4 tephra deposits in northeastern Iceland (Larsen & Thorarinsson, 1977; Meara et al., 2019), that matches with the thickness of NYK3 98. The presence of the H4 tephra has also been reported in the sediment sequences of lake Lögurinn (Gudmundsdóttir et al., 2016) and is therefore known to occur in lakes located close to the northeastern study area.

The major element chemical composition of NYK4 29 correlates with the geochemical composition of tephra layers identified as H3 (Fig. 16; Larsen et al., 2002; Sverrisdottir, 2007; Óladóttir, 2009; Meara, 2011; Óladóttir et al., 2011; Gudmundsdóttir et al., 2016; Meara et al., 2019). As previously mentioned, the H3 tephra typically has broad ranges in concentrations of SiO_2, TiO_2, FeO, which were also analyzed for the NYK4 29 tephra. However, the ranges of NYK4 29 appear to be slightly narrower than published analyses (Fig. 16). H3 tephra layers are suggested to have been deposited around Vopnafjörður (Fig. 35) and deposits in this area should have a thickness of ~2 cm (Larsen & Thorarinsson, 1977; Meara et al., 2019). This would agree with the thickness of the tephra layers situated in NYK2 at 116-117 cm and NYK3 at 55-58 cm (Fig. 16), that are assumed to consists of the same volcanic material as the NYK4 29 tephra. The correlation of NYK4 29 to H3 is also supported by the stratigraphic position of the NYK2 116-117 cm and NYK3 55-58 cm above the NYK3 98 layer, based on the assumption that both layers consists of the same material as NYK4 29. The geochemical identification is further supported by a the light grey color, observed in NYK4 29, which has been previously observed in tephra deposits of the H3 eruption (e.g., Gudmundsdóttir et al., 2016; Meara et al., 2019).

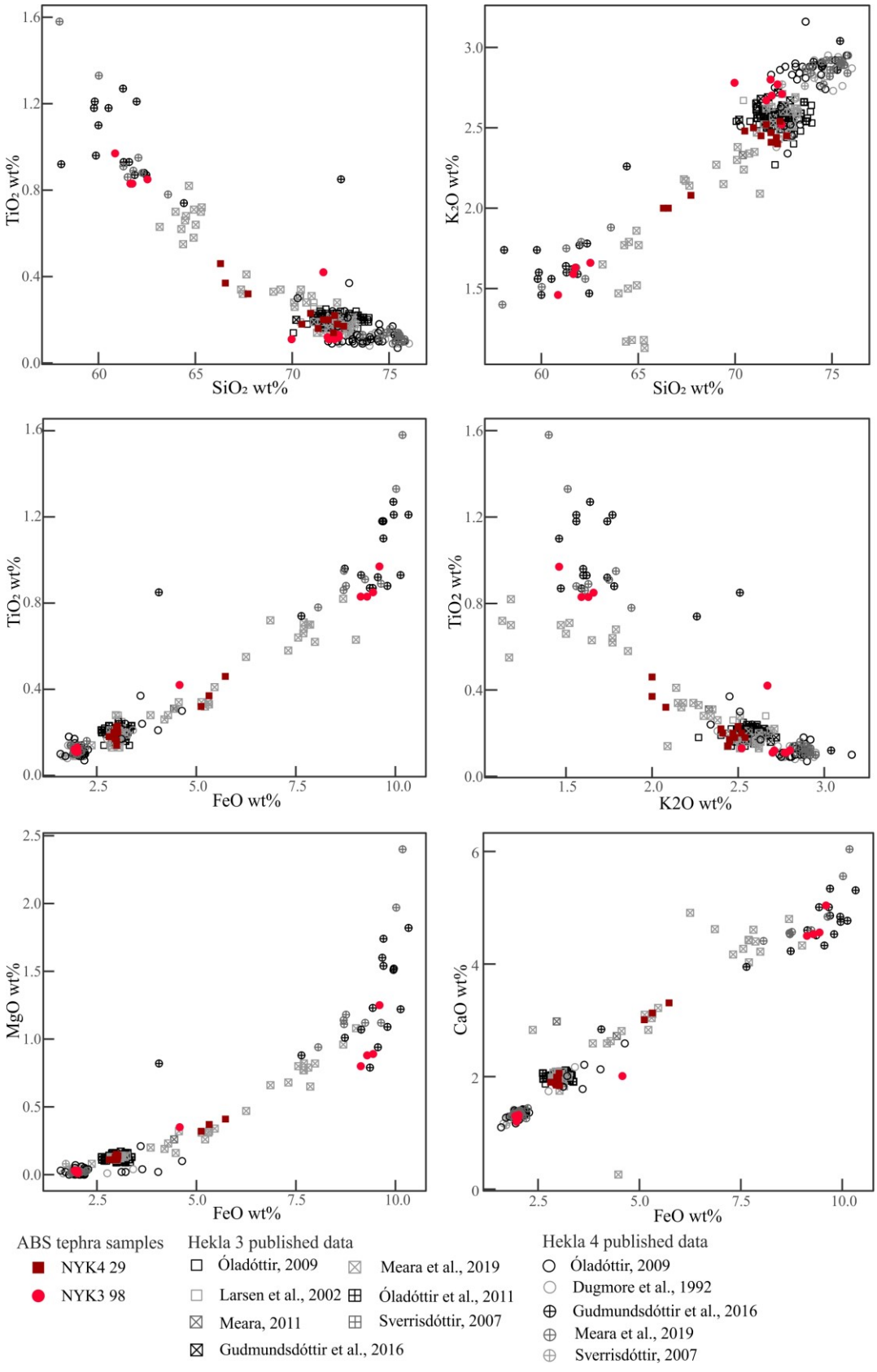

Figure 16. *Binary plots of major element oxide values analyzed for the NYK silicic tephra layers. Plots show the correlation of NYK4 29 and NYK3 98 with the Hekla 4 and Hekla 3 marker layer, respectively.*

Description of basaltic tephra layers

Two tephra layers (NYK1 61 & NYK3 1) are characterized by their basaltic geochemical composition with low SiO_2 concentrations (~49-51 wt%; Fig. 17). In core section NYK1, a continuous tephra layer is situated at 58-64 cm (NYK1 61). The tephra layer consists of fine ash with a dark grey-black color. The major element composition of NYK1 61 shows narrow ranges in the SiO_2 (49.24-51.35 wt%), TiO_2 (1.76-2.05 wt%), Al_2O_3 (13.20-15.20 wt%), FeO (11.28-13.30 wt%), K_2O (0.22-0.26 wt%), MgO (6.44-7.55 wt%) and CaO (10.73-11.80 wt%) concentrations (Fig. 17).

In core section NYK3, a continuous tephra layer is situated at 0-6 cm (NYK3 1). The layer consists of dark grey, fine ash (Fig. 15). The concentrations of SiO_2 (49.69-50.24 wt%), TiO_2 (1.75-1.88 wt%), Al_2O_3 (13.56-14.15 wt%), FeO (12.25-12.93 wt%), K_2O (0.21-0.25 wt%), MgO (6.38-6.86 wt%), CaO (11.12-11.86 wt%) show narrow ranges.

Identification of basaltic tephra layers

The NYK3 1 tephra is very similar to NYK1 61 in its visual characteristics and major element composition. Both tephra layers have TiO_2 concentrations of ~1.9 wt%, that are characteristic for tephra layers originating at the Veiðivötn-Bárðarbunga volcanic system (Larsen et al., 2002). The major element chemical compositions of NYK1 61 and NYK3 1 correlates well with the composition of V1477 (Fig. 17; Larsen et al., 2002; Gudmundsdóttir et al., 2011, 2016; Vakhrameeva et al., 2020). However, published analyses of the V1477 tephra show slightly broader ranges than the geochemical data of both analyzed basaltic tephra layers (Fig. 17). Dispersal maps show that during the V1477 eruption volcanic material got deposited in the eastern half of Iceland and therefore V1477 tephra deposits can be expected in the Vopnafjörður area (Fig. 35; Larsen & Thorarinsson, 1977; Larsen et al., 2002; Gudmundsdóttir et al., 2011). The previously described V1477 layer, situated in the sediment record of lake Lögurinn (Gudmundsdóttir et al., 2016) and ÞUR2 1 are visually very similar to NYK1 61 and NYK3 1. The visual correlation of both basaltic tephra layers with an identified V1477 marker layer therefore supports the geochemical correlation.

In core section NYK2, another dark grey tephra layer is situated at 0-7 cm. The layer visually resembles the NYK1 61 and NYK3 1 layers and is therefore assumed to display the same tephra marker layer.

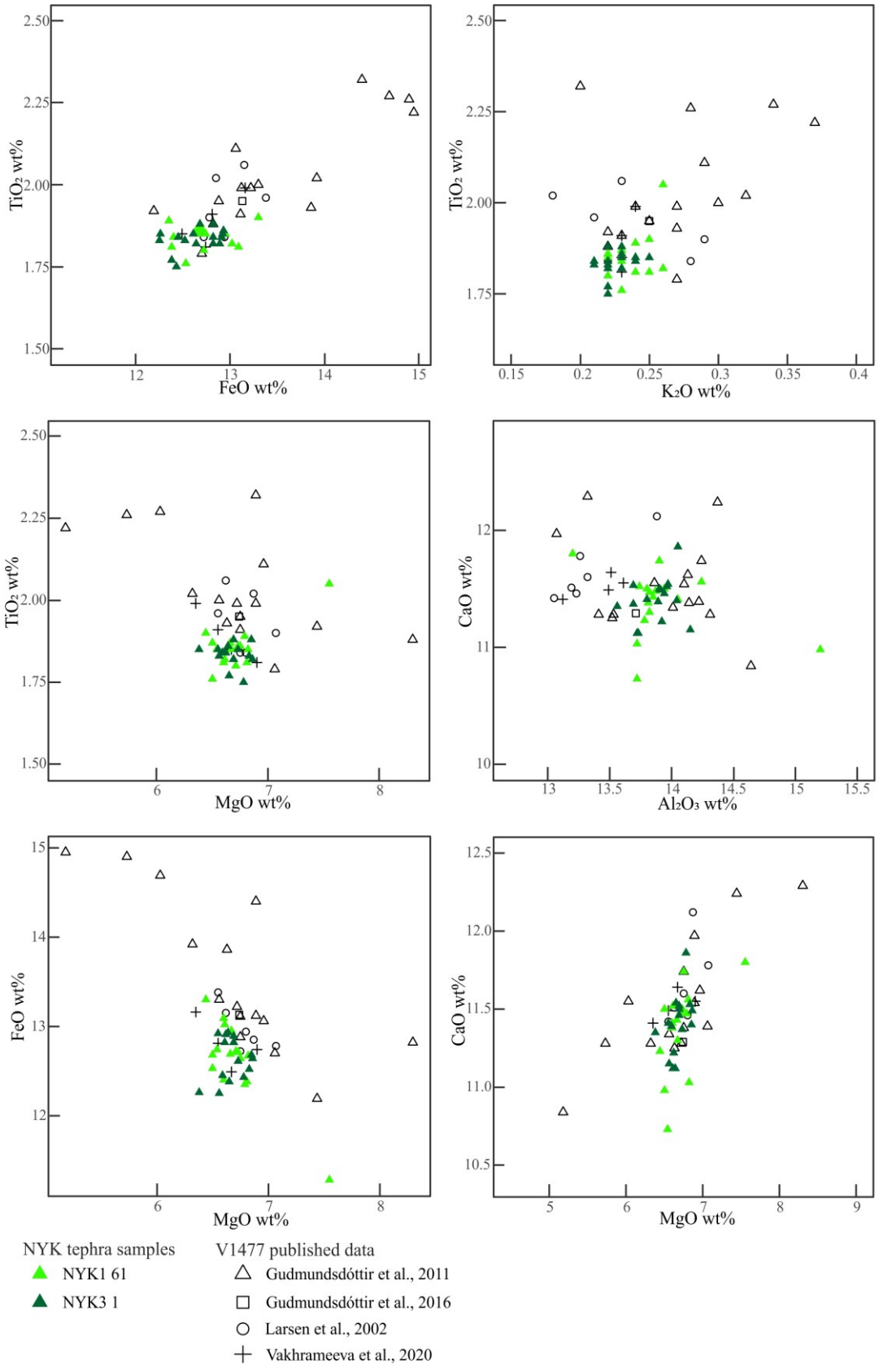

Figure 17. *Binary plots of major element oxide values analyzed for the NYK basaltic tephra layers. Plots show the correlation of the NYK1 61 and NYK3 1 tephra layer with the V1477 marker layer.*

5.2.1.4 Ásbrandsstaðavatn sediment core – tephra marker layers

In the sediment sequence of Ásbrandsstaðavatn, four tephra layers were identified as marker layers. Two silicic tephra layers have been identified to originate at Hekla volcano and have been correlated to the marker layers H3 and H4. A third silicic tephra layer, that originates from the Askja volcano, has been correlated to the Askja S marker layer (Table 3). Two samples collected from a massive basaltic tephra layer have been identified as the Saksunarvatn Ash, originating from Grímsvötn (Table 3). The Askja S layer (ca. 10.8 cal. kyr BP) is the oldest identified marker layer in the ABS sediment sequence, and the Hekla 3 layer is the youngest identified marker layer. The positions of the tephra layer in the core sequences are shown in Fig. 24.

Description of silicic tephra layers

Four tephra layers (ABS1 130, ABS2 22, ABS2 63 and ABS4 97), have been observed in the ABS sediment sequence. In core section ABS1 a continuous tephra layer with a thickness of ~1.5 cm is situated at 130-131 cm (ABS1 130). The tephra layer has a light grey color and consist of fine ash (Fig. 18). The ABS1 130 tephra is characterized by a wide range in the SiO_2 concentration (65.43-72.87 wt%). The concentration of TiO_2 (0.16-0.39 wt%), K_2O (1.98-2.54 wt%), MgO (0.1-0.66 wt%) and CaO (1.89-3.21 wt%) show relatively narrow ranges, whereas the FeO concentration range is broader. The geochemical data of ABS1 130 shows outliers (Fig. 19) with very low K_2O concentration (0.68 wt%) and slightly higher CaO concentration (3.92 wt%) than the average.

In core section ABS2, a tephra sample (ABS2 22) was taken from a discontinuous tephra layer or patch at 22 cm. The tephra patch consists of light grey, fine ash, similar to the material of ABS1 130 (Fig. 18). SiO_2 concentrations measured in ABS2 22 lie between 69.1 wt% and 72.09 wt%. The geochemistry of the ABS2 2 tephra is characterized by small ranges in TiO_2 (0.17-0.21 wt%), FeO (3.0-3.34 wt%), K_2O (2.38-2.45 wt%), MgO (0.09-0.17 wt%) and CaO concentrations (1.89-2.02 wt%) (Fig. 19). Only few tephra shards could be measured for ABS2 22, resulting in only few data points. Because of the shape of the tephra deposit, it is uncertain if the tephra patch is a dislocated rip-up clast, being transported and redeposited at a different depth. However, because the tephra deposit was situated in the center of the core and not on the edge it was assumed that the deposit was not dragged down.

A second continuous tephra layer (ABS2 63) with a thickness of 2 cm, is located in core section ABS2 between 62 cm and 65 cm. The tephra layer is dark grey and consists of medium and fine ash that is fining upwards (Fig. 18). ABS2 63 shows a wide range in the SiO_2 concentration (60.37-74.28 wt%). Similar broad ranges can be seen in the FeO (1.17-9.71 wt%) and CaO concentrations (1.26-4.62 wt%), whereas the concentrations of TiO_2 (0.07-0.9 wt%), K_2O (1.5-2.84 wt%) and MgO (0.01-1.05 wt%) show a narrower range.

In the bottom of core section ABS4, a continuous tephra layer with a thickness of 11 cm is situated at 93-104 cm (ABS4 97). The tephra layer has a grey color and consists of fine ash material (Fig. 18). ABS4 97 has a relatively small range in the SiO_2 concentration (69.52-75.48 wt%). Similar small ranges were measured in TiO_2 (0.24-0.38 wt%), FeO (2.48-2.77 wt%), K_2O (2.32-2.59 wt%), MgO (0.21-0.32 wt%) and CaO (1.41-1.61 wt%) concentrations.

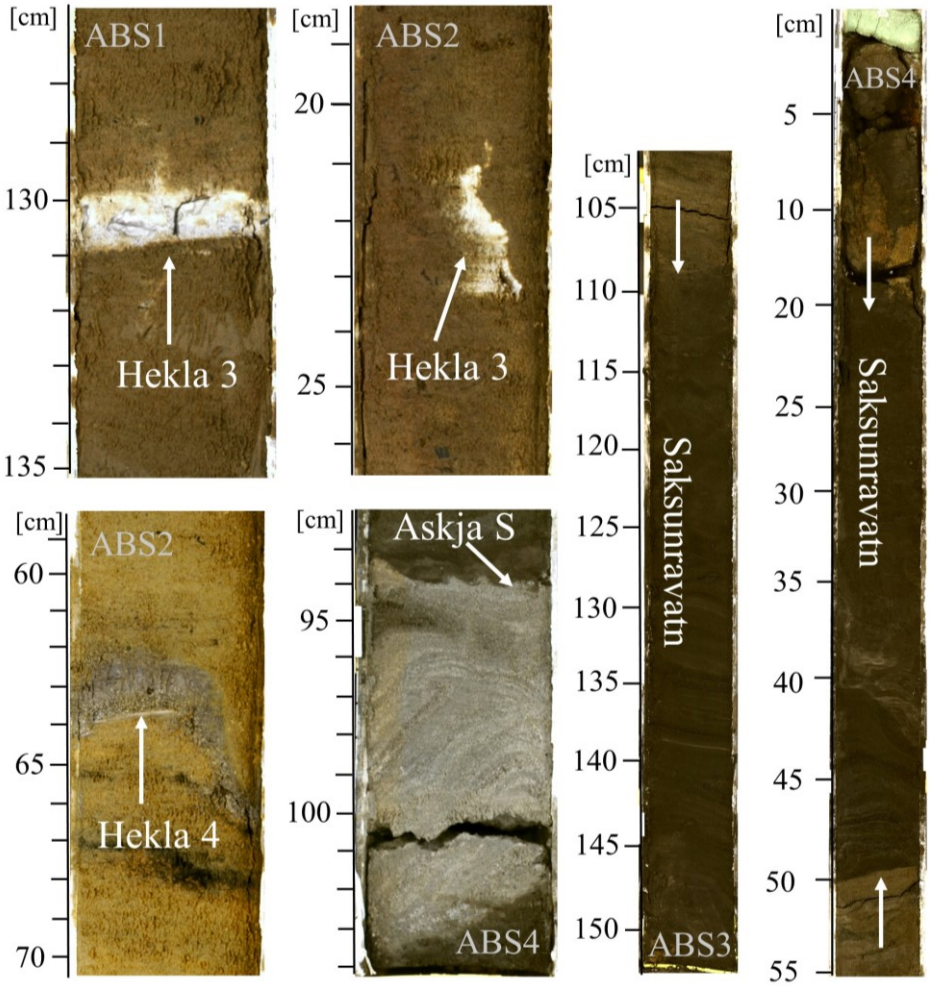

Figure 18. *Visual tephra layers contained in the sediment sequences of Ásbrandsstaðavatn. Four different tephra marker layers have been identified: Hekla 3, Hekla 4, Saksunarvatn and Askja S.*

Identification of silicic tephra layers

The silicic tephra layers ABS1 130, ABS2 22 and ABS2 63 are characterized by low TiO_2 concentrations, affiliated to the Hekla volcano (Larsen et al., 2002). The major element compositions of ABS1 130 and ABS2 22 correlate with geochemical compositions of tephra layers, identified as H3 (Fig. 19; Larsen et al., 2002; Sverrisdottir, 2007; Óladóttir, 2009; Meara, 2011; Óladóttir et al., 2011; Gudmundsdóttir et al., 2016; Meara et al., 2019). In ABS1, the typical wide range in SiO_2 concentrations (62.10-75.19 wt%) and FeO concentrations (1.05-10.07 wt%) that can be seen in H3 tephras (Meara et al., 2019), can also be observed. The smaller range of SiO_2 concentration in ABS2 22 (Fig. 19) is assumed to be caused by the small number of data points. However, the available range of ABS2 22 fits in the typical H3 SiO_2 concentration range. Concentrations of TiO_2, FeO, K_2O, MgO, CaO from published analysis correlate well with ABS1 130 and ABS2 22. The identification of ABS1 130 and ABS2 22 as H3 is supported by their similar visual characteristics and the lack of other tephra layers in the ABS core that consist of light grey ash. Ásbrandsstaðavatn is located close to Nykurvatn, which suggests that H3 deposits in the lake should have a similar thickness of ~2 cm (Larsen & Thorarinsson, 1977; Meara et al., 2019). This is consistent with the thickness of the ABS1 130 tephra layer. A ^{14}C age of 3750 ± 85 cal. yr BP (Table 3) obtained from the sediments below ABS2 22 further supports the identification as H3, as the marker layer has a younger age of ca. 3.0 cal. kyr BP. Additionally, both ABS1 130 and ABS2 22 look very similar to tephra layers in NYK2 at 116-117 cm and NYK3 at 55-58 cm which have also been identified as H3.

The major element composition of ABS2 63 correlates to the geochemical composition of H4 (Fig. 19; Dugmore et al., 1992; Sverrisdottir, 2007; Óladóttir, 2009; Gudmundsdóttir et al., 2016; Meara et al., 2019). As presented in Fig. 19, both reference data of the H4 tephra and geochemical data of ABS2 63 show a relatively widespread pattern with a rhyolitic and andesitic component. The previously mentioned thickness of H4 deposits in the Vopnafjörður area of ~2 cm (Larsen & Thorarinsson, 1977; Meara et al., 2019), has also been observed in the ABS2 63 layer. The ABS2 63 tephra was located stratigraphically below a ^{14}C age of 3750 ± 85 cal. yr BP, further supporting the correlation to H4 (ca. 4.2 cal. kyr BP; Dugmore et al., 1995). The identification is also supported by a visual correlation of the ABS2 63 layer with the NYK3 98 tephra, which has the same color and has also been correlated to H4.

The major element chemical composition of ABS4 97 correlates to the geochemical composition of Askja S (Gudmundsdóttir et al., 2011; Kearney et al., 2018) The Askja S tephra is characterized by highly evolved SiO_2 concentrations and high MgO and TiO_2 content and low K_2O concentrations, making it relativley easy to geochemically differentiate the tephra from silicic Hekla tephras (Fig. 19; e.g., Larsen et al., 1999; Gudmundsdóttir et al., 2011; Kalliokoski et al., 2018; Kearney et al., 2018). The nearly identical ranges in chemical compositon that have been analyzed for ABS4 97, indicate a strong compositional correlation. Sigvaldason (2002) and Gudmundsdóttir et al. (2011) suggest that the Askja S tephra have been transported to and deposited in Northeast Iceland (Fig. 35). It can therefore be expected to find the Askja S marker layer in the sediment sequence of ABS. The identification of ABS4 97 as Askja S is also supported by the stratigraphic position below a massive black tephra layer situated in the ABS core (later) identified as the Saksunarvatn Ash.

Description of basaltic tephra layers

One massive tephra layer has been observed in the ABS sediment sequence. Four samples were collected from two core sections (ABS3 117, ABS3 147, ABS4 18 and ABS4 48). The tephra samples are characterized by their basaltic composition with low concentrations in SiO_2 (~49-50 wt%).

Samples ABS3 117 and ABS3 147 were collected from a ca. 40 cm thick basaltic tephra layer, located in the bottom of core section ABS3 between 108-152 cm. The tephra layer is black and consists of fine ash (Fig. 18). Several grey layers have been observed in the massive tephra deposit (Fig. 18). ABS3 117 is characterized by high TiO_2 (2.55-3.13 wt%), FeO (13.75-15.07 wt), MgO (5.14-5.98 wt%) and CaO (9.32-10.66 wt%) concentrations and low K_2O concentration (0.31-0.49 wt%). ABS3 117 shows several outliers in its geochemistry data with higher K_2O values (~1.3 wt%) and lower MgO values (~4.51 wt%). ABS3 147 shows nearly identical ranges in TiO_2 (2.41-3.08 wt%), FeO (13.27-13.33 wt%), MgO (5.15-5.95 wt%), CaO (9.74-10.67 wt%) and K_2O (0.36-0.46 wt%).

Samples ABS4 18 and ABS4 48 were collected from a ca. 53 cm thick tephra layer, located at the top of core section ABS4 between 0-53 cm. The tephra layer consists of black fine ash and several grey layers have been overserved in the deposit (Fig. 18). The layer is visually very similar to the black tephra located in ABS3.

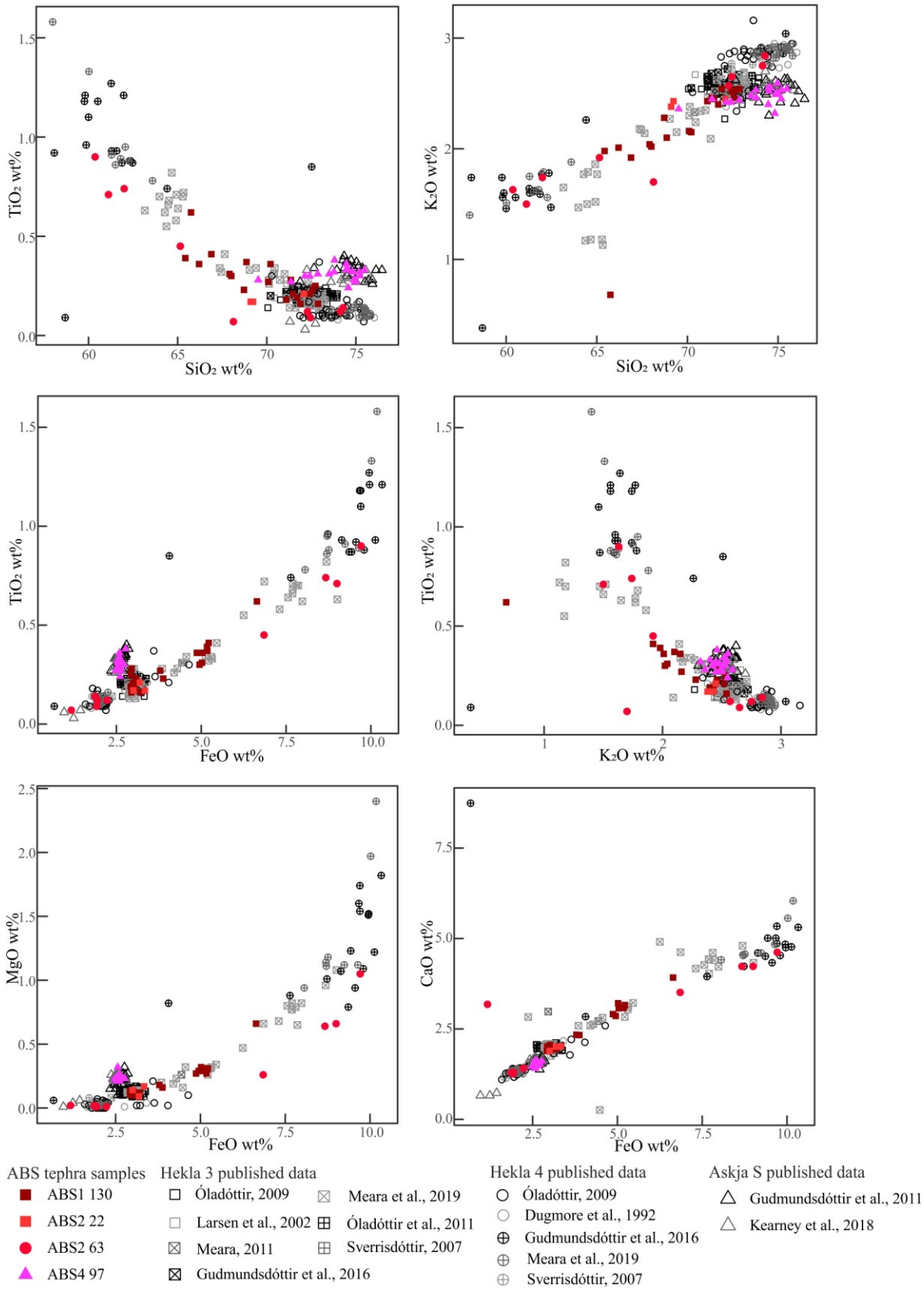

***Figure 19**. Binary plots of major element oxide values analyzed for the ABS silicic tephra layers. Plots show the correlation of ABS1 130, ABS2 22, ABS2 63 and ABS4 97 with the Hekla 3, Hekla 4 and Askja S marker layer.*

ABS4 18 is characterized by high TiO_2 (1.36-3.22 wt%), FeO (11.35-15.38 wt%), MgO (4.21-7.66 wt%) and CaO (8.72-12.40 wt%) concentrations and low K_2O concentrations.The major element composition of ABS4 48 shows ranges in TiO_2 (2.53-3.16 wt%), FeO (13.23-14.50 wt%), MgO (3.97-6.11 wt%), CaO (9.41-10.93 wt%) and K_2O (0.37-0.54 wt%), that are very similar to ABS4 18.

Identification of basaltic tephra layers

The massive basaltic tephra layers situated in the ABS3 and ABS4 have been identified as the Saksunarvatn Ash (Table 3). Four samples, ABS3 117, ABS3 147, ABS4 18 and ABS4 48, taken from two visually very similar layers, all have low SiO_2 and TiO_2 concentrations of ~2.2-3.5 wt% affiliated with the Grímsvötn volcanic system (Larsen & Eiríksson, 2008).

The major element chemical compositions measured in the samples correlate with the composition of tephra layers that were previously identified as Saksunarvatn Ash (Fig. 20; Mangerud et al., 1986; Björck et al., 1992; Ingólfsson, et al., 1995; Birks et al., 1996; Kristjánsdóttir et al., 2007; Gudmundsdóttir et al., 2011). The published analyses of the Saskunarvatn Ash show near identical ranges in concentrations of K_2O, MgO, TiO_2, Al_2O_3 and FeO to the concentrations analyzed in the basaltic ABS layers (Fig. 20). The geochemical identification of all four samples as the Saksunarvatn Ash is supported by the very similar visual characteristics of the two tephra deposits. As previously mentioned, deposits of the wide-spread Saksunarvatn Ash can be found almost all over Iceland (Fig. 35; Gudmundsdóttir et al., 2011; Óladóttir et al., 2020), supporting the finding of the marker layer in the sediment sequence of ABS. The tephra deposit found in the ABS core sections also has very similar visual characteristic to previously described the Saksunarvatn Ash deposits (Óladóttir et al., 2020). Another characteristic supporting the identification of ABS3 117, ABS3 147, ABS4 18 and ABS4 48 as Saksunarvatn tephra is the thickness of the tephra layer. No other tephra layers originating from Grímsvötn of a similar thickness have been identified on Iceland (Óladóttir et al., 2020). Gudmundsdóttir et al. (2016) also identified the Saksunarvatn marker layer in a sediment sequence of lake Lögurinn, ~60 km southeast of Ásbrandsstaðavatn (Fig. 1B). The layer in ABS is also visually and geochemically very similar to a basaltic tephra layer (TDV2-6 129; TDV2-7 16) situated in the TDV core, that was identified as the Saksunarvatn Ash.

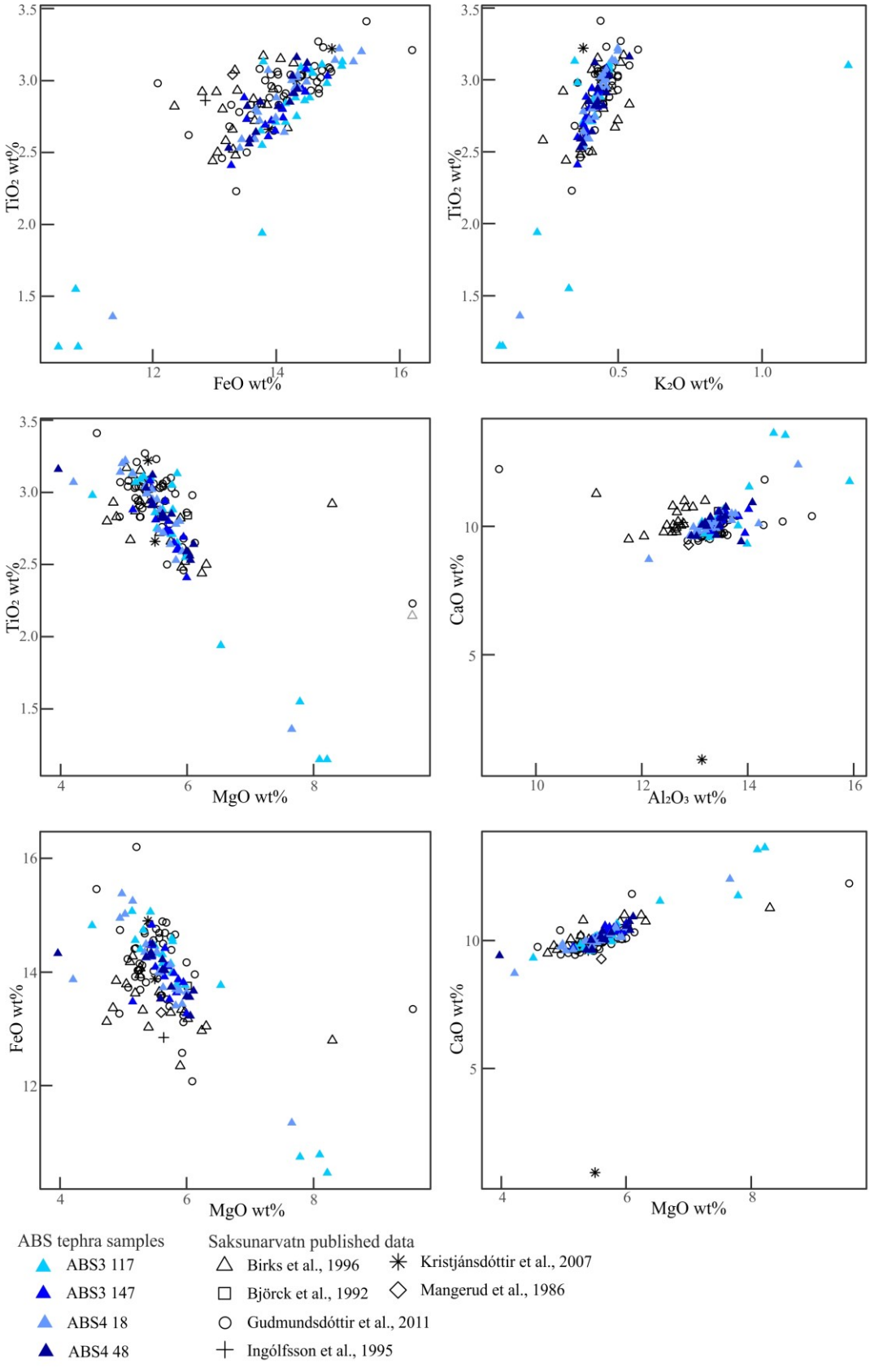

Figure 20. *Binary plots of major element oxide values analyzed for the ABS basaltic tephra layers. Plots show the correlation of ABS3 117 and ABS3 147 with the Saskunarvatn marker layer.*

5.3 Alignments of sediment core sections

5.3.1 Alignment of Torfdalsvatn core sections

The continuous lacustrine record of Torfdalsvatn consists of seven overlapping core sections. The correlation of the individual TDV core sections is rather difficult, as the sections seem to only have minor overlaps and similar lithologies.

The correlation of the core sections TDV2-1 and TDV2-2 is primarily based on a tephra marker, Hekla 1104, located in TDV2-1 at 114-115 cm (Fig. 21). The sediments of TDV2-2 do not contain a tephra layer correlating with the H1104 tephra marker, indicating that the position of TDV2-2 is below the TDV2-1 tephra layer. Similar trends in the MS and Ti/(inc+coh) in both core sections suggest that the sediments between 119 cm and 125 cm in TDV2-1 overlap with the sediments from 0 cm to 17 cm in TDV2-2. The overlapping sediment section (thickness ~6 cm) in TDV2-1 is compressed compared to the same interval in TDV2-2. After inserting the tie-points into AnalySeries, a composite depth of TDV2-2 at 112-241 cm was constructed.

Core sections TDV2-2 and TDV2-3 were aligned partly based on two basaltic (unidentified) tephra layers located at 129 cm and at 131 cm in TDV2-2, that are represented by two peaks in the Ti/(inc+coh) data (Fig. 21). No comparable geochemical signals and tephra layers were found in core section TDV2-3. It was therefore assumed that sediments below the tephra layers in TDV2-2 therefore overlap with the TDV2-3 sediments. The MS and Ti/(inc+coh) data in the lower sediments of TDV2-2 (131-139.5 cm) and upper sediments of TDV2-3 (0-14 cm) show similar trends (Fig. 21) and are believed to correlate. Similar to the alignment of TDV2-1 and TDV2-2, the sediments in TDV2-2 are compressed compared to the overlapping sediment section in TDV2-3. The composite depth of TDV2-3 was determined to be 232-370 cm.

The alignment of TDV2-3 and TDV2-4 was partly based on the same tephra layer, that is presumably contained in the sediments of both core sections. A tephra layer (identified as H3) located between 1-2 cm in core section TDV2-4, had a similar Ti/(inc+coh) signal as a tephra layer in TDV2-3 at ~137 cm (Fig. 21). The geochemical signal may be caused by an identical tephra layer that is not as visible in TDV2-3. The sediments at that depth appear to be of similar color as the tephra layer in TDV2-4, which might indicate that the H3 layer is also

contained in the TDV2-3 core. It was, therefore, assumed that the tephra layer represents a tie-point between the core sections. Based on the tephra and Ti/(inc+coh) data, an overlap between these core sections was identified at 135-141 cm in TDV2-3 and between 0-8 cm in TDV2-4. The overlapping sediments in TDV2-3 are less thick than TDV2-4 and comparably slightly compressed. Based on these correlations the composite depth of TDV2-4 was constructed to be from 364 cm to 469 cm.

The core section TDV2-4 contains a ca. 1 cm thick, rhyolitic tephra layer that is located at ~ 99 cm (Fig. 21) and was identified as the H4 layer. No comparable tephra layer was found within the sediments of TDV2-5. It was therefore assumed that the TDV2-5 core section is positioned stratigraphically below the H4 layer in TDV2-4. The correlation of the similar trending Ti/(inc+coh) and MS data, suggested an overlap of the core sections between 141 cm and 146 cm in TDV2-4 with 0 cm to 28 cm in TDV2-5. Based on the position of the tie-points, the alignment of TDV2-4 and TDV2-5 revealed a composite depth of 464-549 cm for TDV2-5.

The overlap of core segments TDV2-5 and TDV2-6 was determined based on two (unidentified) tephra layers (Fig. 21). Two black tephra layers, located in TDV2-5 at 132 cm and at 136 cm, have also been observed in TDV2-6 at 8 cm and at 11 cm (Fig. 21). The layers show the same geochemical signals in both cores (note that the scale of Ti/(inc+coh) is different for TDV2-5 and TDV2-6). Therefore, as suggested by the geochemical data and correlating tephra layers, an overlap of sediments in TDV2-5 between 121 cm and 139.5 cm with the sediments of TDV2-6 between 0 cm and 17 cm was determined. The overlap is confirmed by another tephra layer, contained in the sediments of TDV2-6 at 15-16 cm (Fig. 21), which is believed to have caused a strong increase in Ti. The same tephra layer cannot be seen in TDV2-5, suggesting that the core sections is located stratigraphically above the tephra layer in TDV2-6. The overlapping section of TDV2-6 is slightly compressed compared to the overlapping sediments in TDV2-5. Through the alignment a composite depth of 537-632 cm was constructed for TDV2-6.

The alignment of the sections TDV2-6 and TDV2-7 is based on the presence of the same tephra marker in both cores (i.e., TDV2-6 129 and TDV2-7 16; Fig. 21). In TDV2-6, the Saksunarvatn Ash can be found between 127 cm and 131 cm (Fig. 10). The same tephra

marker is located in TDV2-7 at 0-17 cm (Fig. 21). A peak in the Ti/(inc+coh) data, identified in both core segments, was used as a tie-point for determining the overlap. Based on the tie-point the lower part of the tephra layer in TDV2-6 (~128-131 cm) is overlapping with the upper part of the tephra layer in TDV2-7 (~0-4 cm). The composite depth of TDV2-7 is 630-715 cm.

The composite length of the TDV core after aligning the individual core section is 715 cm. However, because of the small overlaps between the core sections only a few tie-points were put into AnalySeries, which may make the correlation less reliable. Therefore, the composite depth and locations of certain tephra markers within the TDV core were compared to the length of sedimentary records from the same lake by Björck et al. (1992); Rundgren (1995) and Florian (2016) and found to be consistent.

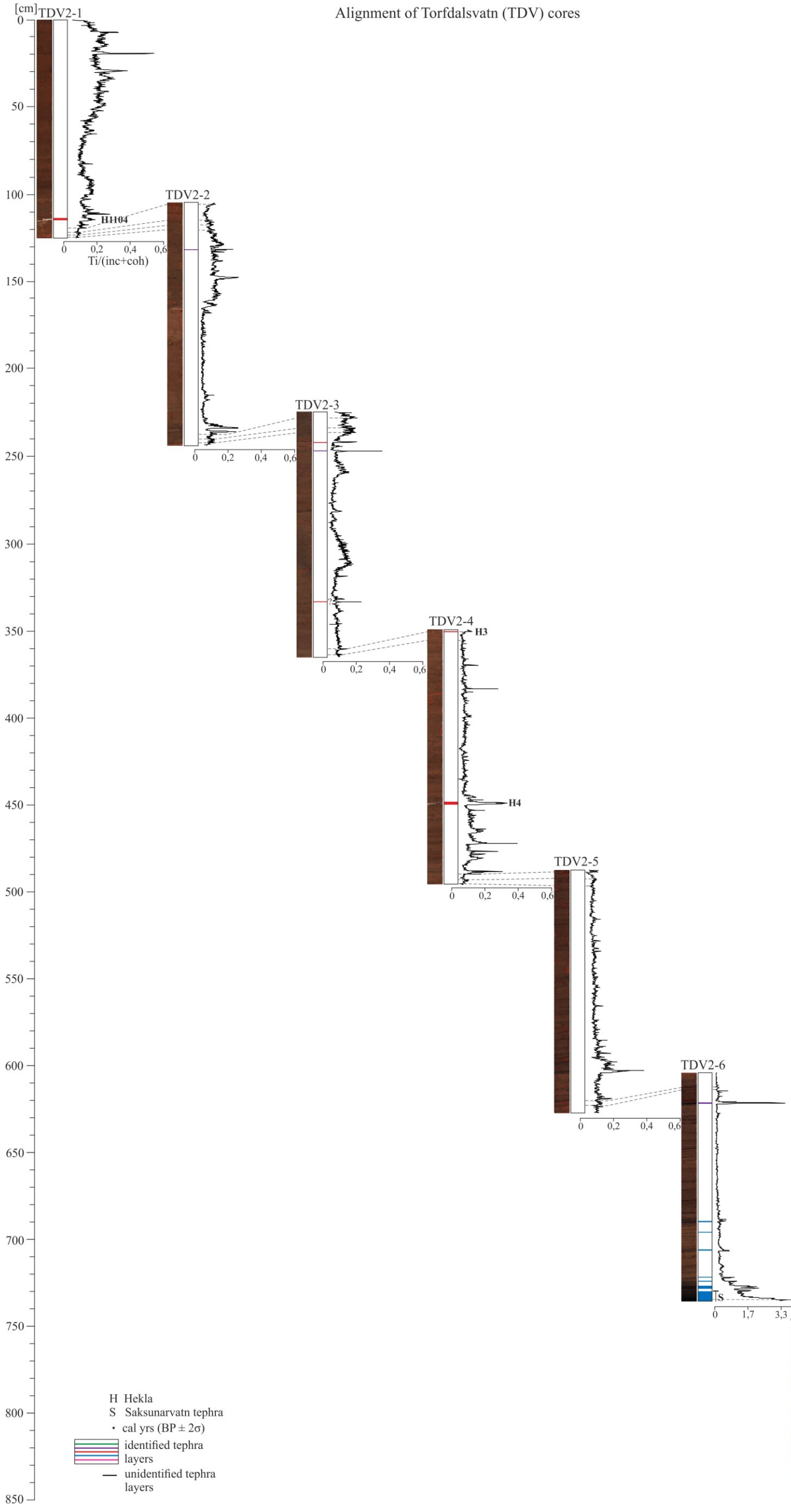

Figure 21. *Alignment of the Torfdalsvatn core sections showing the lithology, Ti/(inc+coh) data [cps], and position of tephra layers within the individual core sections (colors refer to volcanic systems in Fig. 5). Tie-points used for aligning the core sections and construction composite depths in AnalySeries are indicated as dashed lines.*

5.3.2 Alignment of Þuríðarvatn core sections

The continuous lacustrine record of Þuríðarvatn consists of two core sections (Fig. 22). In core section ÞUR1, a radiocarbon date, located between 135-136 cm (Fig. 22), was determined to have an age of 387 ± 49 cal. yr BP (Table 2). The core section ÞUR2 contains a ca. 4 cm thick basaltic tephra layer, located between 0 cm and 4 cm (Fig. 22). The tephra layer was identified as V1477, having an age of 470 cal. yr BP (Table 3). The absence of the V1477 tephra layer in the sediments of ÞUR1 led to the assumption that the core sections do not overlap but directly align. This assumption is supported by the older age of the V1477 tephra layer in ÞUR2, than the radiocarbon dated material contained in ÞUR1. The alignment is furthermore supported by the Ti/Sum data from both cores, which show distinct trends. Additionally, sedimentological variations between the core sections further support the assumption that they do not overlap. As no sediments are contained above the V1477 layer in the ÞUR2 core section, it has been assumed that the core sections directly align. However, it might also be also possible that a hiatus is present between the two core sections and the core sections do not directly align. To confirm the alignment and determine if a hiatus is present another core would need to be collected from the lake.

Because the cores are believed to directly align no tie-points were put into the program AnalySeries for the alignment, meaning that both cores retain their original length. The composite depth of ÞUR1 is 0-151 cm and the composite depth of ÞUR2 is from 151 cm to 304 cm. The total length of the ÞUR core after alignment is 304 cm.

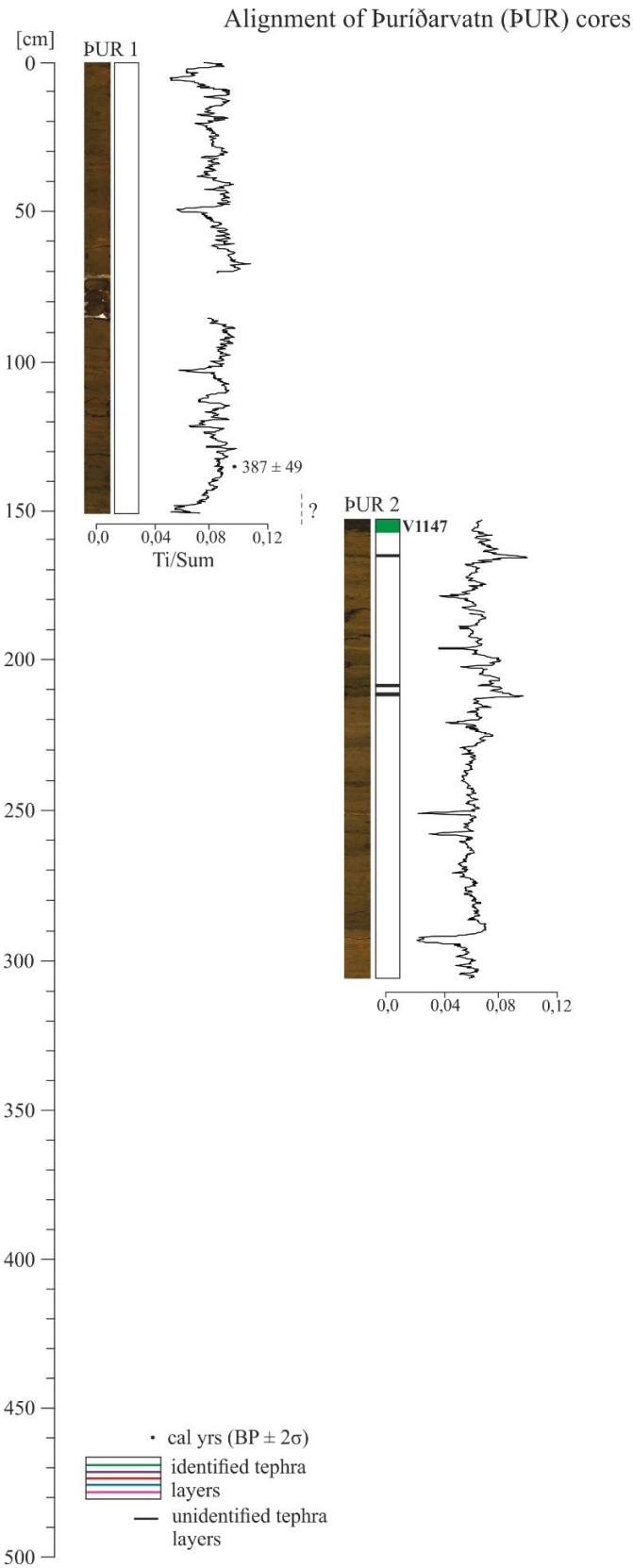

Figure 22. *Alignment of the Þuríðarvatn core sections showing the lithology, Ti/Sum data [cps], position of radiocarbon date and position of tephra layers within the individual core sections (colors refer to volcanic systems in Fig. 5).*

5.3.3 Alignment of Nykurvatn core sections

The continuous record of Nykurvatn consists of five overlapping core sections (Fig. 23). The overlap of NYK1 and NYK2 is partially based on a tephra layer, identified as V1477, which was found in both sequences. The ca. 7 cm thick, basaltic tephra layer is located at 59-64 cm in NYK1 and at 0-8 cm in NYK2 (Fig. 23). The identification of the same tephra marker in both cores, indicates that the sediments in NYK1 stratigraphically below the V1477 layer are overlapping with sediments from NYK2. Based on their similar geochemical signal, a second basaltic tephra layer located at 81 cm in NYK2, was aligned to a basaltic tephra layer found in NYK1 at 124 cm (Fig. 23). The tephra layer is located at the bottom of the NYK1 core section, and was therefore used as a lower boundary. The sediments located between both tephra layers, are aligned by similar trends in the Ti/Sum data. It was determined that the sediments of NYK1 between 59 cm and 126 cm are overlapping with the sediments of NYK1 between 0 cm and 84 cm. As shown in Fig. 23, the sediments of NYK1 between 60-105 cm appear to be stretched compared with the overlapping sediments in NYK2 between 0-50 cm. The overlapping sediments of NYK1 between 105 cm and 126 cm are, however, compressed compared to the NYK2 sediments between 50 and 84 cm. The composite depth of NYK2, after the alignment, was constructed by AnalySeries to be 60-182 cm.

The same basaltic tephra layer (V1477 layer) that was found in NYK1 and NYK2 is also present in the core section NYK3 at 0-7 cm (Fig. 23). The layer was used as an upper boundary for the alignment of NYK2 and NYK3. A prominent rhyolitic tephra layer (H3), was also found in both cores and is therefore used as a tie-point for the alignment. The silicic layer is located at 116-118 cm in NYK2 and at 55-58 cm in NYK3 (Fig. 23). Two other correlating basaltic tephra layers contained in both core section and located at 25 cm and 81 cm in NYK2 and at 16 cm and 39 cm in NYK3, combined with the Ti/Sum data, are used for aligning the sediments between the V1477 layer and H3 layer. Three basaltic tephra layers located at 29 cm, 31 cm and 33 cm in NYK2 were also observed in NYK3 at 20 cm, 21 cm and 23 cm (Fig. 23), confirming the alignment. Another basaltic tephra layer found in both core sections (NYK2 at 147-148 cm and NYK3 at 76-77 cm; Fig. 23), identified to originate from the Katla volcano, has been used for a lower boundary for the alignment. A rhyolitic tephra layer (H4), located at 97-100 cm in NYK3 (Fig. 23) has not been observed in NYK2, which supports the assumption that the overlap ends above this layer. The sediments between the (assumed) H3 layer and the lower basaltic Katla layer are aligned by trends in the Ti/Sum

data. The correlation of the tephra layers and Ti/Sum data indicates that the full length of NYK2 overlaps with the sediments in NYK3 from 0 cm to 82 cm. The complete overlapping section of NYK3 is compressed compared to the sediments of NYK2. The brownish color of the overlapping sediments is similar between the core sections, supporting the alignment. The composite depth of the NYK3 core sections was determined to be 60-230 cm. (Note: both the V1477 layer and the Katla layer located at NYK2 81 cm were used for aligning NYK1 and NYK2 and therefore also show an overlap in the NYK1 and NYK3 core sections).

The alignment of NYK3 and NYK4 is mainly based on the Ti/Sum data of both core section, as well as a few tephra layers. The H4 tephra layer, located at 97-100 cm in NYK3 (Fig. 23), cannot be found in NYK4, which indicates that the overlap begins stratigraphically below the tephra layer. A basaltic tephra layer found in both NYK3 (at 145 cm) and NYK 4 (at 88 cm) was used as lower end of the alignment. The tephra layer in NYK3 was identified to originate from Katla, as presented in Fig. 23. The sediments in NYK3, which are stratigraphically below the H4 layer, have been aligned to the NYK4 sediments by comparing trends in the Ti/Sum data. An overlap of sediments between 106 cm and 151 cm in NYK3 with the sediments in NYK4 between 0 cm and 80 cm was thereby determined. The overlapping sediments in NYK3 are compressed compared to the overlapping section in NYK4. After correlating the core sections, NYK4 was found to have a composite depth of 200-258 cm.

The NYK5 core section is characterized by a thick basaltic tephra layer, that was found to originate from two volcanic systems (i.e., Veiðivötn-Bárðarbunga and Katla). No comparable tephra layer is contained in the sediments of core section NYK4. Additionally, two ^{14}C dates, obtained from macrofossils collected in NYK5 at 62-63 cm and 133-134 cm (Fig. 23), have ages of >7.0 cal. kyr BP, and are therefore significantly older than the H4 layer in NYK3. It was therefore determined that the NYK5 is located stratigraphically below the tephra layer and that the core sections directly align. Based on this alignment, the composite depth of NYK5 was determined to be 258-410 cm. The alignment of NYK5 with the other four core sections might be less reliable, because the core section was collected at a different location in Nykurvatn and because of the possibility of a hiatus between NYK4 and NYK5. The presence of a hiatus cannot be determined without resampling the lake and it was therefore decided to directly align the cores. The length of the continuous NYK core, after aligning all five core sections, is 410 cm.

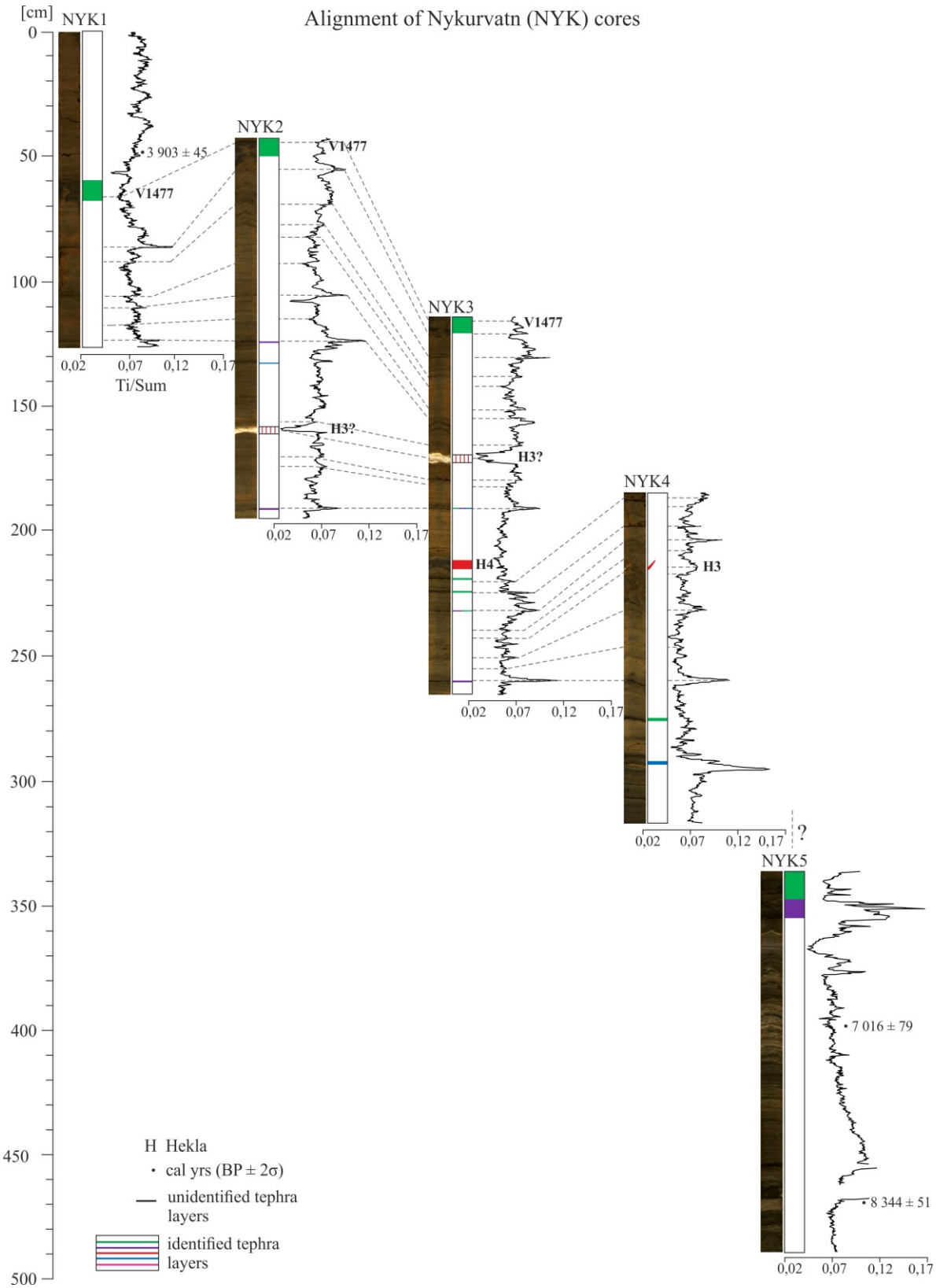

Figure 23. *Alignment of the Nykurvatn core sections showing the lithology, Ti/Sum data [cps], position of radiocarbon date and position of tephra layers within the individual core sections (colors refer to volcanic systems in Fig. 5). Tie-points used for aligning the core sections and construction composite depths in AnalySeries are indicated as dashed lines.*

5.3.4 Alignment of Ásbrandsstaðavatn core sections

The sediment record of Ásbrandsstaðavatn (ABS) consists of four overlapping core sections (Fig. 24). The overlap of ABS1 and ABS2 was determined based on a prominent silicic tephra layer, identified as H3, was found in both core sections and used as a tie-point (Fig. 24). In ABS1 the continuous silicic layer is located at 130-131 cm and in ABS2 at 20-23 cm. Another tie-point was identified through the geochemical signal (i.e. Ti/Sum) of a basaltic (Katla and Veiðivötn-Bárðabunga) tephra layer located at 113-116 cm in ABS1, that shows a very similar Ti/Sum data signal as sediments in ABS2 at 6-8 cm. The sediments located stratigraphically below the H3 tephra layer were aligned based on Ti/Sum data. Based on several tie-points (Fig. 24), the sediments of ABS1 at 104-147 cm are believed to overlap with the sediments of ABS2 from 0-39 cm. The overlapping sediments of ABS2 are compressed compared to the corresponding sediments of ABS1. The composite depth of ABS2 after the alignment is 102-214 cm.

The core section ABS2 contains the H4 tephra layer, which has not been observed in ABS3. This suggests that an overlap of both core sections begins below the H4 tephra layer. A basaltic tephra layer, located in ABS2 at 97-98 cm and characterized by a peak in Ti/Sum, can also be observed in ABS3 at 2 cm (Fig. 24). Both tephra layers were identified to originate from the Veiðivötn-Bárðabunga volcanic system and can therefore be assumed to display the same layer. The correlating basaltic tephra layer is used as a tie-point and represents the start of the overlap. The sediments in ABS2 (98-147 cm) that are stratigraphically below the basaltic tephra layer are characterized by a dark brown color. Sediments of similar color have been observed in ABS3 between 2-24 cm. The sediments in ABS3 below 24 cm show a change in color to olive-brown, that cannot be seen in the bottom sediments of ABS2. The lithology and tephra layer suggest that the cores overlap from 94-147 cm (ABS2) with 0-24 cm (ABS3). The sediments in ABS3 appear to be compressed (thickness of 24 cm), compared to the corresponding sediments in ABS2 (thickness of 53 cm). Through alignment the composite depth of ABS3 was determined to be 181- 304 cm.

The exact overlap of core sections ABS3 and ABS4 is difficult to determine. Both core sequences contain the massive Saksunarvatn tephra. The tephra layer in ABS3 is located at the bottom between 108-152 cm and in ABS4 at the top between 0-53 cm (Fig. 24). An overlap of the core segments based on the Ti/Sum can be constructed, however the

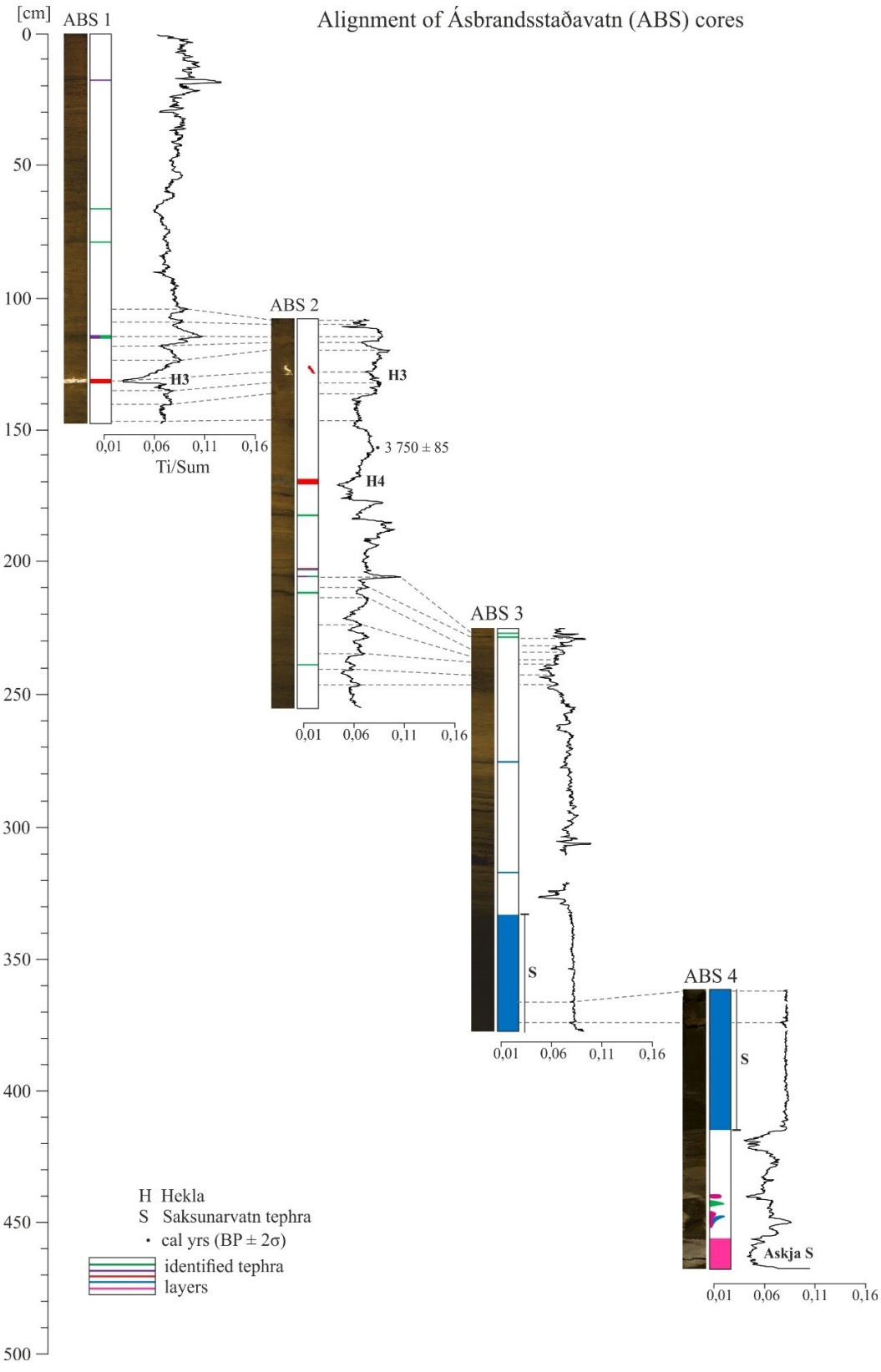

***Figure 24**. Alignment of the Ásbrandsstaðavatn core sections showing the lithology, Ti/Sum data [cps], position of radiocarbon date and position of tephra layers within the individual core sections (colors refer to volcanic systems in Fig. 5). Tie-points used for aligning the core sections and construction composite depths in AnalySeries are indicated as dashed lines.*

geochemical signal of the tephra layer does not show any significant trends, making the alignment more complicated. Therefore, two minor decreases in the Ti/Sum values within the Saksunarvatn tephra layer, observable in both core sections, were used as tie-points for the alignment. Based on these tie-points, it is assumed that the sediments between 140-152 cm in ABS3 overlap with the sediments between 0-16 cm in ABS4. The gap within the Saksunarvatn tephra layer in ABS4 explains the variation in thickness of the overlapping sections. The composite depth of core section ABS4, after aligning it to ABS3, is 297-380 cm. The continuous core length of ABS after aligning the four core sections is 380 cm.

5.4 Lithostratigraphy and Age-depth models

In the sediment sequences of Torfdalsvatn, Þuríðarvatn, Nykurvatn and Ásbrandsstaðavatn, three main sedimentary facies were identified: (1) An olive to brown gyttja facies with sand layers is characterized by organic content of 6-25%. (2) A clay or clayey gyttja facies that shows high MS and Ti values and low LOI values (0.4-4.5%). (3) Tephra deposits of varying thickness (between 1 mm and 64 cm) and geochemical composition that have been observed in both clay and gyttja facies and were interpreted as airfall material (e.g., Larsen & Eiríksson, 2008; see Chapter 5.2).

5.4.1 Torfdalsvatn sediment core

5.4.1.1 Description

The TDV sediment core is 715 cm long and has been divided into two sedimentary units: 1.1 and 1.2 (Fig. 25). MS counts and the Ti/(inc+coh) record are changing according to the units with higher values in Unit 1.1 and lower values in Unit 1.2.

Unit 1.1 (715-648 cm) consists of two facies: clay and clayey gyttja with several tephra layers (between 5 mm and 2 cm). In the lower part of the unit at 715-680 cm, grey homogeneous clay is present. In the upper part of the unit between 680-648 cm the core consists of grey-olive clayey gyttja (Fig. 25). The unit is characterized by high MS counts (up to 1500 10^{-5} SI) that decrease with increasing gyttja content. The Ti/(inc+coh) record of the units also contains high values with a similar decreasing trend observed in the MS counts. Both MS and Ti/(inc+coh) concentrations fluctuate throughout the unit with positive and negative peaks. Peaks in both records occur at the same depths that tephra layers were identified.

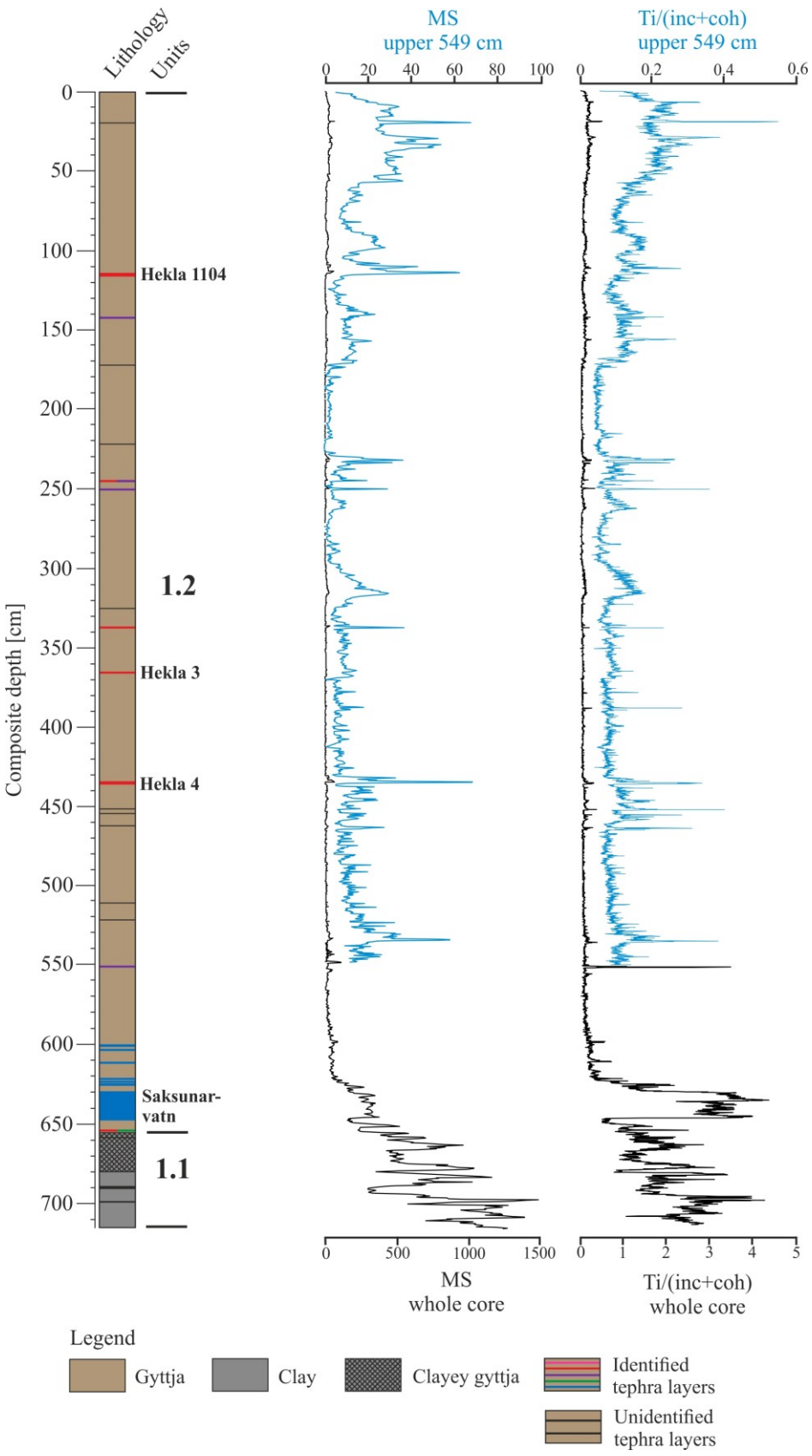

***Figure 25**. Lithological core log of TDV showing the unit divisions, facies, color, structures and tephra layers (colors refer to volcanic systems in Fig. 5). Magnetic Susceptibility and Ti/Sum records are displayed.*

Unit 1.1 and 1.2 are separated by an 18 cm thick Saksunarvatn tephra layer identified between 648-630 cm (Fig. 25). The tephra marker layers are highlighted by relatively high Ti/(inc+coh) values and MS counts of ~400 10^{-5} SI.

Unit 1.2 (630-0 cm) consists of massive olive-brown and brown gyttja with several tephra layers, including tephra marker layers at 435 cm (H4), 365 cm (H3) and 114 cm (H1104). The organic-rich sediments are characterized by low MS values (average ~12 10^{-5} SI) and low Ti/(inc+coh) concentrations with varying shades of color and amounts of plant macrofossils. Four changes in color were observed within the unit, with olive-brown gyttja between 648-318 cm, brown gyttja between 318-295 cm, olive-brown gyttja between 295-175 cm and brown gyttja in the upper part of the unit between 175-0 cm. The brown gyttja between 318-295 cm and 175-0 cm are characterized by a slight increase in MS values and Ti/(inc+coh) concentration compared to the lower part of the olive-brown gyttja. The MS and Ti/Sum record shows both negative and positive peaks which are consistent with depths of tephra layers.

5.4.1.2 Age-depth model and sedimentation rate

The age-depth model of the continuous TDV sediment core integrates four geochemically identified tephra marker layers (i.e., H1104, H3, H4 and Saksunarvatn; Table 3). The age-depth model shows that the 715 cm long core covers the last ca. 11 cal. kyr BP (Fig. 26). Unit 1.1 was deposited before 10.3 cal. kyr BP and Unit 1.2 was deposited between 10.3 cal. kyr BP and recent times and, therefore, covers the remainder of the Holocene. Calculated average sedimentation rates in Unit 1.2 between the four tephra marker layers are 32.5 cm/ka, 58.3 cm/ka, 116.7 cm/ka and 134.1 cm/ka for the core intervals between 630-435 cm, 435-365 cm, 365-114 cm and 114-0 cm. This clear trend indicates an increase in the sedimentation rates in modern times.

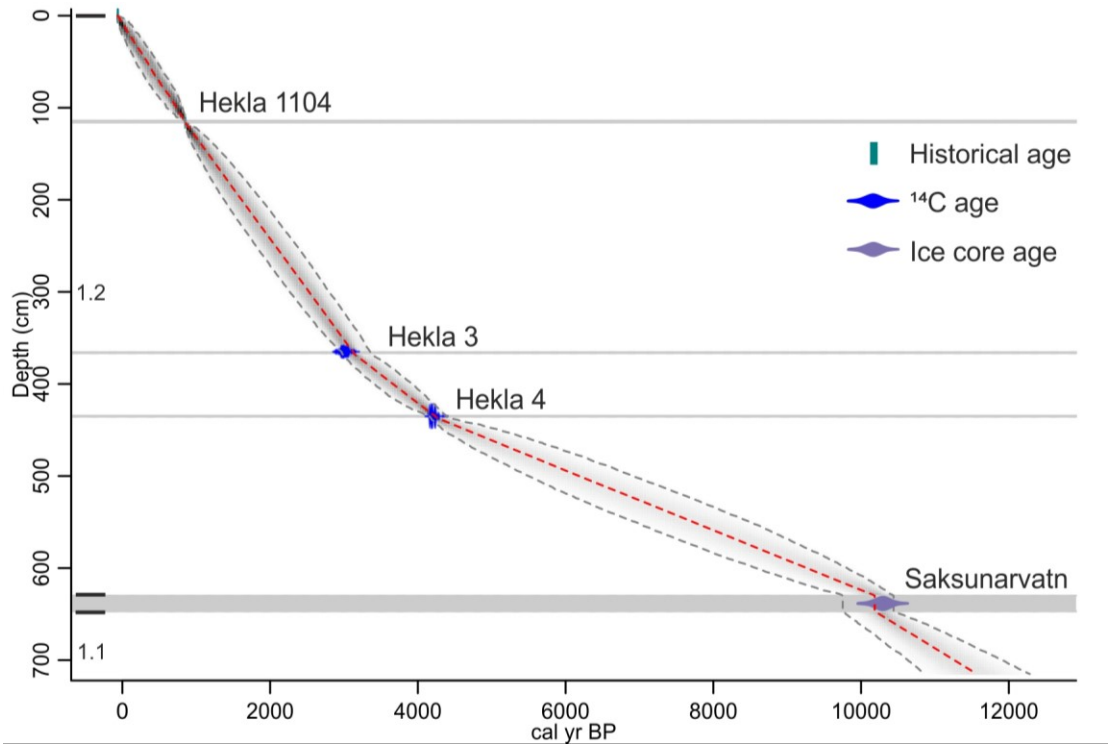

Figure 26. *Age-depth model of Torfdalsvatn. Includes four tephra marker layers: H1104, H3, H3 and Saksunarvatn tephra.*

5.4.2 Þuríðarvatn sediment core

5.4.2.1 Description

The ÞUR core consists of a 304 cm long sedimentary sequence with one unit (2.1; Fig. 27). Unit 2.1 (304-0 cm) consists of organic olive to brown gyttja with several dark grey-black tephra layers (Fig. 27). Changes in color and varying amounts of plant material have been observed throughout the unit. The bottom part of the sequence (304-155 cm) consists of organic olive-brown to dark brown gyttja with several tephra layers (2 mm to 1 cm). Darker sediments appear to be mixed with tephra. The marker layer V1477 is located at 155-151 cm. The upper part of the core (151-0 cm) consists of brown homogeneous gyttja with fewer tephra layers. The LOI values fluctuate between 305-151 cm (0.4-14.6%). Between 151-0 cm, the organic content is higher (ca. 10.5%) and relatively stable. The Ti/Sum shows slightly higher values between 151-0 cm than between 305-151 cm. The LOI and Ti/Sum record shows both negative and positive peaks which are consistent with depths of tephra layers.

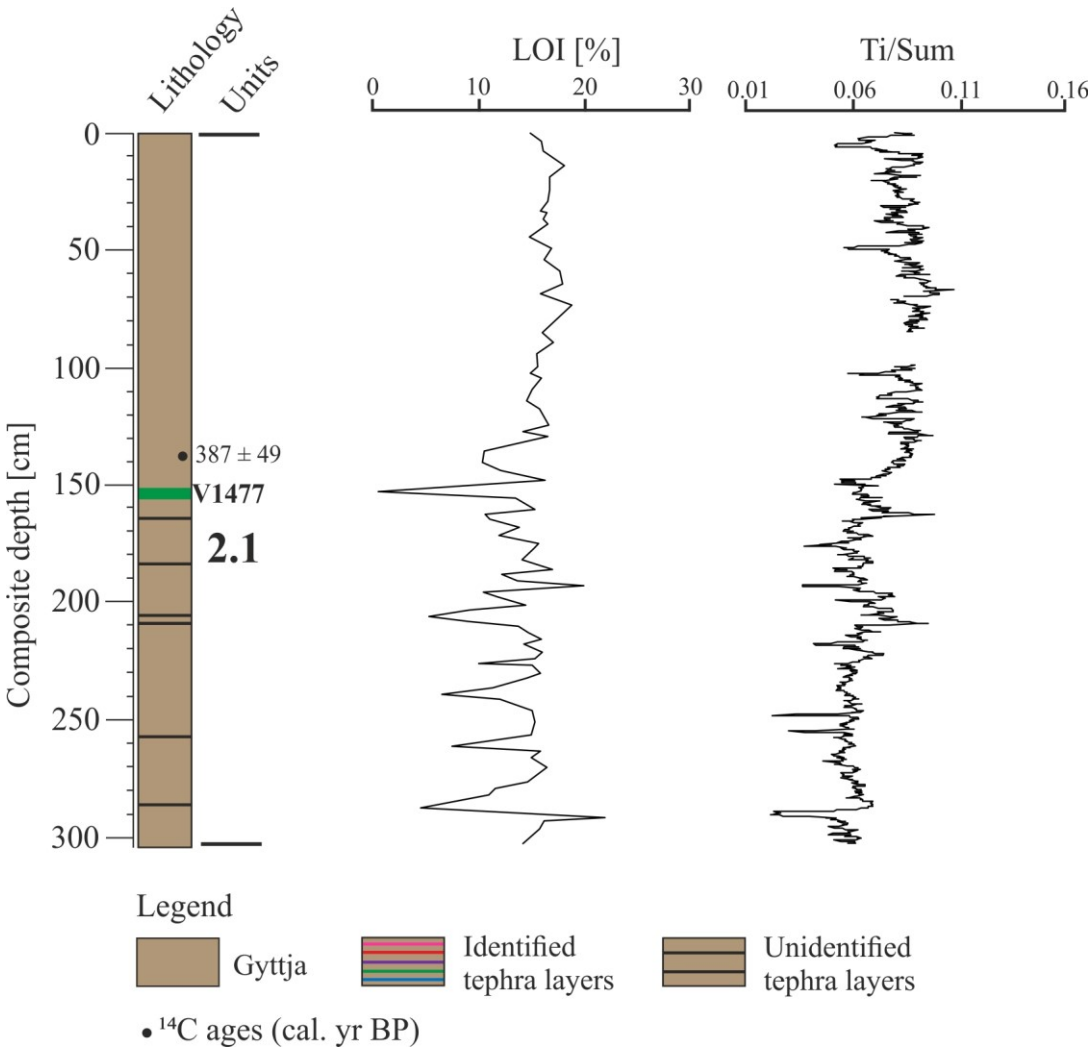

Figure 27. *Lithological core log of ÞUR showing the unit divisions, facies, color, structures and tephra layers (colors refer to volcanic systems in Fig. 5). Ti/Sum and Loss-on-ignition records are displayed.*

5.4.2.2 Age-depth model and sedimentation rate

The chronology of the ÞUR core was established using one ^{14}C age (135.5 cm, 387 ± 49 cal. yr BP) and the V1477 tephra (151-155 cm, 470 cal. yr BP). The age-depth model suggests that the ÞUR sediment sequence was deposited during the last 1200 cal. yr BP (Fig. 28). However, the model is based on only two ages, both located between ca. 130-150 cm, resulting in a higher age uncertainty for sediment between 304-155 cm. The calculated age range of the sediments between 151-0 cm is assumed to be more reliable. Calculated average sedimentation rate between the V1477 tephra marker and surface sediments is 321 cm/ka for the core interval between 151-0 cm. This suggests that the sedimentation rate in the lake was extremely high in recent times.

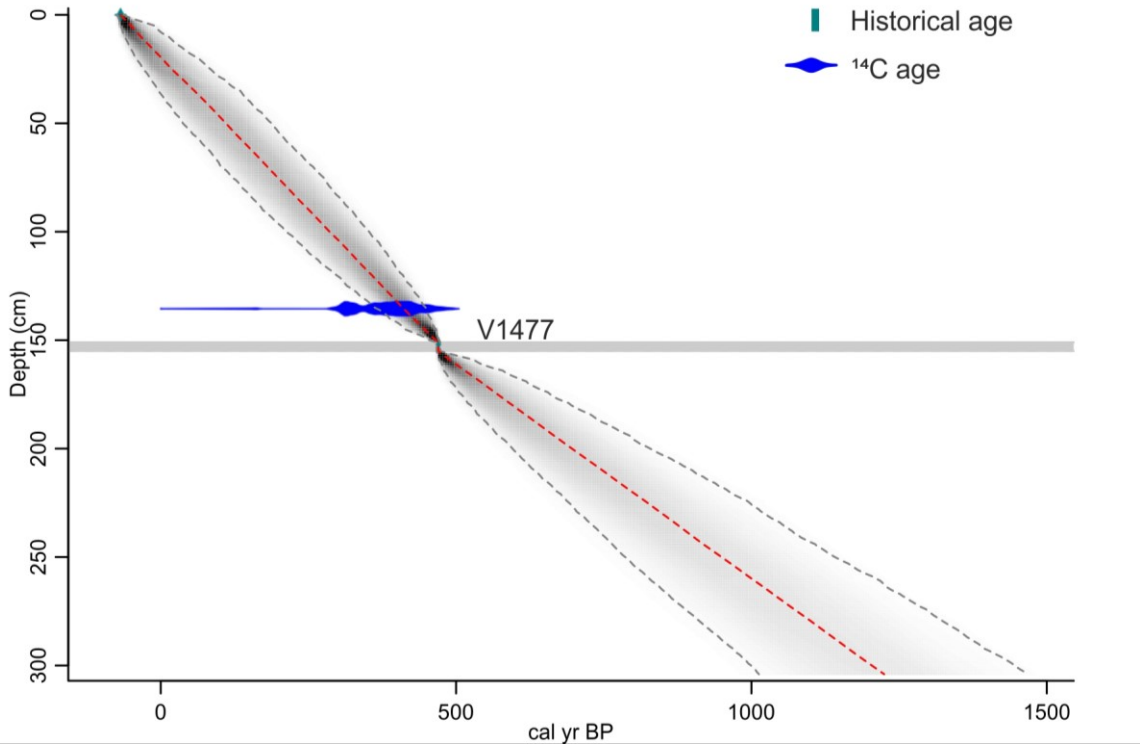

Figure 28. *Age-depth model of Þuríðarvatn. Includes one ^{14}C age (387± 49 cal. yr BP) and one tephra marker layer (V1477).*

5.4.3 Nykurvatn sediment core

5.4.3.1 Description

The NYK sediment core is 410 cm long and contains one sedimentary unit (Unit 3.1, Fig. 29). Unit 3.1 (410-0 cm) consists of olive to brown gyttja with several tephra and sand or silt layers (Fig. 29). Three tephra marker layers (V1477 at 58-64 cm, H3 at 151-153 cm and H4 at 193-195 cm) have been identified within the sediment sequence. Throughout the unit several changes in color and amount of plant material have been observed. The sediments between 410-258 cm consist of olive-brown to brown gyttja rich in aquatic mosses that is interlayered with tephra layers of varying thickness (1 mm to 18 cm) and sand or silt layers. Sediments situated between 258-0 cm are more homogenous and consist of gyttja with several tephra with thickness between 6 cm to 1 mm. The color of the gyttja varies through this upper part of the unit from dark brown (258-240 cm), to olive-brown (240-64 cm) to brown (58-0 cm).

The LOI values between 410-258 cm are relatively low (~4%) with a local maximum of ~11% at 370 cm (Fig. 29). Between 258-0 cm the LOI record is generally increasing (from

5% to 11%, average ~6%) and strongly fluctuates with a local minimum at ca. 60 cm (~2%). The Ti/Sum record is relatively stable throughout the unit with maximum values between 277-258 cm and minimum values between 294-284 cm (Fig. 29). Fluctuations in the organic content are consistent with depths of minerogenic horizons (negative peaks) and horizons with increased organic material amount (positive peaks). The Ti/Sum record also appears to decrease and increase according to the position and geochemistry of the tephra layers situated in the sediment sequence.

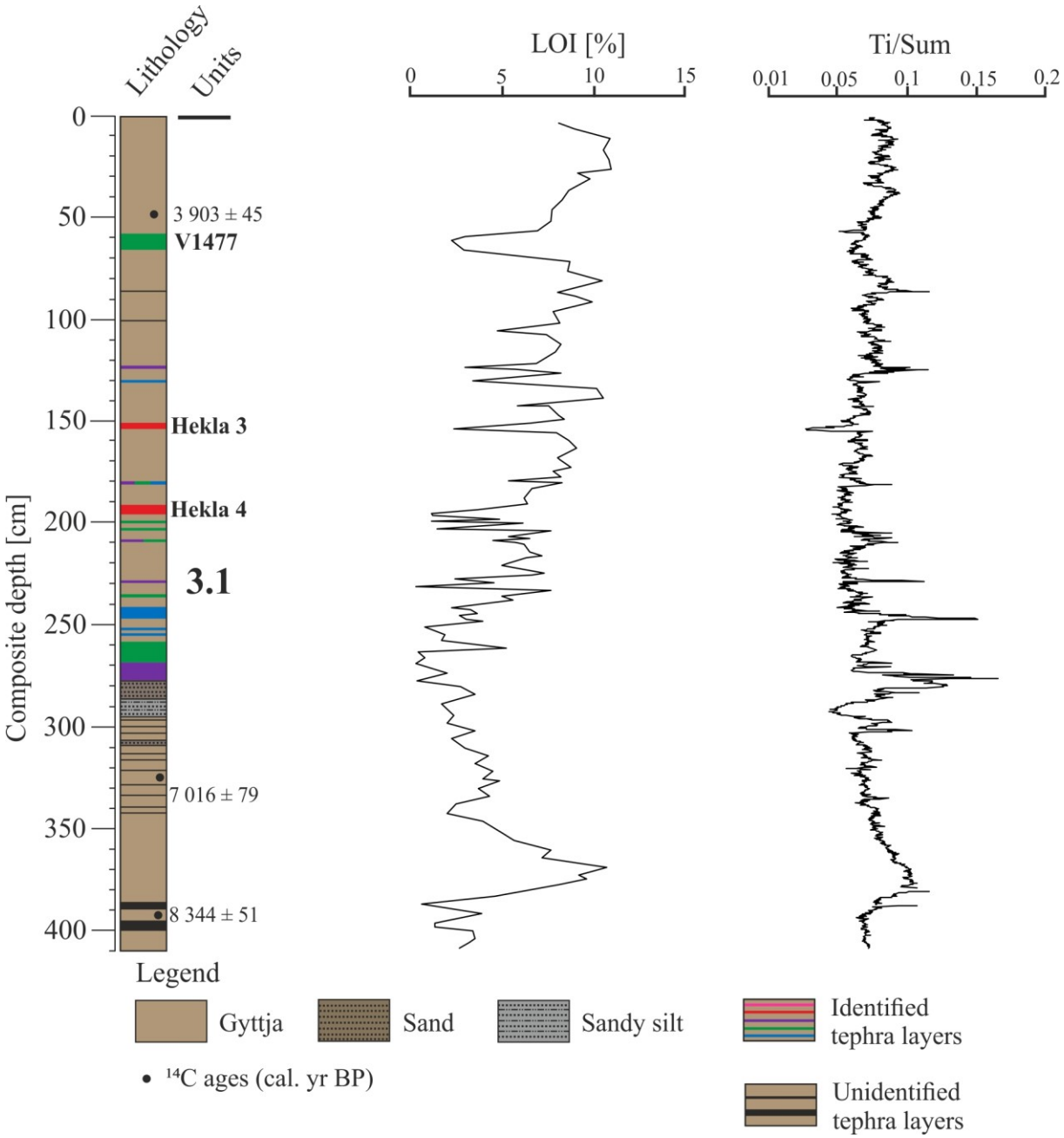

***Figure 29**. Lithological core log of NYK showing the unit divisions, facies, color, structures and tephra layers (colors refer to volcanic systems in Fig. 5). Ti/Sum and Loss-on-ignition records are displayed.*

5.4.3.2 Age-depth model and sedimentation rate

The age-depth model of the NYK core is based on three tephra marker layers (V1477 at 58-64 cm, H3 at 151-153 cm and H4 at 193-195 cm; Table 3) and two ^{14}C ages (7,016 ± 79 cal. yr BP at 320.5 cm and 8,344 ± 51 cal. yr BP at 391.5 cm; Table 2). The age-depth model suggests that the NYK sediment sequence covers the last ca. 8.7 cal. kyr BP (Fig. 30). Calculated average sedimentation rates between the five ages resulted in 53.5 cm/ka, 45.4 cm/ka, 35 cm/ka, 36.8 cm/ka and 123.5 cm/ka for the core intervals between 391.5-320.5 cm, 320.5-193 cm, 193-151 cm, 151-58 cm and 58-0 cm. The trend indicates an increase in sedimentation rates in modern times or that sediments located in the upper core are less compressed.

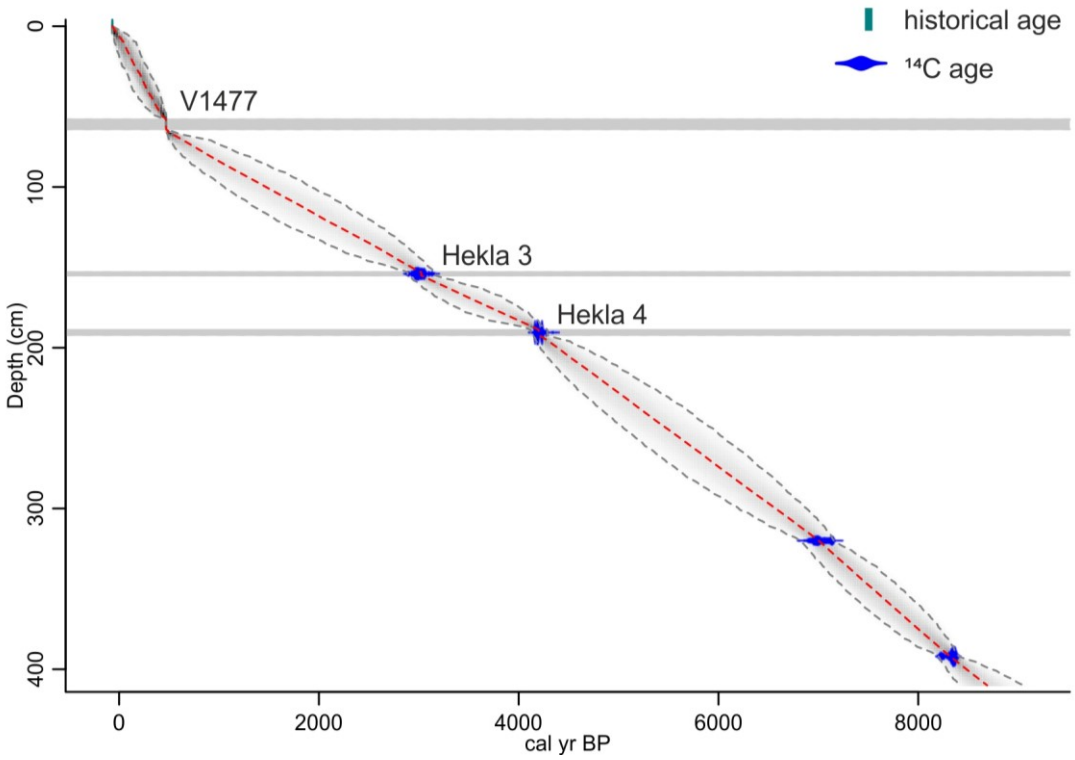

***Figure 30**. Age-depth model of Nykurvatn. Includes two ^{14}C ages (7,016 ± 79 cal. yr BP and 8,344 ± 51 cal. yr BP) and three tephra marker layers (V1477, H3 and H4).*

5.4.4 Ásbrandsstaðavatn sediment core

5.4.4.1 Description

The ABS sediment core is 380 cm long and has been divided into two main stratigraphic units: 4.1 and 4.2 (Fig. 31). Throughout the core, both organic content and the Ti/Sum record

are varying accordingly to the lithostratigraphic units with lower values in Unit 4.1 and higher values in Unit 4.2.

At the bottom of the ABS core a grey tephra layer identified as Askja S, is located between 380-371 cm. The tephra layer is characterized by LOI values of ~2.5% and the Ti/Sum ratio reaches a local minimum. Both LOI and Ti/Sum show little variation within the tephra layer.

Unit 4.1 (371-337 cm) consists of clay and clayey gyttja with several tephra layers. Between 371-355 cm the core consists of dark grey-olive clayey gyttja and tephra layers that are highly disturbed or reworked. Discontinuous layers and 'patches' of basaltic and silicic tephra are located in a clayey gyttja matrix. Between 355-350 cm a transition from grey clayey gyttja at the bottom to grey clay at the top has been observed. The clay sediments contained coarser material and were either mixed with tephra or very fine sand. The upper part of the unit (350-337 cm) consists of grey-olive clayey gyttja that contains aquatic mosses. LOI values measured in Unit 4.1 are generally low (average ~3%) and fluctuate slightly. The Ti/Sum record is generally low and fluctuates mostly in the bottom part of the unit where sediments appear disturbed.

Units 4.1 and 4.2 are separated by a massive tephra layer identified as Saksunarvatn Ash, that is located at 337-273 cm. The tephra layer contains almost no organic material (LOI ~0.6%) and has a stable Ti/Sum record.

Unit 4.2 (273-0 cm) consists of olive and dark brown gyttja with several tephra layers (4 mm - 4 cm). Two tephra marker layers have been identified in Unit 4.2, H3 at 130 cm and H4 at 162 cm. Several changes in color and amount of plant material has been observed within the sediments of this unit. Between 273-240 cm and 240-214 cm the color of the gyttja changes from olive-grey to olive and the amount of aquatic mosses observed at the sediment surface decreases. Other changes in color can be observed at 214-190 cm (olive-brown gyttja), 190-77 cm (olive gyttja) and 77-0 cm (brown-olive gyttja). The organic content in Unit 4.2 (average ~6%) is generally higher than in Unit 4.1 and strongly flucutates. The highest LOI values (max. 23%) have been observed between 214-240 cm. Throughout the unit, Ti/Sum is fluctuating and shows an increase in the upper ~50 cm. Fluctuations in the organic content is consistent with the depth of minerogenic horizons (negative peaks) and horizons with increase

organic material amount (positive peaks). The Ti/Sum record decreases and increases accordingly to the position and geochemistry of the tephra layers.

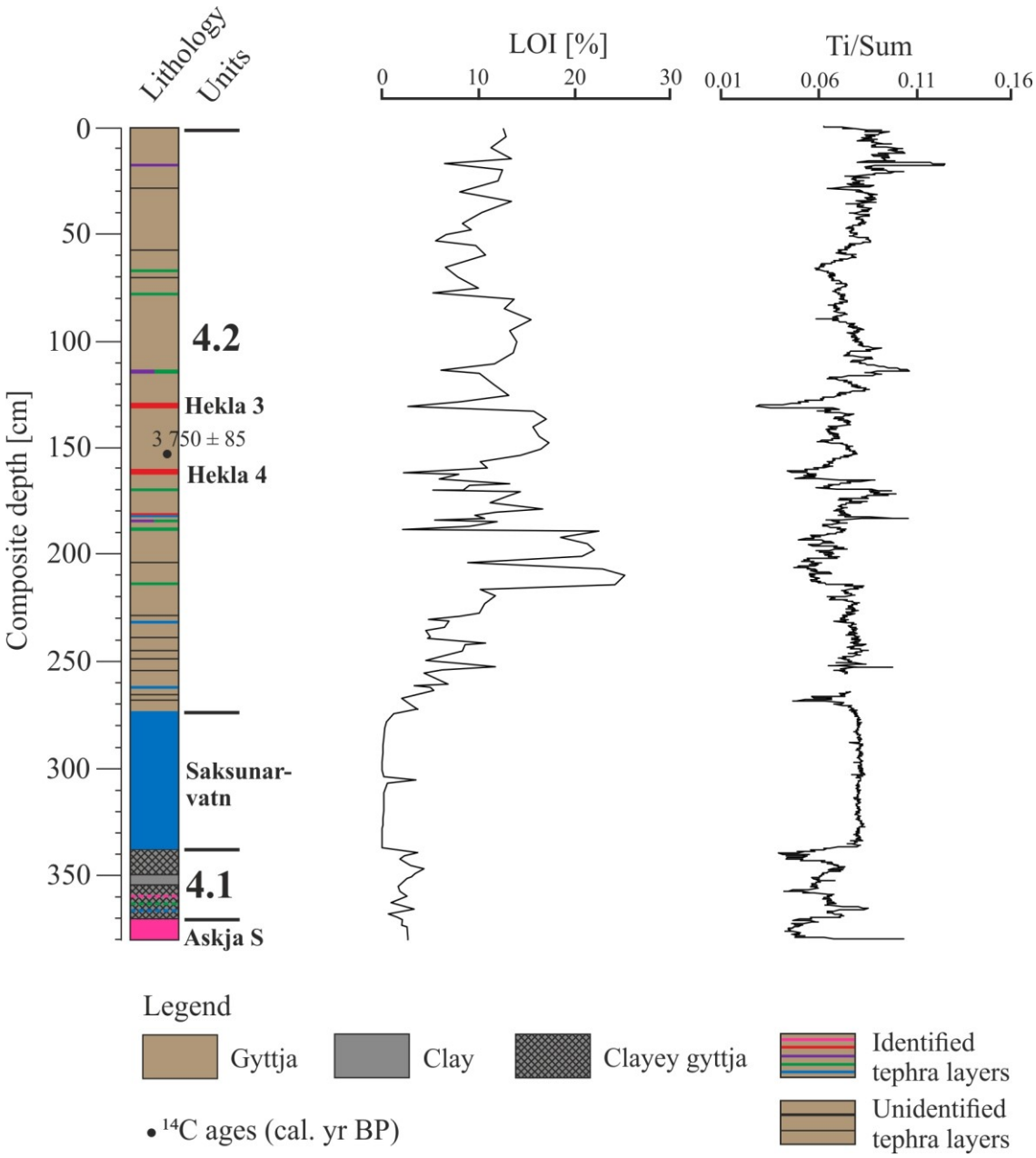

Figure 31. *Lithological core log of ABS showing the unit divisions, facies, color, structures and tephra layers (colors refer to volcanic systems in Fig. 5). Results of select elemental ratios using the X-Ray Fluorescence and Loss-on-ignition.*

5.4.4.2 Age-depth model and sedimentation rate

The age-depth model of the ABS core is based on four tephra marker layers (H3 at 130 cm, H4 at 162 cm, Saksunarvatn Ash at 273-337 cm and Askja S at 371-380; Table 3) and one ^{14}C

age (3,750 ± 85 cal. yr BP at 152 cm; Table 2). The age-depth model suggests that the ABS sediment sequence covers the last ca. 10.8 cal. kyr BP (Fig. 32).

Calculated average sedimentation rates between the five ages resulted in 43.3 cm/ka, 29.3 cm/ka, 22.2 cm/ka, 18.2 cm/ka and 52.3 cm/ka for the core intervals between 371-337 cm, 273-162 cm, 162-152 cm, 152-130 cm and 130-0 cm. The trend indicates a slight increase in sedimentation rates in modern times.

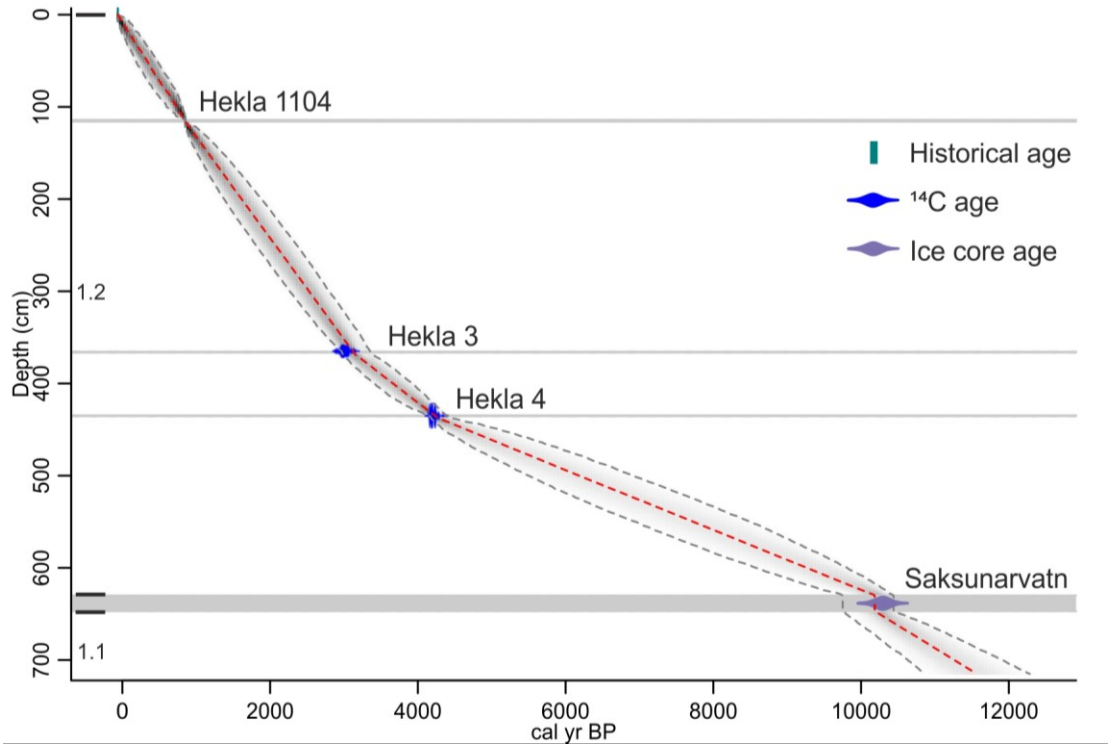

Figure 32. *Age-depth model of Ásbrandsstaðavatn. Includes one ^{14}C age (3,750 ± 85 cal. yr BP) and four tephra marker layers (H3, H4, Saskunarvatn, Askja S. Gray horizontal layers indicate position and thickness of tephra layers.*

6 Discussion

6.1 Challenges and improvements for a correct alignment and correlation of lake sediment sequences

Lake cores often require individual overlapping core sections to be aligned. The alignment is the initial and crucial step in constructing the composite depth of a continuous core record. Depending on the applied proxies, a misalignment is likely to affect reconstructions that are based on these lacustrine records, potentially leading to wrongful conclusions. Despite the importance of aligning overlapping lake core sections, there is a lack of publications explaining the 'correct' methodology and/or a detailed approach for such alignments. Most publications only shortly mention the rather complex alignment-step without going into detail (e.g., Turner et al., 2008; Blumentritt et al., 2013; Stockhecke et al., 2014; Peti & Augustinus, 2019).

6.1.1 Common approaches in the alignment of core sections

Blaauw (2012) summarized different approaches for aligning or correlating different archives (i.e., marine, terrestrial, ice core records) in order to construct age-depth models (a tuning-based chronological framework). The alignment of archives depends largely on the principles of superposition and lateral continuity. Based on those principles it can be assumed that distinct layers produced by major geological events (e.g., volcanic eruptions; tephra layers) were deposited on a wide spatial scale at the same time and are expected to extend horizontally in all directions (Blaauw, 2012). Alignments of different records are often built on the visual identification of identical simultaneous events being used as tie-points between different archives (e.g., Schimmelmann et al., 1990; Turner et al., 2008; Blaauw, 2012; Peti & Augustinus, 2019). This approach can also be used for the alignment of cores sections collected from the same lake. However, there is no necessity of marker layers, that are used as tie-points, to be deposited on a wide scale.

In homogenous sediment records, where marker layers or prominent sediment features are absent, sediments are commonly aligned by correlating distinct features such as down-core elemental or isotopic variations (i.e., XRF-, MS-, isotope-based correlation) (e.g., Stockhecke et al., 2014; Peti & Augustinus, 2019). However, the correlation of core sections without distinct layers is often made with less confidence (e.g., Peti & Augustinus, 2019). A high

number of tie-points will generally result in a better and more reliable alignment of individual core sections.

In addition to having a high number of visual tie-points, the alignment of a sediment sequence can be improved by tuning of the record (e.g., Lisiecki & Herbert, 2007; Blaauw, 2012; Schomacker et al., 2019). During the tuning process, tie-points between two time series are manually added into a tuning software (e.g., AnalySeries), which then aligns tie-points of one series with the tie-point of the other series (Fig. 8, Fig. 33; Blaauw, 2012). This approach is especially helpful if there are variations in sediment thickness between different cores. By stretching or compressing data between tie-points it becomes easier to observe potential correlations between records. The tuning of data can be particularly useful for the alignment of lake sediment cores, especially since sediments sequences in core sections often vary in thickness.

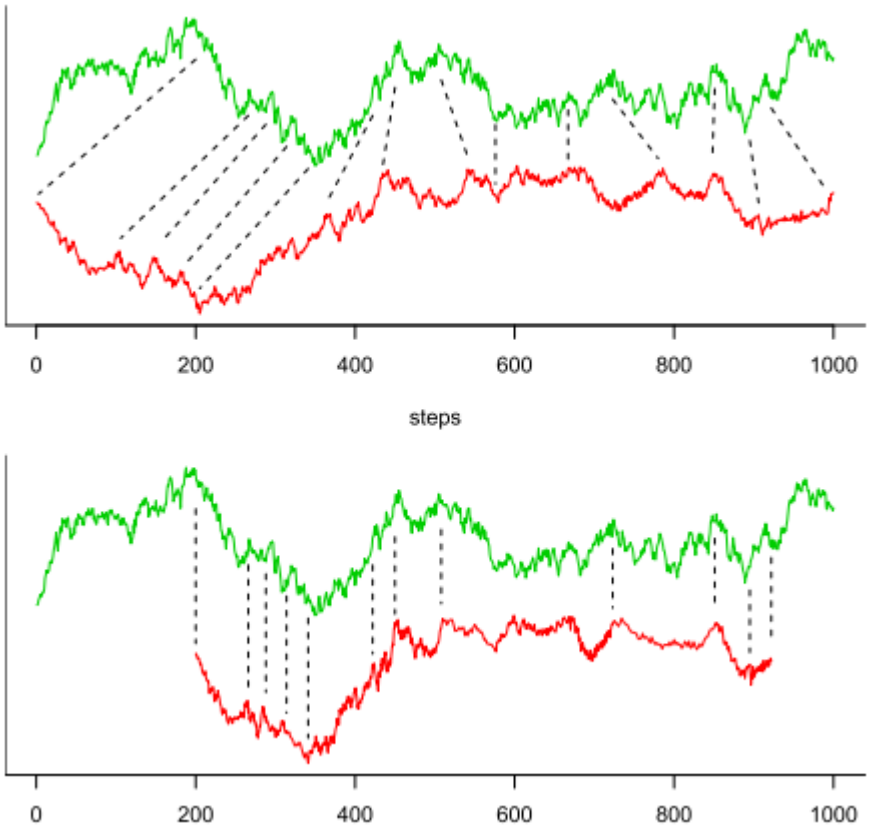

***Figure 33**. Example for tuning of data. Top: Two data curves before tuning. Bottom: Red curved has been stretched/compressed during tuning process, so both curves align (from Blaauw, 2012).*

As described in Chapter 5.3, the alignment of the sediment core sections of this study is based on visual identification of marker layers and/or distinct elemental features. Core sections were also tuned through stretching and/or compressing of data by adding tie-points into AnalySeries. The alignments of this study therefore seem to follow the most common approaches of core correlations.

6.1.2 Issues with core alignments

The described approaches for aligning core sections contain several issues. One potential problem is that the tie-points are selected visually. In visual alignment there is often subjectivity involved in this selection of tie-points, especially when aligning data curves (Lisiecki & Herbert, 2007; Blaauw, 2012). Because of the often very similar shaped peaks within a core, the tuning of data could lead to inaccurate correlations. The correlation of peaks can also be problematic due to measurement uncertainties (e.g., XRF) that can lead to incorrect visual correlations (Blaauw, 2012). Tuned data is therefore more reliable when distinct features that are found in two cores are used as tie-points (e.g., tephra layers in this study). In studies were tuning was involved in the alignment of core sections it may be important to provide reconstructed accumulation or sedimentation rates to allow the reader to have a critical opinion on the alignment (Blaauw, 2012).

Another problem in the alignment of cores and/or core sections are hiati within sediment sequences. This can lead to incorrect composite depth of continuous core records and consequently false conclusion about the paleoenvironment (e.g., Lisiecki & Herbert, 2007). This issue has been observed between the sediment core sections ÞUR1 and ÞUR2, and NYK4 and NYK5. In both cases the stratigraphically lower section had a tephra layer at the top of the core, which had not been observed in the upper core section. It is therefore difficult to determine whether a gap between both core sections is present or if the sediments are directly aligned.

6.1.3 Possible improvements in core aligning

To achieve better alignments, and consequently improve paleoenvironmental lacustrine studies, the issues that may come along with alignment approaches should be discussed and if possible fixed. It may be difficult to detect gaps between two core sections without re-coring the lake. However, the visual and subjective selection of tie-points may be approached in a

less biased way. Blaauw (2012) therefore suggests that alignments of core sections should be based on tie-points that were selected by more objective, numerical approaches (e.g., Clark & Thompson, 1979; Haam & Huybers, 2010). An objective and numerical selection of tie-points could be achieved by developing statistical methods that allow the quantification of proxy event shapes. Statistical methods could also allow for the assessment of the reliability of an alignment and check if alternative alignments are possible (Blaauw, 2012; Clark & Thompson, 1979). This approach is particularly useful when no distinct features that can be used as tie-points are present in the core sections. The alignments in this study are largely based on the use of identified tephra layers as tie-points and may therefore be viewed as reliable. However, they could also profit from a numerical selection of tie-points between geochemical data to avoid subjectivity.

6.2 Tephra stratigraphy in North and Northeast Iceland

The tephra stratigraphy of the TDV sediment sequence revealed that at least four tephra marker layers (H1104, H3, H4 and Saksunarvatn; Fig. 34) have been deposited on Skagi. The tephra stratigraphy of sediment sequences NYK, ÞUR and ABS from the Vopnafjörður area preserved least five tephra marker layers (V1477, H3, H4, Saksunarvatn, Askja S; Fig. 34).

6.2.1 Comparison and correlation of tephra stratigraphies from this study

The results from tephra marker identification showed that three of the tephra markers, including H3, H4 and Saksunarvatn tephra, have been found in both study areas (Fig. 34). The tephra marker H1104 has only been observed in Torfdalsvatn. Tephra markers that were only identified in Northeast Iceland include the V1477 (Þuríðarvatn and Nykurvatn) and the Askja S (Ásbrandsstaðavatn) marker layers.

H1104 has not been identified within the sediments of lakes located near Vopnafjörður. A dispersal map and an isopach map based on previous studies (both marine and terrestrial) show that deposits of the H1104 eruption can potentially be found in lakes located near Vopnafjörður (Fig. 35; Larsen et al., 2002; Gudmundsdóttir et al., 2011; Meara et al., 2019). However, potential H1104 deposits situated in the sediment sequences of Þuríðarvatn, Nykurvatn and Ásbrandsstaðavatn would be relatively thin (~0.2 cm) (Meara et al., 2019), possibly making it difficult to detect layers. The Hekla 1104 marker layer identified in the TDV sediment sequence had a thickness of ~1 cm and it was therefore easy to visually detect

the tephra. Such a difference in the deposit thickness was caused by the fact that the main axis of deposition during the H1104 eruption was due north (Meara et al., 2019).

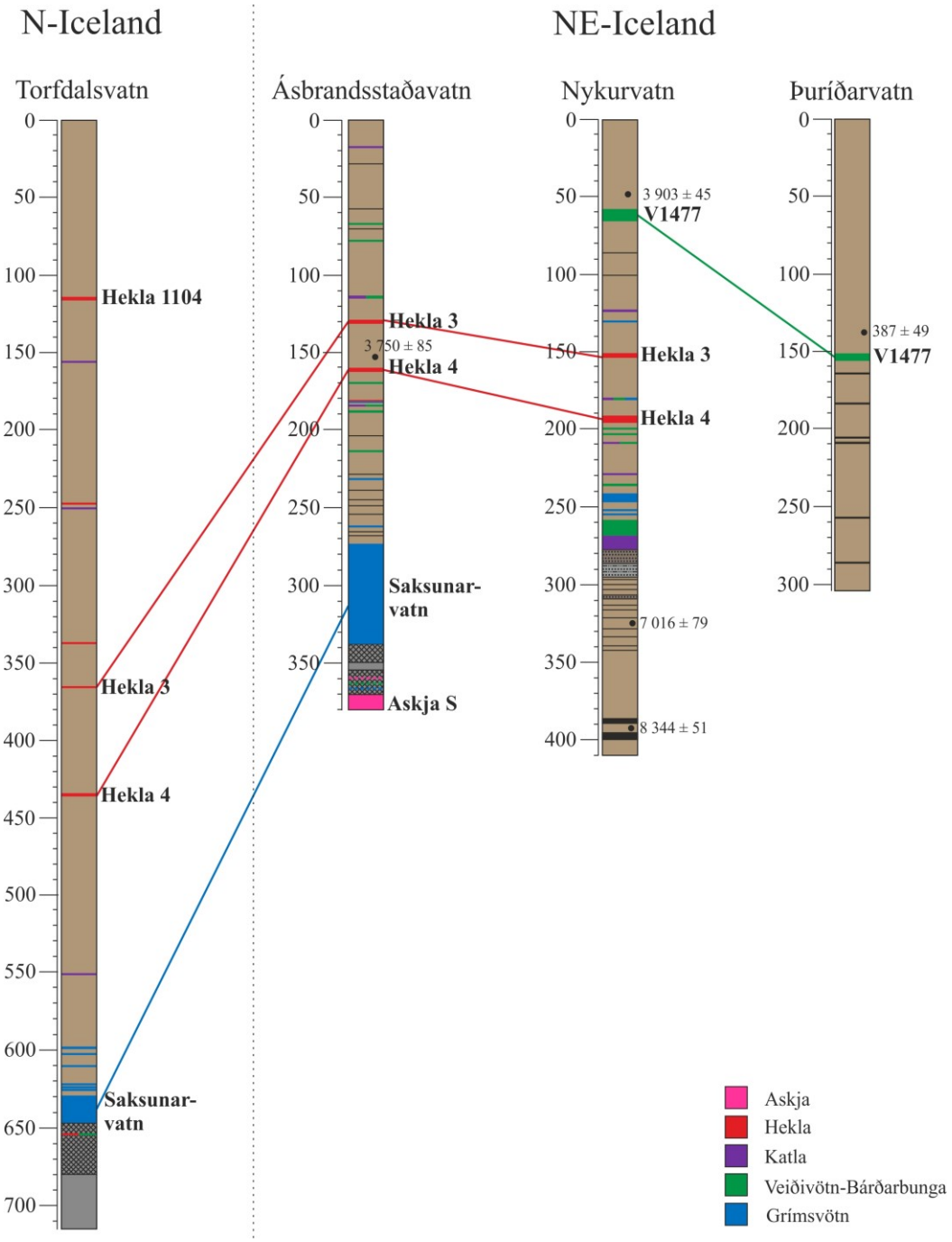

Figure 34. *Correlation of the tephra stratigraphy from North and Northeast Iceland showing the identified tephra markers.*

The V1477 marker layer has been identified in the sediment sequences of two lakes, Þuríðarvatn and Nykurvatn, in the Vopnafjörður area (Fig. 34). The sediment sequence of the third lake, Ásbrandsstaðavatn, did not seem to contain the tephra marker. However, as

displayed in the sedimentary log of the ABS core (Fig. 31), two tephra layers originating from the Veiðivötn-Bárðarbunga volcanic system have been observed. Both layers were much thinner (~1-2 mm) than the V1477 layer in the NYK and ÞUR record. However, it is possible, that one of the basaltic layers may be the V1477 marker. Differences in tephra thickness might be explained by the greater distance of Ásbrandsstaðavatn to the volcanic systems.

Both V1477 and Askja S were not detected in the TDV sediment sequence. Dispersal maps based on previous tephra marker findings show that both tephra markers are not expected to be found on Skagi (Fig. 35; Larsen et al., 2002; Gudmundsdóttir et al., 2011; Kearney et al., 2018) explaining the missing of the marker layers.

6.2.2 Comparison of the tephra stratigraphies with previous records

North Iceland

The analysis of the sediment sequence from Torfdalsvatn revealed that the local tephra stratigraphy includes four tephra marker layers spanning almost the entire Holocene (ca. 10.3 cal. kyr BP). In a previous study, Björck et al. (1992) identified two important marker layers in the bottom of a Torfdalsvatn sediment core, including the Saksunarvatn Ash and the 12.1 cal. kyr BP (Lane et al., 2012) old Vedde Ash (Fig. 36). The Saksunarvatn tephra has also been found in the TDV record but the Vedde tephra has not been identified (Fig. 34). As illustrated by Björck et al. (1992) in a lithological log, the Vedde tephra is situated below the Saksunarvatn tephra and within a clay facies (Fig. 36). Below the Vedde marker layer another thinner tephra layer was observed in the sediments (Björck et al., 1992). The TDV sediment sequence also contained a clay facies with two tephra layers at 689 cm and 698 cm. Based on the thickness of the layers and the stratigraphical position it may be suggested that the layer located at 689 cm is the Vedde tephra. This would indicate that sediments in the TDV core deposited below the tephra layer are older than 12.1 cal. kyr BP. However, without major-element analysis of the layer it can not be determined if the layer actually is the Vedde Ash.

Florian (2016) visually identified several tephra layers within a Torfdalsvatn sediment record, including the Vedde Ash. Other marker layers found in the sediment sequences are H4, Settlement (V877), H1104, H1300 and H1766. The marker layers H4 and H1104 were also identified in the TDV record (Fig. 34). The findings of Florian (2016) suggest that more marker layers are contained in the sediments of the TDV core but have not been identified.

The comparison of data in this thesis with previous studies seems to confirm the identification of tephra marker layers in Torfdalsvatn.

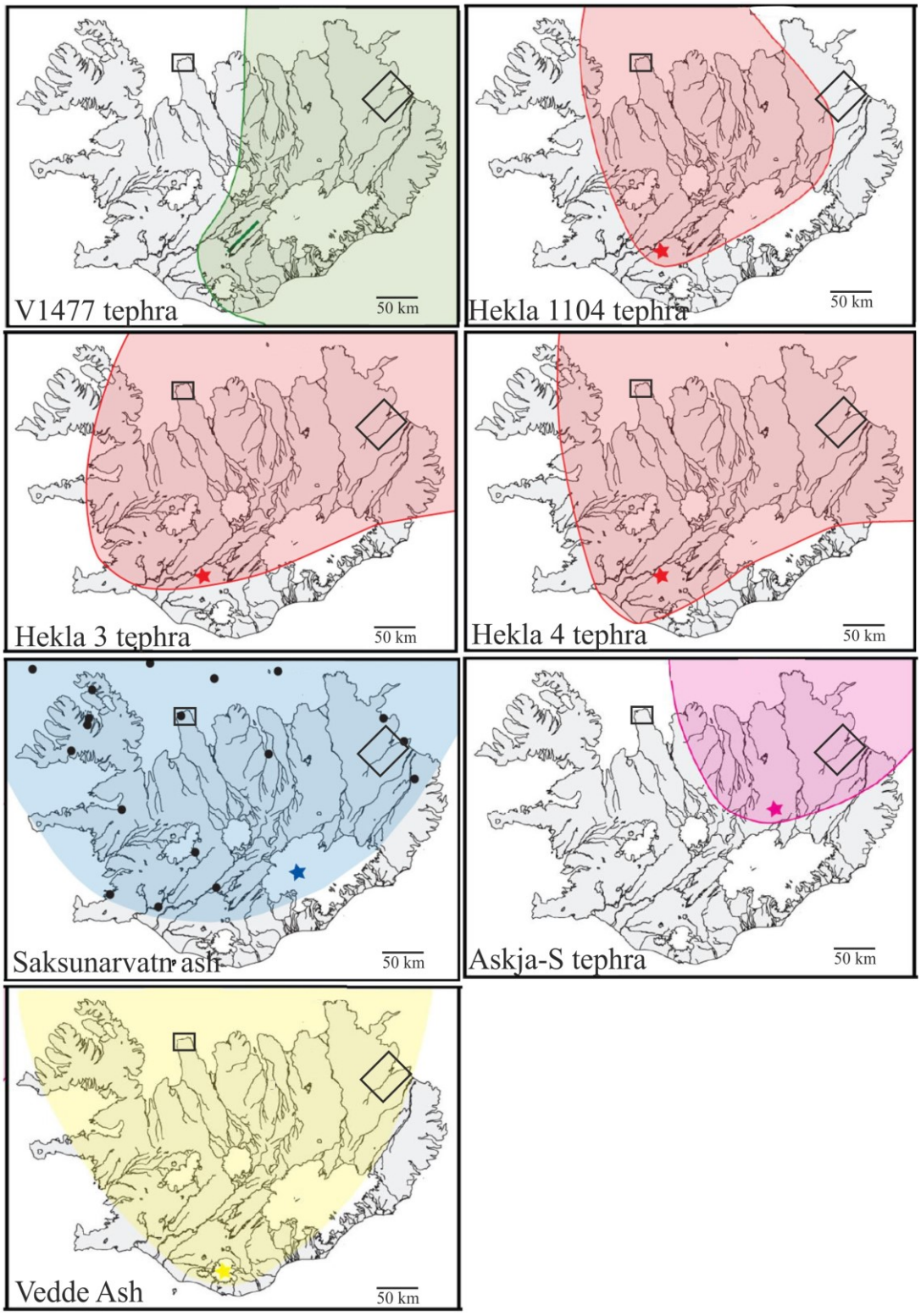

Figure 35. *Dispersal maps of the V1477, H1104, Askja S and Vedde tephra (modified from Gudmundsdóttir et al., 2011). Black boxes indicate position of the study areas.*

Northeast Iceland

A high-resolution Holocene tephra stratigraphy from lake Lögurinn, located in eastern Iceland (Fig. 1), comprises 19 tephra marker layers (Striberger et al., 2012; Gudmundsdóttir et al., 2016). The Lögurinn tephra stratigraphy is the most detailed and continuous record for East Iceland and therefore findings of the Vopnafjörður area are compared to these results. The identified marker layers in Lögurinn include V1477, H3 and H4 tephra (Gudmundsdóttir et al., 2016), which have also been found in lake sediments from northeastern Iceland (ÞUR, NYK and ABS cores). The Saksunarvatn Ash and Askja S tephra, that were found in the ABS record, have not been identified in sediments from Lögurinn (Gudmundsdóttir et al., 2016). The absence of both marker layers can be explained by the fact that the ABS record covers the last ca. 10.8 cal. kyr BP, and the Lögurinn record consists of sediments deposited after the Saksunarvatn eruption (Gudmundsdóttir et al., 2016). However, both Saksunarvatn and Askja S marker layers have been previously observed in northeastern Iceland in other records (e.g., Sigvaldason, 2002; Kearney et al., 2018). The comparison of data in this thesis with previous studies confirms the identification of tephra marker layers in Þuríðarvatn, Nykurvatn and Ásbrandsstaðavatn.

6.2.3 Saksunarvatn Ash or G10ka series?

The Saksunarvatn tephra marker is crucial for the construction of chronologies for terrestrial, marine and ice core records from the North Atlantic region (Óladóttir et al., 2020). The most widely used age of ca. 10.3 cal. kyr BP for the Saksunarvatn was established from an ice-core record from Greenland (Óladóttir et al., 2020) and was also used in this study. However, several studies proposed that the often massive Saksunarvatn tephra was not produced by a single eruption, but by a series of eruptions of the Grímsvötn volcanic system occurring between 10.4-9.9 cal. kyr BP, called the G10 ka series. These eruptions are believed to having produced several widespread tephra layers with very similar geochemical compositions (Óladóttir et al., 2020). The Saksunarvatn Ash was identified to represent one of these multiple eruptions (Jóhannsdóttir et al., 2005; Neave et al., 2017; Harning et al., 2018; Óladóttir et al., 2020). However, because of the similar geochemistry individual layers cannot be distinguised and most studies therefore described and identify these massive tephra deposists as the well known Saksunarvatn Ash (Óladóttir et al., 2020).

The Saksunarvatn layers identified in the TDV and ABS records may show evidence for the layer to be produced by several eruptions. Both layers almost completely consist of black ash, however in both deposits grey layers have been observed (Figs 10, 18). Björck et al. (1992) also observed such layers in the Saskunarvatn Ash deposit and identified them as diatomite. These layers may be interpreted as an indicator for several eruptions (Óladóttir et al., 2020). Because such layers have also been observed in the Saksunarvatn layers of TDV and ABS, it is suggested that the layers have been produced by multiple eruptions. However it was determined that the two layers in this study would be described as the widely used Saksunarvatn tephra rather than the G10ka series.

6.3 Reconstruction of the paleoenvironment in North and Northeast Iceland

6.3.1 Paleoenvironmental conditions of Torfdalsvatn

The reconstruction of the paleoenvironmental conditions of Torfdalsvatn has been divided into two sections. The first section covers the time period from deglaciation to deposition of the Saksunarvatn Ash, and the second section covers the remainder of the Holocene.

6.3.1.1 Deglaciation to Saksunarvatn Ash (>12.0 to ca. 10.3 cal. kyr BP)

During the Late Glacial and early Holocene, the depositional environment at Torfdalsvatn is believed to have changed significantly which can be seen from the lithostratigraphy in the TDV sediment record. The lithology of Unit 1.1 indicates glacial advances in northern Skagi during the Younger Dryas and Early Holocene, followed by a deglaciation. The lithostratigraphy suggests that northern Skagi was fully deglaciated by 10.3 cal. kyr BP.

Sediments of Unit 1.1, composed of three facies (clay, clayey gyttja and gyttja) are situated stratigraphically below the identified Saksunarvatn tephra which indicates that the unit has been deposited prior to ca. 10.3 cal. kyr BP (Table 3). A second tephra layer situated at 690 cm within the clay facies (Fig. 36), might be the 12.1 cal. kyr BP old Vedde Ash (explained in Chapter 6.2.2), which would suggest that the clay facies was deposited during the YD around 12.1 cal. kyr BP. The clay facies, characterized by high MS and Ti/(inc+coh) values, is interpreted as deposited during periods with inflow of glacial meltwater (e.g., Briner et al., 2010; Larsen et al., 2015; Harning et al., 2016; Schomacker et al., 2016). This would suggest that a glacier has been occupying the catchment of Torfdalsvatn during the time clay was

deposited which indicates that temperatures were relatively cold.
Above the clay facies a more organic-rich facies (clayey gyttja) has been deposited which may indicate a decrease in glacial meltwater input over time, caused by a retreating glacier (e.g., Harning et al., 2016). The increase in organic material might also suggest an increase in autochthonous material and/or increased input of allochthonous plant material into the lake (e.g., Tarasov et al., 1996; Meyers & Lallier-Vergès, 1999; Valpola & Ojala, 2006). The reduction in minerogenic input (i.e., glacial meltwater) and increasing organic content is also reflected by the decrease in MS values within the clayey gyttja facies. Both, a decrease in glacial meltwater inflow and increasing organic matter indicate that temperatures were increasing during the time of deposition.
The upper part of Unit 1.1 consists of gyttja that is interpreted as a deposit of lacustrine sedimentation. The deposition of gyttja indicates that the area surrounding Torfdalsvatn was fully deglaciated (i.e., glacier completely retreated from the catchment) shortly before the deposition of the Saksunarvatn tephra (10.3 cal. kyr BP).

During the YD and early Holocene, coastal areas that have been ice-free since the beginning of the Bølling interstadial, were covered by the expanding IIS and local glaciers (Fig. 2C; Norðdahl & Pétursson, 2005; Norðdahl et al., 2008; Ingólfsson et al., 2010; Patton et al., 2017). However, a reconstruction of the ISS during this time showed that the ice sheet did not readvance onto Skagi (Fig. 2C; Patton et al., 2017). Ingólfsson et al. (1997) however suggested that cirque glaciers were present on Skagi during the YD and early Holocene. Similar observations indicating cold conditions and glacial advances on northern Skagi during the this time, have been made by Björck et al. (1992) and Rundgren (1998). Both studies worked with sediment cores from Torfdalsvatn and described a clay deposit below a tephra layer, that has been identified as the Saksunarvatn Ash, which is very similar to the clay facies in the TDV record. Lithological logs suggest that sediments described by Björck et al. (1992) go furthest back in time, as they described a silty clay facies (Fig. 36) which has not been detected within the TDV core or the study conducted by Rundgren (1998). This lower sequence, consisting of silty clays and clays has been interpreted by Björck et al. (1992) to indicate glacial conditions, and therefore supports the interpretation of the clay facies from the TDV core. Both Björck et al. (1992) and Rundgren (1998) also describe that sediments situated above the silty clays and clays appear to have increase in organic content, very similar to the transition in facies observed in TDV record core (Fig. 36).

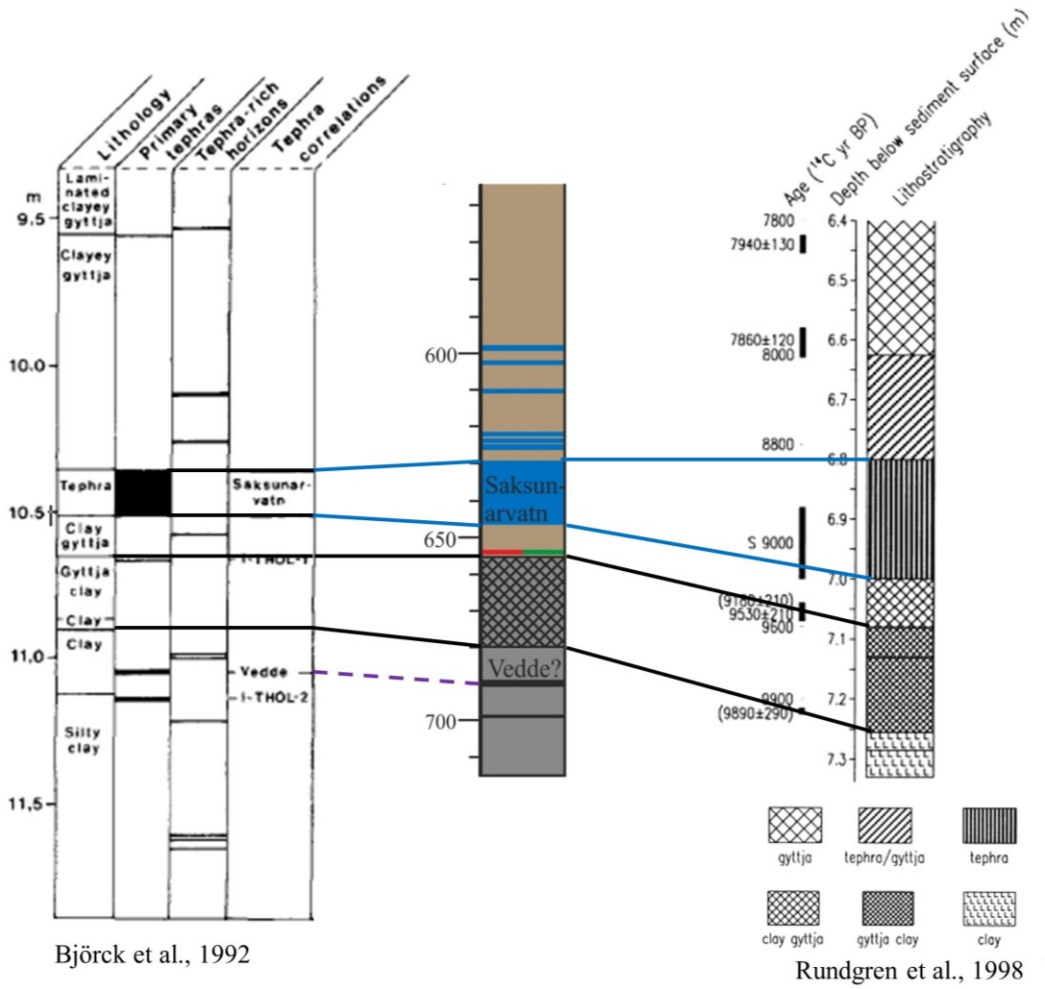

Figure 36. *Lithological logs of Torfdalsvatn from Björck et al., 1992 (left), this study (middle) and Rundgren et al., 1998 (right). All studies identified clayey facies located below the Saksunarvatn tephra.*

Other records also seem to support the interpretations of the sediments from Unit 1.1 of the TDV record. Pollen and macrofossil records from Torfdalsvatn suggest that plants appeared on Skagi at ca. 12.5 cal. kyr BP and are associated with the Bølling-Allerød warmth (Björck et al., 1992; Rundgren, 1995). A decrease in the amount of pollen within the sediments deposited during the Younger Dryas and early Holocene was believed to indicate cold conditions and a short-lived phase of glacier growth (Rundgren, 1997). This evidence for cold conditions and glacial advances is believed to be reflected by the deposition of clay (Unit 1.1) in the TDV record. Pollen records also indicate a marked warming on Skagi around 10.6 cal. kyr BP (Rundgren, 1995), which seems to be consistent with the start of deposition of organic-rich gyttja (Unit 1.1). The theory in which conditions became increasingly warm is also supported by a diatom record from Torfdalsvatn, which indicates that there is a very high limnic productivity ca. 10.6 cal. kyr BP (Björck et al., 1992; Rundgren, 1995, 1998). Based

on these different proxies it was concluded that the deglaciation continued into the Holocene and may have been completed by ca. 10.3 cal. kyr BP (Björck et al., 1992; Rundgren, 1998), which supports the interpretation of Unit 1.1 from this study.

Another paleoenvironmental reconstruction of Torfdalsvatn was conducted by Florian (2016) based on several proxies including Biogenic silica (BSi), diatom pigments and C:N ratio. Findings in the study of Florian (2016) seem to be consistent with assumptions made about the depositional environment from this study. Sediments that have been interpreted to be deposited during the deglaciation show an increase in aquatic productivity after ca. 10.6 cal. kyr BP, which also confirms previous findings by Björck et al. (1992) and Rundgren (1998).

The reconstruction of the paleoenvironment of Torfdalsvatn in this study and previous publications is also supported by findings from marine studies. Diatom and foraminifera records of marine core MD99-2269, located on the northern shelf of Iceland, indicated particular cold temperatures between 11.7-11.5 cal. kyr BP (Justwan et al., 2008; Ólafsdóttir et al., 2010). This observation seems to be consistent with the deposition of clay in Torfdalsvatn. The foraminifera record also indicates rapidly increasing SST from ca. 10.5 cal. kyr BP, caused by a northward extension of the IC, brought warm water to the northern shelf of Iceland (Justwan et al., 2008; Ólafsdóttir et al., 2010) which subsequently led to increasing air temperatures. The timing of increasing temperatures also seems to agree with the lithological findings in the TDV record, where gyttja was deposited before 10.3 cal. kyr BP. The $\delta^{18}O$ records from a different marine core situated along the northern shelf on Iceland, also indicated similar warming trends after ca. 11 cal. kyr BP (Castañeda et al., 2004). The reconstructions of the SSTs are highly consistent with the deposition of glacial and non-glacial facies, suggesting that the IC had a strong influence on the North Icelandic shelf during the deglaciation (>12.0 cal. kyr BP).

6.3.1.2 Holocene (ca. 10.3 cal. kyr BP to present)

From ca. 10.3 cal. kyr BP to present, no significant changes in the depositional environment for Torfdalsvatn can be observed from the lithostratigraphy of the TDV sediment record. The lithology of Unit 1.2 in the TDV record reveals that lacustrine conditions prevailed during this time on Skagi. (Variations in lithology and MS or Ti record were used to interpreted changes in the paleoenvironment during the Holocene, however it should be noted that based on the

available data these changes cannot be confirmed and other proxies would need to be analyzed to confirm the interpretations).

The sediments of Unit 1.2 consist of mostly homogenous organic-rich gyttja indicating that warm conditions prevailed throughout the time of deposition (e.g., Briner et al., 2010; Håkansson et al., 2014; Kaplan et al., 2002; Schomacker et al., 2016). Low MS values suggest that after the deposition of the Saksunarvatn tephra no or very little minerogenic material, was transported into the lake. Peaks in the MS record within Unit 1.2 have been interpreted as being the result of tephra deposition (e.g., Harning et al., 2016; Schomacker et al., 2016). Fluctuations in the sedimentation rate throughout Unit 1.2 may indicate fluctuations in the water level, algal productivity and/or input of allochthonous plant material into the lake occurred during the Holocene (e.g., Tarasov et al., 1996; Meyers & Lallier-Vergès, 1999; Valpola & Ojala, 2006).

Based on comparison to previous studies (e.g., Florian, 2016) it was possible to identify a potential change in the depositional environment of Torfdalsvatn during the last 1.8 cal. kyr BP. Increasing MS values between 170-0 cm suggest an increased input in minerogenic material. Florian (2016) interpreted the increasing MS values to indicate two cooling periods and destabilizations of soil and suggested that a first cooling occurred around 1.8 cal. kyr BP. A second cooling is believed to have occurred 1.1 cal. kyr BP and increasing MS values may also indicate the beginning of human settlement in Iceland (Andrews et al., 2001; Florian, 2016). No other changes in the paleoenvironment occurring during Holocene have been identified from the Torfdalsvatn core (Florian, 2016).

6.3.2 Paleoenvironmental conditions of Þuríðarvatn, Nykurvatn and Ásbrandsstaðavatn

The reconstruction of the paleoenvironmental conditions have been divided into two sections: Deglaciation and Holocene. The Holocene section is further divided into two sub-sections: Early- to Mid-Holocene and Late Holocene.

6.3.2.1 Deglaciation to Saksunarvatn Ash (10.8 to ca. 10.3 cal. kyr BP)

During the early Holocene, the depositional environment in the Vopnafjörður area is believed to have experienced a change from glacial to increasingly lacustrine conditons, which can be seen from the lithostratigraphy of the ABS sediment core (Unit 4.1, Fig. 31). The lithology of

Unit 4.1 indicates that during the early Holocene a local glacier was present in the Vopnafjörður area. Based on the lithology it is believed that that the Vopnafjörður area has been fully deglaciated by 10.3 cal. kyr BP when the Saksunarvatn Ash has been deposited.

Sediments of Unit 4.1, composed of two facies (clay and clayey gyttja), are situated between the Askja S tephra and the Saksunarvatn Ash indicating that the unit has been deposited between ca. 10.8-10.3 cal. kyr BP. Based on the lithofacies (clayey gyttja and clay) Unit 4.1 has been interpreted as deposits of glacial meltwater inflow into the lake (e.g., Briner et al., 2010; Larsen et al., 2015; Harning et al., 2016; Schomacker et al., 2016). These findings might suggest that between 10.8-10.3 cal. kyr BP, a local glacier occupied the catchment of Ásbrandsstaðavatn. However, the upcore transition in the deposition from clayey gyttja to clay to clayey gyttja (Fig. 31) suggests that the amount of glacial meltwater inflow was fluctuating over time. The age-depth model of ABS suggests that the clay facies has been deposited around 10.5 cal. kyr BP. This indicates an increase in meltwater inflow during this time, possibly caused by a short-lived advance of the glacier into the catchment. The deposition of clayey gyttja prior to and after 10.5 cal. kyr BP might indicate that the glacier generally was retreating from the catchment. The low LOI values that have been observed throughout the unit also indicate increased input of minerogenic material and low organic content and therefore support the theory of a glacier influencing the depositional environment. However, Ti values are not as high as in the glacial Unit 1.1 of the TDV record, which may suggest that more minerogenic material was entering Torfdalsvatn or that material from a different source was deposited into the lake.

Reconstructions of the IIS show that the ice sheet had rapidly retreated from its maximum position during the Bølling-Allerød interstadial, and later re-advanced during the YD and early Holocene (Andrews et al., 2000; Norðdahl & Pétursson, 2005; Patton et al., 2017). A reconstruction of the IIS by Patton et al. (2017) indicated that the ice sheet had re-advanced to the head of Vopnafjörður at ca. 11.6 cal. kyr BP (Fig. 2C), before it rapidly retreated from the area. Based on their model it has been suggested that the IIS completely retreated from the study area by ca. 11.4 cal. kyr BP (Patton et al., 2017) suggesting that the ice sheet could not have had any influence on the sediments observed in the ABS core. However, the model also indicates that local glaciers were present around the fjord head after the retreat of the ice sheet

(Patton et al., 2017) and may have had an influence on the depositional environment of Ásbrandsstaðavatn.

Geomorphological evidence presented in previous studies (e.g., Norðdahl & Hjort, 1987; Sæmundsson, 1995; Norðdahl & Pétursson, 2005) suggest that the glaciers in Vopnafjörður experienced episodic standstill and/or readavanced during the final deglaciation. Two sets of glacial striations have been observed in the Vopnafjörður area and have been divided into an older and a younger set. The older striae reveal an easterly ice-flow and are believed to have been formed during the late YD when glaciers completely covered the Vopnafjörður area (Sæmundsson, 1995). Norðdahl & Pétursson (2005) also reported that during the YD, a glacier was situated in the Hofsárdalur valley (i.e., Hofsárdalur glacier) which experienced a standstill during the late YD and a subsequent rapid retreat (Norðdahl & Pétursson, 2005). As previously mentioned, the sediments in the ABS core are deposited after 10.8 cal. kyr BP and therefore do not contain information about glacial advances in the YD. The younger set of striae shows a northeasterly ice-flow direction, parallel to the direction of the Hofsárdalur and Vesturárdalur valleys and has been interpreted to be formed during glacial re-advances in the early Holocene (Sæmundsson, 1995). Glaciers situated in the Vopnafjörður area are believed to have been fairly extensive during early Holocene times (Norðdahl, 1991; Sæmundsson, 1995) and the Hofsárdalur glacier reportedly experienced several episodes of standstill and re-advances during the early Holocene (Norðdahl & Hjort, 1987; Sæmundsson, 1995). The presence of a glacier in Hofsárdalur indicates that the glacial sediments of Unit 4.1 in the ABS core that were deposited between 10.8-10.3 cal. kyr BP, may have received glacial meltwater from the Hofsárdalur glacier. The upcore increase in organic content in Unit 4.1 suggests that the glacier was retreating rather than re-advancing.

A previous study from lake Lögurinn, ~50 km southeast of Vopnafjörður (Fig. 2C), showed sediments that have been interpreted as glacially derived had a relatively low magnetic signals (Striberger et al., 2012). Striberger et al. (2012) found that glacial sediments deposited in lake Lögurinn have relatively low concentrations of ferrimagnetic minerals, causing the low MS signal. This might explain why Unit 4.1 deposited in Ásbrandsstaðavatn shows relatively low Ti values because glaciers transporting minerogenic material potentially eroded the same type of bedrock.

6.3.2.2 Holocene (ca. 10.3 cal. kyr BP – present)

From ca. 10.3 cal. kyr BP to present, the lithostratigraphy in Þuríðarvatn (Unit 2.1), Nykurvatn (Unit 3.1) and Ásbrandsstaðavatn (Unit 4.2) shows that lacustrine conditions prevailed in the three lakes. Sedimentological evidence suggests that the depositional environments of NYK and ÞUR did not change significantly during the Holocene. (Variations in lithology and LOI or Ti records were used to interpreted changes in the paleoenvironment, however it should be noted that based on the available data these changes cannot be confirmed and other proxies would need to be analyzed to confirm the interpretations).

Observations and interpretations made about the sediments of the three sediment during the Holocene have been divided into Early to Mid-Holocene and Late Holocene. Reconstructions of the early to mid-Holocene are based on the sediments from the ABS (10.8 cal. kyr BP – present) and NYK (ca. 8.7 cal. kyr BP – present) records. Late Holocene reconstructions are based on sediments from ABS and NYK and partly ÞUR (ca. 1.2 cal. kyr BP – present) record.

Early to Mid-Holocene (10.3-4.5 cal. kyr BP)

Between 10.3-7.0 cal. kyr BP organic-rich sediments of Unit 4.2 (gyttja, Fig. 31) that characterized by a gradually increasing LOI record have been deposited in Ásbrandsstaðavatn. The increase in LOI might indicate high algal productivity caused by a gradual rise in temperatures during the early to mid Holocene that follow colder conditions in the early Holocene. Climate reconstructions based on subfossil chironomids records from the sediment record of lake Stóra Viðarvatn, located ~75 km northwest of Vopnafjörður, indicate a gradual warming throughout the early and mid Holocene, following colder conditions during the early Holocene (Axford et al., 2007). This observation might agree with the higher LOI values observed in the ABS record between 10.3 cal. kyr BP and ca. 8.0 cal. kyr BP. In a study of Lögurinn (Fig. 2C) by Striberger et al. (2012) indications for the 8.2 cal. kyr BP cold event, which interrupted the general warming trend. The event was identified based on decreasing BSi concentrations and it was noted by the author that no lithological changes have been observed in association with this finding. No indications for such colder climatic conditions could be observed from the available data of the ABS sediment record.

Gyttja that has been deposited between 7.0-5.7 cal. kyr BP (214-190 cm, Unit 4.2 ABS) shows maximum values in the LOI record (Fig. 31). This maximum in organic content may

indicate a very high lake productivity occurring at that time (e.g., Tarasov et al., 1996; Valpola & Ojala, 2006). The sediments in the NYK core that are believed to have been deposited during the mid Holocene (ca. 8.5-5 cal. kyr BP) also show an increase in the LOI record between 7.9-7.7 cal. kyr BP (ca. 360-370 cm). However, similarly high values have been observed in sediments in the upper core. Decreases in LOI prior and after the increase have been interpreted to be tephra-related and therefore do not give any insight about changing paleoenvironmental conditions. In lake sediments from Tröllskagi (N-Iceland; Fig. 2), chironomid-inferred temperature reconstructions show that the HTM occurred between 7.6 and 6.8 cal. kyr BP (Caseldine et al., 2006). The increase in LOI observed in the ABS record between ca. 7.0-5.7 cal. kyr BP therefore might be caused by increased temperatures during HTM. The sediments of Lögurinn revealed that between 9.0-4.4 cal. kyr BP no glacially derived sediments have been deposited, suggesting lacustrine conditions and warmer temperatures (Striberger et al., 2012). Striberger et al. (2012) also identified a sub-unit in the sediment sequence of Lögurinn that has been characterized by high BSi concentrations and consisted of dark-colored homogenous sediments. The sub-unit is believed to represent the HTM, and the peak in BSi is the result of sustained algal blooms developed during warm spring temperatures (Striberger et al., 2012). The sediments in the ABS record between, 214-190 cm, show a similar dark color that may have also been caused by an algal bloom. This similar change in lithology in both lakes might therefore be used as evidence that the HTM occurred around 7.0-5.7 cal. kyr BP in the Vopnafjörður area.

Gyttja deposited after 5.7 cal. kyr BP (Unit 4.2 ABS) has a decreasing amount of organic matter as indicated by the LOI record. The lower LOI values might suggest a reduced lake productivity which might indicate decreasing temperatures (e.g., Tarasov et al., 1996; Valpola & Ojala, 2006). Following the HTM temperatures in Iceland started to decline around 6.0 cal. kyr BP as suggested by Caseldine et al. (2006). This seems to be consistent with the decreasing organic content that might indicate decreasing temperatures observed in the ABS core, starting at ca. 5.7 cal. kyr BP.

Late Holocene (ca. 4.2 cal. kyr BP to present)

The sediments of NYK that have been deposited during the late Holocene (4.2-0 cal. kyr BP) are characterized by a homogenous organic-rich gyttja lithology, relatively stable Ti/Sum record and a slightly upcore increasing LOI record. The gyttja facies generally indicates

lacustrine sedimentation (e.g., Briner et al., 2010; Schomacker et al., 2016). The increase in LOI may indicate increasing lake productivity caused by warmer temperatures (e.g., Tarasov et al., 1996; Meyers & Lallier-Vergès, 1999; Valpola & Ojala, 2006). This would, however, contradict the generally cooling trend occurring on Iceland during the Neoglaciation (Geirsdóttir et al., 2019). Data from Stóra Viðarvatn suggest that the Neoglacial period in northeast Iceland began after ca. 3.0 cal. kyr BP (Axford et al., 2007). However, it is not possible to confirm this onset of neoglacial cooling with the available data in this study. The increase in organic content could also indicate higher erosion rates that are known to have occurred during the LIA and caused the transportation of limiting nutrients into the lake and correlates to an increase in algal production (e.g., Doner, 2003). As previously mentioned, those changes in the paleoenvironment cannot be confirmed by the data.

In the Ti/Sum record of ABS, an upcore increase can be observed in sediments that have been deposited after ca. 1.1 cal. kyr BP (50-0 cm). This increase in Ti might indicate a higher minerogenic input because of destabilization of soil that might have been caused by a cooling event the human settlement of Iceland around 1.1 cal. kyr BP (Andrews et al., 2001; Blair et al., 2015; Florian, 2016).

The ÞUR sediment record consisting of gyttja indicates that lacustrine conditions prevailed during the Late Holocene from ca. 1.2 cal. kyr BP to the present day (e.g., Briner et al., 2010; Schomacker et al., 2016). No evidence for changes in the climate or environment in this particular sedimentary section have been identified.

7 Conlusions

Sediment cores retrieved from four lakes in north and northeast Iceland were used to construct continuous core records, establish age models, improve the regional tephra stratigraphy and reconstruct environmental conditions during the Late Quaternary. This study resulted in the following conclusions:

- The alignments of the individual sediment core sections were based on identified tephra layers and radiocarbon ages.
- Four tephra marker layers, including H1104, H3, H4, and the Saksunarvatn Ash identified in previous studies in northern Iceland and identified in different records (i.e., marine cores, lake cores, soil profiles) have been geochemically detected in the Torfdalsvatn sediment core.
- Five marker layers (i.e., V1477, H3, H4, the Saksunarvatn Ash, and Askja S) previously identified in different records from northeastern Iceland were also found in the sediment cores of Þuríðarvatn, Nykurvatn and Ásbrandsstaðavatn.
- Sedimentological evidence from Torfdalsvatn suggests that Skagi experienced local glacial advances around ca. 12.0 cal. kyr BP and glaciers had fully retreated from the Torfdalsvatn catchment by 10.3 cal. kyr BP.
- Sedimentological data further indicates that after 10.3 cal. kyr BP lacustrine conditions prevailed in Torfdalsvatn until the present day.
- Sedimentological evidence from Þuríðarvatn, Nykurvatn and Ásbrandsstaðavatn indicates that between 10.8 cal. kyr BP and 10.3 cal. kyr BP, a local glacier was present in Hofsárdalur, Vopnafjörður area. The glacier is believed to have fully retreated from the lake catchments by 10.3 cal. kyr BP.
- After 10.3 cal. kyr BP until present day lacustrine conditions prevailed in the three lakes in the Vopnafjörður area.

References

Alley, R. B., & Ágústsdóttir, A. M. (2005). The 8k event: cause and consequences of a major Holocene abrupt climate change. *Quaternary Science Journal*, *24*, 1123–1149. https://doi.org/10.1016/j.quascirev.2004.12.004

Alley, R. B., Mayewski, P. A., Sowers, T., Stuiver, M., Taylor, K. C., & Clark, P. U. (1997). Holocene climatic instability: A prominent, widespread event 8200 yr ago. *Geology*, *25*, 483–486. https://doi.org/10.1130/0091-7613(1997)025<0483

Andersen, C., & Koç, N. (2004). Nonuniform response of the major surface currents in the Nordic Seas to insolation forcing: Implications for the Holocene climate variability. *Paleoceanography*, *19*, 1–16. https://doi.org/10.1029/2002PA000873

Andrés, N., Palacios, D., Sæmundsson, Þ., Brynjólfsson, S., & Fernández-Fernández, J. M. (2019). The rapid deglaciation of the Skagafjörður fjord, northern Iceland. *Boreas*, *48*(1), 92–106. https://doi.org/10.1111/bor.12341

Andrews, J. T., Caseldine, C., Weiner, N. J., & Hatton, J. (2001). Late Holocene (ca. 4 ka) marine and Reykjarfjördur, north Iceland: climate and/or settlement?†. *Journal of Quaternary Science*, *16*(2), 133–143.

Andrews, J. T., Hardardóttir, J., Helgadóttir, G., Jennings, A. E., Geirsdóttir, Á., Sveinsbjörnsdóttur, À. E., Schoolfield, S., Krisjánsdóttir, G. B., Smith, L. M., Thors, K., Syvitski, J. P. M. (2000). The N and W Iceland Shelf: insights into Last Glacial Maximum ice extent and deglaciation based on acoustic stratigraphy and basal radiocarbon AMS dates. *Quaternary Science Reviews*, *19*, 619–631.

Axford, Y., Briner, J. P., Miller, G. H., & Francis, D. R. (2009). Paleoecological evidence for abrupt cold reversals during peak Holocene warmth on Baffin Island, Arctic Canada. *Quaternary Research*, *71*(2), 142–149. https://doi.org/10.1016/j.yqres.2008.09.006

Axford, Y., Geirsdóttir, Á., Miller, G. H., & Langdon, P. G. (2009). Climate of the Little Ice Age and the past 2000 years in northeast Iceland inferred from chironomids and other lake sediment proxies. *Journal of Paleolimnology*, *41*(1), 7–24. https://doi.org/10.1007/s10933-008-9251-1

Axford, Y., Miller, G. H., Geirsdóttir, Á., & Langdon, P. G. (2007). Holocene temperature history of northern Iceland inferred from subfossil midges. *Quaternary Science Reviews*, *26*(25–28), 3344–3358. https://doi.org/10.1016/j.quascirev.2007.09.003

Ben-Dor, E., & Banin, A. (1989). Determination of organic matter content in arid-zone soils using a simple “loss-on-ignition” method. *Communications in Soil Science and Plant Analysis*, *20*(15–16), 1675–1695. https://doi.org/10.1080/00103628909368175

Bergthórsson, P. (1969). An estimate of drift ice and temperature in Iceland in 1000 years. *Jökull*, 95–101.

Birks, H. H. (2001). Plant macrofossils. In *Tracking Environmental Change Using Lake Sediments.* (Vol. 3, pp. 49–74).

Birks, H. H., Gulliksen, S., Haflidason, H., Mangerud, J., & Possnert, G. (1996). New Radiocarbon Dates for the Vedde Ash and the Saksunarvatn Ash from Western Norway. *Quaternary Research*, *45*, 119–127.

Björck, S., Ingólfsson, Ó., Haflidason, H., Hallsdöttir, M., & Anderson, N. J. (1992). Lake Torfadalsvatn: a high resolution record of the North Atlantic ash zone I and the last glacial-interglacial environmental changes in Iceland. *Boreas*, *21*(1), 15–22. https://doi.org/10.1111/j.1502-3885.1992.tb00009.x

Björnsson, H., & Pálsson, F. (2008). Icelandic glaciers. *Jökull*, *58*, 365–386.

Blaauw, M. (2012). Out of tune: The dangers of aligning proxy archives. *Quaternary Science*

Reviews, *36*, 38–49. https://doi.org/10.1016/j.quascirev.2010.11.012
Blaauw, M., & Christen, J. A. (2011). *Bacon manual – v2.3.5*. 1–14.
Blair, C. L., Geirsdóttir, Á., & Miller, G. H. (2015). A high-resolution multi-proxy lake record of Holocene environmental change in southern Iceland. *Journal of Quaternary Science*, *30*(3), 281–292. https://doi.org/10.1002/jqs.2780
Blumentritt, D. J., Engstrom, D. R., & Balogh, S. J. (2013). A novel repeat-coring approach to reconstruct recent sediment, phosphorus, and mercury loading from the upper Mississippi River to Lake Pepin, USA. *Journal of Paleolimnology*, *50*(3), 293–304. https://doi.org/10.1007/s10933-013-9724-8
Borgatti, L., & Soldati, M. (2013). Hillslope Processes and Climate Change. *Treatise on Geomorphology*, *7*, 306–319. https://doi.org/10.1016/B978-0-12-374739-6.00180-9
Bowman, S. (1990). *Radiocarbon dating*. Berkley and Los Anglees: University of California Press.
Briner, J. P., Stewart, H. A. M., Young, N. E., Philipps, W., & Losee, S. (2010). Using proglacial-threshold lakes to constrain fl uctuations of the Jakobshavn Isbræ ice margin, western Greenland, during the Holocene. *Quaternary Science Journal*, *29*, 3861–3874. https://doi.org/10.1016/j.quascirev.2010.09.005
Carroll, A. R., & Bohacs, K. M. (1999). Stratigraphic classification of ancient lakes: Balancing tectonic and climatic controls. *Geology*, *27*(2), 99–102.
Caseldine, C. J., Geirsdóttir, Á., & Langdon, P. (2003). Efstadalsvatn – a multi-proxy study of a Holocene lacustrine sequence from NW Iceland. *Journal of Paleolimnology*, *30*(1), 55–73.
Caseldine, C. J., Langdon, P., & Holmes, N. (2006). Early Holocene climate variability and the timing and extent of the Holocene thermal maximum (HTM) in northern Iceland. *Quaternary Science Reviews*, *25*, 2314–2331. https://doi.org/10.1016/j.quascirev.2006.02.003
Castañeda, I. S., Smith, L. M., Kristjánsdóttir, G. B., & Andrews, J. T. (2004). Temporal changes in Holocene δ18O records from the northwest and central North Iceland Shelf. *Journal of Quaternary Science*, *19*(4), 321–334. https://doi.org/10.1002/jqs.841
Cherapanova, M. V., Snyder, J. A., & Brigham-Grette, J. (2007). Diatom stratigraphy of the last 250 ka at Lake El'gygytgyn, northeast Siberia. *Journal of Paleolimnology*, *37*, 155–162. https://doi.org/10.1007/s10933-006-9019-4
Clark, R. M., & Thompson, R. (1979). A new statistical approach to the alignment of time series. *Geophysical Journal of the Royal Astronomical Society*, *58*(3), 593–607. https://doi.org/10.1111/j.1365-246X.1979.tb04796.x
Coakley, J. P., & Rust, B. R. (1968). Sedimentation in an Arctic Lake. *SEPM Journal of Sedimentary Research*, *Vol. 38*(4), 1290–1300. https://doi.org/10.1306/74d71b59-2b21-11d7-8648000102c1865d
Cohen, A. S. (2003). *Paleolimnology: the history and evolution of lake systems*. New York ; Oxford : Oxford University Press.
Coulter, S. E., Pilcher, J. R., Hall, V. A., Plunkett, G., & Davies, S. M. (2010). Testing the reliability of the JEOL FEGSEM 6500F electron microprobe for quantitative major element analysis of glass shards from rhyolitic tephra. *Boreas*, *39*(1), 163–169. https://doi.org/10.1111/j.1502-3885.2009.00113.x
Crochet, P., Jóhannesson, T., Jónsson, T., Sigurdsson, O., Björnsson, H., Pálsson, F., & Barstad, I. (2007). Estimating the spatial distribution of precipitation in Iceland using a linear model of orographic precipitation. *Journal of Hydrometeorology*, *8*(6), 1285–1306. https://doi.org/10.1175/2007JHM795.1

Croudace, I. W., Rindby, A., & Rothwell, R. G. (2006). ITRAX: Description and evaluation of a new multi-function X-ray core scanner. *Geological Society Special Publication*, *267*, 51–63. https://doi.org/10.1144/GSL.SP.2006.267.01.04

Davies, S. M. (2015). Cryptotephras: the revolution in correlation and precision dating. *Journal of Quaternary Science*, *30*(2), 114–130. https://doi.org/10.1002/jqs.2766

Dean, W. E. (1974). Determination of carbonate and organic matter in calcareous sediments and sedimentary rocks by loss on ignition: comparison with other methods. *Journal of Sedimentary Petrology*, *44*(1), 242–248. https://doi.org/10.1128/JCM.01030-15

Denk, T., Grimsson, F., Zetter, R., & Símonarson, L. a. (2011). Introduction to the Nature and Geology of Iceland. In *Late Cainozoic Floras of Iceland* (pp. 1–29). https://doi.org/10.1007/978-94-007-0372-8

Doner, L. (2003). Late-Holocene paleoenvironments of northwest Iceland from lake sediments. *Palaeogeography, Palaeoclimatology, Palaeoecology*, *193*(3–4), 535–560. https://doi.org/10.1016/S0031-0182(03)00265-7

Dugmore, A., & Buckland, P. (1991). Tephrochronology and late Holocene soil erosion in south Iceland. In J. K. Maizels & C. Caseldine (Eds.), *Environmental Changes in Iceland: Past and Present* (pp. 147–159). Kluwer, Dordrecht.

Dugmore, A. J., Larsen, G., & Newton, A. J. (1995). Seven tephra isochrones in Scotland. *Holocene*, *5*(3), 257–266. https://doi.org/10.1177/095968369500500301

Dugmore, Andrew J, Newton, A. J., & Sugden, D. E. (1992). Geochemical stability of fine-grained silicic Holocene tephra in Iceland and Scotland. *Journal of Quaternary Science*, *7*(2), 173–183.

Eddudóttir, S. D., Erlendsson, E., & Gísladóttir, G. (2017). Effects of the Hekla 4 tephra on vegetation in Northwest Iceland. *Vegetation History and Archaeobotany*, *26*(4), 389–402. https://doi.org/10.1007/s00334-017-0603-5

Eddudóttir, S. D., Erlendsson, E., & Gísladóttir, G. (2020). Landscape change in the Icelandic highland: A long-term record of the impacts of land use, climate and volcanism. *Quaternary Science Reviews*, *240*. https://doi.org/10.1016/j.quascirev.2020.106363

Einarsson, M. Á. (1979). Climatic conditions of the Lake Mývatn area. *Oikos*, *32*(1), 29–37.

Einarsson, M. Á. (1984). Climate of Iceland. In H. van Loon (Ed.), *Climates of the Oceans* (pp. 673–697). Amsterdam: Elsevier.

Einarsson, T. (1973). Geology of Iceland. In M. Pitcher (Ed.), *Arctic Geology* (Am. Assoc., pp. 171–175). Proc. of the Second International Symposium.

Eiríksson, J., Knudsen, K. L., Haflidason, H., & Henriksen, P. (2000). Late-glacial and Holocene palaeoceanography of the North Icelandic shelf. *Journal of Quaternary Science*, *15*, 23–42.

Florian, C. R. (2016). *Multi-Proxy Reconstructions of Holocene Environmental Change and Catchment Biogeochemistry Using Algal Pigments and Stable Isotopes Preserved in Lake Sediment from Baffin Island and Iceland*. Retrieved from PhD thesis, University of Iceland

Flowers, G. E., Björnsson, H., Geirsdóttir, Á., Miller, G. H., Black, J. L., & Clarke, G. K. C. (2008). Holocene climate conditions and glacier variation in central Iceland from physical modelling and empirical evidence. *Quaternary Science Reviews*, *27*, 797–813. https://doi.org/10.1016/j.quascirev.2007.12.004

Forwick, M. (2013). *How to use XRF core scanner data acquired with the Avaatech XRF core scanner at the Department of Geology , University of Tromsø*. 1–9.

Fritz, S. C. (2008). Deciphering climatic history from lake sediments. *Journal of Paleolimnology*, *39*(1), 5–16. https://doi.org/10.1007/s10933-007-9134-x

Froggatt, P. C. (1992). Standardization of the chemical analysis of tephra deposits. Report of the ICCT Working Group. *Quaternary International*, *13–14*(C), 93–96. https://doi.org/10.1016/1040-6182(92)90014-S

Fujifilm Corperation. (2009). *Fujifilm Technical Handbook: The Fundamentals of Industrial Radiography*. Retrieved from https://www.fujifilmusa.com/shared/bin/ix-film_fundamentals_of_industrial_radiography.pdf

Geirsdóttir, Á., Andrews, J. T., Helgadóttir, G., & Hardardóttir, J. (2002). A 36 Ky record of iceberg rafting and sedimentation from north-west Iceland. *Polar Research*, *21*(2), 291–298.

Geirsdóttir, Á., Miller, G. H., Andrews, J. T., Harning, D. J., Anderson, L. S., Florian, C., Larsen, D. J., Thordarson, T. (2019). The onset of neoglaciation in Iceland and the 4.2 ka event. *Climate of the Past*, *15*, 25–40.

Geirsdóttir, Á., Miller, G. H., Axford, Y., & Sædís Ólafsdóttir. (2009). Holocene and latest Pleistocene climate and glacier fluctuations in Iceland. *Quaternary Science Reviews*, *28*(21–22), 2107–2118. https://doi.org/10.1016/j.quascirev.2009.03.013

Geotek. (2016). *Manual: Multi-Sensor Core Logger*. Retrieved from https://www.geotek.co.uk/wp-content/uploads/2016/04/MSCL-manual-1-Nov-16.pdf

Godwin, H. (1962). Half-life of Radiocarbon. *Nature*, *195*(4845), 984–984.

Gudmundsdóttir, E. R., Eiríksson, J., & Larsen, G. (2011). Identification and definition of primary and reworked tephra in Late Glacial and Holocene marine shelf sediments off North Iceland. *Journal of Quaternary Science*, *26*(6), 589–602.

Gudmundsdóttir, E. R., Larsen, G., Björck, S., Ingolfsson, Ó., & Striberger, J. (2016). A new high-resolution Holocene tephra stratigraphy in eastern Iceland: Improving the Icelandic and North Atlantic tephrochronology. *Quaternary Science Reviews*, *150*, 234–249. https://doi.org/10.1016/j.quascirev.2016.08.011

Gudmundsdóttir, E. R., Larsen, G., & Eiríksson, J. (2012). Tephra stratigraphy on the North Icelandic shelf: extending tephrochronology into marine sediments off North Iceland Iceland. *Boreas*, 1–17. https://doi.org/10.1111/j.1502-3885.2012.00258.x

Gudmundsdóttir, E. R., Schomacker, A., Brynjólfsson, S., Ingólfsson, Ó., & Larsen, N. K. (2018). Holocene tephrostratigraphy in Vestfirðir, NW Iceland. *Journal of Quaternary Science*, *33*(7), 827–839. https://doi.org/10.1002/jqs.3063

Gudmundsson, H. J. (1997). A review of the Holocene environmental history of Iceland. *Quaternary Science Reviews*, *16*(1), 81–92. https://doi.org/10.1016/S0277-3791(96)00043-1

Haam, E., & Huybers, P. (2010). A test for the presence of covariance between time-uncertain series of data with application to the Dongge Cave speleothem and atmospheric radiocarbon records. *Paleoceanography*, *25*(2), 1–14. https://doi.org/10.1029/2008PA001713

Haflidason, H., Eiriksson, J., & Van Kreveld, S. (2000). The tephrochronology of Iceland and the North Atlantic region during the Middle and Late Quaternary: a review. *Journal of Quaternary Science*, *15*(1), 3–22.

Hajdas, I. (2008). Radiocarbon dating and its applications in Quaternary studies. *Quaternary Science Journal*, *57*(1–2), 2–25.

Håkansson, L., Briner, J. P., Andresen, C. S., Thomas, E. K., & Bennike, O. (2014). Slow retreat of a land based sector of the West Greenland Ice Sheet during the Holocene Thermal Maximum: evidence from threshold lakes at Paakitsoq. *Quaternary Science Reviews*, *98*, 74–83. https://doi.org/10.1016/j.quascirev.2014.05.016

Haldar, S. K., & Tišljar, J. (2014). Chapter 5 – Sedimentary Rocks. In *Introduction to*

Mineralogy and Petrology (pp. 121–212). https://doi.org/10.1016/B978-0-12-408133-8.00005-5
Hall, V. A., & Pilcher, J. R. (2002). Late-Quaternary Icelandic tephras in Ireland and Great Britain: detection, characterization and usefulness. *The Holocene*, *12*(2), 223–230. https://doi.org/10.1191/0959683602hl538rr
Hallsdóttir, M., & Caseldine, C. J. (2005). The Holocene vegetation history of Iceland, state-of-the-art and future research. In C. J. Caseldine, A. Russel, J. Hardardóttir, & Ó. Knudsen (Eds.), *Iceland - Modern Processes and Past Environments* (pp. 319–334).
Hanna, E., Jónsson, T., & Box, J. E. (2001). Recent changes in Icelandic climate. *Royal Metrological Society*, *61*, 3–9.
Hanna, E., Jónsson, T., & Box, J. E. (2004). An analysis of Icelandic climate since the nineteenth century. *International Journal of Climatology*, *24*(10), 1193–1210. https://doi.org/10.1002/joc.1051
Hansen, B., & Østerhus, S. (2000). North Atlantic – Nordic Seas exchanges. *Progress in Oceanography*, *45*, 109–208.
Harning, D. J., Geirsdóttir, A., Miller, G. H., & Zalzal, K. (2016a). Early Holocene deglaciation of Drangajökull, Vestfirðir, Iceland. *Quaternary Science Reviews*, *153*, 192–198. https://doi.org/10.1016/j.quascirev.2016.09.030
Harning, D. J., Geirsdóttir, Á., Miller, G. H., & Zalzal, K. (2016b). Early Holocene deglaciation of Drangajökull, Vestfirðir, Iceland. *Quaternary Science Reviews*, *153*, 192–198. https://doi.org/10.1016/j.quascirev.2016.09.030
Harning, D. J., Thordarson, T., Geirsdóttir, Á., Zalzal, K., & Miller, H. (2018). Provenance, stratigraphy and chronology of Holocene tephra from. *Quaternary Geochronology*, *46*, 59–76. https://doi.org/10.1016/j.quageo.2018.03.007
Hatfield, R. G., & Maher, B. A. (2009). Fingerprinting upland sediment sources: particle size-specific magnetic linkages between soils, lake sediments and suspended sediments. *Earth Surface Processes and Landforms*, *34*, 1359–1373. https://doi.org/10.1002/esp
Hayward, C. (2012). High spatial resolution electron probe microanalysis of tephras and melt inclusions without beam-induced chemical modification. *The Holocene*, *22*(1), 119–125. https://doi.org/10.1177/0959683611409777
Heiri, O., Lotter, A. F., & Lemcke, G. (2001). Loss on ignition as a method for estimating organic and carbonate content in sediments: Reproducibility and comparability of results. *Journal of Paleolimnology*, *25*(1), 101–110. https://doi.org/10.1023/A:1008119611481
Hunt, J. B., & Hill, P. G. (1993). Tephra geochemistry: a discussion of some persistent analytical problems. *The Holocene*, *3*(3), 271–278.
Hunt, J. B., & Hill, P. G. (2001). Tephrological implications of beam size - Sample-size effects in electron microprobe analysis of glass shards. *Journal of Quaternary Science*, *16*(2), 105–117. https://doi.org/10.1002/jqs.571
Ingólfsson, Ó. (2019). Paleo icestreams in NE-Iceland. *Talk given at UiT*.
Ingólfsson, Ó. (1988). Glacial history of the lower Borgarfjördur area, western Iceland. *Geologiska Föreningens i Stockholm Förhandlingar*, *110*, 293–309. https://doi.org/10.1080/11035898809452664
Ingólfsson, Ó. (1991). A review of the Late Weichselian and early Holocene glacial and environmental history of Iceland. In J. L. Maizels & C. J. Caseldine (Eds.), *Environmental Changes in Iceland: Past and Present* (pp. 13–29). Kluwer, Dordrecht.
Ingólfsson, Ó., Björck, S., Haflidason, H., & Rundgren, M. (1997). Glacial and climatic events in Iceland reflecting regional North Atlantic climatic shifts during the Pleistocene-Holocene transition. *Quaternary Science Reviews*, *16*, 1135–1144.

Ingólfsson, Ó., & Norðdahl, H. (1994). A review of the environmental history of Iceland, 13 000 - 9000 yr BP. *Journal of Quaternary Science*, *9*, 147–150.
Ingólfsson, Ó., Norddahl, H., & Haflidason, H. (1995). Rapid isostatic rebound in southwestern Iceland at the end of the last glaciation. *Boreas*, *24*, 245–259.
Ingólfsson, Ó., Norddahl, H., & Schomacker, A. (2010). 4 Deglaciation and Holocene Glacial History of Iceland. *Developments in Quaternary Science*, *13*, 51–68. https://doi.org/10.1016/S1571-0866(09)01304-9
Ingólfsson, Ó., & Norðdahl, H. (2001). High Relative Sea Level during the Bolling Interstadial in Western Iceland : A Reflection of Ice-sheet Collapse and Extremely Rapid Glacial Unloading High Relative Sea Level during the Bolling Interstadial in Western Iceland : a Reflection of Ice-sheet Co. *Arctic, Antarctic, and Alpine Research*, *33*(2), 231–243. https://doi.org/10.1080/15230430.2001.12003426
Jakobsson, S. P. (1979). Petrology of Recent basalts of the Eastern Volcanic Zone, Iceland. *Acta Naturalia Islandia*, *26*, 1–103.
Jakobsson, S. P., Jónasson, K., & Sigurdsson, I. A. (2008). The three igneous rock series of Iceland. *Jökull*, *58*, 117–138.
Jenkins, R., & Vries, J. L. D. (1970). *Practical X-ray spectometry* (Second edition). London: Macmillan and Co LTD.
Jennings, A., Syvitski, J., Gerson, L., Grönvold, K., Geirsdóttir, Á., Hardardóttir, J., Andrews, J., Hagen, S. (2000). Chronology and paleoenvironments during the late Weichselian deglaciation of the southwest Iceland shelf. *Boreas*, *29*(3), 167–183.
Jiang, H., Seidenkrantz, M.-S., Knudsen, K. L., & Eiríksson, J. (2002). Late-Holocene summer sea-surface temperatures based on a diatom record from the north Icelandic shelf. *The Holocene*, *12*(2), 137–147.
Jóhannesson, H., & Sæmundsson, K. (1989). Geological map of Iceland, 1:500.000. *Bedrock Geology. Icelandic Museum of Natural History and Iceland Geodetic Survey. Reykjavik.*
Jóhannsdóttir, G. E., Thordarson, T., Geirsdóttir, Á., & Larsen, G. (2005). The widespread ~10 ka Saksunarvatn Tephra: a product of three large basaltic phreatoplinian eruptions? *Geophysical Research Abstract*, *7*(05991).
Justwan, A., Koç, N., & Jennings, A. E. (2008). Evolution of the Irminger and East Icelandic Current systems through the Holocene, revealed by diatom-based sea surface temperature reconstructions. *Quaternary Science Reviews*, *27*(15–16), 1571–1582. https://doi.org/10.1016/j.quascirev.2008.05.006
Kaldal, I., & Víkingsson, S. (1990). Early Holocene deglaciation in Central Iceland. *Jökull*, *40*, 51–66.
Kalliokoski, M., Wastegård, S., & Saarinen, T. (2018). Rhyolitic and dacitic component of the Askja 1875 tephra in southern and central Finland: first step towards a Finnish tephrochronology. *Journal of Quaternary Science*, 1–11. https://doi.org/10.1002/jqs.3078
Kaplan, M. R., Wolfe, A. P., & Miller, G. H. (2002). Holocene Environmental Variability in Southern Greenland Inferred from Lake Sediments. *Quaternary Research*, *58*, 149–159. https://doi.org/10.1006/qres.2002.2352
Karlén, W. (1976). Lacustrine Sediments and Tree-Limit Variations as Indicators of Holocene Climatic Fluctuations in. *Geografiska Annaler: Series A, Physical Geography*, *58*(1–2), 1–34. https://doi.org/10.1080/04353676.1976.11879921
Kaufman, D. S. (2009). An overview of late Holocene climate and environmental change inferred from Arctic lake sediment. *Journal of Paleolimnology*, *41*(1), 1–6. https://doi.org/10.1007/s10933-008-9259-6

Kaufman, D. S., Ager, T. A., Anderson, N. J., Anderson, P. M., Andrews, J. T., Bartlein, P. J., Brubaker, L. B., Coats, L. L., Cwynar, L. C., Duvall, M. L., Dyke, A. S., Edwards, M. E., Eisner, W. R., Gajewski, K., Geirsdóttir, A., Hu, F. S., Jennings, A. E., Kaplan, M. R., Kerwin, M. W., Lozhkin, A. V., MacDonald, G. M., Miller, G. H., Mock, C. J., Oswald, W. W., Otto-Bliesner, B. L., Porinchu, D. F., Rühland, K., Smol, J. P., Steig, E. J., Wolfe, B. B. (2004). Holocene thermal maximum in the western Arctic (0-180°W). *Quaternary Science Reviews*, *23*(5–6), 529–560. https://doi.org/10.1016/j.quascirev.2003.09.007

Kearney, R., Albert, P. G., Staff, R. A., Pál, I., Veres, D., Magyari, E., & Ramsey, C. B. (2018). Ultra-distal fine ash occurrences of the Icelandic Askja-S Plinian eruption deposits in Southern Carpathian lakes: New age constraints on a continental scale tephrostratigraphic ma ... Ultra-distal fi ne ash occurrences of the Icelandic Askja-S Plinian e. *Quaternary Science Reviews*, (April). https://doi.org/10.1016/j.quascirev.2018.03.035

Kido, Y., Koshikawa, T., & Tada, R. (2006). Rapid and quantitative major element analysis method for wet fine-grained sediments using an XRF microscanner. *Marine Geology*, *229*, 209–225. https://doi.org/10.1016/j.margeo.2006.03.002

Kottek, M., Grieser, J., Beck, C., Rudolf, B., & Rubel, F. (2006). World map of the Köppen-Geiger climate classification updated. *Meteorologische Zeitschrift*, *15*(3), 259–263. https://doi.org/10.1127/0941-2948/2006/0130

Kristjánsdóttir, G. B., Stoner, J. S., Jennings, A. E., Andrews, J. T., & Grönvold, K. (2007). Geochemistry of Holocene cryptotephras from the North Iceland Shelf (MD99-2269): intercalibration with radiocarbon and palaeomagnetic chronostratigraphies. *The Holocene*, *17*(2), 155–176.

Kylander, M. E., Ampel, L., Wohlfarth, B., & Veres, D. (2011). High-resolution X-ray fluorescence core scanning analysis of Les Echets (France) sedimentary sequence: new insights from chemical proxies. *Journal of Quaternary Science*, *26*(1), 109–117. https://doi.org/10.1002/jqs.1438

Lane, C. S., Blockley, S. P. E., Mangerud, J., Smith, V. C., Lohne, Ø. S., Tomlinson, E. L., Matthews, I. P., Lotter, A. F. (2012). Was the 12.1 ka Icelandic Vedde Ash one of a kind ? *Quaternary Science Reviews*, *33*, 87–99. https://doi.org/10.1016/j.quascirev.2011.11.011

Larsen, D. J., Miller, G. H., Geirsdóttir, Á., & Ólafsdóttir, S. (2012). Non-linear Holocene climate evolution in the North Atlantic: a high-resolution , multi-proxy record of glacier activity and environmental change from Hvítárvatn, central Iceland. *Quaternary Science Reviews*, *39*, 14–25. https://doi.org/10.1016/j.quascirev.2012.02.006

Larsen, D. J., Miller, G. H., Geirsdóttir, Á., & Thordarson, T. (2011). A 3000-year varved record of glacier activity and climate change from the proglacial lake Hvítárvatn, Iceland. *Quaternary Science Reviews*, *30*(19–20), 2715–2731. https://doi.org/10.1016/j.quascirev.2011.05.026

Larsen, G. (1981). Tephrochronology by Microprobe Glass Analysis. In S. Self & R. S. J. Sparks (Eds.), *Tephra Studies* (Nato Advan, pp. 95–102). Springer, Dordrecht.

Larsen, G. (2000). Holocene eruptions within the Katla volcanic system, south Iceland: Characteristics and environmental impact. *Jökull*, *49*(49), 1–28.

Larsen, G. (2010). Katla: Tephrochronology and Eruption History. *Developments in Quaternary Science*, *13*, 23–49. https://doi.org/10.1016/S1571-0866(09)01303-7

Larsen, G., Dugmore, A., & Newton, A. (1999). Geochemistry of historical-age silicic tephras in Iceland. *The Holocene*, *9*, 463–471.

Larsen, G., & Eiríksson, J. (2008). Late Quaternary terrestrial tephrochronology of Iceland — frequency of explosive eruptions, type and volume of tephra deposits. *Journal of Quaternary Science*, *23*(2), 109–120. https://doi.org/10.1002/jqs

Larsen, G., Eiriksson, J., Knudsen, K. L., & Heinemeier, J. (2002). Correlation of late Holocene terrestrial and marine tephra markers, north Iceland: implications for reservoir age changes. *Polar Research*, *21*(2), 283–290.

Larsen, G., Newton, A. J., Dugmore, A. J., & Vilmundardóttir, E. G. (2001). Geochemistry, dispersal, volumes and chronology of Holocene silicic tephra layers from the Katla volcanic system, Iceland. *Journal of Quaternary Science*, *16*(2), 119–132. https://doi.org/10.1002/jqs.587

Larsen, G., & Thorarinsson, S. (1977). H and other acidic Hekla tephra layers. *Jökull*, *27*, 28–46.

Larsen, N. K., Kjær, K. H., Lecavalier, B., Bjørk, A. A., Colding, S., Huybrechts, P., Jakobsen, K. E., Kjeldsen, K. K., Knudsen, K. L., Odgaard, B. V., Olsen, J. (2015). The response of the southern Greenland ice sheet to the Holocene thermal maximum. *Geology*, *43*(4), 291–294. https://doi.org/10.1130/G36476.1

Leeder, M. R. (2011). Part 3: Transporting sediments. In *Sedimentology and Sedimentary Basins: From Turbuence to Tectonics* (2nd Editio, pp. 113–198). Wiley-Blackwell.

Lisiecki, L. E., & Herbert, T. D. (2007). Automated composite depth scale construction and estimates of sediment core extension. *Paleoceanography*, *22*(4), 1–12. https://doi.org/10.1029/2006PA001401

Lofi, J., & Weber, O. (2001). SCOPIX - digital processing of X-ray images for the enhancement of sedimentary structures in undisturbed core slabs. *Geo-Marine Letters*, *20*, 182–186. https://doi.org/10.1007/s003670000051

Lowe, D. J. (2011). Quaternary Geochronology Tephrochronology and its application: A review. *Quaternary Geochronology*, *6*(2), 107–153. https://doi.org/10.1016/j.quageo.2010.08.003

Lowe, J. J., & Walker, M. J. C. (2014). Chapter 5 - Dating methods. In *Reconstructing Quaternary Environments* (pp. 237–297).

Löwemark, L, Chen, H., Yang, T., Kylander, M., Yu, E., Hsu, Y., Lee, T. Q., Song, S. R., Jarvis, S. (2011). Normalizing XRF-scanner data: A cautionary note on the interpretation of high-resolution records from organic-rich lakes. *Journal of Asian Earth Science*, *40*, 1250–1256. https://doi.org/10.1016/j.jseaes.2010.06.002

Löwemark, L., Bloemsma, M., Courdace, I., Daly, J. S., Edwards, R. J., Francus, P., Galloway, J. M., Gregory, B. R. B., Huang, J. J., Jones, A. F., Kylander, M., Luo, Y., Maclachlan, S., Ohlendorf, C., Patterson, R. T., Pearce, C., Profe, J., Reinhardt, E. G., Stranne, C., Tjallingii, R., Turner, J. N. (2019). Practical guidelines and recent advances in the Itrax XRF core-scanning procedure. *Quaternary International*, *514*, 16–29.

Mangerud, J., Furnes, H., & Jóhansen, J. (1986). SHORT PAPERS. A 9000-Year-Old Ash Bed on the Faroe islands. *Quaternary Research*, *26*, 262–265.

Marty, C., Skaugen, T., Pecho, J., & López-Moreno, J. I. (2010). *ETC- AAC Technical Paper on „Impacts of changing climate on Europe ' s snow and ice "Chapter 1: Ice and snow regions in Europe"*.

Meara, R. H. (2011). *Geochemical fingerprinting of Icelandic silicic Holocene tephra layers*. Retrieved from PhD thesis, University of Edinburgh

Meara, R. H., Thordarson, T., Pearce, N. J. G., Hayward, C., & Larsen, G. (2019). A catalogue of major and trace element data for Icelandic Holocene silicic tephra layers. *Journal of Quaternary Science*, 1–21. https://doi.org/10.1002/jqs.3173

Meija, J., Coplen, T. B., Berglund, M., Brand, W. A., De Bièvre, P., Gröning, M., Holden, N. E., Irrgeher, J., Loss, R., Walczyk, T., Prohaska, T. (2016). Isotopic compositions of the elements 2013 (IUPAC Technical Report). *Pure and Applied Chemistry*, *88*(3), 293–306. https://doi.org/10.1515/pac-2015-0503

Meyers, P. A., & Ishiwatari, R. (1993). Lacustrine organic geochemistry - an overview of indicators of organic matter sources and diagenesis in lake sediments. *Organic Geochemistry*, *20*(7), 867–900.

Meyers, Philip A, & Lallier-Vergès, E. (1999). Lacustrine sedimentary organic matter records of Late Quaternary paleoclimates. *Journal of Paleolimnology*, *21*, 345–372.

Molina-Cruz, A. (1991). Holocene palaeo-oceanography of the northern Iceland Sea , indicated by Radiolaria and sponge spicules. *Journal of Quaternary Science*, *6*(4), 303–312.

Neave, D. A., Hartley, M. E., Maclennan, J., & Edmonds, M. (2017). Volatile and light lithophile elements in high-anorthite plagioclase-hosted melt inclusions from Iceland. *Geochimica et Cosmochimica Acta*, *205*, 100–118. https://doi.org/10.1016/j.gca.2017.02.009

Norðdahl, H. (1991). A review of the glaciation maximum concept and the deglaciation of Eyjaförður, north Iceland. In J. L. Maizels & C. J. Caseldine (Eds.), *Environmental Changes in Iceland: Past and Present* (pp. 31–47). Kluwer, Dordrecht.

Norðdahl, H., & Hjort, C. (1987). Aldur jökulhörfunar í Vopnafirði, Abstract volume. *Jarðfræðafélag Íslands*, 18–19.

Norðdahl, H., Ingólfsson, Ó., Pétursson, H., & Hallsdóttir, M. (2008). Late Weichselian and Holocene environmental history of Iceland. *Jökull*, *58*, 343–364.

Norðdahl, H., & Pétursson, H. G. (2005). Relative sea-level changes in Iceland: new aspects of the Weichselian deglaciation of Iceland. In *Iceland - Modern Processes and Past Environments*.

Ogilvie, A. E. J., Barlow, L. K., & Jennings, A. E. (2000). North Atlantic climate c. AD 1000: Millennial reflections on the Viking discoveries of Iceland, Greenland and North America. *Weather*, *55*(2), 34–45. https://doi.org/10.1002/j.1477-8696.2000.tb04028.x

Óladóttir, B. A. (2009). *Holocene eruption history and magmatic evolution of the subglacial volcanoes, Grímsvötn, Bárdarbunga and Kverkfjöll beneath Vatnajökull, Iceland*. Retrieved from PhD thesis, University of Blaise-Pascal and University of Iceland, 142 pp

Óladóttir, B. A., Larsen, G., Thordarson, T., & Sigmarsson, O. (2005). The Katla volcano S-Iceland: Holocene tephra stratigraphy and eruption frequency. *Jökull*, *55*(May 2014), 53–74.

Óladóttir, B. A., Sigmarsson, O., Larsen, G., & Devidal, J. (2011). Provenance of basaltic tephra from Vatnajökull subglacial volcanoes, Iceland, as determined by major- and trace-element analyses. *The Holocene*, *21*(7), 1037–1048.

Óladóttir, B. A., Sigmarsson, O., Larsen, G., & Thordarson, T. (2008). Katla volcano, Iceland: Magma composition, dynamics and eruption frequency as recorded by Holocene tephra layers. *Bulletin of Volcanology*, *70*(4), 475–493. https://doi.org/10.1007/s00445-007-0150-5

Óladóttir, B. A., Thordarson, T., Geirsdóttir, Á., Jóhannsdóttir, G. E., & Mangerud, J. (2020). The Saksunarvatn Ash and the G10ka series tephra. Review and current state of knowledge. *Quaternary Geochronology*, *56*.

Ólafsdóttir, R., & Guòmundsson, H. J. (2002). Holocene land degradation and climatic change in northeastern Iceland. *The Holocene*, *2*, 159–167.

Ólafsdóttir, R., Schlyter, P., & Hörður, V. H. (2001). Simulating Icelandic vegetation cover

during the Holocene. Implications for long-term land degradation. *Geografiska Annaler*, *83 (A)*(4), 203–215.
Ólafsdóttir, S., Jennings, A. E., Geirsdóttir, Á., Andrews, J., & Miller, G. H. (2010). Marine Micropaleontology Holocene variability of the North Atlantic Irminger current on the south- and northwest shelf of Iceland. *Marine Micropaleontology*, *77*(3–4), 101–118. https://doi.org/10.1016/j.marmicro.2010.08.002
Ólafsson, H., Furger, M., & Brümmer, B. (2007). The weather and climate of Iceland. *Meteorologische Zeitschrift*, *16*(1), 5–8. https://doi.org/10.1127/0941-2948/2007/0185
Østerhus, S., Turrell, W. R., Steingrímur, J., & Hanse, B. (2005). Measured volume, heat, and salt fluxes from the Atlantic to the Arctic Mediterranean. *Geophysical Journal International*, *32*, 10–13. https://doi.org/10.1029/2004GL022188
Paillard, D., Labeyrie, L., & Yiou, P. (1996). AnalySeries 1.0: a Macintosh software for the analysis of geophysical time-series. *Eos, Transactions American Geophysical Union*, *77*, 379.
Patton, H., Hubbard, A., Bradwell, T., & Schomacker, A. (2017). The configuration, sensitivity and rapid retreat of the Late Weichselian Icelandic ice sheet. *Earth-Science Reviews*, *166*, 223–245. https://doi.org/10.1016/j.earscirev.2017.02.001
Perry, P. K. (1986). Bathymetry. In B. G. Hurdle (Ed.), *The Nordic Seas*. https://doi.org/https://doi.org/10.1007/978-1-4615-8035-5_9
Peti, L., & Augustinus, P. C. (2019). Stratigraphy and sedimentology of the Orakei maar lake sediment sequence (Auckland Volcanic Field, New Zealand). *Scientific Drilling*, *25*, 47–56. https://doi.org/10.5194/sd-25-47-2019
Pétursson, H., Norðdahl, H., & Ingólfsson, Ó. (2015). Late Weichselian history of relative sea level changes in Iceland during a collapse and subsequent retreat of marine based ice sheet. *Cuadernos de Investigacion Geografica*, *41*(2), 261–277. https://doi.org/10.18172/cig.2741
Principato, S. M. (2008). Geomorphic evidence for Holocene glacial advances and sea level fluctuations on eastern Vestfirðir, northwest Iceland. *Boreas*, *37*, 132–145. https://doi.org/10.1111/j.1502-3885.2007.00003.x
Principato, S. M., Geirsdóttir, Á., Jóhannsdóttir, G. E., & Andrews, J. T. (2006). Late Quaternary glacial and deglacial history of eastern Vestfirdir, Iceland using cosmogenic isotope (36Cl) exposure ages and marine cores. *Journal of Quaternary Science*, *21*(3), 271–285. https://doi.org/10.1002/jqs.978
R Core Team. (2017). *A language and environment for statistical computing. R Foundation for Statistical Computing*. Retrieved from https://www.r-project.org/ (2017)
Ramsey, C. B., van der Pflicht, J., & Weninger, B. (2001). “Wiggle matching” radiocarbon dates. *Radiocarbon*, *43*(2A), 381–389.
Rasmussen, S. O., Andersen, K. K., Svensson, A. M., Steffensen, J. P., Vinther, B. M., Clausen, H. B., Siggaard-Andersen, M. L., Johnsen, S. J., Larsen, D. B., Bigler, M., Fischer, H. (2006). A new Greenland ice core chronology for the last glacial termination. *Journal of Geophysical Research*, *111*, 1–16. https://doi.org/10.1029/2005JD006079
Reimer, P. J., Bard, E., Bayliss, A., Beck, J. W., Blackwell, P. G., Bronk, C., Buck, C. E., Cheng, H., Edwards, R. L., Friedrich, M., Grootes, P. M., Guilderson, T. P., Haflidason, H., Hajdas, I., Hatté, C., Heaton, T. J., Hoffmann, D. L., Hogg, A. G., Hughen, K. A., Kaiser, F., Kromer, B., Manning, S. W., Niu, M., Reimer, R. W., Richards, D. A., Scott, E. M., Southon, J. R., van der Pflicht, J. (2013). Intcal13 and marine13 radiocarbon age calibration curves 0 – 50,000 years cal BP. *Radiocarbon*, *55*(4), 1869–1887.
Richter, T. O., Van Der Gaast, S., Koster, B., Vaars, A., Gieles, R., De Stigter, H. C., De Has,

H., Van Weering, T. C. E. (2006). The Avaatech XRF Core Scanner: Technical description and applications to NE Atlantic sediments. *Geological Society Special Publication*, *267*, 39–50. https://doi.org/10.1144/GSL.SP.2006.267.01.03

Rundgren, M. (1995). Biostratigraphic Evidence of the Allerød-Younger Dryas-Preboreal Oscillation in Northern Iceland. *Quaternary Research*, *44*, 405–413.

Rundgren, M. (1997). *Late Weichselian and early Holocene changes of vegetation, climate and sea level on the Skagi peninsula, northern Iceland* (Lund University). Retrieved from LUNQUA Thesis 40

Rundgren, M. (1998). Early-Holocene vegetation of northern Iceland: Pollen and plant macrofossil evidence from the Skagi peninsula. *The Holocene*, *8*(5), 553–564.

Rundgren, M. (1999). A summary of the environmental history of the Skagi peninsula, northern Iceland, 11300-7800 BP. *Jökull*, *47*, 1–19.

Rundgren, M., & Ingólfsson, Ó. (1999). Plant survival in Iceland during periods of glaciation? *Journal of Biogeography*, *26*, 387–396.

Rundgren, M., Ingolfsson, O., Björck, S., Jiang, H., & Haflidason, H. (1997). Dynamic sea-level change during the last deglaciation of northern Iceland. *Boreas*, *26*, 201–215.

Sæmundsson, K. (1977). Geological map of Iceland, sheet 7, NE-Iceland. *Museum of Natural History and the Icelandic Geodetic Survey, Reykjavik.*

Sæmundsson, K. (1978). Fissure swarms and central volcanoes of the neovolcanic zones of Iceland. *Geological Journal Special Issue*, *10*, 451–432.

Sæmundsson, K. (1979). Outline of the Geology of Iceland. *Jökull*, *29*, 7–28.

Sæmundsson, T. (1995). *Deglaciation and shoreline displacement in Vopnafjørdur, North-eastern Iceland* (Lund University). Retrieved from LUNQUA Thesis 33

Santisteban, J. I., Mediavilla, R., López-Pamo, E., Dabrio, C. J., Zapata, M. B. R., García, M. J. G., Castano, S., Martínez-Alfaro, P. E. (2004). Loss on ignition: a qualitative or quantitative method for organic matter and carbonate mineral content in sediments? *Journal of Paleolimnology*, *32*, 287–299.

Schnurrenberger, D., Russell, J., & Kelts, K. (2003). Classification of lacustrine sediments based on sedimentary components. *Journal of Paleolimnology*, *29*(2), 141–154. https://doi.org/10.1023/A:1023270324800

Schomacker, A., Brynjólfsson, S., Andreassen, J. M., Gudmundsdóttir, E. R., Olsen, J., Odgaard, B. V., Håkansson, L., Ingólfsson, Ó., Larsen, N. K. (2016). The Drangajökull ice cap, northwest Iceland, persisted into the early-mid Holocene. *Quaternary Science Reviews*, *148*, 68–84. https://doi.org/10.1016/j.quascirev.2016.07.007

Schomacker, A., Farnsworth, W. R., Ingólfsson, Ó., Allaart, L., Håkansson, L., Retelle, M., Siggaard-Anderson, M. L., Korsgaard, N. J., Rouillard, A., Kjellman, S. E. (2019). Postglacial relative sea level change and glacier activity in the early and late Holocene: Wahlenbergfjorden, Nordaustlandet, Svalbard. *Scientific Reports*, *9*(1), 1–13. https://doi.org/10.1038/s41598-019-43342-z

Schomacker, A., Krüger, J., & Larsen, G. (2003). An extensive late Holocene glacier advance of Kötlujökull, central south Iceland. *Quaternary Science Reviews*, *22*(14), 1427–1434. https://doi.org/10.1016/S0277-3791(03)00090-8

Serreze, M. C., Carse, F., Barry, R. G., & Rogers, J. C. (1997). Icelandic low cyclone activity: Climatological features, linkages with the NAO, and relationships with recent changes in the Northern Hemisphere circulation. *Journal of Climate*, *10*(3), 453–464. https://doi.org/10.1175/1520-0442(1997)010<0453:ILCACF>2.0.CO;2

Sicre, M. A., Jacob, J., Ezat, U., Rousse, S., Kissel, C., Yiou, P., Eiríksson, J., Knudsen, K. L., Jansen, E., Turon, J. L. (2008). Decadal variability of sea surface temperatures off North

Iceland over the last 2000 years. *Earth and Planetary Science Letters*, *268*(1–2), 137–142. https://doi.org/10.1016/j.epsl.2008.01.011
Sigvaldason, G. E. (2002). Volcanic and tectonic processes coinciding with glaciation and crustal rebound: An early Holocene rhyolitic eruption in the Dyngjufjöll volcanic centre and the formation of the Askja caldera, north Iceland. *Bulletin of Volcanology*, *64*(3–4), 192–205. https://doi.org/10.1007/s00445-002-0204-7
Simpson, I. A., Guðmundsson, G., Thomson, A. M., & Cluett, J. (2004). Assessing the Role of Winter Grazing in Historic Land Degradation, Mývatnssveit, Northeast Iceland. *Geoarchaeology: An International Journal*, *19*(5), 471–502.
Smith, J. G. (2003). Aspects of the loss-on-ignition (LOI) technique in the context of clay-rich, glaciolacustrine sediments. *Geografiska Annaler*, *85*(A), 91–97.
Snæbjörnsdóttir, S. Ó., Wiese, F., Fridriksson, T., Ármansson, H., Einarsson, G. M., & Gislason, S. R. (2014). CO2 storage potential of basaltic rocks in Iceland and the oceanic ridges. *Energy Procedia*, *63*, 4585–4600. https://doi.org/10.1016/j.egypro.2014.11.491
Spagnolo, M., & Clark, C. D. (2009). A geomorphological overview of glacial landforms on the Icelandic continental shelf. *Journal of Maps*, *5*(1), 37–52. https://doi.org/10.4113/jom.2009.1049
Steinthórsson, S., & Thorarinsson, S. (1997). Iceland. In E. M. Mores & R. W. Fairbridge (Eds.), *Encyclopedia of Europe and Asia regional geology* (pp. 341–352). London/New York: Chapman.
Stockhecke, M., Kwiecien, O., Vigliotti, L., Anselmetti, F. S., Beer, J., Çağatay, M. N., Channell, J. E. T., Kipfer, R., Lachner, J., Litt, T., Pickarski, N., Sturm, M. (2014). Chronostratigraphy of the 600,000 year old continental record of Lake Van (Turkey). *Quaternary Science Reviews*, *104*, 8–17. https://doi.org/10.1016/j.quascirev.2014.04.008
Stolt, M. H., & Lindbo, D. L. (2010). 17 - Soil Organic Matter. In G. Stoops, V. Marceline, & F. Mees (Eds.), *Interpretation of Micromorphological Features of Soils and Regoliths* (pp. 369–396). Elsevier B.V.
Stoner, J. S., Channell, J. E. T., & Hillaire-Marcel, C. (1996). The magnetic signature of rapidly deposited detrital layers from the deep Labrador Sea: Relationship to North Atlantic Heinrich layers. *Paleoceanography*, *11*(3), 309–325. https://doi.org/10.1029/96PA00583
Striberger, J., Björck, S., Holmgren, S., & Hamerlík, L. (2012). The sediments of Lake Lögurinn - A unique proxy record of Holocene glacial meltwater variability in eastern Iceland. *Quaternary Science Reviews*, *38*, 76–88. https://doi.org/10.1016/j.quascirev.2012.02.001
Sverrisdottir, G. (2007). Hybrid magma generation preceding Plinian silicic eruptions at Hekla, Iceland: evidence from mineralogy and chemistry of two zoned deposits. *Geological Magazine*, *144*(4). https://doi.org/10.1017/S0016756807003470
Synal, H. A., Stocker, M., & Suter, M. (2007). MICADAS: A new compact radiocarbon AMS system. *Nuclear Instruments and Methods in Physics Research, Section B: Beam Interactions with Materials and Atoms*, *259*(1), 7–13. https://doi.org/10.1016/j.nimb.2007.01.138
Syvitski, J. P., Jennings, A. E., & Andrews, J. T. (1999). High-resolution Seismic Evidence for Multiple Glaciation across the Southwest Iceland Shelf. *Arctic, Antarctic, and Alpine Research*, *31*(1), 50–57. https://doi.org/10.1080/15230430.1999.12003280
Telford, R. J., Heegaard, E., & Birks, H. J. B. (2004). All age – depth models are wrong: but how badly ? *Quaternary Science Journal*, *23*, 1–5. https://doi.org/10.1016/j.quascirev.2003.11.003

Thorarinsson, S., Einarsson, T., & Kjartansson, G. (1959). On the Geology and Geomorphology of Iceland. *Geografiska Annaler*, *41*(2–3), 135–169. https://doi.org/10.1080/20014422.1959.11904385
Thordarson, T., & Larsen, G. (2007). Volcanism in Iceland in historical time: Volcano types, eruption styles and eruptive history. *Journal of Geodynamics*, *43*, 118–152. https://doi.org/10.1016/j.jog.2006.09.005
Thordarson, T., Self, S., Miller, D. J., Larsen, G., & Vilmundardóttir, E. G. (2003). Sulphur release from flood lava eruptions in the Veidivötn, Grimsvötn and Katla volcanic systems, Iceland. *Geological Society, London, Special Publications*, *213*, 103–121.
Turner, R., Roberts, N., & Jones, M. D. (2008). Climatic pacing of Mediterranean fire histories from lake sedimentary microcharcoal. *Global and Planetary Change*, *63*(4), 317–324. https://doi.org/10.1016/j.gloplacha.2008.07.002
Vakhrameeva, P., Portnyagin, M., Ponomareva, V., Abbott, P. M., Repkina, T., Novikova, A., … Pross, J. (2020). Identification of Icelandic tephras from the last two millennia in the White Sea region (Vodoprovodnoe peat bog, northwestern Russia). *Journal of Quaternary Science*, *35*(4), 493–504. https://doi.org/10.1002/jqs.3190
Vink, G. E. (1984). A Hotspot Model for Iceland and the Vøring Plateau. *Journal of Geophysical Research*, *89*(4), 9949–9959.
Ward, P. L. (1971). New interpretation of the geology of Iceland. *Bulletin of the Geological Society of America*, *82*(11), 2991–3012.
Wastegård, S., Björck, S., Possnert, G., & Wohlfarth, B. (1998). Evidence for the occurrence of Vedde Ash in Sweden: radiocarbon and calendar age estimates. *Journal of Quaternary Science*, *13*(3), 271–274.
Weltje, J. G., & Tjallingii, R. (2008). Calibration of XRF core scanners for quantitative geochemical logging of sediment cores: Theory and application. *Earth and Planetary Science Letters*, *274*, 423–438. https://doi.org/10.1016/j.epsl.2008.07.054
White, R. S., Bown, J. W., & Smallwood, J. R. (1995). The temperature of the Iceland plume and origin of outward-propagating V-shaped ridges. *Journal of the Geological Society*, *152*, 1039–1045. https://doi.org/10.1144/GSL.JGS.1995.152.01.26
Wiedenbeck, M. (2015). MICADAS: New instrumentation for carbon-14 dating. *Elements*, 75–76.
Wohlfarth, B., Skog, G., Possnert, G., & Holmquist, B. (1998). Pitfalls in the AMS radiocarbon-dating of terrestrial macrofossils. *Journal of Quaternary Science*, *13*(2), 137–145.
Wolfe, A. P., Miller, G. H., Olsen, C. A., Forman, S. L., Doran, P. T., & Holmgren, S. U. (2004). Geochronology of high latitude lake sediments. *Long-Term Environmental Change in Arctic and Antarctic Lakes*, 19–52. https://doi.org/10.1007/978-1-4020-2126-8_2
Wolfe, C. J., Bjarnason, I. T., VanDecar, J. C., & Solomon, S. C. (1997). Seismic structure of the Icelandic mantle plume. *Nature*, *385*, 245–247.
Zolitschka, B., Francus, P., Ojala, A. E. K., & Schimmelmann, A. (2015). Varves in lake sediments - a review. *Quaternary Science Reviews*, *117*, 1–41.
Zuo, R. (2013). ITRAX: A potential tool to explore the physical and chemical properties of mineralized rocks in mineral resource exploration. *Journal of Geochemical Exploration*, *132*, 149–155. https://doi.org/10.1016/j.gexplo.2013.06.010

Appendix

Tabel A. *Major element composition of the analyzed tephra layers showing sample composite depth and if identified tephra marker. The colors of the data refer to the volcanic system shown in Fig. 5.*

Tephra layer	Composite depth	Tephra marker	SiO_2	TiO_2	Al_2O_3	FeO	MnO	MgO	CaO	Na_2O	K_2O	P_2O_5	Total
TDV2-1 115	114-115 cm	Hekla 1104	72.38	0.22	14.35	3.15	0.12	0.10	1.94	4.69	2.62	0.03	99.59
			72.14	0.21	14.26	3.25	0.09	0.10	1.89	4.82	2.52	0.00	99.28
			72.06	0.24	14.85	2.93	0.12	0.11	2.02	5.00	2.46	0.01	99.80
			71.70	0.21	13.96	3.23	0.12	0.10	1.87	4.99	2.72	0.02	98.92
			71.57	0.22	14.11	3.17	0.09	0.11	1.96	4.79	2.67	0.06	98.75
			71.53	0.17	14.30	3.25	0.14	0.11	1.93	4.62	2.62	0.03	98.69
			71.47	0.19	14.11	3.12	0.08	0.12	1.92	4.81	2.67	0.08	98.57
			71.38	0.18	14.33	3.13	0.12	0.13	1.79	4.94	2.68	0.00	98.67
			71.36	0.23	14.29	3.14	0.10	0.11	1.97	4.73	2.67	0.05	98.65
			71.14	0.24	14.21	3.24	0.12	0.14	1.93	5.12	2.69	0.01	98.84
			70.95	0.22	14.15	3.22	0.07	0.13	1.90	4.95	2.69	0.03	98.30
			70.88	0.23	14.02	3.25	0.10	0.12	1.94	4.81	2.68	0.04	98.07
			70.61	0.14	14.66	3.21	0.09	0.10	1.81	4.94	2.69	0.03	98.29
			70.60	0.21	14.04	3.20	0.10	0.08	1.89	4.74	2.72	0.04	97.63
			70.58	0.22	14.01	3.14	0.11	0.14	1.97	4.77	2.62	0.00	97.56
			70.55	0.22	14.05	3.25	0.12	0.12	1.97	4.69	2.79	0.01	97.77
			70.52	0.20	14.00	3.12	0.14	0.12	1.85	4.53	2.67	0.06	97.21
			70.32	0.19	13.64	3.02	0.06	0.12	1.78	4.43	2.69	0.01	96.26
			69.75	0.24	13.98	3.31	0.10	0.14	2.03	4.94	2.70	0.02	97.22
			69.12	0.62	14.97	4.65	0.12	0.85	2.62	4.84	2.41	0.06	100.25
		Mean	**71.03**	**0.23**	**14.21**	**3.25**	**0.11**	**0.15**	**1.95**	**4.81**	**2.65**	**0.03**	**98.42**
		stdv	**0.81**	**0.10**	**0.31**	**0.34**	**0.02**	**0.16**	**0.17**	**0.17**	**0.09**	**0.02**	**0.96**

Tephra layer	Composite depth	Tephra marker	SiO_2	TiO_2	Al_2O_3	FeO	MnO	MgO	CaO	Na_2O	K_2O	P_2O_5	Total
TDV2-2 27	143 cm		73.95	0.14	13.32	2.18	0.09	0.01	1.33	4.37	2.83	0.00	98.22
			47.01	4.54	12.93	14.91	0.22	4.92	9.39	3.19	0.76	0.58	98.44
			47.46	4.52	13.19	15.26	0.26	4.97	9.81	3.18	0.82	0.61	100.07
			47.35	4.52	12.96	15.10	0.24	4.86	9.64	3.25	0.78	0.56	99.26
			47.07	4.51	12.97	14.91	0.21	4.95	9.69	3.05	0.78	0.58	98.72
			47.38	4.49	13.05	14.66	0.24	5.01	9.66	3.17	0.78	0.59	99.02
			46.54	4.49	12.79	14.83	0.23	5.00	9.58	3.16	0.78	0.57	97.97
			46.95	4.47	12.86	14.87	0.26	4.77	9.46	3.16	0.80	0.55	98.15
			47.54	4.43	13.14	15.04	0.22	4.87	9.59	3.08	0.78	0.52	99.21
			47.21	4.43	12.90	14.91	0.22	4.90	9.49	3.19	0.76	0.55	98.56
			46.92	4.43	12.94	14.81	0.26	4.90	9.63	3.13	0.76	0.55	98.32
			46.41	4.43	12.90	14.35	0.24	4.59	9.37	3.02	0.70	0.64	96.65
			47.89	4.42	13.32	15.05	0.26	4.97	9.70	2.89	0.83	0.54	99.87
			47.29	4.42	12.75	15.04	0.21	4.92	9.76	3.14	0.79	0.59	98.91
			46.77	4.29	12.85	15.02	0.23	4.92	9.66	3.09	0.78	0.57	98.17
		Mean	**47.13**	**4.46**	**12.97**	**14.91**	**0.23**	**4.90**	**9.60**	**3.12**	**0.78**	**0.57**	**98.67**
		stdv	**0.40**	**0.06**	**0.16**	**0.22**	**0.02**	**0.11**	**0.13**	**0.09**	**0.03**	**0.03**	**0.86**
			49.30	3.03	13.11	14.41	0.25	5.51	9.86	2.70	0.44	0.40	99.01
			49.25	3.00	13.11	14.48	0.25	5.58	9.90	2.68	0.45	0.39	99.08
			50.04	1.88	14.14	14.10	0.21	6.02	11.31	2.69	0.18	0.20	100.77
			49.60	1.87	13.72	12.94	0.21	6.45	11.38	2.45	0.22	0.15	98.99

Tephra layer	Composite depth	Tephra marker	SiO_2	TiO_2	Al_2O_3	FeO	MnO	MgO	CaO	Na_2O	K_2O	P_2O_5	Total
TDV2-3 17	245 cm		71.93	0.10	12.90	2.04	0.09	0.01	1.27	4.23	2.73	0.00	95.30
			71.86	0.19	13.14	2.27	0.08	0.16	1.45	4.38	2.70	0.01	96.25
			71.68	0.20	12.66	2.90	0.10	0.01	0.62	4.22	3.39	0.00	95.78
			68.45	0.33	15.30	5.02	0.16	0.29	3.03	4.41	2.13	0.06	99.19
			67.28	0.10	12.09	1.89	0.07	0.02	1.18	3.77	2.56	0.03	88.98
			67.10	0.43	15.53	4.32	0.15	0.54	1.83	4.97	4.24	0.05	99.16
			64.14	0.66	15.59	7.75	0.24	0.78	4.11	4.39	1.79	0.25	99.69
		Mean	**68.92**	**0.29**	**13.89**	**3.74**	**0.13**	**0.26**	**1.93**	**4.34**	**2.79**	**0.06**	**96.34**
		stdv	**3.01**	**0.20**	**1.52**	**2.13**	**0.06**	**0.30**	**1.22**	**0.36**	**0.81**	**0.09**	**3.72**
			47.91	4.48	13.29	14.56	0.22	4.66	9.49	3.00	0.86	0.57	99.04
			48.13	4.47	13.09	14.34	0.22	4.65	9.12	3.11	0.85	0.59	98.58
			48.08	4.43	13.22	14.60	0.27	4.59	9.33	3.01	0.87	0.52	98.92
			46.69	4.31	13.11	14.95	0.24	5.22	10.17	2.87	0.68	0.45	98.70
		Mean	**47.70**	**4.42**	**13.18**	**14.61**	**0.24**	**4.78**	**9.53**	**3.00**	**0.82**	**0.53**	**98.81**
		stdv	**0.68**	**0.08**	**0.09**	**0.25**	**0.02**	**0.29**	**0.45**	**0.10**	**0.09**	**0.06**	**0.21**
			49.57	2.62	13.58	13.21	0.21	5.63	10.31	2.70	0.42	0.30	98.55
			49.83	2.52	13.56	13.55	0.23	5.35	10.24	2.69	0.40	0.28	98.66
			49.30	1.80	13.95	12.29	0.19	7.04	11.87	2.32	0.18	0.15	99.09
			49.75	1.76	14.03	12.32	0.22	6.85	11.74	2.13	0.19	0.17	99.16
			49.78	1.70	13.94	12.40	0.22	6.85	11.91	2.39	0.19	0.18	99.56
			48.86	1.68	13.84	12.06	0.19	7.16	12.18	2.35	0.20	0.16	98.67

Tephra layer	Composite depth	Tephra marker	SiO_2	TiO_2	Al_2O_3	FeO	MnO	MgO	CaO	Na_2O	K_2O	P_2O_5	Total
TDV2-3 22	250 cm		47.78	4.43	13.31	14.45	0.20	4.72	9.41	3.07	0.82	0.57	98.77
			47.62	4.43	13.15	14.59	0.24	4.83	9.48	3.28	0.83	0.49	98.94
			47.93	4.42	13.01	14.54	0.24	4.53	9.49	3.15	0.87	0.58	98.75
			47.61	4.42	13.05	14.76	0.24	4.66	9.36	3.16	0.88	0.48	98.62
			47.86	4.41	13.16	14.70	0.23	4.59	9.48	3.21	0.84	0.55	99.03
			47.55	4.41	12.89	14.69	0.21	4.86	9.55	3.14	0.84	0.61	98.75
			47.12	4.39	13.08	14.53	0.24	4.66	9.36	3.26	0.81	0.50	97.95
			47.28	4.38	12.96	14.53	0.22	4.76	9.55	3.13	0.86	0.56	98.23
			47.21	4.37	13.00	14.37	0.21	4.87	9.39	3.25	0.84	0.55	98.06
			47.59	4.34	12.87	14.49	0.23	4.52	9.32	3.36	0.85	0.57	98.14
			47.47	4.32	13.07	14.48	0.22	4.82	9.37	3.38	0.80	0.56	98.48
			48.17	4.29	12.80	14.68	0.25	3.96	8.93	3.30	0.93	0.60	97.91
			47.81	4.26	13.26	14.76	0.25	4.50	9.51	3.30	0.80	0.53	98.98
			47.49	4.16	13.06	14.84	0.21	4.88	9.29	3.12	0.76	0.55	98.36
			47.44	4.06	12.93	14.59	0.24	4.66	9.29	3.25	0.83	0.56	97.84
			48.62	3.92	12.69	15.79	0.28	5.13	9.56	2.30	0.60	0.47	99.36
		Mean	**47.66**	**4.31**	**13.02**	**14.67**	**0.23**	**4.68**	**9.40**	**3.17**	**0.82**	**0.55**	**98.51**
		stdv	**0.37**	**0.15**	**0.16**	**0.32**	**0.02**	**0.25**	**0.15**	**0.25**	**0.07**	**0.04**	**0.46**
			49.53	2.96	13.45	14.27	0.24	5.44	9.84	2.73	0.42	0.32	99.20
			46.74	2.71	15.50	13.19	0.18	6.23	10.51	2.57	0.45	0.27	98.36
			49.02	1.76	14.01	12.16	0.21	7.07	11.92	2.37	0.19	0.15	98.85
			58.05	*0.39*	*15.97*	*5.09*	*0.16*	*0.37*	*2.70*	*3.47*	*1.76*	*0.10*	*88.06*

Tephra layer	Composite depth	Tephra marker	SiO_2	TiO_2	Al_2O_3	FeO	MnO	MgO	CaO	Na_2O	K_2O	P_2O_5	Total
TDV2-3 109	337 cm		75.10	0.13	13.56	1.82	0.06	0.00	1.20	4.41	2.92	0.02	99.22
			69.08	0.21	13.76	3.00	0.10	0.11	1.86	4.30	2.38	0.01	94.81
			64.67	0.57	15.22	7.06	0.20	0.65	3.83	4.41	1.89	0.20	98.70
			62.20	0.75	15.20	8.19	0.24	0.87	4.52	4.57	1.70	0.26	98.50
			61.20	0.76	14.79	8.08	0.20	0.95	4.23	4.28	1.63	0.25	96.37
			65.89	0.54	15.44	6.66	0.23	0.57	3.73	4.49	1.89	0.16	99.59
			64.93	0.57	15.42	7.07	0.21	0.66	3.92	4.34	1.90	0.17	99.19
			60.72	0.50	17.72	6.58	0.20	0.61	3.73	4.05	1.69	0.19	95.99
			61.59	0.84	15.42	8.76	0.23	1.05	4.59	4.29	1.70	0.31	98.77
			60.31	0.69	14.78	7.84	0.21	0.90	4.38	4.12	1.61	0.25	95.09
			64.50	0.64	15.63	7.54	0.24	0.79	4.03	4.43	1.82	0.20	99.81
			64.01	0.72	15.56	8.02	0.23	0.86	4.19	4.36	1.74	0.23	99.93
			62.56	0.78	15.44	8.38	0.27	1.02	4.56	4.37	1.66	0.30	99.34
			66.36	0.40	15.97	5.79	0.20	0.41	3.29	4.60	2.07	0.06	99.14
			57.42	0.73	14.20	7.55	0.21	0.85	4.13	4.18	1.26	0.22	90.75
			67.81	0.36	15.04	5.27	0.16	0.33	3.04	4.21	2.17	0.06	98.45
			63.24	0.41	19.75	5.51	0.20	0.41	3.17	4.11	1.86	0.10	98.76
			64.47	0.66	15.22	7.25	0.24	0.71	3.95	4.39	1.82	0.17	98.88
		Mean	**63.24**	**0.62**	**15.68**	**7.22**	**0.22**	**0.73**	**3.96**	**4.33**	**1.78**	**0.19**	**97.95**
		stdv	**2.63**	**0.15**	**1.31**	**1.04**	**0.02**	**0.22**	**0.48**	**0.16**	**0.21**	**0.07**	**2.38**
			63.13	*0.10*	*11.37*	*1.79*	*0.07*	*0.01*	*1.07*	*3.66*	*2.39*	*0.01*	*83.59*

Tephra layer	Composite depth	Tephra marker	SiO_2	TiO_2	Al_2O_3	FeO	MnO	MgO	CaO	Na_2O	K_2O	P_2O_5	Total
TDV2-4 1	365 cm		73.16	0.11	13.05	1.97	0.07	0.02	1.28	4.69	2.82	0.02	97.19
			66.93	0.78	16.73	8.57	0.25	0.97	4.66	5.41	2.17	0.37	100.06
		Hekla 3	66.93	0.37	15.17	4.99	0.18	0.39	3.14	4.45	2.17	0.07	97.85
			66.01	0.42	15.17	5.62	0.14	0.36	3.34	4.15	2.04	0.06	97.32
			65.69	0.49	15.04	6.45	0.19	0.55	3.59	4.69	1.97	0.15	98.81
			65.50	0.54	15.34	6.57	0.18	0.57	3.53	4.83	1.96	0.15	99.17
			65.44	0.54	15.29	6.64	0.22	0.58	3.81	4.80	1.89	0.20	99.41
			65.40	0.52	15.36	6.36	0.25	0.54	3.53	5.06	1.92	0.13	99.07
			65.17	0.57	15.15	6.87	0.18	0.55	3.55	4.70	1.91	0.15	98.81
			64.82	0.42	14.87	6.02	0.15	0.50	3.46	4.92	1.88	0.12	97.16
			64.13	0.57	15.20	7.02	0.24	0.64	4.10	4.60	1.82	0.20	98.51
			64.04	0.50	16.73	5.71	0.14	0.50	4.59	5.41	1.48	0.16	99.26
			63.15	0.63	15.46	7.08	0.24	0.70	4.35	4.74	1.75	0.21	98.31
			63.13	0.76	15.56	8.57	0.22	0.95	4.53	4.33	1.68	0.34	100.06
			63.11	0.63	15.21	8.05	0.20	0.91	4.28	4.52	1.77	0.18	98.86
			63.00	0.70	15.21	7.93	0.22	0.86	4.33	4.59	1.76	0.26	98.86
			62.78	0.74	15.57	7.68	0.16	0.79	4.66	4.87	1.29	0.23	98.76
			62.74	0.67	15.20	8.05	0.19	0.87	4.09	4.99	1.71	0.20	98.71
			62.54	0.78	15.56	8.20	0.20	0.96	4.36	4.61	1.72	0.37	99.31
			62.08	0.49	15.20	6.07	0.17	0.60	4.48	5.38	1.23	0.20	95.90
			61.20	0.35	13.38	4.96	0.13	0.34	3.01	5.29	1.97	0.11	90.75
			61.14	0.78	15.21	8.29	0.22	0.97	4.46	4.77	1.67	0.29	97.80
			60.46	0.60	14.44	7.38	0.20	0.76	3.83	4.51	1.73	0.15	94.06
			58.96	0.41	19.81	4.20	0.12	0.47	6.33	5.78	0.88	0.15	97.11
			54.86	*0.63*	*13.26*	*7.79*	*0.20*	*0.84*	*3.49*	*3.94*	*1.56*	*0.24*	*86.81*
			53.58	*0.40*	*12.19*	*5.09*	*0.12*	*0.42*	*2.96*	*3.45*	*1.57*	*0.10*	*79.88*
		Mean	**63.52**	**0.57**	**15.42**	**6.76**	**0.19**	**0.65**	**4.06**	**4.82**	**1.74**	**0.19**	**97.90**
		stdv	**2.01**	**0.13**	**1.14**	**1.20**	**0.04**	**0.20**	**0.71**	**0.38**	**0.29**	**0.08**	**2.08**

Tephra layer	Composite depth	Tephra marker	SiO_2	TiO_2	Al_2O_3	FeO	MnO	MgO	CaO	Na_2O	K_2O	P_2O_5	Total
TDV2-4 100	434-435 cm	Hekla 4	74.03	0.14	13.34	2.03	0.06	0.02	1.37	4.76	2.84	0.05	98.63
			73.44	0.10	13.12	1.95	0.07	0.01	1.30	4.82	2.77	0.00	97.57
			73.15	0.07	13.06	1.97	0.09	0.02	1.33	4.58	2.75	0.03	97.04
			73.01	0.12	13.13	1.93	0.07	0.02	1.22	4.56	2.82	0.00	96.88
			72.91	0.03	13.07	1.93	0.03	0.01	1.26	4.76	2.71	0.02	96.73
			72.78	0.15	12.99	1.92	0.09	0.01	1.19	4.58	2.91	0.01	96.63
			72.38	0.11	12.87	1.90	0.06	0.03	1.25	4.57	2.79	0.00	95.95
			72.24	0.10	12.75	1.90	0.10	0.01	1.27	4.76	2.81	0.01	95.95
			72.14	0.10	12.93	1.85	0.08	0.01	1.31	4.66	2.75	0.00	95.83
			72.07	0.09	13.05	1.89	0.06	0.01	1.28	4.59	2.72	0.03	95.78
			71.93	0.16	13.09	2.09	0.12	0.08	1.36	4.60	2.74	0.01	96.19
			71.83	0.09	12.72	1.88	0.08	0.01	1.16	4.42	2.75	0.00	94.94
			71.75	0.07	13.18	1.89	0.13	0.02	1.23	4.50	2.72	0.01	95.49
			71.25	*0.06*	*12.92*	*1.87*	*0.06*	*0.01*	*1.25*	*4.36*	*2.71*	*0.02*	*94.51*
			70.47	*0.10*	*13.47*	*1.84*	*0.10*	*0.02*	*1.18*	*4.18*	*2.60*	*0.01*	*93.97*
			70.19	*0.13*	*12.71*	*1.91*	*0.08*	*0.00*	*1.27*	*4.20*	*2.59*	*0.02*	*93.09*
			70.12	*0.10*	*12.57*	*1.80*	*0.05*	*0.01*	*1.26*	*4.04*	*2.63*	*0.04*	*92.61*
			70.00	*0.13*	*13.76*	*1.88*	*0.10*	*0.01*	*1.18*	*4.55*	*2.74*	*0.02*	*94.37*
			69.18	*0.09*	*12.57*	*2.16*	*0.09*	*0.01*	*1.18*	*4.58*	*2.68*	*0.09*	*92.63*
			67.70	*0.06*	*13.11*	*1.73*	*0.09*	*0.03*	*1.17*	*3.93*	*2.53*	*0.00*	*90.34*
			62.67	0.08	23.79	1.67	0.07	0.03	1.06	4.05	2.32	0.06	95.81
		Mean	**72.59**	**0.10**	**13.02**	**1.93**	**0.08**	**0.02**	**1.27**	**4.63**	**2.78**	**0.01**	**96.43**
		stdv	**0.69**	**0.04**	**0.17**	**0.07**	**0.03**	**0.02**	**0.06**	**0.12**	**0.06**	**0.02**	**0.97**

Tephra layer	Composite depth	Tephra marker	SiO_2	TiO_2	Al_2O_3	FeO	MnO	MgO	CaO	Na_2O	K_2O	P_2O_5	Total
TDV2-6 17	551 cm		48.31	4.15	13.26	14.53	0.23	4.80	9.77	3.10	0.78	0.47	99.40
			47.93	3.98	13.18	13.75	0.23	4.91	9.53	3.07	0.84	0.51	97.93
			48.17	4.17	13.31	14.95	0.24	4.94	9.70	3.11	0.81	0.48	99.88
			48.23	4.22	13.36	14.51	0.23	4.92	9.74	3.07	0.83	0.45	99.56
			47.76	3.99	13.27	14.25	0.22	4.99	9.82	3.15	0.78	0.55	98.78
			48.10	4.10	13.32	14.46	0.21	5.04	9.76	3.33	0.80	0.50	99.63
			48.23	3.90	13.05	14.24	0.22	5.16	9.88	3.15	0.83	0.45	99.10
			48.15	4.20	13.27	14.88	0.21	5.12	9.96	3.05	0.83	0.46	100.13
			48.75	4.25	13.82	14.78	0.21	4.87	9.71	2.37	0.79	0.45	99.99
			47.86	4.26	13.23	14.45	0.22	4.89	9.53	3.17	0.79	0.51	98.91
			47.92	4.03	13.35	14.47	0.22	4.97	9.72	3.13	0.79	0.49	99.08
			48.28	4.23	13.34	14.31	0.24	4.70	9.49	3.15	0.80	0.47	99.01
			48.19	4.22	13.24	14.45	0.21	4.99	9.76	3.23	0.85	0.45	99.58
			48.15	4.20	13.25	14.61	0.22	4.99	9.67	3.11	0.79	0.48	99.47
			48.65	4.15	13.50	14.97	0.22	4.94	9.84	3.02	0.81	0.47	100.58
			48.08	3.94	13.54	14.77	0.24	4.90	9.51	2.98	0.82	0.48	99.26
		Mean	**48.17**	**4.12**	**13.33**	**14.52**	**0.22**	**4.95**	**9.71**	**3.07**	**0.81**	**0.48**	**99.39**
		stdv	**0.26**	**0.12**	**0.17**	**0.31**	**0.01**	**0.11**	**0.14**	**0.21**	**0.02**	**0.03**	**0.62**

Tephra layer	Composite depth	Tephra marker	SiO_2	TiO_2	Al_2O_3	FeO	MnO	MgO	CaO	Na_2O	K_2O	P_2O_5	Total
TDV2-6 86	600 cm		49.45	2.85	13.24	14.17	0.23	5.62	9.84	2.63	0.45	0.31	98.78
			49.90	2.78	13.33	14.08	0.24	5.49	9.98	2.63	0.42	0.28	99.13
			50.01	3.03	13.40	15.26	0.25	5.38	9.19	2.81	0.67	0.38	100.38
			49.82	2.83	13.42	13.68	0.23	5.73	10.40	2.72	0.41	0.24	99.49
			49.08	2.45	13.66	13.27	0.24	6.11	11.05	2.76	0.37	0.21	99.20
		Mean	**49.65**	**2.79**	**13.41**	**14.09**	**0.24**	**5.67**	**10.09**	**2.71**	**0.46**	**0.28**	**99.39**
		stdv	**0.38**	**0.21**	**0.16**	**0.74**	**0.01**	**0.28**	**0.69**	**0.08**	**0.12**	**0.06**	**0.60**
			46.44	0.02	35.21	0.46	0.00	0.21	18.33	1.18	0.01	0.00	101.87

Tephra layer	Composite depth	Tephra marker	SiO_2	TiO_2	Al_2O_3	FeO	MnO	MgO	CaO	Na_2O	K_2O	P_2O_5	Total
TDV2-6 91	604 cm		69.83	0.68	13.54	6.05	0.13	0.25	1.28	4.85	3.43	0.05	100.10
			49.18	2.78	13.16	14.23	0.26	5.61	9.92	2.74	0.47	0.31	98.65
			49.66	3.03	13.10	14.17	0.24	5.58	9.94	2.72	0.45	0.36	99.25
			49.72	2.84	13.15	14.19	0.24	5.60	10.01	2.70	0.44	0.30	99.19
			49.51	2.97	13.26	14.16	0.24	5.55	9.98	2.63	0.44	0.32	99.06
			50.21	2.99	13.45	14.41	0.23	5.36	9.75	2.64	0.47	0.33	99.84
			49.77	2.93	13.49	14.29	0.23	5.47	9.77	2.59	0.46	0.31	99.32
			49.48	2.98	10.86	14.62	0.24	7.18	11.10	2.36	0.40	0.28	99.50
			49.37	2.92	13.34	13.86	0.26	5.34	10.00	2.75	0.45	0.31	98.60
			49.52	2.92	13.04	13.98	0.23	5.56	9.94	2.66	0.43	0.35	98.63
			50.42	3.07	13.50	15.03	0.26	5.32	9.99	2.23	0.52	0.35	100.68
			50.67	3.06	13.62	14.16	0.20	5.50	10.31	2.51	0.38	0.31	100.73
			49.57	2.70	13.16	14.01	0.23	5.43	9.99	2.64	0.44	0.34	98.50
			49.56	2.96	13.08	14.39	0.24	5.51	9.81	2.70	0.47	0.31	99.04
			50.03	3.01	13.19	14.06	0.25	5.44	10.09	2.58	0.47	0.33	99.44
		Mean	**49.76**	**2.94**	**13.10**	**14.25**	**0.24**	**5.60**	**10.04**	**2.60**	**0.45**	**0.32**	**99.32**
		stdv	**0.42**	**0.11**	**0.67**	**0.30**	**0.02**	**0.46**	**0.33**	**0.15**	**0.03**	**0.02**	**0.70**
			46.39	4.67	12.64	15.14	0.24	5.27	10.18	3.27	0.67	0.68	99.15

Tephra layer	Composite depth	Tephra marker	SiO_2	TiO_2	Al_2O_3	FeO	MnO	MgO	CaO	Na_2O	K_2O	P_2O_5	Total
TDV2-6 101	611 cm		50.04	2.34	13.77	12.81	0.24	6.21	11.16	2.77	0.34	0.23	99.91
			49.77	2.27	13.94	12.51	0.25	6.42	10.91	2.76	0.32	0.23	99.38
			49.81	2.37	13.87	12.35	0.22	6.83	11.12	2.72	0.33	0.22	99.85
			49.48	2.38	13.60	12.83	0.22	6.31	10.94	2.70	0.33	0.20	98.99
			49.44	2.20	13.62	13.05	0.18	6.47	10.87	2.78	0.34	0.24	99.19
			49.76	2.37	13.55	13.50	0.22	6.36	11.02	2.75	0.37	0.23	100.13
			50.29	2.41	14.04	12.46	0.23	6.67	11.19	2.68	0.33	0.19	100.49
			49.83	2.47	13.42	13.47	0.26	6.17	10.78	2.61	0.32	0.23	99.56
			50.20	2.33	14.18	12.26	0.23	6.73	11.46	2.81	0.28	0.20	100.68
			49.70	2.27	13.63	12.81	0.20	6.27	10.95	2.73	0.32	0.22	99.11
			49.82	2.21	14.01	13.41	0.24	6.04	10.73	2.82	0.37	0.26	99.91
			49.58	2.32	13.72	13.27	0.22	6.24	10.85	2.73	0.32	0.23	99.48
			49.64	2.35	13.83	13.28	0.20	5.96	10.83	2.75	0.31	0.23	99.38
			49.92	2.29	13.72	12.02	0.22	7.65	11.70	2.55	0.25	0.21	100.53
			49.68	2.37	13.73	12.58	0.21	6.80	11.16	2.78	0.33	0.24	99.88
			50.15	2.33	13.85	13.30	0.21	6.38	10.96	2.36	0.32	0.20	100.06
			49.56	2.90	13.31	14.23	0.23	5.54	9.87	2.77	0.44	0.35	99.20
		Mean	**49.80**	**2.36**	**13.75**	**12.95**	**0.22**	**6.41**	**10.97**	**2.71**	**0.33**	**0.23**	**99.75**
		stdv	**0.25**	**0.15**	**0.22**	**0.56**	**0.02**	**0.45**	**0.38**	**0.11**	**0.04**	**0.03**	**0.52**

Tephra layer	Composite depth	Tephra marker	SiO_2	TiO_2	Al_2O_3	FeO	MnO	MgO	CaO	Na_2O	K_2O	P_2O_5	Total
TDV2-6 116	621 cm		49.85	3.84	12.56	15.16	0.27	4.47	8.80	2.93	0.63	0.56	99.07
			48.23	3.64	12.80	14.93	0.27	5.50	10.05	2.71	0.48	0.42	99.03
			49.83	3.38	12.80	14.97	0.23	4.76	9.04	3.00	0.61	0.47	99.09
			48.95	3.10	12.87	14.74	0.23	5.29	9.66	2.66	0.45	0.33	98.28
			49.21	3.01	13.19	14.27	0.25	5.52	9.92	2.80	0.44	0.35	98.97
			49.32	2.98	13.23	14.47	0.24	5.57	10.02	2.73	0.42	0.31	99.30
			49.20	2.94	13.33	14.38	0.23	5.41	9.74	2.70	0.45	0.35	98.73
			49.62	2.92	13.10	14.19	0.25	5.46	10.02	2.59	0.44	0.34	98.94
			49.56	2.92	13.30	14.05	0.24	5.54	9.88	2.57	0.44	0.30	98.79
			49.42	2.92	13.15	14.40	0.27	5.45	9.61	2.73	0.45	0.35	98.75
			49.41	2.90	13.21	14.40	0.23	5.58	9.93	2.68	0.45	0.30	99.09
			48.84	2.89	13.11	14.10	0.25	5.42	9.94	2.72	0.43	0.32	98.02
			49.37	2.88	13.39	14.10	0.21	5.46	9.80	2.61	0.43	0.30	98.55
			49.98	2.82	13.33	14.78	0.26	5.27	10.06	2.63	0.56	0.34	100.03
			49.32	2.77	13.22	14.29	0.25	5.57	9.32	2.55	0.43	0.30	98.02
			49.33	2.55	13.60	13.57	0.24	5.98	10.32	2.61	0.40	0.30	98.90
		Mean	**49.34**	**3.03**	**13.14**	**14.43**	**0.25**	**5.39**	**9.76**	**2.70**	**0.47**	**0.35**	**98.85**
		stdv	**0.43**	**0.33**	**0.26**	**0.41**	**0.02**	**0.34**	**0.40**	**0.12**	**0.07**	**0.07**	**0.49**

Tephra layer	Composite depth	Tephra marker	SiO_2	TiO_2	Al_2O_3	FeO	MnO	MgO	CaO	Na_2O	K_2O	P_2O_5	Total
TDV2-6 119	623 cm		47.18	4.36	12.99	14.85	0.25	5.00	9.37	3.12	0.76	0.46	98.33
			47.00	3.94	13.23	14.33	0.19	5.12	9.85	3.03	0.72	0.49	97.90
			49.42	3.00	13.30	14.53	0.25	5.47	9.99	2.66	0.44	0.36	99.42
			49.46	2.97	12.94	14.58	0.26	5.44	9.83	2.60	0.44	0.38	98.90
			49.31	2.97	13.12	14.71	0.23	5.43	9.71	2.64	0.45	0.31	98.89
			49.21	2.97	13.24	14.43	0.27	5.35	10.01	2.71	0.46	0.35	99.00
			48.85	2.97	13.12	14.26	0.22	5.67	9.74	2.86	0.45	0.30	98.44
			49.16	2.96	13.33	14.40	0.23	5.54	9.84	2.71	0.44	0.29	98.90
			49.77	2.95	13.28	13.73	0.23	6.03	10.17	2.60	0.42	0.34	99.53
			49.52	2.95	13.24	14.16	0.25	5.62	10.12	2.66	0.44	0.34	99.30
			49.66	2.94	13.44	15.10	0.23	5.14	9.88	2.44	0.45	0.31	99.60
			49.09	2.92	13.23	15.01	0.24	5.63	10.26	2.22	0.40	0.28	99.28
			49.22	2.90	13.07	14.33	0.24	5.57	9.59	2.70	0.45	0.33	98.40
			49.08	2.90	13.41	14.32	0.26	5.50	9.93	2.71	0.44	0.35	98.90
			49.51	2.86	13.53	14.27	0.25	5.47	9.92	2.64	0.43	0.33	99.21
			49.26	2.86	13.21	13.95	0.23	5.58	9.94	2.70	0.43	0.35	98.50
			49.32	2.82	13.23	14.31	0.25	5.53	9.90	2.66	0.44	0.34	98.79
		Mean	**49.32**	**2.93**	**13.25**	**14.41**	**0.24**	**5.53**	**9.92**	**2.63**	**0.44**	**0.33**	**99.00**
		stdv	**0.24**	**0.05**	**0.15**	**0.36**	**0.01**	**0.19**	**0.18**	**0.14**	**0.01**	**0.03**	**0.38**

Tephra layer	Composite depth	Tephra marker	SiO_2	TiO_2	Al_2O_3	FeO	MnO	MgO	CaO	Na_2O	K_2O	P_2O_5	Total
TDV2-6 121	625 cm		46.28	4.65	12.90	15.55	0.29	4.91	9.63	3.15	0.63	0.81	98.80
			49.99	3.16	13.30	15.33	0.26	5.28	10.00	2.27	0.49	0.32	100.40
			49.63	2.96	13.34	14.45	0.24	5.45	10.01	2.71	0.44	0.33	99.56
			49.68	2.94	13.45	14.37	0.22	5.50	10.10	2.61	0.42	0.35	99.64
			49.43	2.93	13.38	14.43	0.24	5.49	9.91	2.72	0.45	0.32	99.31
			49.43	2.93	13.28	14.47	0.22	5.38	9.74	2.63	0.43	0.37	98.89
			49.19	2.93	13.11	14.19	0.23	5.64	9.97	2.71	0.43	0.33	98.74
			48.95	2.93	13.19	13.93	0.26	5.46	10.02	2.60	0.44	0.33	98.12
			49.19	2.92	13.20	14.38	0.22	5.51	9.92	2.70	0.45	0.33	98.82
			49.50	2.90	13.33	14.20	0.23	5.60	10.09	2.73	0.44	0.37	99.39
			49.04	2.89	13.20	14.39	0.23	5.40	9.79	2.70	0.44	0.31	98.40
			49.55	2.87	13.30	13.96	0.26	5.46	10.04	2.69	0.44	0.35	98.91
			49.30	2.86	13.19	13.87	0.26	5.44	9.87	2.64	0.43	0.31	98.18
			49.75	2.85	13.12	14.31	0.25	5.55	9.92	2.59	0.44	0.34	99.12
			49.36	2.84	13.21	14.29	0.23	5.47	10.03	2.60	0.44	0.33	98.80
			49.42	2.70	13.23	14.02	0.25	5.26	9.83	2.97	0.50	0.37	98.55
			49.22	2.63	13.52	13.41	0.22	5.90	10.35	2.51	0.38	0.31	98.45
		Mean	**49.41**	**2.89**	**13.27**	**14.25**	**0.24**	**5.49**	**9.97**	**2.65**	**0.44**	**0.34**	**98.95**
		stdv	**0.27**	**0.11**	**0.11**	**0.40**	**0.02**	**0.15**	**0.14**	**0.14**	**0.03**	**0.02**	**0.60**

Tephra layer	Composite depth	Tephra marker	SiO_2	TiO_2	Al_2O_3	FeO	MnO	MgO	CaO	Na_2O	K_2O	P_2O_5	Total
TDV2-6 129	630-648 cm	Saksunar vatn	49.83	3.16	13.28	14.96	0.25	5.45	10.11	2.44	0.48	0.32	100.28
			50.49	3.13	13.62	14.14	0.22	5.55	10.10	2.67	0.47	0.33	100.72
			49.63	3.06	13.15	16.30	0.25	4.77	9.64	2.25	0.48	0.34	99.87
			49.61	3.04	13.10	14.77	0.26	5.14	9.76	2.62	0.45	0.40	99.14
			49.56	3.02	13.33	14.61	0.25	5.22	9.93	2.85	0.47	0.35	99.59
			49.41	3.01	13.31	14.58	0.25	5.70	10.14	2.75	0.44	0.33	99.93
			49.35	2.95	12.91	14.70	0.24	5.32	9.59	2.78	0.46	0.38	98.68
			49.74	2.93	13.27	14.21	0.21	5.60	9.90	2.66	0.44	0.33	99.28
			49.48	2.93	13.00	14.23	0.26	5.40	9.83	2.59	0.45	0.36	98.52
			49.67	2.88	13.26	14.23	0.24	5.53	10.06	2.78	0.44	0.33	99.42
			49.36	2.85	13.34	14.20	0.23	5.53	10.11	2.61	0.43	0.34	98.99
			49.34	2.85	13.18	14.32	0.24	5.58	10.05	2.75	0.43	0.31	99.05
			49.43	2.83	13.30	14.34	0.23	5.48	9.47	2.62	0.47	0.32	98.50
			49.23	2.78	13.48	14.23	0.22	5.68	10.04	2.69	0.42	0.31	99.08
			49.46	2.68	13.53	13.95	0.23	5.62	10.03	2.52	0.40	0.30	98.72
			49.38	2.60	13.57	13.59	0.24	5.89	10.47	2.67	0.37	0.25	99.02
			49.43	2.56	13.57	13.58	0.26	6.04	10.57	2.58	0.39	0.31	99.29
		Mean	**49.55**	**2.90**	**13.31**	**14.41**	**0.24**	**5.50**	**9.99**	**2.64**	**0.44**	**0.33**	**99.30**
		stdv	**0.29**	**0.17**	**0.20**	**0.61**	**0.01**	**0.29**	**0.28**	**0.14**	**0.03**	**0.03**	**0.62**

Tephra layer	Composite depth	Tephra marker	SiO_2	TiO_2	Al_2O_3	FeO	MnO	MgO	CaO	Na_2O	K_2O	P_2O_5	Total
TDV2-7 16	630-648 cm	Saksunar	49.52	3.40	12.84	16.38	0.26	4.69	9.52	2.79	0.46	0.40	100.26
		vatn	50.12	3.13	13.18	14.76	0.23	5.07	9.76	2.81	0.47	0.31	99.84
			49.66	3.04	13.46	14.62	0.22	5.03	9.87	2.92	0.48	0.31	99.61
			49.97	3.02	13.43	14.88	0.25	5.46	9.96	2.46	0.45	0.30	100.19
			50.66	3.01	13.53	14.14	0.24	5.27	9.98	1.99	0.45	0.35	99.62
			49.34	2.99	13.27	14.36	0.21	5.68	10.02	2.69	0.44	0.29	99.29
			49.57	2.99	13.29	14.22	0.22	5.70	10.02	2.71	0.43	0.32	99.47
			49.40	2.95	13.29	14.44	0.23	5.58	9.94	2.67	0.44	0.34	99.27
			49.99	2.94	13.64	14.64	0.21	5.27	9.95	2.69	0.47	0.31	100.10
			49.66	2.94	13.21	14.47	0.23	5.38	9.92	2.72	0.46	0.32	99.30
			49.63	2.93	13.22	14.64	0.21	5.28	9.83	2.79	0.47	0.35	99.34
			49.48	2.91	13.31	14.32	0.23	5.58	10.03	2.66	0.43	0.32	99.27
			49.48	2.89	13.20	14.40	0.22	5.42	9.86	2.65	0.45	0.34	98.91
			49.86	2.88	13.41	14.32	0.22	5.57	10.07	2.71	0.44	0.34	99.81
			49.64	2.86	13.36	14.15	0.26	5.58	9.91	2.79	0.44	0.25	99.24
			49.13	2.76	13.12	14.21	0.23	5.53	9.91	2.70	0.44	0.29	98.32
			49.62	2.75	13.28	14.43	0.25	5.57	10.24	2.71	0.44	0.34	99.63
		Mean	**49.69**	**2.96**	**13.30**	**14.55**	**0.23**	**5.39**	**9.93**	**2.67**	**0.45**	**0.32**	**99.50**
		stdv	**0.35**	**0.15**	**0.18**	**0.52**	**0.02**	**0.27**	**0.15**	**0.20**	**0.01**	**0.03**	**0.48**

Tephra layer	Composite depth	Tephra marker	SiO_2	TiO_2	Al_2O_3	FeO	MnO	MgO	CaO	Na_2O	K_2O	P_2O_5	Total
TDV2-7 26	654 cm		46.30	3.13	*15.21*	14.52	0.22	6.31	10.20	2.87	0.47	0.31	99.54
			46.57	3.12	*15.23*	14.34	0.22	6.23	10.18	2.68	0.48	0.32	99.37
			46.59	3.07	*15.36*	14.48	0.20	6.37	10.04	2.76	0.48	0.34	99.69
			46.58	3.01	*15.30*	14.44	0.22	6.41	10.10	2.81	0.46	0.28	99.61
			46.35	3.00	*15.10*	14.40	0.23	6.23	10.03	2.77	0.47	0.30	98.88
			45.91	2.98	*15.14*	14.39	0.23	6.47	9.97	2.91	0.49	0.30	98.79
			46.75	2.98	*15.15*	14.70	0.24	6.32	9.64	2.81	0.47	0.30	99.36
			46.10	2.98	*14.97*	14.32	0.24	6.39	10.08	2.77	0.49	0.31	98.64
			46.14	2.98	*15.22*	14.42	0.20	6.42	9.96	2.76	0.47	0.35	98.92
			46.53	2.96	*15.29*	14.45	0.23	6.44	9.94	2.87	0.47	0.29	99.46
			46.90	2.95	*15.18*	14.42	0.18	6.23	10.14	2.81	0.48	0.35	99.64
			46.42	2.94	*15.13*	14.26	0.19	6.39	10.02	2.61	0.48	0.29	98.73
			46.29	2.88	*15.02*	14.10	0.21	6.37	10.08	2.73	0.49	0.31	98.49
			46.54	2.86	15.30	14.55	0.20	6.27	9.76	2.72	0.46	0.35	99.02
		Mean	**46.43**	**2.99**	**15.19**	**14.41**	**0.22**	**6.35**	**10.01**	**2.78**	**0.48**	**0.31**	**99.15**
		stdv	**0.27**	**0.08**	**0.11**	**0.14**	**0.02**	**0.08**	**0.15**	**0.08**	**0.01**	**0.02**	**0.41**
			49.27	2.87	13.54	14.43	0.23	5.96	10.70	2.52	0.33	0.31	100.16
			50.73	1.82	14.06	13.01	0.22	6.11	11.19	1.79	0.26	0.17	99.36
			50.13	1.77	13.78	13.17	0.20	6.36	11.18	2.38	0.25	0.17	99.39
			49.82	1.75	14.00	13.54	0.22	6.14	11.10	2.59	0.28	0.14	99.59
			50.33	1.74	13.97	13.06	0.22	6.37	11.13	2.37	0.27	0.15	99.61
		Mean	**50.25**	**1.77**	**13.95**	**13.20**	**0.22**	**6.25**	**11.15**	**2.28**	**0.27**	**0.16**	**99.49**
		stdv	**0.38**	**0.04**	**0.12**	**0.24**	**0.01**	**0.14**	**0.04**	**0.34**	**0.01**	**0.01**	**0.13**

Tephra layer	Composite depth	Tephra marker	SiO_2	TiO_2	Al_2O_3	FeO	MnO	MgO	CaO	Na_2O	K_2O	P_2O_5	Total
TDV2-7 31	659 cm		72.22	0.29	13.69	4.05	0.14	0.20	1.29	1.45	3.33	0.03	96.69
			70.95	0.33	13.85	4.03	0.15	0.20	1.29	4.90	3.48	0.06	99.24
			70.48	0.34	13.80	3.90	0.13	0.20	1.32	4.79	3.42	0.04	98.42
			70.43	0.34	13.82	3.99	0.18	0.22	1.29	5.13	3.40	0.04	98.85
			58.09	1.80	14.08	9.83	0.22	3.02	6.69	3.52	1.10	0.37	98.72
			48.19	4.29	13.17	14.65	0.20	4.76	9.37	3.27	0.85	0.50	99.25
			49.40	4.12	13.52	14.25	0.23	4.26	9.22	3.16	0.93	0.52	99.61
			48.77	2.78	13.43	14.26	0.22	6.03	10.86	2.56	0.32	0.24	99.47
			49.54	2.55	13.22	14.37	0.22	5.08	9.76	2.82	0.44	0.28	98.29
			49.56	2.47	13.60	14.07	0.21	5.54	10.04	2.67	0.42	0.22	98.79
			50.80	1.80	14.25	13.01	0.22	5.69	10.85	2.93	0.28	0.20	100.03
			50.43	0.06	31.47	0.87	0.01	0.17	14.64	3.19	0.07	0.00	100.91

Tephra layer	Composite depth	Tephra marker	SiO_2	TiO_2	Al_2O_3	FeO	MnO	MgO	CaO	Na_2O	K_2O	P_2O_5	Total
ÞUR2 1	151-155 cm	V1477	50.87	1.94	14.24	12.59	0.20	6.29	10.98	2.18	0.25	0.20	99.74
			50.14	1.89	14.13	12.58	0.21	6.52	11.46	2.51	0.24	0.10	99.78
			50.03	1.90	14.09	12.76	0.21	6.54	11.60	2.50	0.23	0.19	100.05
			49.82	1.84	14.00	12.91	0.23	6.61	11.19	2.57	0.21	0.16	99.54
			50.50	1.86	14.14	12.74	0.25	6.51	11.41	2.60	0.24	0.16	100.42
			49.89	1.82	14.03	11.97	0.27	6.48	11.04	2.13	0.22	0.17	98.02
			50.12	1.85	14.12	12.68	0.23	6.65	11.51	2.54	0.23	0.18	100.11
			50.60	1.75	13.79	11.92	0.23	6.38	11.07	2.59	0.24	0.17	98.74
			50.57	1.92	14.01	12.76	0.17	6.59	11.21	2.22	0.22	0.13	99.81
			50.20	1.83	13.94	12.43	0.24	6.55	11.26	2.25	0.22	0.18	99.10
			50.75	1.84	14.09	12.10	0.16	6.45	11.55	2.56	0.23	0.20	99.93
			49.96	1.77	13.91	12.44	0.21	6.41	11.22	2.62	0.22	0.16	98.92
			50.12	1.83	13.84	12.32	0.16	6.77	11.24	2.29	0.23	0.21	99.00
			50.19	1.82	13.93	12.57	0.23	6.76	11.53	2.32	0.22	0.15	99.71
			50.13	1.88	14.11	12.40	0.20	6.39	11.46	2.50	0.25	0.18	99.49
			49.79	1.91	13.25	13.03	0.27	6.62	11.38	2.46	0.22	0.10	99.03
			49.78	1.87	13.73	12.92	0.19	6.45	11.59	2.99	0.25	0.14	99.91
			50.05	1.83	14.09	12.55	0.25	6.65	11.49	2.31	0.24	0.19	99.65
			50.45	1.89	13.94	12.59	0.21	6.56	11.44	2.23	0.22	0.13	99.67
			50.11	1.83	14.00	12.52	0.26	6.54	11.34	2.56	0.22	0.16	99.55
			50.28	1.84	14.09	12.92	0.27	6.39	11.31	2.16	0.23	0.17	99.66
			50.58	1.82	14.29	12.73	0.26	6.52	11.47	2.43	0.21	0.19	100.49
		Mean	**50.22**	**1.85**	**13.99**	**12.57**	**0.22**	**6.53**	**11.35**	**2.43**	**0.23**	**0.17**	**99.56**
		stdv	**0.31**	**0.05**	**0.21**	**0.30**	**0.03**	**0.12**	**0.18**	**0.20**	**0.01**	**0.03**	**0.57**

Tephra layer	Composite depth	Tephra marker	SiO_2	TiO_2	Al_2O_3	FeO	MnO	MgO	CaO	Na_2O	K_2O	P_2O_5	Total
NYK1 61	58-64 cm	V1477	49.60	1.80	13.87	12.72	0.20	6.71	11.48	2.32	0.22	0.17	99.09
			49.64	1.89	13.82	12.35	0.29	6.79	11.47	2.31	0.24	0.16	98.96
			50.11	1.76	13.94	12.53	0.22	6.50	11.50	2.42	0.23	0.17	99.39
			50.27	1.82	13.74	13.02	0.23	6.61	11.52	1.96	0.26	0.22	99.64
			49.24	1.87	15.20	12.68	0.19	6.50	10.98	2.43	0.23	0.16	99.48
			50.26	1.85	13.72	12.74	0.22	6.54	10.73	2.46	0.24	0.22	98.99
			49.87	1.84	14.05	12.40	0.22	6.60	11.41	2.69	0.23	0.14	99.45
			49.64	1.86	13.80	12.71	0.25	6.73	11.50	2.50	0.22	0.24	99.44
			51.35	2.05	13.20	11.28	0.23	7.55	11.80	2.25	0.26	0.18	100.15
			50.37	1.85	13.82	12.95	0.24	6.67	11.30	2.67	0.22	0.22	100.31
			50.05	1.81	13.81	13.09	0.24	6.60	11.38	2.45	0.25	0.21	99.89
			50.52	1.81	14.24	12.38	0.25	6.81	11.56	2.10	0.24	0.18	100.08
			50.25	1.85	13.72	12.67	0.20	6.82	11.03	2.41	0.23	0.15	99.33
			50.41	1.90	13.78	13.30	0.23	6.44	11.23	2.00	0.25	0.13	99.67
			49.98	1.87	13.85	12.69	0.22	6.66	11.43	2.66	0.23	0.16	99.75
			49.99	1.86	13.90	12.64	0.23	6.75	11.74	2.21	0.22	0.25	99.78
		Mean	**50.10**	**1.86**	**13.90**	**12.63**	**0.23**	**6.71**	**11.38**	**2.37**	**0.24**	**0.18**	**99.59**
		stdv	**0.48**	**0.06**	**0.40**	**0.45**	**0.02**	**0.25**	**0.28**	**0.22**	**0.01**	**0.04**	**0.40**
			50.01	2.89	13.20	13.76	0.24	5.38	10.06	3.04	0.44	0.31	99.32

Tephra layer	Composite depth	Tephra marker	SiO_2	TiO_2	Al_2O_3	FeO	MnO	MgO	CaO	Na_2O	K_2O	P_2O_5	Total
NYK2 82	122 cm		49.47	1.90	13.80	13.01	0.24	6.72	11.04	2.52	0.22	0.17	99.09
			49.73	1.92	13.68	12.71	0.20	6.57	11.96	2.37	0.22	0.18	99.54
			47.89	4.21	13.26	14.65	0.23	4.82	9.54	3.08	0.78	0.53	98.98
			48.25	4.41	13.39	14.78	0.23	4.41	9.18	3.41	0.87	0.57	99.50
			47.91	4.45	13.20	14.69	0.22	4.93	9.58	3.15	0.80	0.52	99.45
			49.49	1.82	13.88	12.75	0.22	6.64	11.75	2.47	0.20	0.15	99.37
			48.43	4.25	13.23	14.44	0.20	4.82	9.58	3.01	0.82	0.46	99.24
			47.71	4.35	13.43	14.83	0.21	5.09	9.45	3.24	0.81	0.45	99.58
			47.40	4.54	13.16	14.73	0.23	4.99	9.68	3.17	0.80	0.52	99.22
			47.79	4.36	13.27	14.71	0.22	4.91	9.78	3.16	0.78	0.49	99.48
			47.91	4.30	13.27	14.88	0.23	4.89	9.44	3.16	0.80	0.49	99.38
			47.67	4.43	13.23	14.42	0.23	4.92	9.63	3.23	0.77	0.50	99.03
			47.58	4.28	13.22	14.57	0.24	4.91	9.55	3.07	0.79	0.51	98.73
			49.73	1.92	13.68	12.71	0.20	6.57	11.96	2.37	0.22	0.18	99.54
			47.88	4.35	13.33	14.86	0.27	4.96	9.49	3.06	0.81	0.52	99.54
			47.87	4.45	12.93	14.78	0.23	4.63	9.50	3.07	0.84	0.46	98.77
		Mean	**48.11**	**4.01**	**13.32**	**14.41**	**0.23**	**5.11**	**9.87**	**3.05**	**0.72**	**0.45**	**99.27**
		stdv	**0.69**	**0.91**	**0.23**	**0.73**	**0.02**	**0.66**	**0.85**	**0.28**	**0.22**	**0.13**	**0.29**

Tephra layer	Composite depth	Tephra marker	SiO_2	TiO_2	Al_2O_3	FeO	MnO	MgO	CaO	Na_2O	K_2O	P_2O_5	Total
NYK2 90	129 cm		60.96	0.94	15.30	9.47	0.26	1.31	4.72	4.21	1.46	0.42	99.05
			50.74	1.13	3.25	10.36	0.28	16.16	18.02	0.30	0.00	0.00	100.25
			49.65	1.73	13.95	12.01	0.20	7.14	12.15	2.26	0.18	0.13	99.40
			49.41	1.65	13.95	11.86	0.22	7.27	12.03	2.34	0.18	0.16	99.07
			46.23	3.13	14.61	14.59	0.22	6.20	9.95	2.76	0.48	0.34	98.50
			46.15	2.55	16.01	12.71	0.18	7.21	10.80	2.73	0.43	0.24	99.01
			46.39	3.29	14.67	14.81	0.25	6.14	10.32	3.01	0.50	0.33	99.71
			53.06	2.14	14.59	12.05	0.29	3.36	7.21	3.93	1.04	1.26	98.93
			46.71	2.82	15.51	13.87	0.21	7.17	10.84	2.64	0.43	0.27	100.46
			53.11	2.37	14.74	12.13	0.28	3.46	7.22	3.80	1.09	1.19	99.38
			53.21	2.31	14.47	12.34	0.29	3.44	7.07	3.82	1.16	1.23	99.33
			46.30	2.79	15.41	13.57	0.19	6.91	10.53	2.74	0.44	0.30	99.18
			46.75	2.55	15.85	13.23	0.18	6.95	10.77	2.71	0.43	0.27	99.69
			46.38	2.43	16.29	12.42	0.17	7.49	10.75	2.58	0.40	0.24	99.14
			46.59	2.40	16.36	13.09	0.22	7.12	11.19	2.40	0.21	0.21	99.79
		Mean	**48.26**	**2.62**	**15.32**	**13.16**	**0.23**	**5.95**	**9.70**	**3.01**	**0.60**	**0.53**	**99.38**
		stdv	**3.13**	**0.36**	**0.73**	**0.96**	**0.05**	**1.67**	**1.65**	**0.56**	**0.33**	**0.45**	**0.52**

Tephra layer	Composite depth	Tephra marker	SiO_2	TiO_2	Al_2O_3	FeO	MnO	MgO	CaO	Na_2O	K_2O	P_2O_5	Total
NYK2 148	179 cm		50.14	1.46	14.46	11.44	0.22	7.39	12.47	2.26	0.19	0.10	100.13
			49.56	1.55	14.48	11.10	0.21	7.73	12.98	2.18	0.13	0.11	100.03
			47.43	*1.76*	*13.19*	*12.10*	*0.19*	*6.42*	*10.70*	*2.08*	*0.22*	*0.15*	*94.24*
			48.56	4.45	12.72	14.75	0.25	4.45	9.26	3.11	0.93	0.64	99.12
			48.43	4.30	12.82	14.48	0.23	4.63	9.30	3.31	0.88	0.68	99.05
			48.44	4.29	13.02	14.43	0.22	4.49	9.06	3.22	0.86	0.61	98.64
			48.52	4.43	12.98	14.44	0.22	4.35	9.27	3.19	0.90	0.64	98.94
			48.75	4.38	12.90	14.87	0.23	4.27	9.07	3.49	0.96	0.62	99.55
			48.69	4.46	13.03	14.50	0.24	4.61	9.55	3.29	1.00	0.57	99.94
			48.52	4.43	12.84	14.68	0.26	4.53	8.89	3.33	0.86	0.58	98.91
			48.66	4.36	13.16	14.44	0.24	4.51	9.17	3.32	0.86	0.63	99.35
			48.39	4.28	13.20	14.38	0.24	4.60	9.05	3.41	0.87	0.63	99.04
			48.85	4.39	12.97	14.89	0.23	4.32	9.04	3.17	0.88	0.58	99.32
			48.37	4.36	12.95	14.48	0.25	4.64	9.34	3.36	0.85	0.62	99.22
			48.44	4.30	13.02	14.45	0.24	4.46	9.03	3.16	0.87	0.60	98.56
			48.87	4.27	12.76	14.36	0.24	4.50	9.29	3.24	0.88	0.62	99.03
			49.20	4.41	12.74	14.90	0.23	4.39	8.92	2.44	0.93	0.65	98.82
		Mean	**48.62**	**4.37**	**12.94**	**14.58**	**0.24**	**4.48**	**9.16**	**3.22**	**0.89**	**0.62**	**99.11**
		stdv	**0.23**	**0.07**	**0.15**	**0.20**	**0.01**	**0.12**	**0.18**	**0.25**	**0.04**	**0.03**	**0.36**

Tephra layer	Composite depth	Tephra marker	SiO_2	TiO_2	Al_2O_3	FeO	MnO	MgO	CaO	Na_2O	K_2O	P_2O_5	Total
NYK3 1	58-64 cm	V1477	50.20	1.84	13.92	12.91	0.23	6.62	11.22	2.40	0.24	0.21	99.79
			50.01	1.85	13.56	12.26	0.21	6.38	11.35	2.47	0.25	0.16	98.50
			49.86	1.84	13.89	12.45	0.24	6.59	11.39	2.54	0.21	0.17	99.18
			49.95	1.88	14.04	12.68	0.21	6.85	11.40	2.53	0.22	0.18	99.94
			49.85	1.83	13.69	12.52	0.21	6.83	11.53	2.43	0.21	0.11	99.21
			49.69	1.82	13.94	12.89	0.24	6.69	11.46	2.41	0.23	0.17	99.54
			50.07	1.83	14.15	12.25	0.23	6.56	11.15	2.55	0.22	0.18	99.19
			49.96	1.88	13.90	12.82	0.21	6.69	11.50	2.54	0.23	0.16	99.89
			49.99	1.82	13.96	12.82	0.17	6.69	11.52	2.50	0.23	0.14	99.84
			49.99	1.84	13.73	12.82	0.22	6.61	11.12	2.52	0.22	0.18	99.24
			49.80	1.77	13.97	12.38	0.23	6.65	11.54	2.40	0.22	0.17	99.13
			50.10	1.85	13.69	12.61	0.20	6.73	11.37	2.49	0.23	0.16	99.43
			50.01	1.75	14.05	12.43	0.20	6.78	11.86	2.41	0.22	0.14	99.85
			50.24	1.85	13.80	12.92	0.21	6.55	11.41	2.55	0.24	0.16	99.93
			49.85	1.82	13.91	12.64	0.24	6.86	11.49	2.53	0.22	0.16	99.73
			49.88	1.86	13.72	12.93	0.24	6.64	11.12	2.57	0.23	0.17	99.36
		Mean	**49.97**	**1.83**	**13.87**	**12.65**	**0.22**	**6.67**	**11.40**	**2.49**	**0.23**	**0.16**	**99.48**
		stdv	**0.14**	**0.03**	**0.16**	**0.24**	**0.02**	**0.13**	**0.19**	**0.06**	**0.01**	**0.02**	**0.40**
			47.51	4.31	12.98	14.79	0.22	4.86	9.75	3.11	0.79	0.51	98.84

Tephra layer	Composite depth	Tephra marker	SiO_2	TiO_2	Al_2O_3	FeO	MnO	MgO	CaO	Na_2O	K_2O	P_2O_5	Total
NYK3 74	179 cm		49.45	1.30	14.56	10.38	0.20	8.21	13.14	2.04	0.14	0.08	99.50
			49.38	1.33	14.40	10.51	0.18	8.23	12.97	2.01	0.12	0.14	99.27
			49.56	1.37	14.32	10.59	0.19	7.85	13.06	2.09	0.14	0.12	99.29
			49.58	1.14	14.59	10.35	0.17	8.14	13.52	1.97	0.09	0.11	99.67
			49.50	1.37	14.49	10.18	0.20	8.01	13.35	1.96	0.13	0.09	99.29
		Mean	**49.49**	**1.30**	**14.47**	**10.40**	**0.19**	**8.09**	**13.21**	**2.01**	**0.12**	**0.11**	**99.40**
		stdv	**0.08**	**0.09**	**0.11**	**0.16**	**0.01**	**0.16**	**0.22**	**0.05**	**0.02**	**0.02**	**0.18**
			49.45	2.86	13.21	13.99	0.24	5.62	10.39	2.82	0.38	0.26	99.22
			49.22	2.81	13.16	14.15	0.24	5.64	10.27	2.78	0.38	0.26	98.91
			49.43	2.86	13.09	14.32	0.25	5.60	10.30	2.79	0.39	0.25	99.29
		Mean	**49.37**	**2.84**	**13.15**	**14.15**	**0.24**	**5.62**	**10.32**	**2.80**	**0.38**	**0.26**	**99.14**
		stdv	**0.13**	**0.03**	**0.06**	**0.17**	**0.01**	**0.02**	**0.06**	**0.02**	**0.00**	**0.00**	**0.20**
			48.11	3.95	13.31	14.09	0.23	5.26	9.89	3.09	0.78	0.49	99.19
			48.02	4.03	13.40	13.88	0.23	5.05	9.73	3.00	0.80	0.44	98.59
			47.92	4.14	12.95	14.10	0.20	5.29	9.96	3.05	0.80	0.47	98.88
			47.48	4.16	13.34	14.25	0.24	5.16	9.83	3.18	0.78	0.40	98.82
			47.88	4.19	13.29	15.25	0.21	4.84	9.46	3.11	0.76	0.45	99.44
			47.92	4.11	13.42	14.25	0.22	5.04	9.75	2.94	0.78	0.40	98.83
			48.25	4.01	13.41	14.08	0.24	4.75	9.81	3.06	0.83	0.51	98.95
			47.70	4.08	12.98	14.32	0.23	5.13	9.41	3.07	0.79	0.42	98.14
			48.26	4.11	13.33	14.12	0.21	4.93	9.73	3.25	0.84	0.46	99.23
		Mean	**47.95**	**4.09**	**13.27**	**14.26**	**0.22**	**5.05**	**9.73**	**3.08**	**0.79**	**0.45**	**98.90**
		stdv	**0.25**	**0.08**	**0.18**	**0.39**	**0.01**	**0.18**	**0.18**	**0.09**	**0.03**	**0.04**	**0.38**

Tephra layer	Composite depth	Tephra marker	SiO_2	TiO_2	Al_2O_3	FeO	MnO	MgO	CaO	Na_2O	K_2O	P_2O_5	Total
NYK3 98	193-195 cm	Hekla 4	72.42	0.12	13.10	1.94	0.07	0.03	1.30	4.38	2.71	0.00	96.07
			72.40	0.13	13.03	2.01	0.06	0.03	1.26	4.21	2.52	0.00	95.64
			71.89	0.11	13.19	2.02	0.08	0.02	1.32	4.22	2.70	0.00	95.56
			71.83	0.12	13.06	1.99	0.08	0.02	1.27	4.41	2.80	0.01	95.58
			72.19	0.11	13.05	2.02	0.07	0.01	1.30	4.48	2.77	0.00	96.01
			71.61	0.42	12.99	4.58	0.15	0.35	2.01	4.32	2.67	0.09	99.19
			69.97	0.11	12.64	1.97	0.10	0.02	1.20	4.13	2.78	0.00	92.92
			61.65	0.83	14.80	9.13	0.25	0.80	4.50	4.50	1.59	0.30	98.34
			61.75	0.83	14.90	9.29	0.27	0.88	4.53	4.60	1.63	0.24	98.92
			62.53	0.85	15.13	9.44	0.28	0.89	4.56	4.33	1.66	0.33	100.00
			60.86	0.97	15.49	9.60	0.27	1.25	5.04	4.47	1.46	0.42	99.83
			59.15	1.15	15.26	9.72	0.23	1.76	5.16	4.09	1.41	0.52	98.45
			57.26	1.19	14.89	10.59	0.25	1.68	4.92	3.86	1.45	0.55	96.64
			46.62	2.46	15.84	12.68	0.18	7.11	10.83	2.66	0.43	0.30	99.10
			46.20	2.77	15.57	13.57	0.21	6.95	10.84	2.85	0.41	0.28	99.66
			47.40	3.73	13.98	13.92	0.20	6.02	10.79	2.51	0.46	0.34	99.35
			46.31	3.22	14.77	14.66	0.25	5.94	10.13	2.93	0.50	0.35	99.06
		Mean	**61.88**	**1.12**	**14.22**	**7.60**	**0.18**	**1.99**	**4.76**	**3.94**	**1.76**	**0.22**	**97.66**
		stdv	**10.15**	**1.19**	**1.12**	**4.84**	**0.08**	**2.66**	**3.71**	**0.71**	**0.92**	**0.19**	**2.06**
			47.45	4.52	13.12	14.39	0.25	5.01	9.52	2.89	0.86	0.63	98.64
			46.60	4.07	12.96	14.44	0.22	5.39	10.34	3.12	0.63	0.40	98.17
			46.11	0.00	34.82	0.52	0.04	0.19	18.42	1.22	0.01	0.00	101.33

Tephra layer	Composite depth	Tephra marker	SiO_2	TiO_2	Al_2O_3	FeO	MnO	MgO	CaO	Na_2O	K_2O	P_2O_5	Total
NYK3 103	198 cm		50.13	1.59	14.30	11.65	0.21	7.38	12.24	2.30	0.18	0.12	100.09
			49.92	1.55	14.23	11.36	0.19	7.47	12.42	2.13	0.15	0.10	99.52
			49.33	1.47	14.06	11.61	0.21	7.66	12.37	2.26	0.15	0.15	99.28
			49.76	1.59	14.09	11.49	0.20	7.33	12.28	2.24	0.15	0.13	99.26
			49.71	1.52	14.23	11.68	0.17	7.51	12.49	2.28	0.16	0.14	99.89
			49.66	1.51	14.05	11.55	0.19	7.69	12.16	2.25	0.16	0.14	99.36
			50.25	1.56	14.24	11.77	0.22	7.18	12.21	2.36	0.19	0.14	100.11
			50.01	1.43	14.31	11.70	0.20	7.29	12.19	2.21	0.15	0.14	99.63
			49.80	1.55	14.05	11.55	0.21	7.50	12.28	2.29	0.15	0.12	99.51
			49.73	1.62	14.22	11.73	0.19	7.54	12.41	2.34	0.16	0.12	100.05
			50.19	1.60	14.32	11.42	0.22	7.11	11.88	2.40	0.18	0.15	99.47
			50.21	1.52	14.29	11.69	0.20	7.36	12.40	2.21	0.15	0.07	100.11
			49.93	1.51	14.10	11.56	0.22	7.28	11.86	2.25	0.18	0.12	99.01
			49.60	1.51	14.16	11.32	0.22	7.53	12.24	2.38	0.15	0.11	99.23
			49.91	1.58	14.10	11.70	0.21	7.44	12.39	2.31	0.15	0.12	99.90
			50.31	1.56	14.29	11.58	0.23	7.54	12.48	2.22	0.16	0.14	100.50
		Mean	**49.90**	**1.54**	**14.19**	**11.59**	**0.21**	**7.43**	**12.27**	**2.28**	**0.16**	**0.13**	**99.68**
		stdv	**0.27**	**0.05**	**0.10**	**0.13**	**0.02**	**0.16**	**0.19**	**0.07**	**0.01**	**0.02**	**0.42**

Tephra layer	Composite depth	Tephra marker	SiO_2	TiO_2	Al_2O_3	FeO	MnO	MgO	CaO	Na_2O	K_2O	P_2O_5	Total
NYK3 109	202 cm		50.16	1.70	14.10	11.90	0.19	7.02	11.78	2.30	0.21	0.15	99.52
			50.85	1.74	14.10	11.95	0.20	6.64	11.18	2.46	0.27	0.19	99.59
			50.71	1.75	14.24	11.89	0.20	7.04	11.41	2.48	0.24	0.19	100.16
			51.53	1.66	14.11	11.58	0.20	6.60	11.54	2.37	0.26	0.16	100.01
			50.30	1.71	14.07	11.91	0.20	6.96	11.78	2.47	0.23	0.16	99.79
			49.83	1.68	13.86	11.89	0.21	7.07	11.35	2.39	0.23	0.15	98.66
			50.42	1.73	13.97	12.08	0.19	7.00	11.47	2.37	0.22	0.14	99.59
			49.99	1.73	13.78	12.13	0.20	6.93	11.62	2.39	0.23	0.15	99.15
			50.40	1.59	14.02	11.39	0.23	6.92	11.48	2.44	0.28	0.22	98.97
			50.14	1.70	13.95	11.90	0.22	6.99	11.60	2.40	0.22	0.17	99.29
			50.53	1.50	14.33	11.30	0.22	7.74	12.14	2.30	0.16	0.14	100.37
			49.99	1.66	14.11	12.06	0.23	7.18	11.82	2.36	0.22	0.19	99.82
			51.52	1.70	14.03	11.58	0.22	6.37	11.03	2.53	0.33	0.17	99.48
			50.09	1.58	14.29	11.44	0.22	7.39	12.35	2.22	0.18	0.15	99.92
			50.14	1.71	13.94	12.13	0.19	7.06	11.70	2.37	0.21	0.15	99.61
		Mean	**50.44**	**1.68**	**14.06**	**11.81**	**0.21**	**6.99**	**11.62**	**2.39**	**0.23**	**0.17**	**99.59**
		stdv	**0.52**	**0.07**	**0.15**	**0.28**	**0.01**	**0.32**	**0.34**	**0.08**	**0.04**	**0.02**	**0.45**
			49.73	2.35	13.90	12.29	0.19	6.62	11.12	2.54	0.33	0.16	99.23

Tephra layer	Composite depth	Tephra marker	SiO_2	TiO_2	Al_2O_3	FeO	MnO	MgO	CaO	Na_2O	K_2O	P_2O_5	Total
NYK3 117	207 cm		47.49	4.34	13.18	14.78	0.22	4.71	9.91	3.08	0.78	0.47	98.97
			48.17	4.39	13.27	15.14	0.24	4.97	9.89	3.10	0.79	0.49	100.45
			47.53	4.35	12.94	14.80	0.22	5.08	9.96	3.00	0.80	0.43	99.10
			47.78	4.36	13.10	14.91	0.25	4.87	9.68	3.12	0.81	0.49	99.38
			47.52	4.14	13.20	15.11	0.24	5.07	9.90	3.03	0.78	0.51	99.50
			47.91	4.42	13.15	14.95	0.20	5.08	9.76	3.18	0.75	0.47	99.87
			47.82	4.24	13.25	14.94	0.24	4.93	9.52	3.19	0.80	0.48	99.41
		Mean	**47.75**	**4.32**	**13.16**	**14.95**	**0.23**	**4.96**	**9.80**	**3.10**	**0.79**	**0.48**	**99.53**
		stdv	**0.25**	**0.10**	**0.11**	**0.14**	**0.02**	**0.14**	**0.16**	**0.07**	**0.02**	**0.03**	**0.50**
			50.48	3.11	13.00	14.85	0.23	4.42	8.93	3.01	0.63	0.37	99.03
			49.97	3.03	13.10	14.89	0.26	4.59	9.30	2.94	0.67	0.33	99.08
			50.19	3.20	12.67	15.05	0.27	4.16	8.91	3.13	0.73	0.40	98.70
			50.42	3.05	13.17	14.95	0.25	4.17	9.10	3.03	0.68	0.42	99.24
			49.31	3.13	13.07	14.77	0.23	5.33	9.77	2.77	0.48	0.35	99.20
			50.02	2.45	13.63	13.66	0.26	5.55	10.18	2.60	0.43	0.30	99.08
		Mean	**50.07**	**3.00**	**13.11**	**14.70**	**0.25**	**4.70**	**9.37**	**2.91**	**0.60**	**0.36**	**99.06**
		stdv	**0.42**	**0.27**	**0.31**	**0.52**	**0.02**	**0.60**	**0.51**	**0.19**	**0.12**	**0.04**	**0.19**
			48.63	3.89	9.77	14.22	0.25	7.88	11.74	2.26	0.69	0.40	99.74
			49.72	1.23	14.33	10.84	0.19	7.94	12.60	2.04	0.14	0.09	99.12
			50.07	1.73	14.08	12.20	0.21	6.95	11.65	2.33	0.27	0.18	99.67

Tephra layer	Composite depth	Tephra marker	SiO_2	TiO_2	Al_2O_3	FeO	MnO	MgO	CaO	Na_2O	K_2O	P_2O_5	Total
NYK3 145	226 cm		49.51	1.36	14.72	10.85	0.20	7.89	12.93	1.98	0.15	0.12	99.69
			48.72	4.12	13.59	14.80	0.24	4.94	9.75	2.47	0.63	0.50	99.76
			49.04	4.16	13.73	14.89	0.25	4.73	9.77	3.05	0.75	0.42	100.79
			48.17	4.00	13.16	14.32	0.22	5.08	9.66	3.01	0.80	0.51	98.93
			47.05	3.90	13.71	13.96	0.21	5.04	9.66	2.97	0.78	0.44	97.72
			48.18	3.82	13.50	14.39	0.20	5.11	9.79	3.14	0.82	0.42	99.38
			48.25	3.88	13.37	14.10	0.22	5.13	9.77	3.09	0.77	0.47	99.05
			47.96	4.18	13.48	14.60	0.21	5.00	9.91	3.05	0.79	0.48	99.66
			48.19	3.95	13.30	14.42	0.23	5.07	9.47	3.09	0.80	0.45	98.97
			48.65	4.18	13.55	14.56	0.22	4.77	9.68	2.99	0.82	0.47	99.89
			48.28	3.98	13.34	14.12	0.21	4.97	9.67	2.99	0.80	0.47	98.83
			48.14	4.11	13.36	14.24	0.19	4.99	9.89	3.16	0.79	0.43	99.30
			48.53	4.00	13.46	14.29	0.22	5.05	9.52	3.07	0.84	0.43	99.42
			48.70	4.15	13.49	14.66	0.23	5.03	9.90	2.65	0.82	0.45	100.08
			48.71	4.07	13.50	13.79	0.20	4.94	9.87	3.02	0.87	0.52	99.49
		Mean	**48.33**	**4.04**	**13.47**	**14.37**	**0.22**	**4.99**	**9.74**	**2.98**	**0.79**	**0.46**	**99.38**
		stdv	**0.48**	**0.12**	**0.15**	**0.32**	**0.02**	**0.12**	**0.14**	**0.19**	**0.05**	**0.03**	**0.71**

Tephra layer	Composite depth	Tephra marker	SiO_2	TiO_2	Al_2O_3	FeO	MnO	MgO	CaO	Na_2O	K_2O	P_2O_5	Total
NYK 4 29	151-153 cm	Hekla 3	72.32	0.18	14.44	2.95	0.14	0.11	1.85	5.07	2.54	0.02	99.61
			72.19	0.22	14.37	2.99	0.12	0.15	1.98	4.89	2.40	0.08	99.39
			72.66	0.17	14.40	2.96	0.08	0.13	1.99	4.95	2.45	0.02	99.81
			72.13	0.14	14.04	3.00	0.12	0.11	1.93	4.97	2.44	0.01	98.89
			71.86	0.20	14.36	2.96	0.10	0.13	1.94	4.77	2.41	0.01	98.75
			71.85	0.20	14.58	2.93	0.08	0.11	1.88	5.08	2.47	0.00	99.18
			71.61	0.20	14.52	3.03	0.13	0.14	1.84	5.01	2.52	0.00	99.00
			71.34	0.16	14.05	3.00	0.09	0.11	1.90	5.04	2.45	0.00	98.15
			70.95	0.23	14.27	3.02	0.12	0.12	2.06	5.07	2.50	0.00	98.34
			70.50	0.18	13.96	2.81	0.09	0.11	1.90	4.83	2.48	0.00	96.86
			68.61	*0.18*	*13.83*	*2.88*	*0.11*	*0.13*	*1.83*	*4.65*	*2.38*	*0.04*	*94.64*
			67.72	0.32	15.03	5.12	0.24	0.32	3.01	5.18	2.08	0.04	99.05
			66.55	0.37	15.13	5.32	0.19	0.37	3.13	4.81	2.00	0.11	97.98
			66.30	0.46	14.92	5.73	0.23	0.41	3.31	4.81	2.00	0.10	98.27
			65.88	*0.21*	*13.46*	*2.54*	*0.10*	*0.10*	*1.65*	*4.23*	*2.24*	*0.00*	*90.41*
			65.46	*0.14*	*12.82*	*2.81*	*0.11*	*0.12*	*1.84*	*4.70*	*2.26*	*0.00*	*90.27*
			64.44	*0.18*	*13.28*	*2.68*	*0.15*	*0.10*	*1.70*	*4.38*	*2.15*	*0.00*	*89.05*
			64.44	*0.15*	*13.21*	*2.70*	*0.12*	*0.12*	*1.71*	*4.46*	*2.21*	*0.03*	*89.15*
			63.46	*0.31*	*15.22*	*4.79*	*0.14*	*0.23*	*2.75*	*4.73*	*1.99*	*0.01*	*93.63*
			60.39	*0.22*	*13.51*	*2.71*	*0.09*	*0.16*	*1.77*	*3.73*	*2.03*	*0.01*	*84.62*
			60.05	*0.18*	*15.39*	*2.68*	*0.12*	*0.10*	*1.70*	*4.13*	*2.02*	*0.00*	*86.36*
			58.56	*0.33*	*13.37*	*3.87*	*0.15*	*0.24*	*2.34*	*3.89*	*1.70*	*0.07*	*84.53*
		Mean	**70.47**	**0.23**	**14.42**	**3.48**	**0.13**	**0.17**	**2.18**	**4.94**	**2.37**	**0.03**	**98.42**
		stdv	**2.22**	**0.09**	**0.40**	**1.04**	**0.05**	**0.11**	**0.53**	**0.15**	**0.19**	**0.04**	**1.33**

Tephra layer	Composite depth	Tephra marker	SiO_2	TiO_2	Al_2O_3	FeO	MnO	MgO	CaO	Na_2O	K_2O	P_2O_5	Total
NYK4 89	230 cm		49.57	1.64	13.92	12.16	0.20	7.17	11.92	2.33	0.20	0.13	99.24
			50.01	1.97	14.15	12.09	0.19	6.64	11.71	2.54	0.27	0.20	99.76
			50.06	1.72	14.26	11.81	0.24	7.19	12.36	2.42	0.20	0.19	100.45
			49.77	1.65	14.26	11.66	0.20	7.22	12.42	2.28	0.20	0.16	99.83
			49.75	1.66	14.33	11.42	0.19	7.31	12.22	2.29	0.19	0.10	99.47
			49.69	1.59	14.36	11.28	0.21	7.35	12.13	2.31	0.20	0.13	99.25
			49.72	1.88	14.08	12.47	0.22	6.77	11.54	2.36	0.24	0.19	99.47
			51.07	2.92	12.85	14.46	0.26	4.59	8.84	3.08	0.57	0.40	99.04
			50.15	2.05	13.78	12.91	0.22	6.48	11.26	2.44	0.31	0.20	99.81
			49.71	1.65	14.40	11.63	0.21	7.28	12.38	2.23	0.19	0.14	99.81
			50.08	1.95	14.10	12.51	0.19	6.49	11.66	2.42	0.28	0.19	99.88
			49.68	1.94	14.01	14.06	0.25	6.19	11.26	2.48	0.32	0.22	100.42
			49.86	2.11	13.81	12.79	0.23	6.34	11.12	2.46	0.32	0.23	99.26
			50.27	1.75	14.33	10.61	0.18	7.97	13.05	2.24	0.18	0.17	100.75
			49.94	1.84	14.04	11.83	0.21	6.95	11.64	2.36	0.24	0.18	99.23
			49.89	1.79	14.18	11.93	0.21	6.90	11.97	2.36	0.22	0.17	99.61
			50.06	1.63	14.37	11.75	0.21	7.15	12.33	2.30	0.19	0.15	100.13
		Mean	**49.96**	**1.87**	**14.07**	**12.20**	**0.21**	**6.82**	**11.75**	**2.41**	**0.25**	**0.19**	**99.73**
		stdv	**0.35**	**0.32**	**0.37**	**0.96**	**0.02**	**0.73**	**0.90**	**0.19**	**0.10**	**0.06**	**0.49**

Tephra layer	Composite depth	Tephra marker	SiO_2	TiO_2	Al_2O_3	FeO	MnO	MgO	CaO	Na_2O	K_2O	P_2O_5	Total
NYK4 103	239 cm		49.66	2.48	13.93	12.53	0.19	6.31	11.21	2.58	0.36	0.22	99.47
			49.48	2.33	14.07	12.25	0.18	6.60	11.33	2.44	0.33	0.24	99.25
			49.75	2.31	14.19	12.41	0.22	6.54	10.86	2.55	0.35	0.22	99.40
			49.66	2.19	14.42	12.15	0.21	6.75	11.67	2.44	0.30	0.21	100.00
			49.56	2.18	14.21	11.80	0.20	7.09	11.61	2.42	0.30	0.20	99.57
			49.79	2.14	14.25	12.08	0.22	6.94	11.58	2.50	0.32	0.18	100.00
			49.47	2.14	14.23	11.91	0.20	6.90	11.46	2.37	0.31	0.21	99.20
			49.63	2.13	14.22	11.84	0.21	6.86	11.46	2.39	0.30	0.20	99.24
			49.54	2.11	14.17	11.99	0.20	6.99	11.65	2.42	0.29	0.18	99.54
			49.68	2.09	14.36	11.54	0.20	7.13	11.71	2.54	0.30	0.18	99.72
			49.60	2.09	14.60	11.50	0.19	7.16	11.89	2.41	0.28	0.20	99.91
			49.53	2.08	14.48	11.45	0.18	7.21	11.82	2.34	0.26	0.16	99.52
			49.54	2.05	14.28	11.50	0.17	7.16	11.85	2.53	0.31	0.22	99.61
		Mean	**49.61**	**2.18**	**14.26**	**11.92**	**0.20**	**6.90**	**11.55**	**2.46**	**0.31**	**0.20**	**99.57**
		stdv	**0.10**	**0.12**	**0.17**	**0.36**	**0.02**	**0.28**	**0.29**	**0.08**	**0.03**	**0.02**	**0.27**
			49.79	1.47	14.34	10.86	0.20	7.56	12.95	2.09	0.16	0.10	99.53
			49.87	3.51	12.97	14.98	0.24	4.58	8.94	2.97	0.57	0.43	99.06

Tephra layer	Composite depth	Tephra marker	SiO_2	TiO_2	Al_2O_3	FeO	MnO	MgO	CaO	Na_2O	K_2O	P_2O_5	Total
NYK4 120	252 cm		50.80	2.66	13.39	13.76	0.22	5.09	9.70	2.66	0.49	0.34	99.11
			50.10	2.72	13.43	13.51	0.24	5.43	10.00	2.62	0.46	0.30	98.81
			50.24	2.31	14.56	12.01	0.20	6.79	11.41	2.42	0.32	0.22	100.48
			50.83	2.76	13.72	13.89	0.24	4.80	9.75	2.77	0.50	0.34	99.61
			50.38	2.70	13.67	13.73	0.24	5.40	9.86	2.72	0.45	0.31	99.45
			50.70	2.68	13.52	13.94	0.21	5.27	9.72	2.86	0.50	0.32	99.73
			50.97	2.71	13.43	13.67	0.22	5.30	9.64	2.79	0.50	0.35	99.57
			50.48	3.35	12.86	14.64	0.25	4.65	8.96	2.93	0.55	0.37	99.05
			50.33	3.34	13.24	14.52	0.25	4.52	8.99	2.87	0.56	0.40	99.03
			51.17	2.68	13.70	13.72	0.20	5.45	10.05	2.77	0.47	0.28	100.50
			50.51	2.66	13.57	13.57	0.22	5.40	10.00	2.75	0.48	0.30	99.46
			50.96	2.77	13.24	13.63	0.24	5.20	9.61	2.77	0.48	0.34	99.23
			50.61	2.64	13.57	13.78	0.23	5.32	9.77	2.74	0.48	0.30	99.44
		Mean	**50.62**	**2.77**	**13.53**	**13.72**	**0.23**	**5.28**	**9.80**	**2.74**	**0.48**	**0.32**	**99.50**
		stdv	**0.32**	**0.28**	**0.39**	**0.62**	**0.02**	**0.55**	**0.59**	**0.13**	**0.06**	**0.05**	**0.51**
			50.50	1.78	14.36	11.39	0.19	7.18	12.36	2.44	0.22	0.19	100.61
			49.62	1.51	5.49	7.12	0.15	14.93	21.27	0.26	0.01	0.01	100.37

Tephra layer	Composite depth	Tephra marker	SiO_2	TiO_2	Al_2O_3	FeO	MnO	MgO	CaO	Na_2O	K_2O	P_2O_5	Total
NYK4 129	256 cm		49.39	2.68	13.42	13.68	0.23	6.05	10.50	2.68	0.40	0.28	99.30
			49.34	2.80	13.26	13.69	0.24	5.76	10.08	2.64	0.42	0.31	98.54
			49.94	2.75	13.34	13.82	0.23	5.86	10.40	2.60	0.40	0.30	99.64
			49.63	2.61	13.39	13.80	0.22	5.99	10.42	2.60	0.37	0.34	99.37
			49.93	3.04	13.29	14.55	0.26	5.51	9.92	2.74	0.46	0.30	100.00
			50.27	2.00	13.46	13.78	0.21	6.01	10.81	2.48	0.30	0.18	99.50
			50.12	2.94	13.37	14.39	0.23	5.48	9.89	2.74	0.45	0.37	99.98
			50.34	3.04	13.25	14.38	0.24	4.60	9.48	2.84	0.69	0.31	99.17
			49.95	2.98	13.09	14.51	0.25	5.26	9.95	2.72	0.45	0.37	99.53
			49.64	2.84	13.54	14.06	0.23	5.64	10.04	2.61	0.42	0.29	99.31
			49.64	2.74	13.45	13.90	0.23	5.87	10.35	2.55	0.39	0.31	99.43
			49.56	2.61	13.70	13.72	0.21	5.94	10.42	2.53	0.39	0.30	99.38
			50.95	2.00	13.58	13.04	0.23	5.92	10.34	2.61	0.43	0.22	99.32
			49.57	2.85	13.39	14.13	0.24	5.68	10.08	2.64	0.42	0.30	99.30
			49.44	2.87	13.40	13.96	0.25	5.70	10.03	2.63	0.41	0.28	98.97
			49.78	2.42	13.82	13.63	0.21	6.26	10.83	2.51	0.34	0.26	100.06
		Mean	**49.84**	**2.70**	**13.42**	**13.94**	**0.23**	**5.72**	**10.22**	**2.63**	**0.42**	**0.29**	**99.43**
		stdv	**0.42**	**0.32**	**0.18**	**0.39**	**0.01**	**0.39**	**0.35**	**0.09**	**0.08**	**0.05**	**0.38**

Tephra layer	Composite depth	Tephra marker	SiO_2	TiO_2	Al_2O_3	FeO	MnO	MgO	CaO	Na_2O	K_2O	P_2O_5	Total
NYK5 5	258-268 cm		49.45	2.09	13.61	14.89	0.26	5.92	11.42	2.50	0.24	0.16	100.54
			50.13	1.93	14.01	13.17	0.21	6.58	11.61	2.44	0.22	0.18	100.48
			49.53	1.90	13.73	13.02	0.22	6.43	10.97	2.55	0.24	0.19	98.78
			49.34	1.90	13.64	12.39	0.22	6.67	11.33	2.50	0.23	0.16	98.39
			49.56	1.90	13.86	12.90	0.21	6.34	11.28	2.39	0.23	0.18	98.85
			49.55	1.90	13.95	12.90	0.22	6.46	11.24	2.50	0.23	0.18	99.12
			49.68	1.87	13.80	13.21	0.22	6.38	11.22	2.52	0.24	0.16	99.31
			49.50	1.87	13.79	12.57	0.21	6.59	11.41	2.43	0.22	0.17	98.77
			49.96	1.87	13.75	12.94	0.22	6.40	11.39	2.43	0.24	0.15	99.35
			50.52	1.87	14.12	11.15	0.21	7.47	12.28	2.23	0.14	0.16	100.15
			50.05	1.86	13.80	12.72	0.23	6.61	11.28	2.50	0.22	0.18	99.44
			49.97	1.84	14.01	13.74	0.22	6.08	11.41	2.42	0.26	0.13	100.08
			49.89	1.83	14.05	12.93	0.25	6.41	11.39	2.36	0.22	0.17	99.49
			49.51	1.81	13.95	12.85	0.21	6.70	11.42	2.42	0.24	0.18	99.28
			50.40	1.81	14.12	12.63	0.22	6.81	11.71	2.56	0.16	0.16	100.58
			49.24	1.80	13.87	12.83	0.19	6.35	11.25	2.54	0.21	0.17	98.45
		Mean	**49.77**	**1.88**	**13.88**	**12.93**	**0.22**	**6.51**	**11.41**	**2.46**	**0.22**	**0.17**	**99.44**
		stdv	**0.38**	**0.07**	**0.16**	**0.75**	**0.02**	**0.34**	**0.28**	**0.08**	**0.03**	**0.01**	**0.73**
			49.05	1.15	14.55	11.20	0.21	7.77	13.20	2.17	0.08	0.07	99.46

Tephra layer	Composite depth	Tephra marker	SiO_2	TiO_2	Al_2O_3	FeO	MnO	MgO	CaO	Na_2O	K_2O	P_2O_5	Total
NYK5 17	268-277 cm		46.23	5.14	12.90	**16.12**	0.24	4.42	9.32	3.07	0.77	0.53	98.74
			47.62	4.80	13.35	15.86	0.22	4.61	9.51	2.89	0.77	0.54	100.17
			46.74	4.72	13.14	16.11	0.23	5.03	9.93	2.85	0.71	0.53	99.99
			46.78	4.61	13.08	16.09	0.21	4.79	9.62	3.13	0.79	0.53	99.64
			47.79	4.59	13.23	15.29	0.22	4.66	9.40	3.13	0.80	0.60	99.72
			47.44	4.53	13.15	15.29	0.25	4.70	9.72	2.98	0.79	0.62	99.46
			46.88	4.53	13.00	14.43	0.21	4.98	9.91	3.00	0.78	0.62	98.34
			47.14	4.52	12.99	14.89	0.22	4.89	9.62	3.06	0.77	0.57	98.67
			47.69	4.52	13.06	15.40	0.23	4.75	9.74	3.16	0.77	0.58	99.89
			47.03	4.51	13.03	14.79	0.23	4.93	9.59	2.95	0.75	0.51	98.32
			46.94	4.51	13.19	15.15	0.22	5.02	9.97	3.27	0.75	0.59	99.61
			47.07	4.49	12.94	14.66	0.25	4.87	9.65	2.99	0.76	0.59	98.27
			47.09	4.48	13.05	15.04	0.25	4.94	9.76	3.08	0.76	0.50	98.95
			47.48	4.46	13.05	14.90	0.25	4.73	9.74	3.08	0.77	0.51	98.96
			46.83	4.46	13.07	14.73	0.24	5.06	9.64	3.11	0.77	0.58	98.49
			47.37	4.40	12.97	14.53	0.24	5.43	10.10	2.94	0.78	0.58	99.34
			47.25	4.22	12.93	14.96	0.24	4.93	9.87	3.07	0.77	0.62	98.86
		Mean	**47.20**	**4.52**	**13.08**	**15.13**	**0.23**	**4.90**	**9.74**	**3.04**	**0.77**	**0.57**	**99.17**
		stdv	**0.34**	**0.13**	**0.11**	**0.52**	**0.01**	**0.20**	**0.18**	**0.11**	**0.02**	**0.04**	**0.64**

Tephra layer	Composite depth	Tephra marker	SiO_2	TiO_2	Al_2O_3	FeO	MnO	MgO	CaO	Na_2O	K_2O	P_2O_5	Total
NYK5 44	302 cm		50.43	3.25	12.79	14.72	0.25	4.45	8.61	3.03	0.60	0.42	98.55
			50.02	2.54	13.48	13.55	0.24	5.73	10.40	2.60	0.41	0.33	99.30
			50.29	2.37	13.64	13.86	0.27	5.76	10.20	2.62	0.39	0.31	99.71
			49.67	2.29	13.41	13.66	0.22	5.71	10.19	2.49	0.41	0.33	98.39
			49.41	2.13	14.08	12.81	0.21	6.54	11.38	2.41	0.29	0.24	99.50
			50.16	1.95	14.02	13.17	0.19	6.36	11.46	2.14	0.28	0.22	99.95
			49.45	1.93	13.80	12.66	0.19	6.27	11.20	2.49	0.28	0.21	98.48
			49.12	1.90	14.05	12.51	0.21	6.62	11.50	2.56	0.28	0.20	98.96
			49.12	1.82	14.18	11.79	0.20	7.19	12.27	2.41	0.22	0.19	99.39
			49.52	1.80	14.25	11.57	0.20	7.29	12.75	2.32	0.18	0.16	100.04
			50.86	1.77	15.60	10.87	0.22	5.85	11.89	2.89	0.14	0.18	100.27
			49.39	1.76	14.26	11.82	0.19	6.98	12.31	2.26	0.22	0.16	99.34
			49.25	1.69	14.18	11.68	0.19	7.09	12.11	2.24	0.21	0.14	98.78
			49.54	1.65	14.20	11.83	0.23	7.19	12.20	2.30	0.21	0.18	99.53
			49.26	1.65	14.04	11.72	0.22	7.22	12.34	2.32	0.19	0.16	99.12
		Mean	**49.56**	**1.86**	**14.17**	**12.17**	**0.21**	**6.69**	**11.80**	**2.40**	**0.24**	**0.20**	**99.31**
		stdv	**0.50**	**0.19**	**0.51**	**0.79**	**0.02**	**0.55**	**0.69**	**0.19**	**0.07**	**0.05**	**0.60**
			49.79	1.38	8.96	9.60	0.19	12.17	15.69	1.33	0.14	0.10	99.36

Tephra layer	Composite depth	Tephra marker	SiO_2	TiO_2	Al_2O_3	FeO	MnO	MgO	CaO	Na_2O	K_2O	P_2O_5	Total
ABS1 18	18 cm		50.38	1.75	14.04	12.27	0.22	6.81	11.61	2.38	0.23	0.20	99.89
			48.41	4.83	13.29	15.29	0.24	4.60	9.39	3.24	0.92	0.78	100.99
			48.76	4.72	14.33	13.43	0.24	5.31	10.53	3.28	0.60	0.61	101.80
			48.24	4.68	13.24	15.03	0.25	4.56	9.12	3.13	0.84	0.70	99.79
			48.79	4.66	13.21	15.05	0.23	4.55	9.26	2.67	0.86	0.79	100.06
			47.78	4.64	12.96	14.55	0.26	4.84	9.40	3.16	0.84	0.76	99.20
			48.11	4.60	13.24	14.90	0.27	4.58	9.29	2.98	0.88	0.80	99.64
			47.39	4.55	12.95	14.83	0.24	4.89	9.58	3.24	0.82	0.74	99.23
			48.08	4.55	13.12	15.12	0.26	4.64	9.30	3.10	0.85	0.77	99.78
			48.60	4.54	13.21	15.03	0.26	4.70	9.45	2.84	0.84	0.78	100.26
			47.97	4.51	13.04	14.76	0.25	4.72	9.20	3.32	0.85	0.70	99.31
			47.95	4.50	13.15	14.69	0.26	4.69	9.38	3.11	0.80	0.77	99.30
			48.32	4.48	13.10	15.28	0.27	4.74	9.43	3.32	0.92	0.72	100.57
			47.88	4.43	12.92	14.58	0.23	4.73	9.24	3.09	0.84	0.77	98.71
			47.81	4.34	12.87	14.95	0.26	4.66	9.35	3.04	0.84	0.76	98.88
		Mean	**48.15**	**4.57**	**13.19**	**14.82**	**0.25**	**4.73**	**9.42**	**3.11**	**0.83**	**0.75**	**99.82**
		stdv	**0.40**	**0.13**	**0.35**	**0.46**	**0.01**	**0.19**	**0.34**	**0.18**	**0.08**	**0.05**	**0.86**

Tephra layer	Composite depth	Tephra marker	SiO_2	TiO_2	Al_2O_3	FeO	MnO	MgO	CaO	Na_2O	K_2O	P_2O_5	Total
ABS1 66	66-67 cm		42.37	4.19	11.44	14.49	0.24	4.28	8.64	2.35	0.77	0.65	89.42
			49.72	2.93	13.63	14.62	0.24	4.64	9.28	2.81	0.64	0.40	98.91
			51.12	2.09	13.80	13.49	0.20	5.35	9.86	2.76	0.37	0.23	99.27
			51.28	2.09	13.76	13.24	0.22	5.28	9.84	2.71	0.38	0.22	99.02
			50.23	2.02	13.90	13.64	0.20	5.95	10.59	2.72	0.26	0.20	99.72
			49.61	1.82	13.91	12.63	0.20	6.58	11.48	2.42	0.23	0.19	99.06
			50.16	1.80	13.85	12.97	0.27	6.38	11.38	2.44	0.24	0.21	99.70
			49.94	1.80	14.07	12.98	0.24	6.43	11.46	2.49	0.24	0.19	99.84
			50.17	1.79	14.06	12.70	0.23	6.93	11.56	2.55	0.22	0.20	100.40
			49.88	1.79	13.95	12.66	0.22	6.60	11.38	2.32	0.22	0.18	99.21
			50.19	1.77	13.97	12.87	0.23	6.37	11.46	2.48	0.25	0.22	99.81
			49.99	1.77	14.05	12.78	0.24	6.91	11.68	2.14	0.19	0.14	99.90
			50.34	1.76	13.82	12.70	0.23	6.41	11.33	2.49	0.24	0.21	99.53
			49.36	1.76	13.96	12.72	0.21	6.53	11.14	2.40	0.23	0.17	98.47
			50.38	1.75	13.76	10.88	0.20	7.97	12.71	2.33	0.14	0.19	100.31
			50.02	1.74	13.87	12.74	0.21	6.55	11.11	2.46	0.23	0.16	99.10
			50.14	1.72	13.95	12.73	0.23	6.51	11.46	2.45	0.24	0.22	99.64
			49.83	1.51	14.23	11.67	0.22	7.44	12.58	2.20	0.14	0.14	99.96
		Mean	**50.17**	**1.81**	**13.93**	**12.71**	**0.22**	**6.51**	**11.31**	**2.46**	**0.24**	**0.19**	**99.56**
		stdv	**0.48**	**0.15**	**0.13**	**0.65**	**0.02**	**0.66**	**0.76**	**0.17**	**0.06**	**0.03**	**0.51**

Tephra layer	Composite depth	Tephra marker	SiO_2	TiO_2	Al_2O_3	FeO	MnO	MgO	CaO	Na_2O	K_2O	P_2O_5	Total
ABS1 79 cm	79 cm		50.24	1.87	14.07	12.72	0.22	6.50	10.75	2.45	0.24	0.20	99.26
			50.10	2.55	13.77	13.43	0.21	5.51	10.27	2.72	0.42	0.33	99.31
			49.57	2.30	14.19	12.30	0.23	6.64	11.27	2.51	0.32	0.22	99.54
			49.76	3.72	11.74	16.43	0.27	4.63	9.03	2.85	0.54	0.43	99.40
			49.65	2.26	14.32	12.30	0.20	6.55	11.62	2.65	0.33	0.20	100.08
			49.85	2.25	14.02	12.61	0.21	6.17	11.29	2.67	0.36	0.24	99.66
			49.59	2.25	13.86	12.03	0.20	6.40	11.19	2.45	0.33	0.24	98.55
			49.76	2.24	14.24	11.68	0.22	6.52	11.52	2.57	0.33	0.25	99.33
			49.66	2.21	14.28	12.16	0.22	6.43	11.25	2.51	0.33	0.21	99.26
			50.24	2.20	14.17	12.02	0.21	6.35	11.15	2.56	0.36	0.22	99.48
			49.79	2.20	14.26	11.99	0.21	6.38	11.14	2.51	0.34	0.20	99.02
			49.80	2.19	14.25	11.97	0.20	6.60	11.47	2.53	0.32	0.21	99.55
			49.72	2.18	14.30	12.13	0.22	6.56	11.39	2.53	0.32	0.27	99.62
			49.66	2.17	14.22	12.13	0.19	6.47	11.61	2.40	0.33	0.20	99.38
			50.38	2.14	14.30	9.64	0.20	8.41	12.60	2.22	0.22	0.21	100.32
			49.64	2.13	14.32	12.20	0.21	6.59	11.54	2.55	0.32	0.20	99.70
			48.63	2.11	14.02	11.76	0.21	6.36	11.17	2.47	0.32	0.19	97.23
		Mean	**49.72**	**2.19**	**14.20**	**11.89**	**0.21**	**6.60**	**11.46**	**2.51**	**0.32**	**0.22**	**99.32**
		stdv	**0.40**	**0.05**	**0.14**	**0.72**	**0.01**	**0.56**	**0.39**	**0.11**	**0.03**	**0.02**	**0.77**

Tephra layer	Composite depth	Tephra marker	SiO_2	TiO_2	Al_2O_3	FeO	MnO	MgO	CaO	Na_2O	K_2O	P_2O_5	Total
ABS1 114	114 cm		49.48	2.91	13.26	14.97	0.24	4.82	9.71	2.73	0.61	0.38	99.11
			48.47	4.59	13.60	15.01	0.25	4.82	9.53	3.17	0.85	0.54	100.82
			47.67	4.46	13.41	14.33	0.20	4.75	9.69	3.07	0.78	0.52	98.87
			47.51	4.41	13.15	14.55	0.20	4.86	9.36	3.13	0.80	0.56	98.52
			47.50	4.37	13.26	14.72	0.25	4.69	9.49	2.98	0.79	0.53	98.57
			47.76	4.37	13.25	14.39	0.23	4.87	9.61	2.99	0.82	0.55	98.84
			47.98	4.28	13.36	14.93	0.22	4.83	9.78	2.91	0.78	0.52	99.60
			48.20	4.13	13.81	14.28	0.22	5.85	9.71	3.21	0.70	0.53	100.63
			48.23	4.09	12.15	14.06	0.23	6.56	10.96	2.40	0.72	0.52	99.92
			49.70	3.78	13.11	13.59	0.26	4.03	8.77	3.43	1.04	0.94	98.64
		Mean	**48.11**	**4.28**	**13.23**	**14.43**	**0.23**	**5.03**	**9.66**	**3.03**	**0.81**	**0.58**	**99.38**
		stdv	**0.68**	**0.24**	**0.46**	**0.44**	**0.02**	**0.74**	**0.57**	**0.28**	**0.10**	**0.14**	**0.90**
			49.19	1.93	13.64	13.02	0.22	6.42	11.63	2.42	0.22	0.15	98.84
			49.52	1.80	14.09	12.33	0.20	6.97	11.92	2.32	0.19	0.12	99.46
			49.92	1.78	14.23	12.82	0.21	6.86	12.10	2.24	0.21	0.16	100.53
			48.21	1.73	13.57	12.30	0.23	6.41	11.35	2.46	0.21	0.21	96.68
			49.17	1.67	14.27	11.63	0.20	7.35	12.28	2.20	0.21	0.18	99.17
			49.56	1.67	14.00	12.17	0.20	6.93	11.85	2.37	0.20	0.17	99.12
		Mean	**49.26**	**1.76**	**13.97**	**12.38**	**0.21**	**6.82**	**11.86**	**2.34**	**0.21**	**0.17**	**98.97**
		stdv	**0.58**	**0.10**	**0.30**	**0.49**	**0.01**	**0.36**	**0.33**	**0.10**	**0.01**	**0.03**	**1.26**

Tephra layer	Composite depth	Tephra marker	SiO_2	TiO_2	Al_2O_3	FeO	MnO	MgO	CaO	Na_2O	K_2O	P_2O_5	Total
ABS1 130	130-131 cm	Hekla 3	72.87	0.16	14.50	2.94	0.13	0.12	1.91	4.76	2.54	0.06	
			72.73	0.25	14.59	2.93	0.08	0.11	1.99	4.72	2.53	0.01	
			72.57	0.23	14.42	3.08	0.11	0.10	1.98	4.86	2.46	0.04	
			72.43	0.21	14.43	2.99	0.11	0.12	1.96	4.86	2.52	0.00	
			71.89	0.16	14.28	3.21	0.13	0.12	1.95	4.92	2.54	0.05	
			71.70	0.19	14.89	2.92	0.12	0.13	1.89	4.51	2.40	0.00	
			71.47	0.21	14.32	3.02	0.12	0.13	2.06	4.78	2.45	0.04	
			71.35	0.28	14.21	2.95	0.11	0.10	2.02	4.75	2.46	0.00	
			71.10	0.18	14.22	3.05	0.12	0.10	1.92	4.69	2.43	0.04	
			70.21	0.36	15.24	4.87	0.18	0.27	2.91	1.78	2.15	0.06	
			70.09	0.27	14.70	3.79	0.15	0.18	2.34	4.74	2.16	0.07	
			68.86	0.37	15.60	5.18	0.17	0.27	3.08	4.22	2.10	0.07	
			68.72	0.23	14.52	3.88	0.14	0.16	2.33	4.75	2.28	0.02	
			68.29	0.16	13.56	2.86	0.10	0.12	1.83	4.72	2.33	0.02	
			68.01	0.30	15.45	4.95	0.17	0.29	2.86	3.71	2.02	0.08	
			67.91	0.31	15.33	5.02	0.17	0.32	3.21	4.97	2.04	0.10	
			66.89	0.41	15.18	5.22	0.18	0.31	3.16	1.78	1.92	0.04	
			66.20	0.36	14.85	5.04	0.14	0.29	3.07	4.14	2.01	0.11	
			65.75	0.62	15.62	6.64	0.21	0.66	3.92	5.15	0.68	0.21	
			65.43	0.39	15.01	5.17	0.16	0.30	3.09	3.67	1.98	0.08	
		Mean	**69.72**	**0.28**	**14.75**	**3.99**	**0.14**	**0.21**	**2.47**	**4.32**	**2.20**	**0.05**	
		stdv	**2.47**	**0.11**	**0.54**	**1.15**	**0.03**	**0.13**	**0.62**	**0.95**	**0.42**	**0.05**	
			48.42	4.45	13.46	14.47	0.27	4.62	9.68	2.63	0.83	0.54	

Tephra layer	Composite depth	Tephra marker	SiO_2	TiO_2	Al_2O_3	FeO	MnO	MgO	CaO	Na_2O	K_2O	P_2O_5	Total
ABS2 63	161-162 cm	Hekla 4	74.28	0.14	13.45	1.87	0.08	0.02	1.29	4.49	2.84	0.01	98.47
			74.14	0.12	13.64	1.94	0.06	0.01	1.30	4.54	2.75	0.02	98.52
			72.45	0.09	13.02	1.92	0.05	0.01	1.26	4.12	2.65	0.02	95.59
			72.28	0.12	13.39	2.23	0.13	0.01	1.41	4.27	2.57	0.02	96.43
			68.13	0.07	**17.92**	1.17	0.05	0.02	3.18	6.14	1.70	0.00	98.38
			65.15	0.45	14.72	6.85	0.22	0.26	3.51	4.18	1.92	0.10	97.37
			62.00	0.74	14.87	8.67	0.27	0.64	4.23	4.26	1.74	0.21	97.63
			61.12	0.71	**16.74**	9.00	0.30	0.66	4.23	4.11	1.50	0.25	98.61
			60.37	0.90	14.98	9.71	0.26	1.05	4.62	4.29	1.63	0.32	98.14
		Mean	**67.77**	**0.37**	**14.75**	**4.82**	**0.16**	**0.30**	**2.78**	**4.49**	**2.14**	**0.11**	**97.68**
		stdv	**5.75**	**0.33**	**1.65**	**3.64**	**0.11**	**0.39**	**1.45**	**0.64**	**0.55**	**0.12**	**1.06**

Tephra layer	Composite depth	Tephra marker	SiO_2	TiO_2	Al_2O_3	FeO	MnO	MgO	CaO	Na_2O	K_2O	P_2O_5	Total
ABS2 74	168 cm		49.06	1.97	14.40	10.55	0.21	7.29	12.34	2.32	0.26	0.18	98.58
			49.98	1.72	14.06	12.04	0.21	7.01	11.97	2.06	0.23	0.18	99.46
			50.71	1.70	13.98	11.53	0.21	6.15	11.01	2.68	0.32	0.22	98.51
			50.32	1.64	14.01	11.44	0.21	6.68	11.41	2.48	0.28	0.20	98.67
			49.70	1.64	14.16	11.76	0.21	7.19	11.77	2.41	0.21	0.15	99.19
			49.34	1.63	13.97	11.80	0.18	7.44	12.29	2.33	0.15	0.15	99.28
			49.37	1.61	14.11	11.98	0.21	7.41	11.97	2.33	0.17	0.14	99.30
			50.32	1.61	14.06	11.84	0.21	6.78	11.49	2.41	0.25	0.11	99.08
			50.55	1.60	14.07	11.23	0.22	6.82	11.55	2.50	0.26	0.12	98.93
			49.21	1.60	13.92	11.49	0.20	7.51	12.34	2.31	0.18	0.12	98.88
			49.15	1.60	13.95	11.92	0.22	7.57	12.44	2.18	0.16	0.13	99.32
			49.29	1.59	14.02	11.89	0.21	7.19	12.17	2.31	0.17	0.14	98.99
			49.07	1.59	13.99	11.81	0.20	7.45	12.12	2.27	0.16	0.13	98.78
			49.34	1.58	13.97	11.82	0.18	7.37	12.30	2.32	0.17	0.13	99.17
			49.26	1.58	14.29	11.65	0.20	7.30	12.22	2.36	0.19	0.18	99.23
			49.70	1.58	13.97	11.54	0.20	7.01	11.93	2.39	0.22	0.11	98.65
			49.30	1.54	14.11	11.85	0.21	7.32	12.37	2.30	0.17	0.19	99.36
		Mean	**49.63**	**1.63**	**14.06**	**11.66**	**0.21**	**7.15**	**11.98**	**2.35**	**0.21**	**0.15**	**99.02**
		stdv	**0.54**	**0.10**	**0.13**	**0.36**	**0.01**	**0.37**	**0.41**	**0.13**	**0.05**	**0.03**	**0.30**

Tephra layer	Composite depth	Tephra marker	SiO_2	TiO_2	Al_2O_3	FeO	MnO	MgO	CaO	Na_2O	K_2O	P_2O_5	Total
ABS2 95	181 cm		50.26	3.46	13.25	14.62	0.23	4.66	8.73	3.00	0.72	0.45	99.38
			50.20	2.72	13.88	13.83	0.27	5.64	10.96	3.04	0.26	0.26	101.05
			48.84	2.60	13.46	13.44	0.21	6.15	10.82	2.80	0.35	0.24	98.92
			49.04	2.59	13.46	13.09	0.20	6.00	10.43	2.82	0.40	0.32	98.35
			48.87	2.55	13.48	13.24	0.21	6.31	10.66	2.70	0.32	0.28	98.63
			49.36	2.53	13.49	13.65	0.22	6.01	10.57	2.66	0.34	0.24	99.07
			49.23	2.48	13.66	13.28	0.21	6.30	10.89	2.46	0.32	0.24	99.07
			49.41	2.47	13.56	11.69	0.19	7.77	12.22	2.48	0.25	0.25	100.29
			49.36	2.47	13.68	12.75	0.22	6.31	10.98	2.50	0.32	0.25	98.85
			49.15	2.46	13.78	12.86	0.22	6.35	11.29	2.54	0.32	0.24	99.21
			49.10	2.43	13.57	13.00	0.21	6.45	11.00	2.59	0.33	0.22	98.90
			49.30	2.43	13.60	12.73	0.22	6.60	11.30	2.70	0.31	0.28	99.47
			48.87	2.43	13.68	12.96	0.20	6.53	11.22	2.61	0.34	0.26	99.10
			49.04	2.40	13.65	12.95	0.21	6.53	11.18	2.55	0.33	0.25	99.08
			49.45	2.38	14.00	13.02	0.22	6.34	11.15	2.61	0.31	0.22	99.69
			49.24	2.28	13.67	12.62	0.22	6.52	11.27	2.73	0.31	0.21	99.07
		Mean	**49.23**	**2.48**	**13.64**	**13.01**	**0.21**	**6.39**	**11.06**	**2.65**	**0.32**	**0.25**	**99.25**
		stdv	**0.33**	**0.11**	**0.16**	**0.50**	**0.02**	**0.46**	**0.42**	**0.15**	**0.03**	**0.03**	**0.67**
			49.54	1.48	14.37	10.84	0.19	7.61	12.40	2.20	0.18	0.13	98.93

Tephra layer	Composite depth	Tephra marker	SiO_2	TiO_2	Al_2O_3	FeO	MnO	MgO	CaO	Na_2O	K_2O	P_2O_5	Total
ABS2 95	181 cm		72.42	0.17	14.53	2.95	0.10	0.12	1.90	4.90	2.51	0.04	99.64
			72.17	0.15	14.50	3.08	0.12	0.12	1.96	4.86	2.46	0.03	99.45
			72.10	0.18	14.44	3.07	0.15	0.10	1.99	5.21	2.39	0.01	99.64
			71.90	0.23	13.99	3.03	0.13	0.13	1.87	5.02	2.44	0.03	98.77
			70.38	0.17	14.76	2.98	0.11	0.10	1.89	4.95	2.49	0.00	97.83
			69.73	0.16	13.88	3.07	0.11	0.13	1.81	4.77	2.44	0.04	96.14
			69.68	0.20	14.03	2.78	0.12	0.11	1.84	4.65	2.41	0.03	95.85
			69.65	0.13	15.58	2.51	0.12	0.08	2.46	5.60	2.15	0.03	98.31
			69.35	0.27	14.11	3.55	0.13	0.28	2.18	4.67	2.36	0.00	96.90
			69.32	0.17	13.80	2.80	0.12	0.12	1.83	4.95	2.26	0.04	95.41
			68.60	*0.16*	*13.48*	*2.85*	*0.10*	*0.12*	*1.77*	*4.37*	*2.37*	*0.05*	*93.87*
			68.28	0.43	15.13	4.74	0.18	0.32	3.15	4.81	2.17	0.04	99.24
			68.01	*0.12*	*13.92*	*2.90*	*0.11*	*0.12*	*1.76*	*4.57*	*2.22*	*0.00*	*93.73*
			67.92	*0.18*	*13.34*	*2.84*	*0.09*	*0.14*	*1.91*	*4.95*	*2.41*	*0.02*	*93.80*
			67.20	*0.21*	*13.65*	*2.83*	*0.15*	*0.12*	*1.81*	*4.56*	*2.38*	*0.04*	*92.96*
			67.12	*0.18*	*13.54*	*2.81*	*0.10*	*0.13*	*1.78*	*4.10*	*2.28*	*0.06*	*92.09*
			67.00	0.17	16.89	2.69	0.09	0.11	1.91	5.20	2.20	0.02	96.27
			66.71	0.39	15.12	4.78	0.14	0.29	2.90	4.81	2.07	0.03	97.25
			66.20	*0.17*	*16.48*	*2.90*	*0.08*	*0.12*	*1.81*	*4.51*	*2.26*	*0.01*	*94.55*
			65.70	*0.19*	*13.61*	*2.76*	*0.09*	*0.11*	*1.79*	*4.21*	*2.29*	*0.00*	*90.76*
			64.16	*0.17*	*13.03*	*2.61*	*0.11*	*0.10*	*1.67*	*4.44*	*2.27*	*0.02*	*88.58*
			63.86	*0.15*	*13.61*	*2.78*	*0.05*	*0.15*	*1.69*	*4.40*	*2.29*	*0.05*	*89.02*
			63.84	0.30	14.43	4.58	0.13	0.28	2.76	4.71	2.00	0.01	93.04
			63.15	0.19	24.43	2.55	0.09	0.10	1.65	4.20	2.14	0.00	98.50
			57.25	*0.19*	*10.89*	*2.33*	*0.12*	*0.08*	*1.65*	*3.86*	*2.00*	*0.02*	*78.38*
			50.54	*0.15*	*12.25*	*2.00*	*0.08*	*0.11*	*1.34*	*3.21*	*1.70*	*0.00*	*71.38*
		Mean	**69.05**	**0.22**	**15.31**	**3.28**	**0.12**	**0.16**	**2.14**	**4.89**	**2.30**	**0.02**	**97.48**
		stdv	**2.85**	**0.09**	**2.65**	**0.78**	**0.02**	**0.09**	**0.46**	**0.31**	**0.17**	**0.02**	**1.89**

Tephra layer	Composite depth	Tephra marker	SiO_2	TiO_2	Al_2O_3	FeO	MnO	MgO	CaO	Na_2O	K_2O	P_2O_5	Total
ABS2 98	183 cm		47.64	4.41	12.34	14.72	0.21	5.19	9.83	3.02	0.90	0.53	98.79
			47.45	4.20	13.43	15.25	0.23	4.74	9.36	3.31	0.91	0.42	99.30
			49.06	4.18	13.79	15.28	0.20	4.70	7.97	3.08	1.24	0.51	100.01
			47.71	4.13	13.29	14.66	0.22	5.01	9.62	3.16	0.86	0.54	99.21
			47.47	4.09	13.45	14.49	0.21	4.92	9.82	3.10	0.79	0.56	98.90
		Mean	**47.87**	**4.20**	**13.26**	**14.88**	**0.21**	**4.91**	**9.32**	**3.13**	**0.94**	**0.51**	**99.24**
		stdv	**0.68**	**0.12**	**0.55**	**0.36**	**0.01**	**0.20**	**0.78**	**0.11**	**0.17**	**0.05**	**0.48**
			49.78	2.98	13.23	14.92	0.24	4.76	9.16	2.86	0.62	0.43	98.98
			49.31	2.79	13.14	14.15	0.21	5.72	10.37	2.90	0.37	0.28	99.24
			49.37	1.41	14.68	10.93	0.21	7.56	12.93	2.05	0.15	0.09	99.38
			50.89	1.39	14.69	9.95	0.18	8.38	12.96	2.00	0.17	0.12	100.73
			49.36	1.34	14.57	10.71	0.18	7.99	13.35	1.98	0.13	0.10	99.71
			48.46	1.33	14.52	10.41	0.21	8.27	12.73	2.04	0.13	0.09	98.19
			49.28	1.33	14.53	10.77	0.19	8.00	13.21	2.08	0.13	0.10	99.62
			49.16	1.32	14.48	10.78	0.18	8.05	13.12	1.98	0.13	0.11	99.30
			49.51	1.31	14.63	10.41	0.17	7.99	13.38	1.89	0.15	0.14	99.58
			49.27	1.30	14.67	10.38	0.17	7.98	13.08	1.99	0.14	0.13	99.10
			49.48	1.28	14.69	10.60	0.18	8.23	13.08	2.00	0.14	0.11	99.79
		Mean	**49.42**	**1.33**	**14.61**	**10.55**	**0.18**	**8.05**	**13.09**	**2.00**	**0.14**	**0.11**	**99.49**
		stdv	**0.63**	**0.04**	**0.08**	**0.30**	**0.01**	**0.24**	**0.21**	**0.05**	**0.01**	**0.02**	**0.67**
			46.12	0.06	**34.54**	0.79	0.00	0.22	18.23	1.41	0.02	0.01	101.40

Tephra layer	Composite depth	Tephra marker	SiO_2	TiO_2	Al_2O_3	FeO	MnO	MgO	CaO	Na_2O	K_2O	P_2O_5	Total
ABS2 104	187 cm		49.28	2.37	13.17	14.07	0.24	5.82	10.62	2.57	0.37	0.30	98.81
			49.52	2.15	13.73	12.66	0.22	6.57	10.89	2.54	0.31	0.23	98.81
			49.81	2.03	14.15	12.99	0.21	6.45	11.46	2.43	0.28	0.21	100.02
			49.28	1.96	13.94	13.36	0.24	6.08	10.91	2.49	0.32	0.22	98.80
			49.71	1.94	13.85	12.39	0.21	6.67	11.55	2.51	0.28	0.19	99.31
			49.37	1.91	13.93	12.51	0.21	6.71	11.30	2.49	0.29	0.23	98.95
			50.24	1.89	14.38	10.20	0.21	8.05	12.54	2.37	0.21	0.17	100.26
			49.30	1.86	13.85	12.27	0.21	6.75	11.70	2.42	0.24	0.20	98.80
			49.98	1.79	14.43	11.79	0.20	6.96	12.07	2.44	0.22	0.16	100.04
			49.48	1.79	14.25	11.76	0.20	7.16	11.75	2.33	0.23	0.17	99.12
			49.60	1.78	14.17	11.54	0.21	6.98	11.99	2.30	0.23	0.18	98.98
			49.25	1.75	14.28	11.55	0.24	7.12	12.13	2.39	0.23	0.18	99.12
			49.19	1.69	14.24	11.90	0.18	7.23	12.21	2.44	0.20	0.18	99.46
			50.38	1.68	15.40	10.12	0.20	7.44	12.74	2.34	0.15	0.15	100.60
			49.21	1.57	13.98	11.68	0.21	7.31	12.27	2.32	0.18	0.16	98.89
		Mean	**49.59**	**1.84**	**14.18**	**11.91**	**0.21**	**6.96**	**11.82**	**2.42**	**0.24**	**0.19**	**99.37**
		stdv	**0.39**	**0.15**	**0.41**	**0.92**	**0.02**	**0.48**	**0.56**	**0.08**	**0.05**	**0.03**	**0.61**
			49.61	1.17	5.01	7.86	0.20	16.15	19.27	0.23	0.00	0.01	99.51

Tephra layer	Composite depth	Tephra marker	SiO_2	TiO_2	Al_2O_3	FeO	MnO	MgO	CaO	Na_2O	K_2O	P_2O_5	Total
ABS2 131	204 cm		50.87	3.63	13.58	12.91	0.21	4.20	8.32	3.33	1.14	0.52	98.70
			50.51	2.87	13.80	12.19	0.22	6.25	10.31	2.57	0.45	0.32	99.49
			50.18	2.79	13.66	12.29	0.19	6.23	10.40	2.95	0.45	0.32	99.46
			49.03	2.20	14.10	11.80	0.18	7.00	11.38	2.53	0.31	0.21	98.75
			48.92	2.13	14.08	11.81	0.19	7.06	11.54	2.49	0.32	0.21	98.75
			48.62	2.12	14.15	11.69	0.18	7.21	11.77	2.41	0.29	0.16	98.60
			49.06	2.11	14.15	11.35	0.19	6.97	11.85	2.40	0.29	0.22	98.59
			48.81	2.11	14.12	11.96	0.20	6.81	11.33	2.54	0.30	0.23	98.41
			49.19	2.11	14.29	11.61	0.20	6.96	11.66	2.45	0.30	0.24	99.01
			49.46	2.10	14.43	11.69	0.21	6.85	11.60	2.42	0.32	0.22	99.30
			49.08	2.10	14.35	11.85	0.17	6.86	11.31	2.51	0.30	0.23	98.77
			49.10	2.10	14.37	11.27	0.20	6.99	11.75	2.38	0.29	0.20	98.66
			48.62	2.08	14.43	11.75	0.22	7.12	11.76	2.43	0.29	0.24	98.94
			49.31	2.06	14.46	11.60	0.14	7.16	11.95	2.22	0.27	0.20	99.38
			48.97	2.03	14.37	11.55	0.20	7.06	11.82	2.39	0.29	0.26	98.94
			49.06	1.99	14.13	12.20	0.19	6.92	11.59	2.49	0.30	0.21	99.08
			49.01	1.95	14.29	11.29	0.18	7.01	11.89	2.54	0.28	0.25	98.69
		Mean	**49.02**	**2.09**	**14.27**	**11.67**	**0.19**	**7.00**	**11.66**	**2.44**	**0.30**	**0.22**	**98.85**
		stdv	**0.23**	**0.06**	**0.14**	**0.26**	**0.02**	**0.12**	**0.21**	**0.09**	**0.01**	**0.03**	**0.28**

Tephra layer	Composite depth	Tephra marker	SiO_2	TiO_2	Al_2O_3	FeO	MnO	MgO	CaO	Na_2O	K_2O	P_2O_5	Total
ABS3 2	181 cm		49.79	1.63	14.34	13.59	0.25	5.89	11.78	2.67	0.22	0.15	100.30
			49.26	1.59	14.15	11.63	0.22	7.31	12.49	2.15	0.15	0.10	99.05
			49.28	1.58	14.29	11.70	0.20	7.44	12.47	2.21	0.16	0.10	99.42
			50.03	1.58	14.20	12.09	0.22	6.75	12.06	2.30	0.21	0.14	99.57
			49.98	1.58	13.93	11.90	0.21	7.03	12.01	2.36	0.21	0.17	99.38
			50.12	1.57	14.18	11.43	0.20	6.97	11.75	2.34	0.20	0.19	98.94
			49.18	1.56	14.22	11.78	0.20	7.49	12.28	2.26	0.15	0.14	99.26
			49.59	1.55	14.43	11.77	0.20	7.29	12.58	2.20	0.15	0.13	99.90
			49.54	1.55	14.13	11.54	0.20	7.54	12.61	2.19	0.15	0.13	99.58
			49.83	1.54	14.23	12.07	0.24	7.07	12.21	2.17	0.20	0.15	99.71
			49.62	1.53	14.04	11.77	0.17	7.50	12.48	2.20	0.15	0.14	99.61
			48.90	1.52	14.19	11.75	0.20	7.44	12.55	2.10	0.15	0.14	98.94
			50.03	1.52	14.05	11.67	0.22	6.91	11.95	2.40	0.22	0.13	99.10
			50.01	1.50	14.29	12.33	0.20	6.85	12.07	2.11	0.18	0.18	99.72
			49.21	1.50	14.01	11.77	0.20	7.46	12.45	2.20	0.15	0.13	99.07
			49.15	1.49	13.94	11.71	0.21	7.56	12.25	2.19	0.13	0.12	98.75
			49.18	1.44	13.78	11.56	0.19	7.82	12.57	2.14	0.15	0.10	98.93
		Mean	**49.57**	**1.54**	**14.14**	**11.89**	**0.21**	**7.20**	**12.27**	**2.25**	**0.17**	**0.14**	**99.37**
		stdv	**0.39**	**0.05**	**0.17**	**0.49**	**0.02**	**0.45**	**0.29**	**0.14**	**0.03**	**0.03**	**0.41**

Tephra layer	Composite depth	Tephra marker	SiO_2	TiO_2	Al_2O_3	FeO	MnO	MgO	CaO	Na_2O	K_2O	P_2O_5	Total
ABS3 3	183 cm		50.52	1.75	13.86	12.27	0.21	6.35	11.03	2.52	0.32	0.19	99.03
			50.16	1.71	14.08	11.23	0.20	7.39	12.82	2.34	0.18	0.19	100.29
			49.85	1.68	13.89	11.90	0.22	6.87	11.60	2.34	0.24	0.17	98.76
			49.92	1.59	14.27	11.69	0.22	7.34	12.20	2.29	0.19	0.15	99.86
			49.67	1.70	13.92	12.26	0.21	6.97	11.69	2.43	0.23	0.20	99.28
			49.57	1.53	14.17	11.60	0.20	7.29	12.31	2.16	0.17	0.13	99.14
			49.26	1.56	14.11	11.67	0.20	7.47	12.41	2.24	0.17	0.13	99.22
			49.64	1.52	13.79	10.17	0.17	9.01	13.55	1.86	0.23	0.14	100.08
			49.83	1.78	13.83	12.12	0.20	7.00	11.45	2.43	0.21	0.13	98.99
			49.98	1.76	13.99	12.23	0.23	6.84	11.57	2.43	0.25	0.18	99.47
			48.98	2.55	13.31	13.77	0.22	5.81	11.13	2.53	0.38	0.28	98.95
			50.06	1.85	13.85	11.76	0.18	7.23	11.53	2.42	0.26	0.18	99.32
			49.86	1.69	13.93	11.60	0.22	6.96	11.75	2.09	0.20	0.13	98.43
			50.25	1.65	14.03	11.72	0.19	6.89	11.71	2.41	0.24	0.16	99.25
			49.31	1.61	14.06	11.66	0.21	7.50	12.32	2.18	0.15	0.14	99.14
			49.60	1.52	14.05	11.43	0.21	7.50	12.23	2.34	0.19	0.13	99.19
			50.03	1.61	14.19	12.61	0.24	6.76	12.35	1.80	0.18	0.14	99.91
			49.00	1.54	14.03	11.47	0.20	7.45	12.62	2.22	0.14	0.12	98.80
		Mean	**49.75**	**1.70**	**13.96**	**11.84**	**0.21**	**7.15**	**12.02**	**2.28**	**0.22**	**0.16**	**99.28**
		stdv	**0.42**	**0.23**	**0.21**	**0.71**	**0.02**	**0.64**	**0.63**	**0.20**	**0.06**	**0.04**	**0.48**

Tephra layer	Composite depth	Tephra marker	SiO_2	TiO_2	Al_2O_3	FeO	MnO	MgO	CaO	Na_2O	K_2O	P_2O_5	Total
ABS3 50	229 cm		49.69	3.93	11.87	16.12	0.27	4.08	8.63	2.80	0.84	0.52	98.75
			48.58	2.49	13.47	13.49	0.23	6.01	10.38	2.81	0.36	0.23	98.04
			49.14	2.46	13.53	13.24	0.22	6.17	10.48	2.76	0.36	0.31	98.67
			49.20	2.42	13.59	13.31	0.23	5.80	10.52	2.81	0.36	0.27	98.51
			49.21	2.42	13.37	13.17	0.26	6.29	10.53	2.84	0.36	0.20	98.65
			49.28	2.42	13.61	13.35	0.19	6.11	10.66	2.84	0.34	0.26	99.06
			49.14	2.41	13.55	13.46	0.23	5.86	10.27	2.81	0.36	0.23	98.31
			49.38	2.40	13.67	12.79	0.23	6.12	10.36	2.78	0.35	0.24	98.33
			49.04	2.39	13.38	13.60	0.24	6.03	10.55	2.74	0.36	0.26	98.59
			49.99	2.39	13.71	12.15	0.21	7.10	11.67	2.68	0.25	0.26	100.41
			49.27	2.37	13.54	13.39	0.22	6.00	10.67	2.83	0.36	0.28	98.93
			48.80	2.36	13.52	13.01	0.21	6.15	10.65	2.81	0.35	0.28	98.14
			49.20	2.34	13.39	13.30	0.24	5.99	10.62	2.86	0.37	0.22	98.53
			49.06	2.33	13.42	13.34	0.18	6.23	10.71	2.69	0.34	0.23	98.54
			49.33	2.31	13.72	12.89	0.21	6.16	10.76	2.84	0.33	0.23	98.78
			49.84	2.15	13.27	14.29	0.26	5.59	10.13	2.75	0.34	0.21	98.82
		Mean	**49.23**	**2.38**	**13.52**	**13.25**	**0.22**	**6.11**	**10.60**	**2.79**	**0.34**	**0.25**	**98.69**
		stdv	**0.35**	**0.08**	**0.13**	**0.46**	**0.02**	**0.33**	**0.34**	**0.06**	**0.03**	**0.03**	**0.55**
			49.92	1.97	8.52	10.76	0.24	10.99	15.46	1.41	0.19	0.16	99.62

Tephra layer	Composite depth	Tephra marker	SiO_2	TiO_2	Al_2O_3	FeO	MnO	MgO	CaO	Na_2O	K_2O	P_2O_5	Total
ABS3 91	266 cm		49.80	3.59	12.66	15.24	0.24	4.59	8.89	3.11	0.54	0.40	99.07
			49.69	3.12	12.71	15.40	0.26	4.70	8.73	3.01	0.56	0.35	98.53
			49.28	3.01	12.99	14.68	0.27	5.38	9.83	2.61	0.46	0.30	98.80
			50.14	2.86	13.44	14.53	0.26	4.65	9.60	3.07	0.51	0.35	99.42
			49.61	2.84	13.16	14.19	0.23	5.15	9.58	2.75	0.49	0.34	98.34
			50.26	2.82	13.09	13.85	0.25	5.01	9.39	2.93	0.54	0.38	98.51
			50.20	2.80	13.40	14.17	0.24	5.42	9.94	2.83	0.49	0.38	99.87
			50.01	2.78	13.60	14.10	0.23	5.56	9.96	2.71	0.48	0.32	99.75
			50.00	2.75	13.22	13.65	0.22	5.33	9.69	2.84	0.48	0.32	98.50
			49.91	2.75	13.43	13.98	0.22	5.33	9.65	2.83	0.49	0.37	98.96
			49.63	2.73	13.27	13.88	0.23	5.51	9.84	2.70	0.50	0.33	98.62
			49.13	2.73	13.19	14.02	0.23	5.33	9.77	2.91	0.49	0.35	98.15
			49.65	2.71	13.23	13.97	0.21	5.31	9.64	2.86	0.48	0.34	98.40
			50.28	2.69	13.30	13.60	0.25	5.28	8.69	2.84	0.49	0.36	97.77
			49.46	2.66	13.25	13.64	0.25	5.46	9.96	2.81	0.49	0.31	98.29
		Mean	**49.80**	**2.80**	**13.23**	**14.12**	**0.24**	**5.24**	**9.59**	**2.84**	**0.50**	**0.34**	**98.71**
		stdv	**0.37**	**0.13**	**0.22**	**0.48**	**0.02**	**0.28**	**0.41**	**0.12**	**0.03**	**0.03**	**0.60**
			49.22	2.27	14.19	12.12	0.19	6.63	11.63	2.56	0.30	0.20	99.30
			49.43	2.21	13.98	12.48	0.22	6.51	11.19	2.56	0.34	0.23	99.15

Tephra layer	Composite depth	Tephra marker	SiO_2	TiO_2	Al_2O_3	FeO	MnO	MgO	CaO	Na_2O	K_2O	P_2O_5	Total
ABS3 117	273-335 cm	Saksunarva	49.91	3.13	13.31	15.07	0.22	5.14	9.72	2.58	0.49	0.34	99.92
			50.07	3.13	13.54	13.79	0.24	5.85	10.66	2.45	0.35	0.33	100.41
			49.59	3.11	13.18	14.74	0.25	5.32	9.71	2.70	0.47	0.37	99.44
			49.69	3.10	13.27	15.06	0.25	5.43	9.58	2.37	1.30	0.35	100.40
			49.77	3.09	13.25	14.40	0.26	5.27	9.86	2.89	0.47	0.32	99.59
			49.24	3.07	13.02	14.56	0.24	5.19	9.70	2.78	0.47	0.38	98.65
			49.38	3.05	13.17	14.59	0.25	5.77	9.96	2.55	0.46	0.33	99.51
			50.31	2.98	13.98	14.82	0.23	4.51	9.32	3.24	0.36	0.33	100.09
			49.38	2.88	13.42	14.54	0.25	5.78	10.19	2.65	0.42	0.29	99.80
			49.13	2.88	13.29	14.31	0.23	5.62	10.22	2.69	0.44	0.34	99.15
			49.03	2.86	13.14	14.46	0.24	5.50	10.14	2.85	0.42	0.26	98.90
			49.26	2.84	13.47	14.15	0.23	5.62	10.25	2.60	0.43	0.33	99.18
			49.07	2.75	13.13	14.33	0.22	5.53	10.17	2.78	0.42	0.34	98.74
			49.37	2.71	13.81	14.15	0.24	5.75	10.03	2.73	0.38	0.26	99.43
			48.94	2.71	13.41	13.99	0.22	5.77	10.34	2.60	0.41	0.36	98.75
			49.24	2.65	13.51	13.75	0.22	5.85	10.42	2.63	0.39	0.25	98.90
			49.21	2.55	13.42	13.77	0.20	5.98	10.38	2.59	0.38	0.31	98.78
		Mean	**49.45**	**2.91**	**13.37**	**14.38**	**0.23**	**5.52**	**10.04**	**2.69**	**0.47**	**0.32**	**99.39**
		stdv	**0.39**	**0.19**	**0.25**	**0.41**	**0.02**	**0.36**	**0.35**	**0.20**	**0.22**	**0.04**	**0.58**
			49.70	1.94	14.02	13.77	0.21	6.54	11.54	2.54	0.22	0.20	100.68
			48.20	1.55	15.91	10.75	0.20	7.79	11.75	2.25	0.33	0.15	98.89
			49.46	1.15	14.48	10.47	0.19	8.22	13.63	1.92	0.09	0.09	99.70
			49.13	1.15	14.70	10.79	0.20	8.10	13.55	1.93	0.10	0.10	99.74

Tephra layer	Composite depth	Tephra marker	SiO_2	TiO_2	Al_2O_3	FeO	MnO	MgO	CaO	Na_2O	K_2O	P_2O_5	Total
ABS3 147	273-335 cm	Saksunarva	49.21	3.08	13.33	14.48	0.22	5.42	9.97	2.57	0.46	0.37	99.11
			49.34	3.03	13.30	14.83	0.25	5.45	9.81	2.69	0.46	0.36	99.52
			49.71	2.94	13.44	14.42	0.21	5.66	10.58	2.43	0.41	0.29	100.10
			49.05	2.92	13.45	14.47	0.22	5.46	9.98	2.65	0.44	0.30	98.94
			49.03	2.91	13.31	14.27	0.22	5.45	10.00	2.74	0.43	0.28	98.64
			51.10	2.88	13.94	13.48	0.25	5.15	9.74	2.44	0.39	0.29	99.65
			49.24	2.81	13.31	14.09	0.25	5.51	10.08	2.48	0.43	0.35	98.55
			49.11	2.80	13.52	14.10	0.22	5.71	10.21	2.67	0.40	0.32	99.07
			49.22	2.74	13.82	14.11	0.23	5.68	10.39	2.65	0.39	0.30	99.54
			48.82	2.73	13.59	13.52	0.22	5.73	10.52	2.58	0.40	0.35	98.45
			48.98	2.72	13.45	13.92	0.23	5.65	10.02	2.56	0.41	0.30	98.24
			48.94	2.69	13.45	13.82	0.25	5.95	10.33	2.60	0.38	0.27	98.68
			49.28	2.65	13.56	13.98	0.22	5.80	10.50	2.52	0.39	0.30	99.21
			49.33	2.61	13.53	13.87	0.24	5.87	10.35	2.54	0.39	0.29	99.03
			49.59	2.60	13.57	13.64	0.24	5.84	10.55	2.61	0.36	0.31	99.30
			49.70	2.41	14.01	13.27	0.18	6.00	10.67	2.53	0.36	0.25	99.39
		Mean	**49.35**	**2.78**	**13.54**	**14.02**	**0.23**	**5.65**	**10.23**	**2.58**	**0.41**	**0.31**	**99.09**
		stdv	**0.53**	**0.17**	**0.22**	**0.42**	**0.02**	**0.23**	**0.29**	**0.09**	**0.03**	**0.03**	**0.50**
			52.34	0.11	**29.78**	1.07	0.03	0.18	13.13	3.90	0.10	0.02	100.66
			49.37	3.53	13.30	14.82	0.24	4.69	9.17	2.75	0.70	0.38	98.94

Tephra layer	Composite depth	Tephra marker	SiO_2	TiO_2	Al_2O_3	FeO	MnO	MgO	CaO	Na_2O	K_2O	P_2O_5	Total
ABS4 18	273-335 cm	Saksunarva	49.43	3.00	12.98	14.25	0.22	5.37	9.64	2.62	0.46	0.36	98.33
			49.33	3.13	12.90	15.25	0.22	5.15	9.64	2.97	0.49	0.32	99.39
			49.25	1.36	14.94	11.35	0.14	7.66	12.40	2.09	0.16	0.13	99.48
			49.15	2.59	13.24	13.44	0.23	5.93	10.13	2.55	0.40	0.21	97.87
			49.78	2.95	13.28	14.30	0.22	5.46	10.07	2.72	0.44	0.29	99.51
			50.39	2.74	13.44	13.99	0.20	5.56	10.17	2.98	0.42	0.31	100.20
			49.66	3.02	13.07	14.33	0.28	5.45	9.80	2.71	0.44	0.36	99.12
			49.75	3.14	13.00	14.95	0.18	4.95	9.75	2.74	0.48	0.30	99.25
			49.55	2.53	13.49	13.41	0.20	5.83	10.54	2.39	0.38	0.24	98.57
			49.53	2.78	13.76	13.70	0.22	5.83	10.49	2.56	0.38	0.25	99.50
			49.64	2.99	13.27	14.49	0.20	5.36	9.97	2.92	0.45	0.24	99.53
			50.53	3.20	13.20	15.38	0.24	4.98	9.86	2.81	0.50	0.34	101.05
			49.83	2.59	13.69	13.65	0.23	6.00	10.50	2.53	0.39	0.26	99.66
			49.92	3.22	12.98	15.02	0.28	5.03	9.60	2.53	0.50	0.32	99.39
			49.35	2.80	14.20	13.67	0.23	5.89	10.11	2.56	0.41	0.28	99.50
			46.17	3.07	12.13	13.87	0.20	4.21	8.72	2.65	0.46	0.30	91.78
			49.90	3.04	12.97	14.35	0.27	5.34	9.97	2.76	0.45	0.29	99.34
			49.53	2.64	13.69	14.13	0.20	5.74	10.24	2.27	0.38	0.32	99.13
			49.73	2.88	13.09	14.00	0.22	5.58	9.98	2.55	0.43	0.36	98.82
			49.30	2.95	13.40	14.36	0.24	5.53	9.92	2.72	0.46	0.27	99.15
			49.93	2.72	13.37	13.73	0.25	5.63	10.15	2.49	0.40	0.30	98.97
		Mean	**49.51**	**2.83**	**13.34**	**14.08**	**0.22**	**5.55**	**10.08**	**2.62**	**0.42**	**0.29**	**98.93**
		stdv	**0.84**	**0.40**	**0.55**	**0.84**	**0.03**	**0.64**	**0.66**	**0.22**	**0.07**	**0.06**	**1.76**

Tephra layer	Composite depth	Tephra marker	SiO_2	TiO_2	Al_2O_3	FeO	MnO	MgO	CaO	Na_2O	K_2O	P_2O_5	Total
ABS4 48	273-335 cm	Saksunarva	49.09	2.59	13.46	13.57	0.18	6.00	10.56	2.49	0.37	0.27	98.58
			49.18	2.53	13.57	13.23	0.21	6.06	10.40	2.56	0.37	0.30	98.41
			49.29	2.85	13.13	14.22	0.25	5.62	10.06	2.61	0.43	0.37	98.82
			49.36	2.82	13.47	14.03	0.27	5.66	10.04	2.71	0.42	0.30	99.08
			49.45	3.12	13.03	14.50	0.27	5.46	9.62	2.75	0.42	0.35	98.97
			49.70	2.94	13.22	14.34	0.23	5.44	10.01	2.37	0.43	0.29	98.97
			50.25	3.16	13.87	14.33	0.21	3.97	9.41	1.86	0.54	0.28	97.88
			49.13	2.85	13.48	13.74	0.20	5.76	10.31	2.38	0.40	0.30	98.56
			49.16	3.03	12.93	14.26	0.26	5.36	9.63	2.71	0.47	0.32	98.13
			49.42	2.82	13.19	13.53	0.24	5.59	10.15	2.94	0.43	0.22	98.53
			49.54	2.82	13.29	14.04	0.25	5.62	10.36	2.63	0.45	0.33	99.33
			49.34	2.91	13.40	14.29	0.27	5.45	9.66	2.77	0.46	0.34	98.89
			49.39	2.56	13.58	13.56	0.18	6.05	10.75	2.63	0.38	0.29	99.37
			50.15	2.64	14.08	13.67	0.22	6.11	10.93	2.27	0.41	0.40	100.88
		Mean	**49.46**	**2.83**	**13.41**	**13.95**	**0.23**	**5.58**	**10.14**	**2.55**	**0.43**	**0.31**	**98.89**
		stdv	**0.35**	**0.20**	**0.31**	**0.39**	**0.03**	**0.53**	**0.45**	**0.27**	**0.04**	**0.04**	**0.71**
			39.00	0.00	0.01	17.09	0.30	43.38	0.34	0.00	0.00	0.00	100.12

Tephra layer	Composite depth	Tephra marker	SiO_2	TiO_2	Al_2O_3	FeO	MnO	MgO	CaO	Na_2O	K_2O	P_2O_5	Total
ABS4 72	353 cm	Askja S	73.63	0.29	12.21	2.57	0.08	0.23	1.50	4.93	2.51	0.03	97.98
		(disturbed	73.96	0.27	12.38	2.56	0.08	0.22	1.57	4.38	2.51	0.04	97.98
			73.12	0.30	12.05	2.53	0.10	0.25	1.51	4.21	2.47	0.00	96.54
			75.19	0.26	12.20	2.58	0.04	0.21	1.56	4.34	2.49	0.03	98.89
			71.00	0.27	11.70	2.42	0.06	0.24	1.43	3.98	2.42	0.01	93.53
			74.17	0.23	12.23	2.51	0.05	0.26	1.50	4.45	2.50	0.06	97.96
			74.51	0.37	12.25	2.59	0.02	0.25	1.66	4.32	2.50	0.04	98.50
			74.54	0.29	12.28	2.59	0.06	0.24	1.51	4.26	2.52	0.07	98.36
			75.18	0.29	12.42	2.73	0.06	0.22	1.52	4.29	2.60	0.06	99.37
			75.24	0.28	12.60	2.57	0.12	0.22	1.51	4.24	2.50	0.07	99.34
			75.66	0.35	12.47	2.57	0.09	0.23	1.48	4.20	2.52	0.05	99.61
			74.55	0.31	12.31	2.59	0.04	0.24	1.48	4.23	2.55	0.00	98.31
			75.22	0.30	12.39	2.67	0.12	0.24	1.55	4.27	2.53	0.06	99.35
		Mean	**74.31**	**0.29**	**12.27**	**2.58**	**0.07**	**0.24**	**1.52**	**4.32**	**2.51**	**0.04**	**98.13**
		stdv	**1.23**	**0.04**	**0.22**	**0.07**	**0.03**	**0.02**	**0.06**	**0.22**	**0.04**	**0.02**	**1.61**
			48.62	1.92	14.14	10.45	0.19	8.39	12.67	2.28	0.25	0.13	99.05
			49.85	1.72	13.88	12.32	0.23	6.40	11.78	2.36	0.23	0.09	98.86
			49.68	1.44	15.04	10.70	0.22	6.81	12.82	2.14	0.15	0.07	99.07
			49.61	1.16	14.52	10.13	0.13	7.88	13.38	1.85	0.11	0.07	98.83
			49.65	2.62	13.58	13.89	0.25	5.95	9.86	2.51	0.38	0.23	98.92
			54.40	2.61	13.57	13.17	0.26	3.11	7.20	3.37	0.80	0.64	99.13
			50.08	2.41	13.43	13.98	0.21	5.43	10.13	2.68	0.43	0.23	99.01
			49.87	1.72	14.05	11.98	0.24	6.65	11.92	2.31	0.27	0.16	99.16

Tephra layer	Composite depth	Tephra marker	SiO_2	TiO_2	Al_2O_3	FeO	MnO	MgO	CaO	Na_2O	K_2O	P_2O_5	Total
ABS4 74	355 cm	Askja S (disturbed	75.66	0.31	12.72	2.79	0.10	0.23	1.68	4.37	2.66	0.02	100.54
			75.36	0.27	12.51	2.69	0.08	0.22	1.59	4.22	2.49	0.05	99.49
			75.40	0.30	12.49	2.58	0.07	0.27	1.59	4.39	2.55	0.02	99.66
			74.66	0.27	12.34	2.65	0.06	0.22	1.48	4.18	2.51	0.06	98.43
			73.87	0.26	12.25	2.62	0.11	0.23	1.63	4.32	2.51	0.04	97.85
			74.70	0.30	12.36	2.58	0.12	0.22	1.51	4.46	2.43	0.04	98.72
			75.49	0.30	12.56	2.77	0.13	0.25	1.59	4.47	2.58	0.05	100.19
			75.79	0.29	12.47	2.55	0.08	0.22	1.58	4.01	2.49	0.04	99.52
			75.60	0.30	12.61	2.68	0.09	0.20	1.60	4.49	2.46	0.01	100.04
			71.88	0.33	11.94	2.53	0.09	0.22	1.48	4.19	2.36	0.01	95.03
			75.29	0.26	12.39	2.58	0.11	0.25	1.63	4.50	2.56	0.00	99.56
			76.07	0.30	12.70	2.66	0.11	0.22	1.63	4.47	2.52	0.03	100.71
			74.50	0.31	12.43	2.62	0.07	0.24	1.58	4.14	2.45	0.04	98.37
			70.97	*0.26*	*11.62*	*2.56*	*0.08*	*0.23*	*1.45*	*4.29*	*2.46*	*0.04*	***93.97***
			68.79	*0.27*	*11.46*	*2.49*	*0.08*	*0.19*	*1.30*	*3.96*	*2.26*	*0.05*	***90.85***
		Mean	**74.94**	**0.29**	**12.44**	**2.64**	**0.09**	**0.23**	**1.58**	**4.32**	**2.51**	**0.03**	**99.09**
		stdv	**1.10**	**0.02**	**0.20**	**0.08**	**0.02**	**0.02**	**0.06**	**0.16**	**0.07**	**0.02**	**1.49**

Tephra layer	Composite depth	Tephra marker	SiO_2	TiO_2	Al_2O_3	FeO	MnO	MgO	CaO	Na_2O	K_2O	P_2O_5	Total
ABS4 80	360 cm	disturbed	50.50	1.40	14.34	11.49	0.23	7.22	12.25	2.30	0.19	0.13	100.05
			49.96	1.43	14.51	11.75	0.22	7.53	12.15	2.16	0.18	0.11	100.01
			50.52	1.46	14.88	9.95	0.17	7.42	13.41	2.40	0.14	0.13	100.48
			50.24	1.46	14.44	11.51	0.23	7.28	12.40	2.29	0.20	0.09	100.14
			50.25	1.39	14.49	11.20	0.21	7.38	12.25	2.25	0.20	0.12	99.74
			50.09	1.42	14.51	11.43	0.21	7.61	12.44	2.23	0.20	0.13	100.26
			50.28	1.38	14.23	11.35	0.21	7.45	12.23	2.26	0.19	0.12	99.70
			50.22	1.40	14.35	11.31	0.20	7.46	12.37	2.35	0.23	0.11	100.00
			50.39	1.42	14.35	11.40	0.20	7.36	12.04	2.18	0.18	0.12	99.65
			50.29	1.41	14.30	11.19	0.16	7.86	12.46	2.16	0.19	0.11	100.13
			50.11	1.43	14.19	11.44	0.21	7.28	12.48	2.24	0.22	0.12	99.72
			50.37	1.38	14.43	11.47	0.20	7.49	12.31	2.29	0.21	0.12	100.26
			50.39	1.40	14.56	11.47	0.21	7.35	12.22	2.28	0.20	0.15	100.23
			50.12	1.46	14.46	11.43	0.21	7.34	12.20	2.23	0.21	0.12	99.77
			50.36	1.38	14.34	11.62	0.20	7.50	12.49	2.20	0.21	0.14	100.44
		Mean	**50.27**	**1.41**	**14.43**	**11.33**	**0.20**	**7.44**	**12.38**	**2.25**	**0.20**	**0.12**	**100.04**
		stdv	**0.16**	**0.03**	**0.16**	**0.41**	**0.02**	**0.16**	**0.31**	**0.07**	**0.02**	**0.01**	**0.27**

Tephra layer	Composite depth	Tephra marker	SiO_2	TiO_2	Al_2O_3	FeO	MnO	MgO	CaO	Na_2O	K_2O	P_2O_5	Total
ABS4 87	365 cm	disturbed	45.95	2.98	14.96	14.52	0.24	6.51	10.09	3.14	0.51	0.34	99.24
			46.19	3.52	13.76	15.44	0.27	5.81	10.01	3.00	0.57	0.29	98.85
			46.19	3.13	15.12	13.96	0.21	6.54	9.98	2.92	0.48	0.37	98.90
			45.45	3.12	14.78	15.22	0.21	6.15	9.82	2.95	0.56	0.30	98.56
			46.33	2.87	15.10	14.37	0.20	6.62	10.22	2.80	0.46	0.27	99.24
			46.54	3.24	15.07	14.61	0.26	6.13	10.09	3.04	0.49	0.32	99.79
			46.13	2.92	15.05	14.47	0.22	6.53	9.73	2.88	0.46	0.29	98.69
			46.72	3.07	15.03	14.35	0.27	6.46	10.01	3.02	0.46	0.31	99.70
			46.90	3.13	15.43	14.99	0.22	6.14	10.30	2.58	0.49	0.37	100.54
			48.31	3.04	14.38	12.72	0.18	6.03	10.92	2.75	0.50	0.36	99.20
			46.00	3.06	15.07	14.61	0.24	6.54	9.93	2.82	0.46	0.30	99.03
			46.32	2.96	15.24	14.35	0.18	6.44	9.49	2.88	0.47	0.32	98.65
			45.98	3.12	14.88	14.87	0.21	6.23	10.28	2.99	0.51	0.35	99.43
			46.65	3.67	13.84	15.93	0.24	5.66	10.48	2.97	0.61	0.39	100.43
			46.41	3.02	14.75	14.35	0.26	6.60	10.17	2.89	0.48	0.39	99.32
			47.88	2.88	14.10	12.62	0.25	6.34	11.70	2.67	0.50	0.33	99.27
			46.36	3.11	15.01	14.59	0.21	6.38	10.18	3.01	0.51	0.31	99.67
			46.55	3.04	15.01	14.48	0.20	6.39	10.21	2.94	0.48	0.29	99.59
			46.15	3.82	13.39	16.28	0.21	5.48	10.09	3.22	0.56	0.35	99.55
			46.29	3.84	13.44	16.01	0.29	5.59	10.25	2.95	0.61	0.36	99.62
			46.85	3.08	15.46	14.26	0.25	6.42	9.88	2.85	0.49	0.29	99.82
		Mean	**46.48**	**3.17**	**14.71**	**14.62**	**0.23**	**6.24**	**10.18**	**2.92**	**0.51**	**0.33**	**99.39**
		stdv	**0.63**	**0.29**	**0.63**	**0.90**	**0.03**	**0.34**	**0.45**	**0.15**	**0.05**	**0.04**	**0.53**

Tephra layer	Composite depth	Tephra marker	SiO_2	TiO_2	Al_2O_3	FeO	MnO	MgO	CaO	Na_2O	K_2O	P_2O_5	Total
ABS4 97	371-380 cm	Askja S	74.58	0.24	12.18	2.61	0.07	0.25	1.48	4.61	2.55	0.02	98.59
			73.50	0.31	12.18	2.61	0.09	0.21	1.52	4.38	2.48	0.02	97.30
			72.41	0.30	12.06	2.64	0.08	0.25	1.49	3.93	2.42	0.02	95.59
			74.95	0.28	12.70	2.62	0.11	0.23	1.61	4.40	2.59	0.06	99.55
			72.14	0.30	11.69	2.72	0.11	0.23	1.52	3.93	2.42	0.05	95.11
			74.82	0.32	12.31	2.60	0.11	0.26	1.59	4.39	2.32	0.02	98.74
			69.52	0.28	11.26	2.56	0.06	0.32	1.52	4.03	2.36	0.00	91.91
			71.36	0.27	11.84	2.48	0.09	0.23	1.46	3.97	2.45	0.04	94.19
			75.00	0.27	12.37	2.62	0.10	0.24	1.60	4.36	2.50	0.00	99.07
			72.86	0.31	12.18	2.56	0.06	0.25	1.47	4.42	2.44	0.00	96.54
			74.46	0.36	12.48	2.59	0.07	0.23	1.51	4.38	2.55	0.05	98.69
			73.80	0.38	12.22	2.77	0.09	0.23	1.61	4.30	2.46	0.02	97.87
			74.51	0.34	12.42	2.59	0.10	0.22	1.54	4.42	2.52	0.08	98.75
			74.89	0.28	12.52	2.59	0.08	0.23	1.41	4.58	2.50	0.07	99.15
			74.88	0.28	12.43	2.54	0.08	0.23	1.53	4.24	2.49	0.09	98.79
			75.48	0.33	12.61	2.60	0.13	0.25	1.58	4.33	2.54	0.05	99.90
			75.20	0.30	12.50	2.56	0.07	0.21	1.62	4.65	2.53	0.09	99.73
			74.46	0.33	12.06	2.56	0.16	0.25	1.55	4.28	2.40	0.09	98.13
			75.18	0.32	12.62	2.56	0.10	0.24	1.53	4.12	2.45	0.09	99.21
			73.77	0.32	12.30	2.53	0.09	0.21	1.49	4.31	2.53	0.02	97.57
		Mean	**73.89**	**0.31**	**12.25**	**2.60**	**0.09**	**0.24**	**1.53**	**4.30**	**2.48**	**0.04**	**97.72**
		stdv	**1.53**	**0.03**	**0.35**	**0.06**	**0.02**	**0.02**	**0.06**	**0.21**	**0.07**	**0.03**	**2.08**